Mechanisms of action and vulnerabilities associated with the oncogene EZH2 in germinal centre B-cell non-Hodgkin lymphoma

James Nolan

A thesis submitted to Trinity College Dublin
for the degree of Doctor in Philosophy

March 2023

Thesis Supervisor: Professor Adrian Bracken
Cancer Epigenetics Laboratory,
Department of Genetics,
University of Dublin, Trinity College, Dublin 2

Trinity College Dublin
Coláiste na Tríonóide, Baile Átha Cliath
The University of Dublin

Thesis Declaration

I declare that this thesis has not been submitted as an exercise for a degree at this or any other university and it is entirely my own work, except where otherwise acknowledged.

I agree to deposit this thesis in the University's open access institutional repository or allow the library to do so on my behalf, subject to Irish Copyright Legislation and Trinity College Library conditions of use and acknowledgement.

James Nolan

26th September 2022

Date

Summary

Polycomb group (PcG) proteins are highly conserved chromatin regulators that play a critical role as transcriptional repressors in mediating and maintaining cellular identity. PcG proteins assemble into large, distinct, multimeric complexes: Polycomb Repressive Complex 1 and 2 (PRC1 and PRC2). PRC2 comprises core components EZH1/2, EED, SUZ12 and RBBP4/7, with additional substoichiometric components defining mutually exclusive subcomplex assemblies PRC2.1 and PRC2.2. PRC2 core components catalyse post-translational modification of histone H3 by the addition of up to three methyl groups on Lysine at position 27, while substoichiometric components provide varied contributions to PRC2 activity and localisation. EZH2 plays a central role in B-cell lymphopoiesis, though also functions as an oncogene in B-cell lymphoma, whereby recurrent change-of-function hotspot mutations in EZH2 result in increased levels of tri-methylated H3K27. Although enzymatic inhibitors of EZH2 are entering the clinic for the treatment of selected patients with B-cell lymphoma, their utility is limited by inevitable disease progression amongst responders after a short period of time, by as yet undescribed mechanisms. The aim of this PhD thesis was to gain new insight into the mechanism of action of the oncogene EZH2 in lymphoma and to identify novel vulnerabilities in lymphoma amongst other PRC2 components. Firstly, I describe the effects of the change-of-function EZH2 mutation on PRC2 localisation and activity in a lymphoma model and demonstrate that EZH2 asserts its oncogenic role via its methyltransferase activity. Secondly, using a PRC2-directed CRISPR tiling screen, I identify the PRC2.2 component AEBP2 as a specific genetic dependency in germinal centre B-cell lymphoma cell lines and highlight critical domains mediating this dependency. I show that targeting AEBP2 or core PRC2 components can overcome acquired resistance to EZH2 inhibition using a lymphoma cell line model. Finally, through knockdown of AEBP2 in lymphoma cells, I show that AEBP2 inhibits PRC2 methyltransferase activity *in vivo*, with AEBP2 depletion resulting in activation of PRC2 and further elevation of H3K27me3 in EZH2 mutant lymphoma cells and a disrupted balance of PRC2.1 and PRC2.2 components. Taken together, these data contribute an improved understanding of the role of the oncogene EZH2 in B-cell lymphoma biology and of AEBP2 in Polycomb biology and identify an intriguing novel potential target for treating patients with B-cell non-Hodgkin lymphoma.

Publications

Healy E., McCole R., **Nolan J**., Monger C., Brien G.L., Wang C., Neikes H.K., Potjewyd F., Vermeulen M., James L.I., Bracken A.P. (2022) A non-catalytic role of EZH1-PRC2 to promote canonical PRC1 recruitment in quiescent cells. (Manuscript under review at Molecular Cell)

Mucha M., McKenzie N.J., Monger C., Flanigan S.F., Boudes M., Zhang Q., Healy E., Matra F., Hamilton M., Glancy E., **Nolan J**., Davidovich C., Bracken A.P. (2022) PRC2 chromatin binding and histone methyltransferase activities are regulated by alternative AEBP2 isoforms with antagonistic functions. (Manuscript in preparation)

Nolan J., Conway E., Angelov D., Nimmo D., Wang C., Mucha M., Brien G.L., Chen C.W., Bracken A.P. (2022) AEBP2 is a novel genetic dependency in germinal centre B-cell lymphoma. (Manuscript in preparation)

Acknowledgements

First and foremost, I would like to thank Professor Adrian Bracken for being a supportive, enthusiastic and insightful supervisor and giving me the opportunity to work in his lab as a PhD student. I would also like to thank Professor Elisabeth Vandenberghe whose mentorship led me to pursue this PhD and has inspired my ambition to become a clinician scientist. Sincere thanks also to the collaborators who greatly enriched the work in this thesis; Prof. Chun-Wei Chen and his lab at the City of Hope, Los Angeles for generation of the PRC2 tiling library plasmids and processing cell pellets for high-throughput sequencing, Dr. Lindsey James for provision of EED degrader PROTAC compounds and Prof. Richard Flavin, his colleagues and patients at St. James' Hospital for immunohistochemistry on lymphoma material.

I wish to thank the Irish Research Council, Science Foundation of Ireland and Lymphoma Forum of Ireland, whose funding facilitated this research.

Thank you to all past and present members of the Bracken Lab for creating an open, collaborative environment that made it both possible and enjoyable to transition from hospital medicine to scientific research. The culture of mutual mentorship and friendly sharing of ideas is extremely conducive to performing rigorous science. Special thanks to Dr. Eric Conway for giving me a strong start at the bench, to Dr. Daniel Angelov for joining me on the lymphoma project and to Dr. Marlena Mucha for her shared enthusiasm for AEBP2. Thanks to Dr. Cheng Wang, Darragh Nimmo and Dr. Craig Monger for performing bioinformatic analyses for the project.

I am grateful to my parents Deirdre and Michael and my sisters Deanne and Emma, for all of their love and support. Finally to my partner Aidan, for his kindness and encouragement.

Go raibh maith agaibh go léir.

Table of Contents

List of Figures

Chapter 1

Chapter 3

Chapter 4

Chapter 5

List of Tables

Chapter 1

Chapter 2

List of Abbreviations

Ac - Acetylation

AEBP2 – Adipocyte enhancer binding protein 2

AICDA – Activation induced cytidine deaminase

AML – Acute myeloid leukaemia

ARID1A/B – AT-rich interactive domain-containing protein 1A/B

ASX/ASXL – Additional sex combs/like

ATF3 – Activating transcription factor 3

BAP1 – BRCA-associated protein 1

BCL2 – B-cell lymphoma 2 gene

BCL6 – B-cell lymphoma 6 gene

BCL7A – B-cell lymphoma 7A gene

BCR – B cell receptor

BMI-1 – B Lymphoma Mo-MLV insertion region 1 homolog

B-NHL – B-cell non-Hodgkin lymphoma

BRD9 – Bromodomain-containing protein 9

BTK – Bruton's tyrosine kinase

CBX – Chromobox

CCNA2 – Cyclin A2

CDKN1A – Cyclin dependent kinase inhibitor 1A

cDNA – Complementary DNA

CFD – Cutting frequency determination score

CGI – CpG island

ChIP – Chromatin immunoprecipitation

CLL – Chronic lymphocytic leukaemia

CpG – Cytosine-phosphate-Guanine

cPRC1 - Canonical PRC1

CREBBP – Cyclic adenosine monophosphate response element binding protein binding protein

CRISPR – Clustered regularly interspaced palindromic repeats

crRNA – CRISPR RNA

CSR – Class-switch recombination

CTCF – CCCTC-binding factor

DLBCL – Diffuse large B-cell lymphoma (**GCB –** Germinal Centre B-cell) (**ACB** – Activated B-cell)

DNA – Deoxyribonucleic acid

DNMT – DNA methyltransferase

DOT1L – Disruptor of telomere silencing 1-like

EED – Embryonic ectoderm development

EP300 – E1A-associated protein 300

EPOP – Elongin BC and PRC2-associated protein

ESC – Embryonic stem cell

EZH1/2 – Enhancer of Zeste Homolog 1/2

EZHIP – EZH inhibitory protein

FACS – Fluorescence-activated cell sorting

FL – Follicular lymphoma

GC – Germinal centre

gDNA – Genomic DNA

GFP – Green fluorescent protein

HAT – Histone acetyltransferase

H2A – Histone H2A

H2B – Histone H2B

H3 – Histone H3

Hox genes – Homeobox genes

HDAC – Histone deacetylase

IGH/IGHV – Immunoglobulin heavy chain/variable region

IP - Immunoprecipitation

IRF4/MUM1 – Interferon regulatory factor 4

JARID2 – Jumonji and AT-rich interaction domain containing 2

KDM5 – Lysine demethylase 5

Ki-67 – Marker of proliferation Ki-67

KMT2A/B/C/D (MLL) – Lysine methyltransferase 2A/B/C/D (Mixed lineage leukaemia)

MCL – Mantle cell lymphoma

MDS – Myelodysplastic syndrome

me1 – mono-methylated

me2 – di-methylated

me3 – tri-methylated

MHC – Major histocompatibility complex

MOI – Multiplicity of infection

mTORC1 – Mammalian target of rapamycin complex 1

MTF2/PCL2 – Metal response elements binding transcription factor 2

NSD1/2 – Nuclear receptor binding SET domain protein 1/2

OLIG2 – Oligodendrocyte transcription factor 2

ORR – Overall response rate

PALI1/2 – Polycomb associated LCOR isoform 1/2

PAM – Protospacer adjacent motif

PAX5 – Paired box 5

PcG – Polycomb group proteins

PCGF – Polycomb group ring finger

PCR – Polymerase chain reaction

PD-L1 – Programmed death-ligand 1

PHC - Polyhomeotic

PHF1/PCL1 – PHD finger protein 1

PHF19/PCL3 – PHD finger protein 19

PI3K – Phosphatidylinositol 3-kinase

PRC1 – Polycomb repressive complex 1

PRC2 – Polycomb repressive complex 2

PRDM1 – PR domain zinc finger protein 1

PR-DUB – Polycomb repressive deubiquitinase complex

PRMT5 – Protein arginine N-methyltransferase 5

PROTAC – Proteolysis targeting chimera

PTM – Post-translational modification

PUM1 – Pumillo RNA binding family member 1

R-CHOP – Rituximab, cyclophosphamide, doxorubicin, vincristine, prednisolone

RBBP4/7 – Retinoblastoma-binding protein 4/7

RFP – Red fluorescent protein

RING1A/B – Really interesting new gene 1A/B

RNA – Ribonucleic acid

RNAi – RNA interference

RNA-ISH – RNA in-situ hybridisation

R/R – Relapsed/refractory

RT-qPCR – Reverse transcription quantitative PCR

SAE – Serious adverse events

SAM – S-Adenosyl-L-Methionine

SBH – SUZ12 binding helix

SDC1/CD138 – Syndecan 1/Cluster of differentiation 138

SET domain – Su(var)3-9, enhancer-of-zeste and trithorax

SETD2 – SET domain containing 2

sgRNA – Single guide RNA

shRNA – Small hairpin RNA

SHM – Somatic hypermutation

SMARCA4/B1 – SWI-SNF related, matrix associated, actin dependent regulator of chromatin A4/B1

SUZ12 – Suppressor of zeste 12 homolog

SWI-SNF – Switch/sucrose non-fermentable

TAD – Topologically associated domain

T-ALL – T-cell acute lymphoblastic leukaemia

TET – Ten-eleven-translocation

tracrRNA – Trans-activating CRISPR RNA

TrxG – Trithorax group proteins

TSS – Transcriptional start site

UIM – Ubiquitin interacting motif

UTX/KDM6A – Lysine demethylase 6A

UTY/KDM6AL – Lysine demethylase 6A-like

vPRC1 – Variant PRC1

WT – Wild type

XIST – X-inactive specific transcript

YAF2 – YYI associated factor 2

ZF/ZnF – Zinc finger

CHAPTER 1: Introduction

1.1 Determination of cellular identity

Within a multicellular organism, all cells exist somewhere on a spectrum from totipotency to terminal differentiation into any of a vast array of cell types, despite sharing an identical genetic blueprint. A high level of fidelity is required to drive the divergent fates of these totipotent or pluripotent progenitor cells in the process of accurately assembling and maintaining healthy tissues and organs. The integrity of this process is centred around the transcriptional signature of the cell: the combination of genes active and inactive in a cell at a given time. Lineage-committed cells have generally silenced genes responsible for maintenance of pluripotency or "stem-ness" and activated tissue- and stage-appropriate transcriptional programmes. With each "cell fate decision" made by a pluripotent cell, its repertoire of options for terminal differentiation is progressively restricted, as seen in the model system of haematopoiesis (Figure 1B; adapted from (Orkin & Zon, 2008)). This progressive constriction of cell fates was portrayed by Conrad Waddington as a pebble rolling down a hill, following one of a number of possible routes and settling eventually in a valley representing a discrete cellular identity (Figure 1.1A) (Moris et al., 2016; Waddington, 1942). Pluripotency transcription factors such as NANOG are highly expressed in and contribute directly to the maintenance of pluripotent stem cells; however upon initiation of differentiation, these pluripotency factors are lost and subsequent cellular identity is determined by the ebb and flow of lineage-specific transcription factors (Bracken & Helin, 2009). Further downstream, once pluripotent stem cells have committed to, for example, a haematopoietic lineage, the mutually antagonistic transcription factors GATA-1 and PU.1 promote erythroid and myeloid differentiation of haematopoietic stem cells respectively, whereby GATA-1 not only promotes transcription of erythroid-specific genes but also represses the PU.1-dependent myeloid transcriptional programme, and vice versa (Nerlov et al., 2000; P. Zhang et al., 2000).

In order to sustain a healthy stem cell pool or tissue type, with each mitotic cellular division, daughter cells must retain a transcriptional memory of the parental cell from which they were derived. Appropriate genetic programmes are inherited as active or inactive from parental cells to maintain tissue homogeneity (Alabert et al., 2015). This process is governed by numerous mechanisms. One such mechanism involves transcription factors (trans-factors) interacting with discrete DNA sequences such as enhancers (cis-acting elements) leading to the recruitment of co-activators and RNA polymerase II to target genes (T. I. Lee

& Young, 2013). Furthermore, covalent modification of the histone octamer around which DNA is wrapped to form chromatin, or of DNA itself, can direct whether a given gene is available to be activated as euchromatin or is repressed (Jenuwein & Allis, 2001). These modifications (marks), though diluted during mitosis, are transmitted alongside parental histones and DNA to daughter cells, informing the daughter cellular phenotype (Alabert et al., 2015). The dynamic, rigorously controlled regulation of chromosome accessibility for transcription or compaction and resultant silencing is essential for timely, coordinated and appropriately scaled gene expression.

1.2 Covalent methylation of DNA

DNA can be covalently modified by the addition of methyl groups (CH_3) to the fifth position of cytosine to form 5-methyl-cytosine nucleotides. Following replication, symmetrical methylation is restored to hemi-methylated DNA by DNA methyltransferases (DNMTs), which use the parental strand as a template to copy the DNA methylation onto the newly synthesised daughter strand (E. Li & Zhang, 2014).

DNA methylation occurs primarily at cytosines followed directly by a guanine nucleotide in the 5' to 3' direction: so called CpG dinucleotides. Up to 80% of CpG dinucleotides are methylated in somatic cells; however, mammalian genomes are CpG dinucleotide poor (~1% of human genome). CpG dinucleotides are further depleted by C-to-T transitions occurring due to the mutagenic nature of 5-mC (Bird & Taggart, 1980; D. N. Cooper & Krawczak, 1989; Holliday & Grigg, 1993). DNA methylation is generally understood to promote transcriptional repression, supported by its association with heterochromatin formation, X-chromosome inactivation and the repression of transposons and germline-specific genes (Greenberg & Bourc'his, 2019). Deviating from this rule, however, are CpG islands (CGIs), which are ~1-2kb regions of the genome enriched for CpG dinucleotides but which are rarely methylated (Z. D. Smith & Meissner, 2013). Aberrant methylation of CGI promoters of tumour suppressor genes, first described in the context of retinoblastoma (Greger et al., 1989), has since been recognised as a common phenomenon in cancer (Baylin & Jones, 2016).

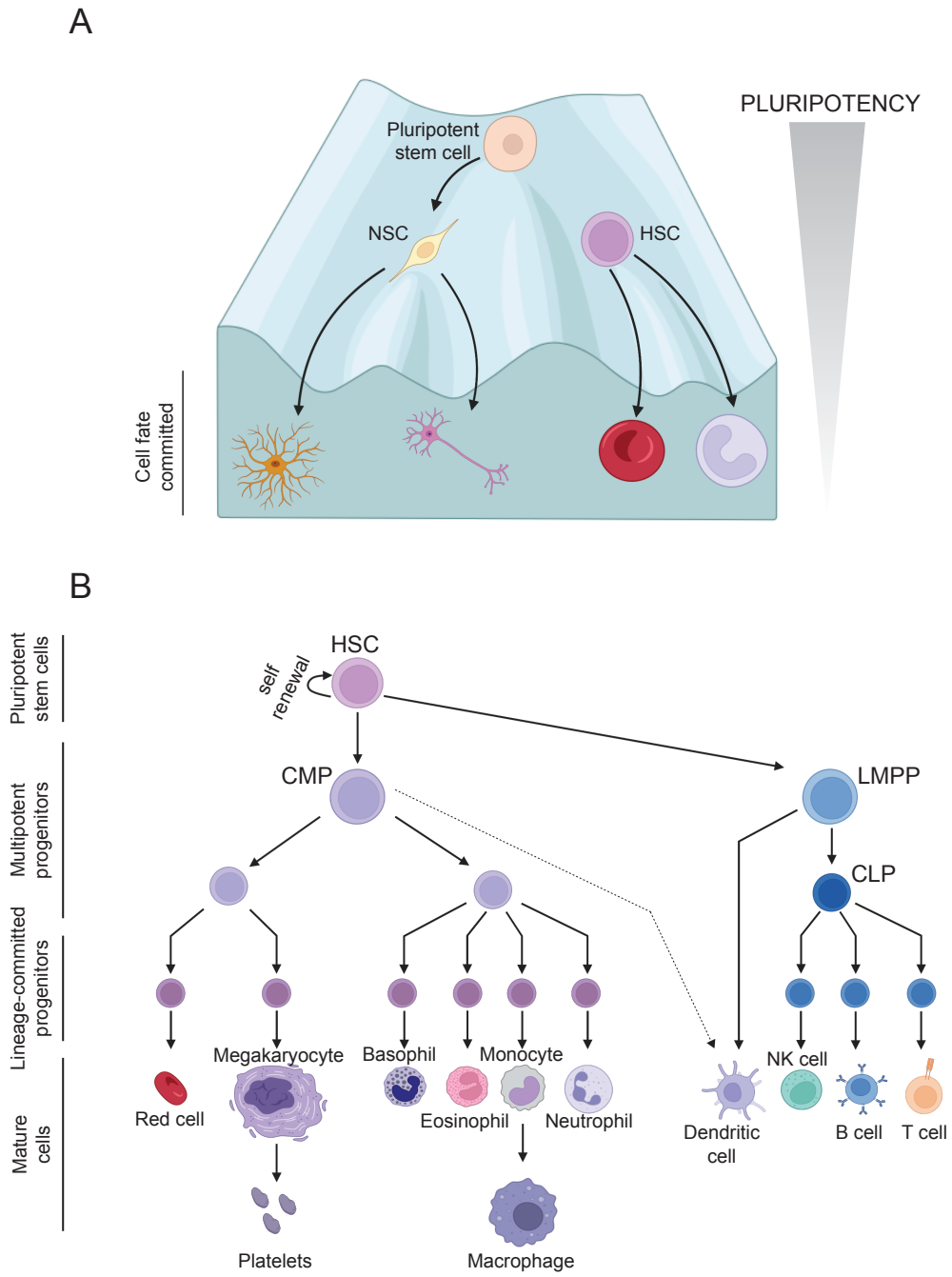

Figure 1.1 Cellular identity

(A) Schematic representation of Waddington's landscape. In this illustration, the pluripotent stem cell can be directed towards numerous multipotent stem cell fates, which in turn can be directed ultimately towards numerous committed cell fates and terminal differentiation.

(B) A model of haematopoiesis, demonstrating that within the blood lineage, there are numerous precursor multipotent cell states.

NSC neural stem cell. HSC haematopoietic stem cell. CMP common myeloid precursor. CLP common lymphoid precursor. LMPP lymphoid primed multipotent progenitor.

Created with BioRender.com

DNMTs are responsible for regulation of DNA methylation, using S-Adenosyl-L-Methionine (SAM) as a methyl donor. DNMT3A and DNMT3B are responsible for *de novo* DNA methylation; while the catalytically inactive DNMT3L positively regulates these enzymes (Bourc'his et al., 2001). DNMT1 is tasked with maintenance and restoration of DNA methylation following cell division and is recruited to the replication fork to copy methylation from the parental to the daughter strand (Nishiyama et al., 2020; Qin et al., 2015). Active DNA demethylation is carried out by the ten-eleven translocation (TET) family of methylcytosine dioxygenases (TET1-3) (Kohli & Zhang, 2013). Strikingly, loss of function mutations in TET2 and DNMT3A are common in an array of haematological malignancies, reflecting the centrality of careful regulation of DNA methylation (Huang & Rao, 2014; Roller et al., 2013; Shlush et al., 2014; Yang et al., 2015).

1.3 Chromatin structure

The human genome comprises ~3 billion base pairs of DNA measuring approximately 2 metres in length and this molecule must be crammed into a nucleus measuring less than 10μm in diameter (Figure 1.2). To do this, DNA is compacted into DNA-protein subunits called nucleosomes, comprising 147 base pairs of DNA wrapped 1.6 times around a histone octamer scaffold (two copies each of histone proteins H2A, H2B, H3 and H4) and a flanking linker DNA of ~10-70 base pairs flanked by histone H1 (Luger et al., 1997). This was first conceptualised when chromatin was observed by electron microscopy to resemble "beads on a string" (Olins & Olins, 1974).

In order for transcriptional machinery to retain access to appropriate target genes, chromatin exists in a dynamic environment whereby chromatin is variably compacted and thereby unavailable/inactive for transcription (heterochromatin) or loosely packed and available for active transcription (euchromatin) (Kieffer-Kwon et al., 2017). These chromatin compaction dynamics are regulated by ATP-dependent chromatin remodelling complexes that alter nucleosome topology to permit DNA assembly, access or editing (Clapier et al., 2017). Four subfamilies of chromatin remodellers are recognised: imitation switch (ISWI), chromatin helicase DNA-binding (CHD), switch/sucrose non-fermentable (SWI-SNF) and INO80.

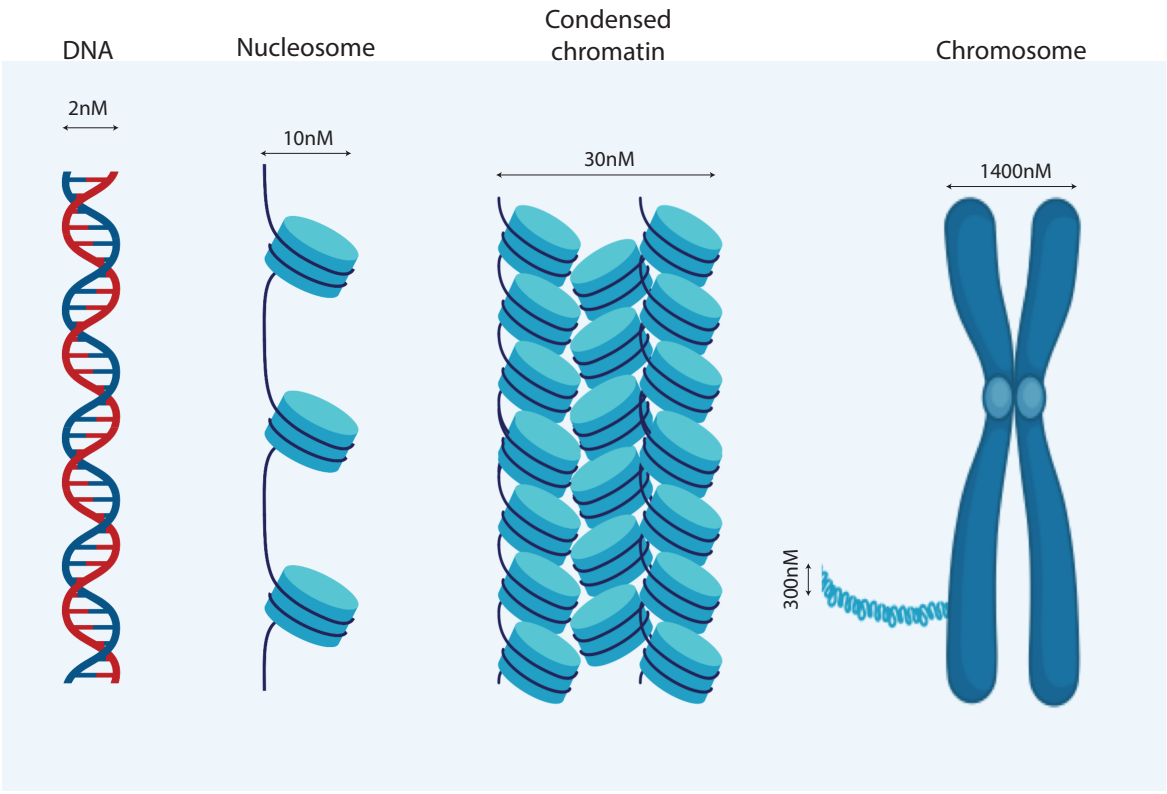

Figure 1.2 Schematic of chromatin compaction

Negatively charged DNA is wrapped around a positively charged histone octamer core to form the nucleosome core particle. Nucleosomes fold together to produce 30nm fibres that themselves condense and form loops averaging 300nm in length. These loops are further compressed and coil tightly to form the chromatid of a nucleosome.

Created using BioRender.com

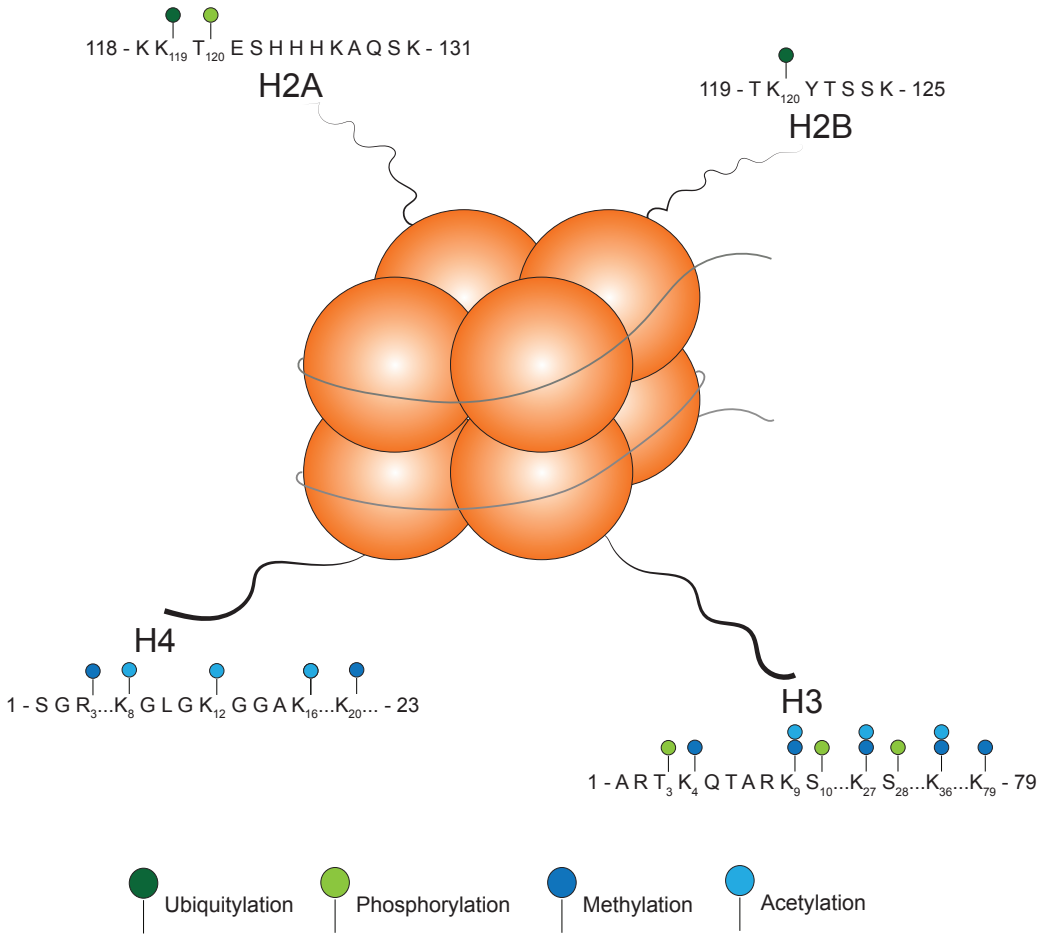

Figure 1.3. Covalent post-translational modification of histone tails

Long, flexible, hydrophilic N-terminal tails protrude from the core nucleosome particle histone octamer and are subject to chemical modification by "writer" enzymes of histone post-translational modifications. These modifications affect transcription both directly and indirectly via actions of recruited effector proteins.

Two copies each of histones H3 and H4 assemble into a tetramer and associate with 2 copies of histone H2A and H3B to form the core histone octamer (Figure 1.3). The linker histone H1 draws flanking linker DNA between nucleosomes together, resulting in a less flexible structure and influencing higher order chromatin structure (Bednar et al., 2017). Recent work has identified an important role for histone H1 in regulating chromatin condensation, with histone H1 deficiency resulting in decompaction of topologically associated domains (TADs) (Willcockson et al., 2021; Yusufova et al., 2021).

In order for transcription to occur, RNA polymerase (Pol) II must passage through chromatin, which innately provides a barrier to Pol II machinery due to extensive contacts between histones and the DNA wrapped around them (Luger et al., 1997). In studies *in vitro*, this required that Pol II displace at least one H2A-H2B dimer to transcribe through a nucleosome (Bevington & Boyes, 2013; Bintu et al., 2011; H. A. Cole et al., 2014), however this conflicted with the finding that most transcribed genes have intact nucleosomes, with only highly transcribed genes showing nucleosomal loss (C. K. Lee et al., 2004; Ramachandran et al., 2017). However, cryo-electron structural models have offered a mechanistic basis for nucleosome retention whereby Pol II helps to retain nucleosomes during transcription by allowing DNA rewrapping back onto the histone octamer surface, thereby avoiding H2A-H2B drop-out (Filipovski et al., 2022; Farnung et al, 2022).

Histone proteins also possess hydrophobic C termini that are buried in the interaction surface of the nucleosome, whilst their hydrophilic N terminal tails protrude from the octamer and are available for post-translational modification (PTM) (Luger et al., 1997).

1.4 Histone post-translational modification

Post-translational modifications (PTMs) can modulate chromatin compaction or rarefaction by addition or removal of chemical modification and thereby can alter gene expression. These marks most commonly include but are not limited to methylation, acetylation, ubiquitylation and phosphorylation (Figure 1.3) (Kouzarides, 2007). Acetylated histone residues most commonly demarcate open or active chromatin, due to mutual repulsion between the negatively charged acetyl group and negatively charged DNA and also the diminished nett positive charge of the modified histone tail. Accordingly, acetylated residues are enriched at the promoters of transcriptionally active genes. Histone

acetyltransferase enzymes (HATs) are responsible for acetylation of target lysine residues, whilst removal of these acetyl marks is catalysed by a family of "eraser" enzymes designated as histone deacetylases (HDAC) (X. J. Yang & Seto, 2007).

The effect of methylation marks on gene transcription is more varied as methylation marks do not alter the charge of the target residue; depending instead on the target residue methylated, the degree of methylation (i.e. mono-, di- or tri-methylation), the topographical location of the mark and which effector proteins are recruited. This reflects the complex, indirect effects of these marks whereby their regulatory effects are imparted by their influence on regulatory "effector" proteins, as will be discussed in section 1.5. For example, H3K4me3 and H3K27me3 are correlated with activation and repression of transcription, respectively. H3K4me3 is typically enriched in proximity to transcriptional start sites (TSS), while H3K4me2 is found slightly downstream from the trimethyl mark and H3K4me1 is found closer to the gene body (Kimura, 2013). In undifferentiated stem cells, regardless of gene expression status, many genes marked with H3K4me3 are also marked by the repressive mark H3K27me3, resulting in bivalent nucleosomes harbouring both marks. These bivalent genes maintain low level expression in ES cells until differentiation and are poised to be silenced upon removal of the H3K4me3 mark (Bernstein et al., 2006; Vastenhouw & Schier, 2012).

Furthermore, epigenetic marks help to inform higher order chromatin structure. Chromosomes can be segregated into sub-megabase scale domains which overlap extensively with distinct patterns of epigenetic marks (Bonev & Cavalli, 2016; Dixon et al., 2012; Nora et al., 2012; Sexton et al., 2012). These topologically associated domains (TADs), bound by numerous factors including insulator binding protein CTCF, appear as square domains along the diagonal of Hi-C maps and most local interactions (enhancer-promoter, promoter-promoter etc) are confined within these boundaries (Shen et al., 2012). TADs are proposed as putative functional units regulating gene expression in development and differentiation due to their preferential marking of these domains by either active (H3K36me3) or inactive (H3K27me3) epigenetic marks (Le Dily et al., 2014; Nora et al., 2012; Sexton et al., 2012). The integrity of these active and inactive TADs has been shown to be disrupted in cancer (Donaldson-Collier et al., 2019; Flavahan et al., 2016; Hnisz et al., 2016; Taberlay et al., 2016).

1.5 Chromatin modifying proteins

Writers, readers and erasers are classes of proteins grouped together based on their ability to regulate histone post-translational modification. Writer proteins "write" or deposit PTMs on histones, which in turn are "read" or recognised by effector reader proteins. Among the first writer proteins to be discovered was the histone methyltransferase SUV39H1, which selectively methylates lysine K9 of histone H3 (H3K9) (Rea et al., 2000). The H3K9me3 mark in turn is recognised by the chromodomain of reader protein HP1γ (Bannister et al., 2001; Lachner et al., 2001) resulting in the compaction and condensation of chromatin (Cheutin et al., 2003). Subsequently, H3K9 can be demethylated by a variety of specific demethylases including JHDM2A (Yamane et al., 2006) and JMJD2B (Fodor et al., 2006). The dynamic nature of histone PTMs is reflected also in the presence of eraser enzymes such as demethylases, deubiquitinases and deacetylases that can remove specific PTMs from histones. This system of checks and balances between writers, whose marks are read by readers and erased by erasers provides a dynamic landscape whereby PTM-directed barriers to transcription may be lifted or drivers for transcription silenced.

Reader proteins contain conserved reader domains such as Tudor domains, bromo domains, chromo domains and PHD domains which confer specificity for particular histone residue modifications (Fischle et al., 2003; Musselman et al., 2012). Figure 1.4 demonstrates two schematics of histone methylation, recognition of that mark by a reader protein and subsequent demethylation. In the first example, SETD2 trimethylates H3K36, writing a mark usually associated with transcriptional activation. The Tudor domain of PHF19 associated with PRC2 subsequently recognises and transiently interacts with this mark. PRC2-PHF19 recruits the demethylase No66, which demethylates H3K36me3, leading to transcriptional silencing (Brien et al., 2012; Kooistra & Helin, 2012b). In the second example, Polycomb Repressive Complex 2 (PRC2) catalyses the trimethylation of H3K27 to generate H3K27me3. This is subsequently read in this example by the WD40 domain of EED, which results in allosteric activation of the PRC2 methyltransferase. UTX or JMJD3 subsequently demethylate H3K27me3, thereby facilitating gene activation (Agger et al., 2007).

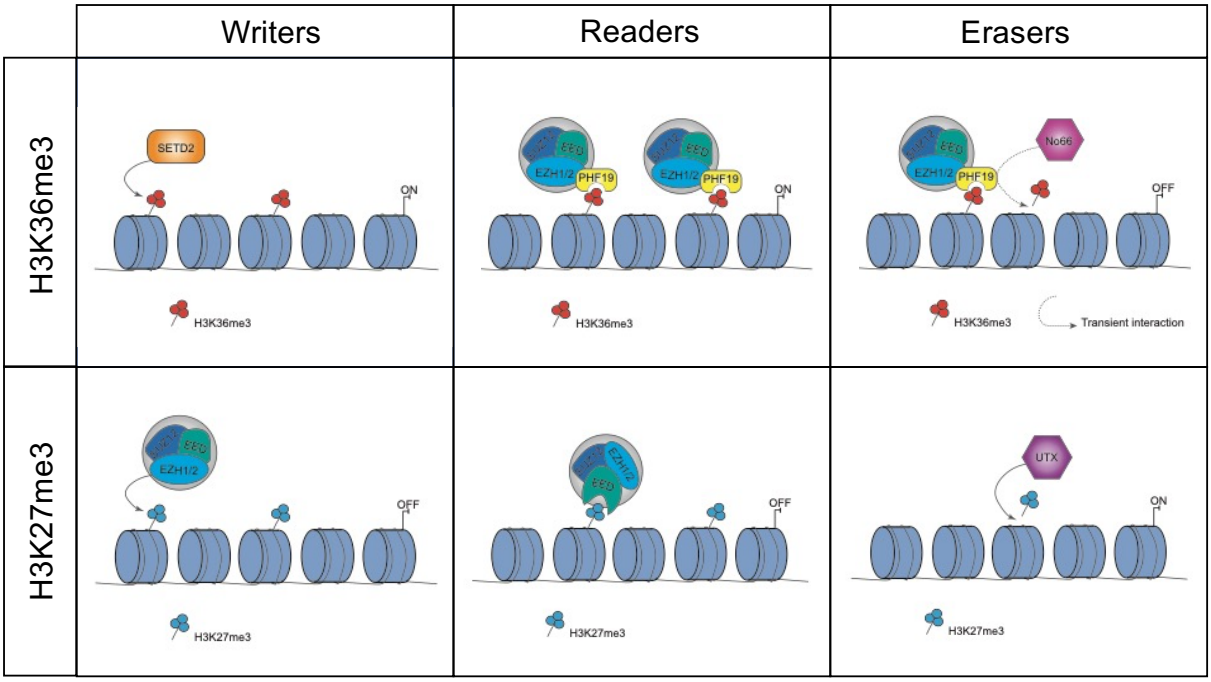

Figure 1.4 Writers, readers and erasers of histone post-translational modifications

Schematic representing two histone marks: H3K36me3 and H3K27me3 and their associated writer, reader and eraser enzymes (note: several reader and eraser proteins have been described for these marks).

1.6 Polycomb group proteins

Polycomb was first proposed as an essential genetic regulator of anterior-posterior segmentation in *Drosophila melanogaster* due to its role in silencing homeotic gene (Hox) expression (Lewis, 1978). Mutagenesis of this protein resulted in posterior homeotic transformation in Drosophila with inappropriate anteriorisation of body segments and additional phenotypic abnormalities. Additional Polycomb group proteins (PcG) were subsequently discovered in Drosophila and mammalian species, perturbation of which resulted in derepression of Hox genes (Adler et al., 1991; T. Akasaka et al., 2001; Takeshi Akasaka et al., 1996; Dura et al., 1987; Kyo-ichi Isono et al., 2005). Genetic knockout of several PcG proteins in mouse studies results has shown an embryonically lethal phenotype due to inappropriate transcriptional programme activation during cellular differentiation (Laugesen & Helin, 2014). In undifferentiated stem cells, PcG proteins are bound to bivalent promoters of lineage-specific genes ensuring their transcriptional silencing. Upon differentiation, they are redistributed to stem cell-specific promoters to allow for expression of lineage-specific genes (Bracken et al., 2006, 2007; Bracken & Helin, 2009).

Also discovered in *Drosophila,* Trithorax group (TrxG) antagonise PcG function; thereby maintaining active gene expression states (Piunti & Shilatifard, 2016; Schuettengruber et al., 2017). Mutations in TrxG genes result in anterior homeotic transformation phenotypes (Ingham, 1983, 1985; Kennison & Tamkun, 1988; Struhl & Akam, 1985). Cooperation between PcG and TrxG proteins is essential to safeguard cellular identity during development and differentiation (Piunti & Shilatifard, 2021; Schuettengruber et al., 2017).

1.7 Polycomb repressive complexes

PcG proteins are highly conserved and form multi-subunit protein complexes denoted Polycomb repressive complexes (PRCs) (Blackledge et al., 2015; Di Croce & Helin, 2013; Levine et al., 2002). Several families of PcG proteins have been described, including Polycomb Repressive Complexes 1 and 2 (PRC1 and PRC2) and the Polycomb Repressive Deubiquitinase complex (PR-DUB), as discussed below. PRC1 is responsible for mono-ubiquitination of lysine K119 of histone H2A (H2AK119ub1) via its Ring-Pcgf E3 ligase heterodimer, while PRC2 is responsible for all mono-, di- and tri-methylation of lysine K27 of histone H3 (Cao et al., 2005; Müller et al., 2002). Numerous possible subcomplex assemblies of both PRC1 and PRC2 exist (Figure 1.5) and both complexes are enriched at

promoters of developmentally repressed genes (Blackledge et al., 2015; Deevy & Bracken, 2019; Healy et al., 2019; Pasini et al., 2007; Schuettengruber et al., 2017).

1.7.1 PRC2

Mammalian PRC2 is composed of four core subunits: EED, SUZ12, RBBP4/7 and either the EZH1 or EZH2 histone methyltransferase (HMT) (Glancy et al., 2021; Kasinath et al., 2020; Laugesen et al., 2019; Poepsel et al., 2018; Yu et al., 2019). EZH1 and EZH2 are paralogous SET domain containing histone methyltransferases (Margueron et al., 2008). Despite sharing significant sequence homology, EZH1-PRC2 is a less efficient methyltransferase enzyme and is proposed to contribute to transcriptional silencing via chromatin compaction (Lavarone et al., 2019; Margueron et al., 2008). EED engages H3K27me3, JARID2-K116me3 (stimulated by PRC2 associated with JARID2) or PALI1-K1241me2/3 via its aromatic cage, resulting in allosteric activation of PRC2 (C. H. Lee, Holder, et al., 2018; Margueron et al., 2009; Sanulli et al., 2015; Q. Zhang et al., 2021). Point mutations in EED or the EZH2 stimulation response motif (SRM) disrupting PRC2 allosteric activation result in significantly reduced H3K27me3 (C. H. Lee, Holder, et al., 2018). SUZ12 indispensably stabilises PRC2 core, whilst also bridging the core complex with substoichiometric accessory components, which are increasingly understood to modulate the enzymatic activity of the core and assist its targeting on chromatin (S. Chen et al., 2018; Ciferri et al., 2012; Glancy et al., 2021; Healy et al., 2019; Højfeldt et al., 2019; Kasinath et al., 2020; Poepsel et al., 2018). Intriguingly, live-cell imaging has shown that only ~20% of PRC2 is stably bound to chromatin, while the remaining 80% is highly mobile and diffused within the nucleus; suggesting that transient, frequent interactions are likely to occur; potentially accounting for dispersed H3K27me2 and H3K27me3 (Youmans et al., 2018). This core complex is responsible for all mono-, di- and tri-methylation of lysine K27 of histone H3 (H3K27me1/me2/me3) (Højfeldt et al., 2018; Smits et al., 2013). Mono-methylated H3K27 (H3K27me1) is preferentially deposited at highly transcribed gene bodies and correlates with H3K36me3 expression, while tri-methylated H3K27 (H3K27me3) is preferentially deposited at the CpG-dense promoters of transcriptionally silent target genes (Bracken et al., 2006; Ferrari et al., 2014; Morey & Helin, 2010; Tanay et al., 2007). H3K27me2, however, is a more abundant mark, covering 70% of H3 in embryonic stem cells, and largely fills space between H3K27me1 and H3K27me3 marks in

intergenic and non-transcribed intragenic genomic space (Ferrari et al., 2014; Lavarone et al., 2019).

PRC2 assembles into two mutually exclusive subcomplex assemblies: PRC2.1 and PRC2.2, which are defined by their substoichiometric accessory components (Alekseyenko et al., 2014; Conway et al., 2018; Grijzenhout et al., 2016; Hauri et al., 2016; Oliviero et al., 2016) (Figure 1.5B). PRC2.1 member EPOP competes with PRC2.2 component JARID2 at the neck region towards the N-terminus of SUZ12. Similarly, polycomb-like proteins 1-3 (PCL1-3: also referred to as PHF1, MTF2 and PHF19 respectively), compete with AEBP2 to bind the central C2 domain of SUZ12 (S. Chen et al., 2018, 2020). Given the mutual exclusivity of PALI1/2 and EPOP in PRC1, it is likely though as yet unproven that they similarly compete for binding with SUZ12. Although it is increasingly understood that PRC2.1 and PRC2.2 have divergent roles, it has been shown that in mouse ESCs they co-occupy the vast majority of target sites and co-operate to modulate gene transcription at those sites (Healy et al., 2019; Laugesen et al., 2019).

PCL proteins are multidomain PRC2.1 proteins involved in enhancing methyltransferase activity of PRC2 and directing its recruitment to chromatin (Casanova et al., 2011; Choi et al., 2017; Sarma et al., 2008; Q. Zhang et al., 2019). Numerous domains within these proteins have been characterised including a Tudor domain, two PHD domains (PHD1/2), an extended helix (EH) domain and a C-terminal reverse chromatin domain. Biochemical assays have demonstrated that the Tudor domain of PCLs recognises and binds to the H3K36me3 mark, potentially recruiting H3K36me3 demethylases (Ballaré et al., 2012; Brien et al., 2012; Cai et al., 2013; Musselman et al., 2012). Additionally the PHD1, PHD2 and EH are all putative DNA-binding domains(Choi et al., 2017; Perino et al., 2018).

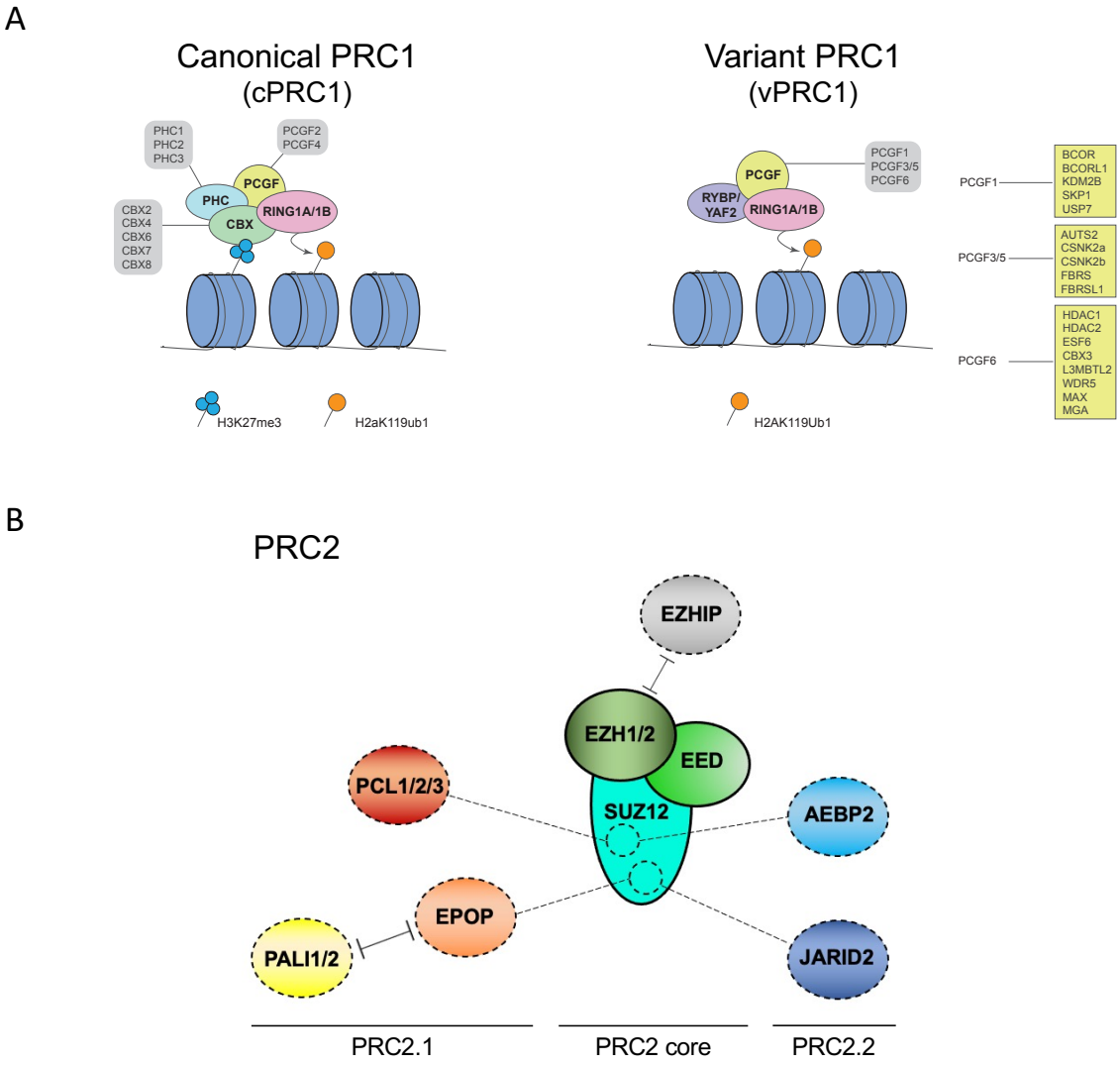

Figure 1.5 The variable compositions of Polycomb repressive complexes

A) Schematic representation of PRC1 subtypes canonical and non-canonical/variant PRC1 with common interactors.

B) Schematic representation of PRC2 illustrating mutual exclusion of numerous substoichiometric accessory components.

EPOP (C17ORF96) binds to Elongin B/C proteins and has also been identified as a PRC2.1 subcomponent. The presence of EPOP in PRC2.1 precludes association with PALI1/2 (Alekseyenko et al., 2014; Beringer et al., 2016; Conway et al., 2018; Hauri et al., 2016; Liefke et al., 2016). Although EPOP enhances PRC2 histone methyltransferase activity *in vitro*, it inhibits the complex *in vivo* (Beringer et al., 2016; Liefke et al., 2016; Z. Zhang et al., 2011). PALI1 was identified more recently and has been shown to interact with numerous chromatin regulators including G9A, USP11 and USP22 and enhance the *in vitro* methyltransferase activity of the complex (Conway et al., 2018). More recently, PALI1 was also shown to allosterically activate PRC2 and facilitate PRC2 binding to DNA via its PIP (PALI interaction with PRC2) domain (Q. Zhang et al., 2021). The role of PALI2 is less well described, although it also contains a PIP domain and when disrupted in addition to PALI1, results in a greater loss of H3K27me3 than is observed by loss of PALI1 alone (Conway et al., 2018).

PRC2.2 comprises core PRC2 in complex with JARID2 and/or AEBP2 (Grijzenhout et al., 2016; Hauri et al., 2016). JARID2 enhances the methyltransferase activity of PRC2 *in vitro* and *in vivo*, including by allosteric activation of PRC2 as previously described due to methylation by PRC2 of JARID2-K116. This protein has also been shown to interact with DNA via its Jumonji-N-term (JmjN) and AT-rich interaction domain (ARID) domains (T. Kim et al., 2004) and with H2AK119ub1 via its N-terminus ubiquitin-interacting motif (UIM) (S. Cooper et al., 2016; Kasinath et al., 2020). Supporting this link between H2AK119ub1 and PRC2.2, mouse ESCs with depleted H2AK119ub1 lose PRC2.2 binding to a greater degree than PRC2.1 binding (Blackledge et al., 2020; Fursova et al., 2019; Healy et al., 2019; Scelfo et al., 2019; Tamburri et al., 2020)

AEBP2 is a C2H2 zinc finger protein with several isoforms arising due to transcription from several discrete promoters (H. Kim et al., 2015). AEBP2 enhances histone methyltransferase activity *in vitro* via its KR motif (C. H. Lee, Holder, et al., 2018) and has been reported to bind GC-rich DNA via three highly conserved C2H2 zinc finger motifs (Xueyin Wang et al., 2017). However, *in vivo* AEBP2 disruption results in a small increase in H3K27me3 levels, likely reflecting either increased activity of PRC2.1 or possibly an inhibitory effect of AEBP2 on PRC2 methyltransferase activity. Furthermore, mice with biallelic knockout of AEBP2 exhibit anterior transformation of the skeleton (a Trithorax phenotype) as opposed to a classical “Polycomb phenotype” posterior homeotic transformation

(Grijzenhout et al., 2016). Recent structural data using Cryo-EM also supports the interaction between AEBP2 zinc fingers and nucleosomal DNA, while demonstrating also a novel interaction between the zinc fingers and H2AK119ub1 and an acidic patch on the surface of H2A-H2B (Kasinath et al., 2020).

A novel PRC2-interacting protein called EZHIP (alternative designations CXORF67 and CATACOMB) has recently been described that is capable of interacting with either PRC2.1 or PRC2.2 (Hübner et al., 2019; Jain et al., 2019; Pajtler et al., 2018; Piunti et al., 2019; Ragazzini et al., 2019). Expression of this protein is usually limited to spermatogonia, though has been identified as being of biological importance in posterior fossa (group A) (PFA) ependymomas. EZHIP mimics the oncohistone H3.3K27M and binds the active site of EZH2, resulting in loss of broad H3K27me3 domains but retention of H3K27me3 at CpG islands.

1.7.2 PRC1

Mammalian PRC1 is an E3 ubiquitin ligase complex responsible for catalysing the H2AK119ub1 mark and exists in a variety of sub-assemblies (Figure 1.5A), with varying catalytic activity depending on its composition (Taherbhoy et al., 2015). The PRC1 catalytic core comprises a heterodimer of the paralogous (Really Interesting New Gene) RING1A and RING1B ubiquitin ligases and one of six PCGF (Polycomb group RING fingers 1-6) proteins (Z. Gao et al., 2012). Depending on its subunit conformation, PRC1 can be categorised as canonical (cPRC1) or non-canonical (variant) (Blackledge & Klose, 2021). Broadly, variant PRC1 (vPRC1) contains one of PCGF1/3/5/6, RING1A/B, either RYBP or YAF2 along with additional subtype-specific interactors (Farcas et al., 2012; Z. Gao et al., 2012). Canonical PRC1 consists of RING1A/B, either PCGF2/4, SCM and PHC along with any of CBX2/4/6/7/8 and is recruited to chromatin by binding of PRC2-mediated H3K27me3 by the highly conserved N-terminal chromodomain of its CBX subunit (Fischle et al., 2003; Min et al., 2003; H. Wang et al., 2004).

PRC1 and PRC2 largely co-localise on chromatin (Boyer et al., 2006; Bracken et al., 2006; Fursova et al., 2019; Schwartz et al., 2006; Tolhuis et al., 2006). vPRC1 additionally functions upstream of PRC2 via varied and incompletely defined recruitment mechanisms, including targeting by long non-coding RNAs such as XIST (C. Y. Wang et al., 2019) and

association with non-PRC2 proteins at CpG islands such as KDM2B (Blackledge & Klose, 2021). Monoubiquitylation of H2AK119 is primarily the responsibility of vPRC1 complexes via its RING/PCGF heterodimer (H. Wang et al., 2004). H2AK119ub1 is enriched at the promoters of developmentally repressed genes, but also found at low levels genome-wide (Conway et al., 2021; Fursova et al., 2019; H. Wang et al., 2004). PRC1-mediated H2AK119ub1 recruits PRC2.2 as both JARID2 via its UIM and AEBP2 via its zinc fingers have the ability to recognise this mark (Blackledge et al., 2020; Fursova et al., 2019; Glancy et al., 2021; Healy et al., 2019; Kasinath et al., 2020; Sugishita et al., 2021; Tamburri et al., 2020). Unlike vPRC1, cPRC1 contributes little to H2AK119ub1 deposition; instead mediating chromatin compaction via oligomerisation of its PHC subunits (Fursova et al., 2019; Kyoichi Isono et al., 2013).

1.7.3 PR-DUB

H2AK119ub1 is removed from histones by the Polycomb Repressive Deubiquitinase Complex (PR-DUB) (Chittock et al., 2017; Scheuermann et al., 2010). *Drosophila menalogaster* PR-DUB was first characterised and comprises a deubiquitinase protein Calypso and its binding partner Additional Sex Combs (ASX). The positively charged C-terminal tail of Calypso (and likely BAP1), has been shown to be necessary for recruitment of PR-DUB to nucleosomes (Foglizzo et al., 2018). Orthologous to *Drosophila* PR-DUB, the mammalian PR-DUB complex contains a deubiquitinase protein BRCA-associated Protein 1 (BAP1) and one of three ASX-like proteins (ASXL1-3) (Daou et al., 2015; Sahtoe et al., 2016). Depletion of BAP1 results in intergenic spreading of H2AK119ub1 due to displacement of PRC1 from polycomb target genes. In turn, this boosts intergenic H3K27me3 while depleting it at polycomb-target promoters (Conway et al., 2021). Resultant transcriptional changes can be rescued by depletion of RING1A/1B (Campagne et al., 2019).

1.8 B-cell maturation and the lymphoid germinal centre

Haematopoietic stem cell (HSC) multipotency is supported by bivalent chromatin signatures, where lineage-affiliated promoters are marked by both activating and repressive marks (Bernstein et al., 2006; Maës et al., 2008; Velichutina et al., 2010; Weishaupt et al., 2010). Monospecific B-cell ontogenesis is triggered by essential transcription factors such as E2A proteins, early b-cell factor (EBF), PAX5 and Ikaros (Dias et al., 2008;

Georgopoulos et al., 1994; Ikawa et al., 2004; O'Riordan & Grosschedl, 1999; Sigvardsson et al., 2002; Velichutina et al., 2010; J. H. Wang et al., 1996).

Progenitor B cells in the bone marrow undergo V(D)J recombination processes to assemble immunoglobulin heavy (IGH) and light chain V regions encoding variable parts of antibody molecules (Rajewsky, 1996). This process involves numerous double-stranded DNA breaks at recombination signal sequences (RSS); first joining an IGHD gene to an IGHJ gene, and then recombining an IGHV gene to the recombined D_HJ_H joint. Exonucleolytic removal of several nucleotides then occurs and non-germline bases are then added to the N-terminus of the heavy chain; which if capable of being expressed, precedes light-chain gene rearrangements to generate the B-cell receptor (BCR). During V(D)J recombination, the ends of rearranging genes in any of the immunoglobulin loci can erroneously join a DNA break in another chromosome resulting in a reciprocal translocation: for example, the t(14;18)(q32;p21), bringing the BCL2 anti-apoptotic gene under the control of IGH locus enhancers (Küppers & Dalla-Favera, 2001; Tsujimoto et al., 1985; Yunis et al., 1987).

Upon antigen stimulation, immature lymphoid cells form germinal centres (GC) (Figure 1.6) (adapted from (Mlynarczyk et al., 2019)). Germinal centres are dynamic microenvironmental compartments within lymphoid organs, where B-cells somatically hypermutate (SHM) the variable regions of their immunoglobulin genes and are selected based on their affinity for antigen to massively proliferate and ultimately differentiate into terminally differentiated antibody-secreting plasma cells and B-cells (Berek et al., 1991; Jacob et al., 1991). Germinal centre B cells constantly shuttle between the dark zone and light zone, experiencing repeated iterations of Activation-induced Cytidine Deaminase (AICDA)-catalysed SHM and compete for selection and survival signals. DNA repair of AICDA-induced lesions is by the error-prone DNA polymerase eta (Polη), introducing new DNA point mutations (Mcheyzer-Williams et al., 2015).

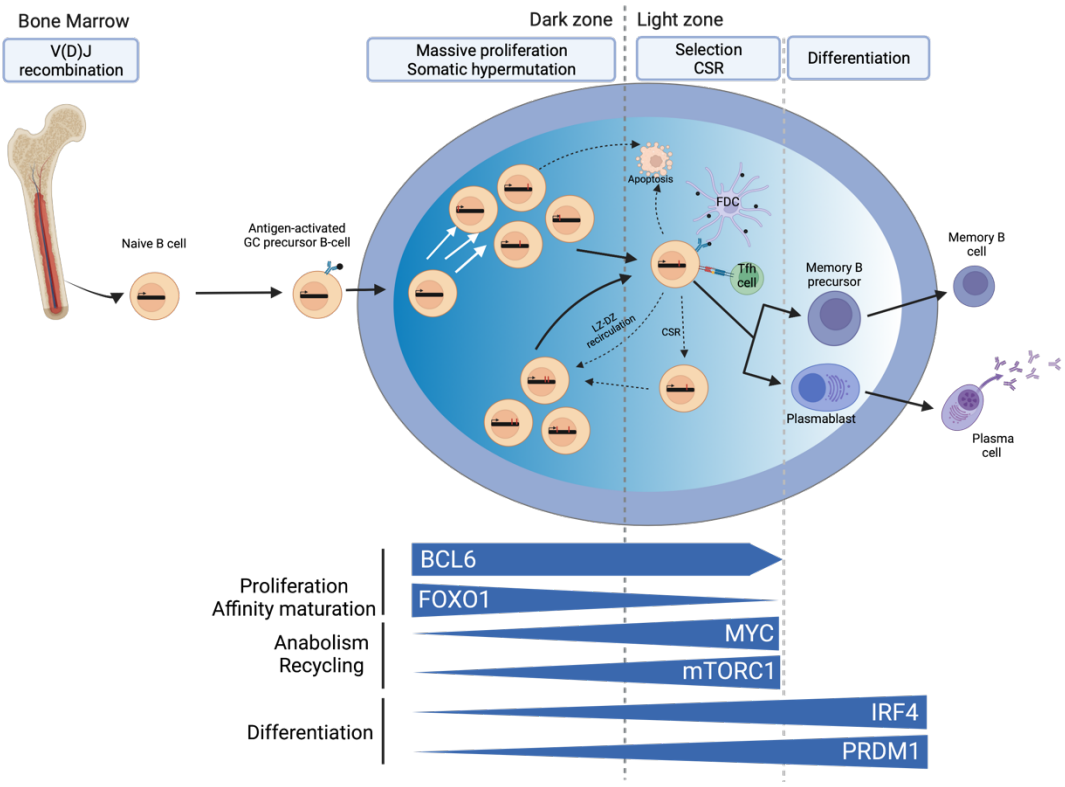

Figure 1.6 The dynamic microenvironment of the lymphoid germinal centre

Antigen-activated B-cells enter the dark zone of the lymphoid germinal centre with T-cell help. Here, they experience AID-induced somatic hypermutation of their immunoglobulin variable regions in order to gain greater affinity for their antigen, whilst also massively expanding. They then shuttle to the immune synapse in the light zone, where upregulation of MYC and mTORC1 and interaction with follicular dendritic cells and T_{fh} cells selects cells based on antibody affinity for recirculation into the dark zone, germinal centre exit and terminal differentiation or apoptosis.

CSR class switch recombination. GC germinal centre. LZ light zone. DZ dark zone.

Adapted from (Mlynarczyk et al., 2019)

Created with Biorender.com

GC B cells feature upregulation of EZH2, without which germinal centres cannot form (Béguelin et al., 2013; Caganova et al., 2013; Raaphorst et al., 2000; Velichutina et al., 2010). EZH2-mediated H3K27me3 marks over 1,000 newly bivalent promoters in GC B-cells, which were marked with only H3K4me3 in naïve resting B cells (Béguelin et al., 2013), many of which are EZH2 target genes specific to GC B-cells, including many genes essential for GC exit and plasma cell differentiation. The mechanism whereby EZH2 mediates transcriptional repression in GC B cells has not been precisely delineated, especially as cPRC1-associated PCGF2/4 (Mel-18/BMI-1) are not expressed in GC centroblast B cells (Raaphorst et al., 2000). However, one group has proposed a vPRC1 complex including CBX8 and BCOR as a candidate PRC1 complex in GC B-cells (Béguelin et al., 2016).

The transcriptional repressor B-Cell Lymphoma 6 (BCL-6) controls a critical transcriptional network driving GC formation and maintenance (Basso & Dalla-Favera, 2010, 2015). BCL6 negatively regulates its own transcription and this is frequently dysregulated in diffuse large B-cell lymphomas (DLBCLs), with both translocations and point mutations disrupting its negative autoregulatory circuit (Cattoretti et al., 2005; Ci et al., 2008; Pasqualucci et al., 2003). Although BCL-6 is a master regulator for the GC, it is dependent on EZH2 in order to form germinal centres (Béguelin et al., 2016).

After SHM and proliferative expansion in the lymphoid dark zone, B cells migrate to the light zone where those with high affinity for antigen are selected for survival and either re-enter the dark zone or terminally differentiate. These differential fates are meted out at the immune synapse between GC B cells and other GC resident cells: T cells and follicular dendritic cells (Gitlin et al., 2014; Nowosad et al., 2016; Victora et al., 2010; Victora & Nussenzweig, 2012). T-cell-derived CD40 signalling resulting in NF-KB activation is necessary for this selection (Basso et al., 2004; Heise et al., 2014). NF-KB activation results in IRF-4-mediated transcriptional repression of BCL-6, releasing the BCL-6-mediated repression of B-cell terminal differentiation genes including PRDM1, encoding BLIMP-1 which is necessary for plasma cell differentiation (Ci et al., 2009). BLIMP-1 in turn implements a plasma cell-specific transcriptional programme, including the acquisition of an antibody-secreting phenotype dependent on XBP1 (Hu et al., 2009; Reimold et al., 2001).

Taken together, these processes are highly error prone and it is perhaps unsurprising that the majority of B-cell lymphomas arise from the lymphoid germinal centre. This is a compartment that hosts cells undergoing massive proliferation and clonal expansion, with inactivation of tumour suppressor genes, genomic instability due to SHM and CSR mediated by AICDA, immune evasion by downregulation of MHC-II and PD-L1 and terminal differentiation blockade. Mutations in chromatin regulators are another hallmark of GC-derived lymphomas and will be discussed in section 1.9 below.

1.9. Chromatin regulators are recurrently disrupted in B-cell lymphomas

Disruptions and mutations in chromatin modifying genes are significantly enriched in germinal centre-derived B-cell lymphomas (Figure 1.7). Table 1.1 outlines mutations and disruptions in chromatin modifying genes arising in GC-derived lymphomas, as well as selected additional mutations in chromatin regulators occurring in other lymphoid neoplasms.

Recurrent monoallelic hotspot mutations in the enzymatic SET domain of EZH2 have been demonstrated in up to 22% of follicular B-cell non-hodgkin lymphoma (B-NHL) and germinal centre subtype diffuse large B-cell lymphoma (GCB-DLBCL), as well as less frequently in other cancer types including malignant melanoma (Bödör et al., 2013; Harms et al., 2014; Hodis et al., 2012; Morin et al., 2010; Yap et al., 2011). These EZH2 SET domain hotspot mutations most frequently affecting Tyrosine Y646 and less frequently Alanine A682 and Alanine A692, and result in a dramatically altered substrate preference of the PRC2 methyltransferase for H3K27me2 and significantly increased global H3K27me3 deposition (McCabe, Ott, et al., 2012; Sneeringer et al., 2010; Yap et al., 2011). The increase in the H3K27me3 mark at Polycomb target loci IRF4 and PRDM1 with resultant repression of transcription of these genes hinders immature B-lymphocytes from exiting the germinal centre reaction and results in malignant centrocyte expansion in the germinal centre light zone (Béguelin et al., 2013, 2020; Mlynarczyk et al., 2019). In a murine model, conditional expression of $EZH2^{Y646F}$ cooperated with the anti-apoptotic protein BCL2 (ubiquitously expressed in the germinal centre of lymph nodes) or P53 inactivation to accelerate B-cell lymphomagenesis. Although this oncogenic mutant largely replaces the repressive blanket of H3K27me2 with H3K27me3, the repressive mark

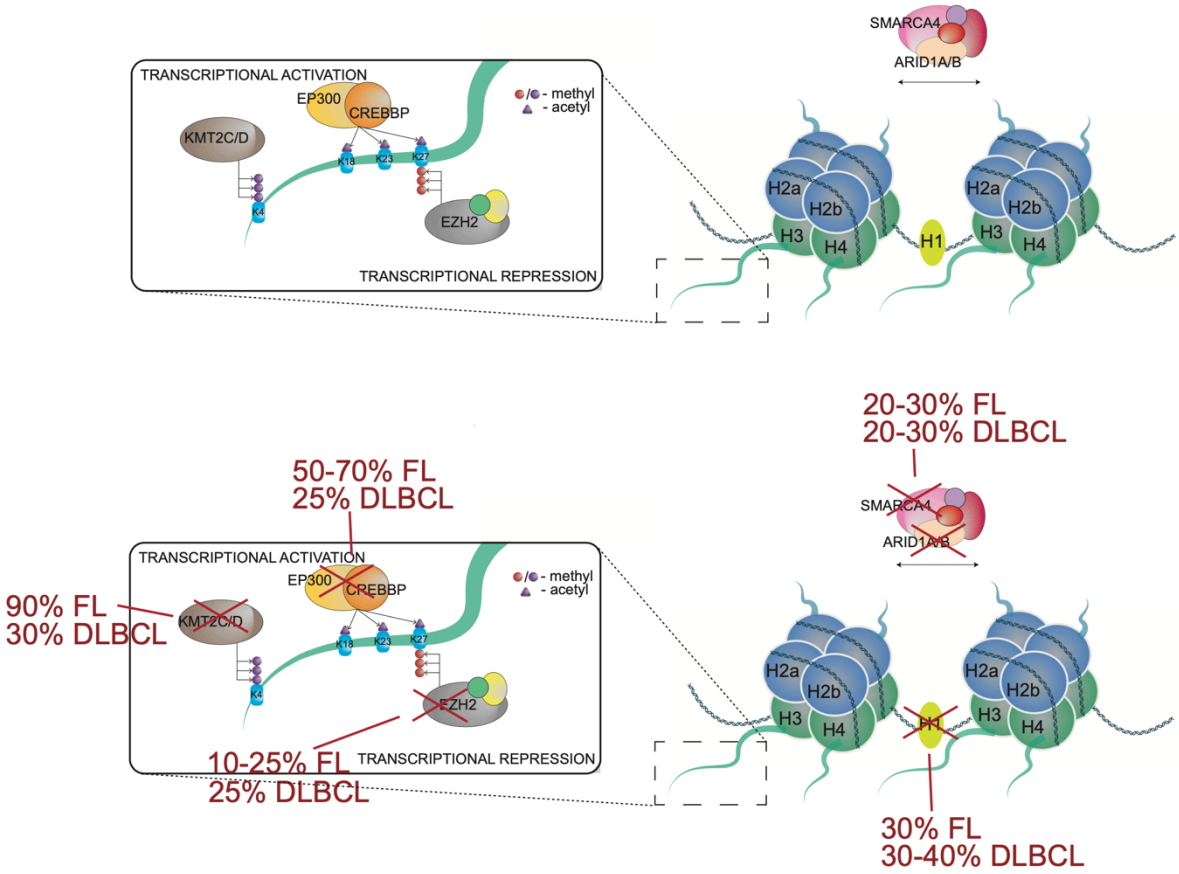

Figure 1.7 Chromatin modifying genes are recurrently mutated in germinal centre B-cell lymphomas

Chromatin regulators are recurrently mutated in B-cell lymphomas, including gain of function mutations in oncogenes (i.e. EZH2) and loss-of-function disruptions of tumour suppressor genes (KMT2C/D, Histone H1), histone acetyltransferase enzymes (CREBBP, EP300) and genes involved in ATP-dependent chromatin remodelling (BAF complex). Modified from (Lunning & Green, 2015).

H3K27me3 is also lost at some genomic loci, reflecting a neofunctionalisation of this mutant protein (Souroullas et al., 2016). Furthermore, where H3K27me3 is gained, its gain is not necessarily equal across all compartments; its fold-change correlates more within TADs compared to adjacent TADs; concordant also with transcriptional activity within TADs (Donaldson-Collier et al., 2019).

This anticorrelation between mRNA level and H3K27me3 fold-change included numerous tumour suppressor genes and even tumour suppressor TADs (Donaldson-Collier et al., 2019; Oricchio et al., 2017). EZH2 mutant lymphomas also demonstrate reduced MHC-1 and MHC-II expression, supporting immune escape (Ennishi et al., 2019).

Intriguingly, biallelic loss or inactivating mutations of EZH2 or the other PRC2 core components SUZ12 and EED have been detected in some T-cell acute lymphoblastic leukaemias and malignant peripheral nerve sheath tumours (Ernst et al., 2010; W. Lee et al., 2014; Ntziachristos et al., 2012). Although this effect is diametrically opposed to the lymphoma gain-of-function mutation in EZH2, one explanation of its oncogenic contribution is epigenetic reprogramming resulting in derepression of cancer-associated genes due to redistribution of H3K27 methylation and acetylation marks (Conway et al., 2015; Muto et al., 2013; Simon et al., 2012). Therefore, EZH2 is a bona fide oncogene or tumour suppressor gene dependent on the cancer context.

Numerous SAM-competitive small molecule inhibitors of EZH2 have been developed (W. Kim et al., 2013; Knutson et al., 2012; McCabe, Graves, et al., 2012; Tan et al., 2007; Xing Wang et al., 2021). Tazemetostat specifically reduces all degrees of H3K27 methylation written by both mutant and wild-type EZH2 alleles, without measurable effect on other methylation marks *in vitro* and equally affects wild-type and mutant alleles in doing so (Béguelin et al., 2013; Knutson et al., 2012; McCabe, Ott, et al., 2012). Cells surviving treatment with Tazemetostat have an increased dependency upon B-cell activation signalling for survival in lymphoma cell lines, with potential synergy predicted between Tazemetostat and kinase inhibitors targeting B-cell activation at various points along the B-cell receptor signalling cascade, including BTK, SYK, PI3K, AKT, mTOR and MEK1 (Brach et al., 2017). Supporting this, activation of these pathways has been shown to confer resistance to EZH2 inhibitor drugs in DLBCL cell lines (Bisserier & Wajapeyee, 2018). Treatment of EZH2 mutant lymphoma cells with EZH2 inhibitor drugs results in upregulation of terminal

differentiation genes and derepression of aberrantly repressed tumour suppressor genes (Béguelin et al., 2013; Donaldson-Collier et al., 2019; Knutson et al., 2012; McCabe, Graves, et al., 2012; Souroullas et al., 2016). Furthermore, Tazemetostat treatment reactivates TADs that have been repressed by ectopic expression of the EZH2 mutant in wild-type lymphoma cells (Donaldson-Collier et al., 2019). Alternative approaches explored so far in targeting PRC2 activity *in vivo* include the EED allosteric inhibitor molecule EED226 (Qi et al., 2017) and EZH2 and EED degrader proteolysis targeting chimera (PROTAC) drugs (J. H. R. Hsu et al., 2020; Z. Liu et al., 2021; Potjewyd et al., 2020).

Recent work has exposed the Histone H1 family genes (H1B, H1C, H1D, H1E: H1-5, H1-2, H1-3 and H1-4, respectively) as driver mutations in B-cell lymphoma (Hongxiu Li et al., 2014; Okosun et al., 2014; Reichel et al., 2015; Wright et al., 2020; Yusufova et al., 2021). Disruption of H1 function resulting in H1 deficiency results in gain of H3K36me2 and/or loss of H3K27me3 at stem cell genes, reflecting de-repression of early developmental genes usually sequestered in inaccessible genomic compartments (Willcockson et al., 2021; Yusufova et al., 2021). These mutations likely arise during mutagenic aberrant SHM by activation-induced cytosine deaminase (Chapuy et al., 2018).

KMT2D/MLL2 loss of function mutations occur in ~80% of follicular lymphomas and ~30% of GCB-DLBCLs and result in loss of H3K4me1, H3K4me2 and H3K4me3 *in vitro* and *in vivo* (Green, 2018; Okosun et al., 2014; Pasqualucci, Trifonov, et al., 2011; Jiyuan Zhang et al., 2015). This perturbation has been shown to cooperate with BCL2 disruption, resulting in massive germinal centre expansion, enhanced GC B cell fitness and the development of lymphoma in mice (Ortega-Molina et al., 2015; Jiyuan Zhang et al., 2015). The KDM5 demethylase family is responsible for demethylation at H3K4 and inhibition of these enzymes has been proposed and proven in pre-clinical (lymphoma cell lines and mouse xenograft) models to be a potential genetic dependency (Heward et al., 2021).

Histone acetyltransferases CREBBP and EP300 are haploinsufficient tumour suppressor genes in DLBCL (Okosun et al., 2014; Pasqualucci, Dominguez-Sola, et al., 2011; Jiyuan Zhang et al., 2017). CREBBP acetylates both histone and non-histone proteins, including BCL6 and p53. CREBBP opposes the actions of BCL6 both by writing H3K27ac at the promoters and enhancers of BCL6 target genes and by direct acetylation of BCL6, which

inactivates the protein (Bereshchenko et al., 2002; Jiang et al., 2017; Pasqualucci, Dominguez-Sola, et al., 2011; Jiyuan Zhang et al., 2017). CREBBP haploinsufficiency therefore enhances the proto-oncogenic function of BCL6. Deletion of CREBBP has also been shown to result in expansion of the GC, accelerate MYC-driven lymphomagenesis and CREBBP inactivation down-regulates the expression of MHC-II proteins, contributing to tumour immune evasiveness (Hashwah et al., 2017). HDAC inhibitor molecules have been proposed as a therapeutic approach to treating these lymphomas (Hashwah et al., 2017; Jiang et al., 2017).

Combined deletion of both CREBBP and EP300 prevents germinal centre formation *in vivo* and impairs DLBCL proliferation *in vitro*, suggesting that CREBBP deficient DLBCL becomes dependent on EP300 and a potential role for EP300 inhibitor drugs in this context (Meyer et al., 2019).

Inactivating mutations in TET2, an enzyme responsible for conversion of 5-methylcytosine to 5-hydroxymethylcytosine and ultimately DNA demethylation, are found in ~12% of DLBCL cases (Asmar et al., 2013; Lemonnier et al., 2012; Reddy et al., 2017). Over 70% of sites gaining DNA methylation as a result of this mutation lie within CpG islands, with a further 18% within 2Kb of a CpG island; particularly enriched for polycomb group protein target promoters (Asmar et al., 2013; Tulstrup et al., 2021). Although hypomethylating agents inhibiting DNMT1 have shown efficacy in numerous TET2-mutant (inactivating) malignancies thus far including Myelodysplastic Syndrome/Acute Myeloid Leukaemia (MDS/AML), T-cell acute lymphoblastic leukaemia (T-ALL) and angioimmunoblastic T-cell lymphoma, evidence is lacking regarding their use in TET2 mutated B-cell Non-Hodgkin Lymphoma (Bejar et al., 2014; Bensberg et al., 2021; Lemonnier et al., 2018).

Table 1.1 Chromatin modifying gene mutations in B-lymphoid neoplasms

Gene	Function	Genetic Lesion	Gross Effect on PTMs	Frequency				References(s)
				GCB-DLBCL	ABC-DLBCL	FL	Other Lymphoid Malignancy	
EZH2	H3K27 HMT (PRC2)	Missense mut (Y646X / A682G / A692G) +7q/locus amplification Deletion/nonsense/missense	GOF: ↑H3K37me3 ↓H3K27me2 GOF: ↑H3K37me3 LOF: ↓H3K27me3	21.7% 7.7% ND	ND ND ND	7.2% - 27.5% 24% ND	 - T-ALL (15-18%)	(Morin et al., 2010), (McCabe, Graves, et al., 2012), (Bödör et al., 2013) (Bouska et al., 2017) (Ntziachristos et al., 2012)
SUZ12	H3K27 HMT (PRC2)	Deletion/nonsense	LOF: ↓H3K27me3	ND	ND	ND	- T-ALL (5-7%)	(Neumann et al., 2015), (Y. Liu et al., 2017), (Ntziachristos et al., 2012)
EED	H3K27 HMT (PRC2)	Deletion/nonsense	LOF: ↓H3K27me3	ND	ND	ND	- T-ALL (3%)	(Ntziachristos et al., 2012)
CREBBP	Lysine HAT	Missense>truncation/deletion	LOF: ↓H3K27ac, ↓H3K18ac	41%	17%	32-64%	- Relapsed ALL (18%)	(Pasqualucci, Dominguez-Sola, et al., 2011), (Okosun et al., 2014), (Mullighan et al., 2011)
EP300	Lysine HAT	Missense>truncation/deletion	LOF: ↓H3K27ac, ↓H3K18ac	5-10%	ND	8.7%		(Pasqualucci, Dominguez-Sola, et al., 2011),
HistoneH1 H1E>H1C >H1D> H1B	Linker Histone	Missense mutations in globular (DNA-binding) domain	LOF: ↓H3K27me3, ↑H3K36me2	27%	24%	30%	- Classical Hodgkin Lymphoma (50%)	(Okosun et al., 2014), (Hongxiu Li et al., 2014), (Reichel et al., 2015), (Wright et al., 2020), (Yusufova et al., 2021)
KDM6A (UTX)	H3K27 demethylase	Deletion>frameshift>nonsense	LOF: ↑H3K37me3	ND	ND	ND	- Multiple Myeloma (10%) - T-ALL (male) (10-20%)	(Van Haaften et al., 2009), (Van Der Meulen et al., 2015)
KMT2D (MLL2)	H3K4 HMT	Nonsense>deletion>splice site >missense	LOF: ↓H3K4me1, ↓H3K4me2	30%	20%	89%	- MCL (12%)	(Morin et al., 2011), (Pasqualucci, Trifonov, et al., 2011), (Chapuy et al., 2018), (Schmitz et al., 2018), (Ferrero et al., 2020)
KMT2C (MLL3)	H3K4 HMT	Nonsense>deletion	LOF: ↓H3K4me1, ↓H3K4me2	13%	ND	5%	- MCL (10%)	(Jenny Zhang et al., 2014), (Green, 2018)
ARID1a	SWI/SNF	Frameshift>nonsense>deletion	LOF	9-12%	7-10%	5-14%	- Burkitt lymphoma (20%)	(Hongxiu Li et al., 2014), (Schmitz et al., 2018), (Reddy et al., 2017), (Burkhardt et al., 2022)
ARID1b	SWI/SNF	Frameshift>nonsense>deletion	LOF	8-10%	6-7%	2%		(Pasqualucci et al., 2014), (Reddy et al., 2017)
SMARCA4	SWI/SNF	Frameshift>nonsense>deletion	LOF	3-8%	6%	2%	- Burkitt lymphoma (21%)	(Hongxiu Li et al., 2014), (Reddy et al., 2017), (Schmitz et al., 2018)
BCL7a	SWI/SNF	Splice site>frameshift>deletion	LOF	8-13%	3-4%	10-15%		(Reddy et al., 2017), (Schmitz et al., 2018), (Baliñas-Gavira et al., 2020), (Krysiak et al., 2017)
TET2	DNA demethylase	Nonsense/frameshift>missense	LOF: promoter hypermethylation	10%	ND	ND	- AITL/PTCL (38-47%)	(Lemonnier et al., 2012), (Asmar et al., 2013), (Reddy et al., 2017)
NSD2	H3K36 HMT	Missense mut (E1109K / T1150A) Overexpression t(4;14)	GOF: ↑H3K36me2, ↓H3K27me3	ND	ND	ND	- MCL (10-15%) - Paediatric ALL (5-10%) - Myeloma (10-20%)	(Beà et al., 2013) (Jaffe et al., 2013), (Loh et al., 2013), (Ferrero et al., 2020) (Keats et al., 2005)

ND = not determined. LOF = loss of function. GOF = gain of function. HAT = histone acetyltransferase. HMT = histone methyltransferase.

T-ALL = T-cell acute lymphoblastic leukaemia. MCL = mantle cell lymphoma. AITL = angioimmunoblastic T-cell lymphoma. PTCL = peripheral T-cell lymphoma.

The SWI/SNF complex (alias BAF) utilises energy from ATP to remodel chromatin by shuffling nucleosomes along DNA (Roberts & Orkin, 2004). Inactivating mutations in ARID1A and SMARCA4 occur (often concurrently) frequently in Burkitt lymphoma (BL) at a frequency of 32% and 35% respectively for paediatric, as compared with 19% and 21% respectively for adult Burkitt lymphoma (Burkhardt et al., 2022). Synthetic lethality screens of ARID1A and SMARCA4 mutant cells have exposed a vulnerability to interference with paralogous SWI/SNF complex components, representing a potential future therapeutic option for SWI/SNF mutant lymphomas (Helming et al., 2014; Hoffman et al., 2014).

1.10 Epigenetic therapies are entering the clinic

Given the high prevalence of mutations and other disruptions in chromatin regulators in cancer, it follows that numerous epigenetic targeted therapies are entering the clinic. In this section I will discuss several epigenetic axes which are being therapeutically targeted in various cancer contexts with a particular focus on B-cell lymphomas, illustrating that this is a promising space with significant ongoing clinical work and burgeoning interest.

In 2020, the EZH2 selective small molecule enzymatic inhibitor Tazemetostat (EPZ-6438) received accelerated approval from the US FDA (Food and Drink Authority) for the treatment of EZH2-mutant lymphoma beyond second line, relapsed/refractory EZH2-wild type lymphoma where no suitable alternative exists, and for unresectable INI1/SMARB1 deficient epithelioid sarcoma (Epizyme (2020) Tazemetostat: Tazverik (Tazemetostat) for oral use. FDA accessdata.fda.gov: reference ID 4627347). Indeed, in both cell lines and patients, the presence of an EZH2 change of function mutation predicted but was not essential for response to Tazemetostat (Brach et al., 2017; Italiano et al., 2018; Izutsu et al., 2021; Knutson et al., 2012; Morschhauser et al., 2020; Munakata et al., 2021). EZH2 inhibitor drugs have also been proposed as a therapy in other cancer contexts including H3K27M-mutant diffuse midline glioma (DIPG) and breast cancer (Brien et al., 2021; Duan et al., 2020; Mohammad et al., 2017; Yaqin Zhang et al., 2017). Numerous trials with data of variable maturity are ongoing to find an appropriate combination therapy for EZH2 inhibitor therapy in B-NHL, including PD-L1 monoclonal antibodies, anti-CD20 therapy (Rituximab), immunomodulator drug Lenalidomide, BCL2 inhibitor Venetoclax and R-CHOP standard chemoimmunotherapy, among others. Table 1.2 provides an overview of available clinical trial data using PRC2

inhibitors in human patients, among dozens of ongoing but as yet unreported clinical trials involving EZH2 inhibitor drugs.

Histone deacetylase (HDAC) inhibitor molecules have become well established in the treatment of T-cell lymphomas, with four molecules approved by the FDA (Bondarev et al., 2021). Numerous studies involving patients with both newly diagnosed and relapsed/refractory B-cell lymphomas have yielded encouraging results, especially in combination with established or other experimental therapies (Kirschbaum et al., 2011; Persky et al., 2018; Straus et al., 2015; P. Wang et al., 2020).

Disruptor of telomere silencing 1-like (DOT1L) is the only known H3K79 methyltransferase. Its H3K79me2/me3 mark is generally found at the gene body of actively transcribed genes and is associated with transcriptional elongation while inhibiting histone deacetylase activity and preventing the formation of H3K9me3 repressive domains (C. W. Chen et al., 2015; Feng et al., 2002; Mohan et al., 2010; Steger et al., 2008). MLL-rearranged leukaemias are critically dependent upon DOT1L and frequently recruit DOT1L to chromatin, resulting in aberrant H3K79 methylation at MLL target genes (Bitoun et al., 2007; Guenther et al., 2008; Krivtsov et al., 2008; Milne et al., 2005). The highly selective DOT1L inhibitor pinometostat had modest activity in MLL-rearranged acute leukaemia (Stein et al., 2018). Subsequent work to target this disruption has resulted in the development of additional compounds to target the interaction between Menin and MLL fusion proteins, which is an essential interaction for MLL fusion-driven gene expression (Grembecka et al., 2012; Krivtsov et al., 2019; Y. Xu et al., 2016; Yokoyama et al., 2005). Lysine specific demethylase 1 (LSD1/KDM1A) is a specific demethylase for H3K4me1/2 and H3K9me1/2 at promoter regions, triggering interest in the enzyme as a potential target in MLL-rearranged acute leukaemias, where MLL SET domain is lost and MLL is fused with a fusion partner, i.e. DOT1L (Fang et al., 2010; Krivtsov & Armstrong, 2007; Salamero et al., 2020; Y. Shi et al., 2004).

PRMT5 is a Type 2 protein arginine methyltransferase responsible for symmetrical arginine methylation at a variety of residues, including H4R3, H3R8 and H2AR3 and can also methylate protein targets including p53 (Shailesh et al., 2018; Stopa et al., 2015). It is overexpressed in a number of cancer types including prostate, breast, lung and colon (Beketova et al., 2022; Poulard et al., 2016), resulting in aberrant repression of various tumour suppressor genes (X. Liu et al., 2018; Pal et al., 2004). The chromosome 9p21 locus is homozygously deleted in 15%

of human cancers, resulting in deletion of CDKN2A and critical tumour suppressors p19-ARF and p16-INK4a (Beroukhim et al., 2010; Kamijo et al., 1997). The gene methylthioadenosine phosphorylase (MTAP), which is immediately proximal to CDKN2A, is homozygously co-deleted in 80-90% of tumours with CDKN2A mutation, resulting in accumulation of its substrate 5'-methylthioadenosine, a potent endogenous inhibitor of PRMT5 (Zappia et al., 1988). Intriguingly, this endogenous inhibition of PRMT5 by the accumulated byproduct of MTAP loss renders the cells sensitive to further PRMT5 loss (Marjon et al., 2016). Therefore, numerous compounds targeting this protein have entered clinical trials for patients with MTAP nul tumours or advanced solid tumours (Siu et al., 2019; C. R. Smith et al., 2022; Watts et al., 2019).

An exciting recent development in oncology is the transition of PROTAC (proteolysis targeting chimera) molecules for targeted protein degradation, to the clinic. PROTACs are heterobifunctional molecules comprising two ligands joined by a linker: one ligand recruits and binds the protein of interest, while the other engages an E3 ubiquitin ligase (e.g. cereblon, Von-Hippel-Lindau) (Figure 1.8) (Sakamoto et al., 2001). In 2019, the first PROTACs entered phase 1 clinical trials in patients: ARV-471, an oestrogen receptor PROTAC in breast cancer, and ARV-110 an androgen receptor PROTAC in metastatic castration-resistant prostate cancer (X. Gao et al., 2022; Snyder et al., 2021). In B-NHL, supported by the efficacy of Bruton's tyrosine kinase (BTK) inhibitors, numerous BTK degraders have been developed and are in trial. The BTK inhibitor Ibrutinib is among the front-line treatment options in TP53-disrupted chronic lymphocytic leukaemia (CLL) and at relapse or in specific scenarios for indolent B-cell lymphomas, with eventual resistance emerging most commonly due to a recurrent hotspot mutation BTKC481S, which attenuates the covalent binding ability of the drug (Chiron et al., 2014; Woyach et al., 2014). Degradation of the target protein may provide a route whereby acquired resistance due to impaired drug binding in this and other cancer contexts could be overcome. Promisingly, based on the demonstration that BRD9 co-localises with the SS18-SSX pathogenic fusion protein in synovial sarcoma, two BRD9 PROTACs are currently in clinical trial (Brien et al., 2018). This demonstrates that where an inhibitor or other molecularly targeted therapy does not exist, development of a PROTAC to degrade the protein of interest is a realistic avenue to bypass this issue and the clinical trial space is accordingly becoming more populated (Table 1.3). Excitingly, numerous tissue-specific E3 ubiquitin ligases have now been described, alluding to the potential future design of PROTACs capable of targeting a specific tissue (or cell) type (Békés et al., 2022; Kannt & Đikić, 2021).

Table 1.2 Published clinical trial data for PRC2 enzymatic inhibitor drugs

Target / Drug	Trial ID	Clinical context	Safety and efficacy	Reference
EZH2 / EPZ-6438	NCT01897571 (Phase 1)	- R/R B-NHL (n=21) - INI1/SMARCA4(-/-) solid tumours (n=13) - Other solid tumours (n=30) - Median 2 (1-5) prior lines	- 9% Grade ≥3 SAE - ORR: 38% B-NHL, duration 12.4months - ORR: INI1/SMARCA4(-/-) 18%, duration NR - ORR: other solid tumours: 0%	(Italiano et al., 2018)
EZH2 / EPZ-6438	NCT01897571 (Phase 2)	- R/R FL (n=45 $EZH2^{MUT}$, n=54 $EZH2^{WT}$) - Median 2 (1-5) prior lines	- 12% Grade ≥3 SAE - ORR: 69% $EZH2^{MUT}$, duration 10.9 months - ORR: 35% $EZH2^{WT}$, duration 13 months	(Morschhauser et al., 2020)
EZH2 / EPZ-6438	NCT03456726 (Phase 2)	- R/R $EZH2^{MUT}$ B-NHL (FL n=17, DLBCL n=3) Median 2 (1-5) prior lines	- 40% Grade ≥3 SAE - ORR 76.5%, median duration not reached (median follow-up 12.9 months)	(Izutsu et al., 2021)
EZH2 / EPZ-6438	NCT02601950 (Phase 2)	- INI1/SMARCB1(-/-) Epithelioid sarcoma (n=62)	- 13% Grade ≥3 SAE - 15% ORR	(Gounder et al., 2020)
EZH2 / EPZ-6438	NCT02860286	- BAP1 inactivated R/R malignant mesothelioma (n=74)	- 34% Grade ≥3 SAE - 3% ORR (+54% stable disease at 12 weeks)	(Zauderer et al., 2020)
EZH2 / SHR2554	NCT03603951 (Phase 1)	- R/R lymphomas (B/T/Hodgkin) (n=113) - 47% ≥3 prior lines	- 41% Grade ≥3 SAE (2% Grade 5) - 46% ORR (no subgroups available)	(Song et al., 2022)
EZH1/2 / Valemetostat	NCT02732275 (Phase 1)	- Adult T-cell leukaemia/lymphoma (n=9) - Median 2 (1-8) lines	- >50% Grade ≥3 SAE - 44% ORR, duration >12 weeks	(Morishima et al., 2019)
EZH2 / EPZ-6438 + R-CHOP	NCT02889523 (Phase 1b)	- (Up front) DLBCL (high-risk: aaIPI 2-3)(n=17 patients)	- 30% Grade ≥3 SAE - 76.5% metabolic CR (median follow-up 20.6 months)	(Sarkozy et al., 2020)
EZH2 / EPZ-6438 +R^2 +Rituximab (CD20 mAB) +Lenalidomide (IMID)	NCT04224493 (Phase 1a/1b)	- R/R lymphomas (B/T/Hodgkin) (n=113) - Median 2 (1-5) prior lines	- 50% Grade ≥3 SAE - ORR 91.7% (median follow-up 16.9 weeks)	(Batlevi et al., 2021)
EED / MAK683	NCT02900651 (Phase 1/2)	- R/R DLBCL - Median 4 (1-16 prior lines)	- 45% Grade ≥3 SAE - 16% ORR	(Ribrag et al., 2021)

R/R = relapsed/refractory. Lines refers to prior lines of therapy. SAE refers to serious adverse events as defined by CTCAE (Common Terminology Criteria for Adverse Events) version 4.0 (National Cancer Institute). ORR = overall response rate. IPI = imternational prognostic index. CR = complete response. PR = partial response. Median duration of response indicated where available.

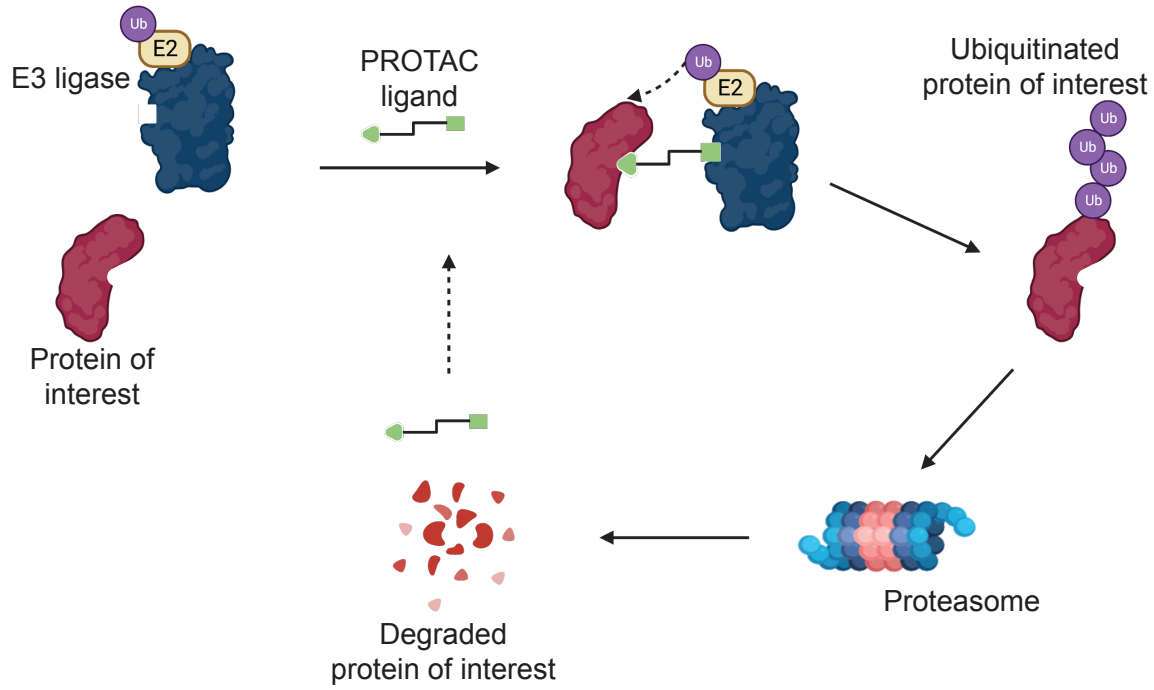

Figure 1.8 Targeted protein degradation via PROTAC

A heterobifunctional PROTAC molecule with affinity for its target protein and also a suitable E3 ubiquitin ligase expressed in the target cell binds both proteins, resulting in ubiquitination of the protein of interest and proteasomal degradation. The PROTAC molecule is not degraded and is recycled for further iterations of degradation of its target protein.
Made with BioRender.com

Table 1.3 List of PROTAC molecules currently in clinical trials

Target / Drug	Trial ID	Clinical context	Year opened
Androgen receptor / ARV-110	NCT03888612	Metastatic castrate-resistant prostate cancer	2019
Androgen receptor / ARV-766	NCT04428788	Metastatic castrate-resistant prostate cancer	2020
Androgen receptor / ARV-766	NCT05067140	Metastatic castrate-resistant prostate cancer	2021
Androgen receptor / AC176	NCT05241613	Metastatic castrate-resistant prostate cancer	2022
Bcl-xL / DT2216	NCT04886622	Relapsed/refractory solid and blood cancers	2021
BRD4 / RNK05047	NCT05487170	Advanced solid tumours / relapsed DLBCL	2022
BRD9 / FHD-609	NCT04965753	Advanced synovial sarcoma	2021
BRD9 / CFT8634	NCT05355753	Locally advanced/metastatic SMARCB1-disrupted cancers	2022
BTK / NX-2127	NCT04830137	Relapsed/refractory B-cell malignancies	2021
BTK / NX-5948	NCT05131022	Relapsed/refractory B-cell malignancies	2021
BTK / BGB-16673	NCT05294731	B-cell malignancies	2022
IRAK4 / KT-474	NCT04772885	Atopic dermatitis / hidradenitis suppurativa	2021
IRAK4 / KT-413	NCT05233033	Relapsed/refractory B-NHL	2022
Oestrogen receptor (ER) / ARV-471	NCT04072952	ER+/HER2- locally advanced/ metastatic breast cancer	2019
Oestrogen receptor (ER) / AC682	NCT05080842	Locally advanced/metastatic ER+ breast cancer	2021
STAT3 / KT-333	NCT05225584	Refractory lymphoma, large granular lymphocytic leukaemia, solid tumours	2022

Correct as of September 2022 (clinicaltrials.gov)

1.11 Aims of thesis

The principal aim of my thesis was to explore the function of the oncogene EZH2 and other Polycomb Repressive Complex 2 (PRC2) components in B-cell Non-Hodgkin lymphoma cell lines. The specific aims of each chapter were as follows.

Chapter 3: Mapping disrupted H3K27 methylation in EZH2 mutant lymphoma and the differential effects of PRC2 enzymatic inhibition and PRC2 degradation

- To examine the effects of the EZH2 gain-of-function mutant on genomic localisation of core PRC2 and H3K27 methylation marks
- To identify differential effects of PRC2 enzymatic inhibition and PRC2 degradation on the genomic localisation or H3K27 methylation marks and the transcriptional landscape in lymphoma cells
- To evaluate PRC2 degradation as a means of overcoming acquired resistance to PRC2 enzymatic inhibition

Chapter 4: A CRISPR tiling screen of PRC2 components in germinal centre B-cell lymphoma reveals AEBP2 as a specific genetic dependency

- To apply CRISPR screening technology to identify novel genetic dependencies relating to the oncogene EZH2 in B-cell lymphoma cell lines
- To identify and describe any new or key functional domains in any identified genetic dependency
- To validate any promising dependency by performing sgRNA negative selection assays and rescue experiments

Chapter 5: AEBP2 disruption in lymphoma leads to PRC2 activation and genome-wide redistribution of H3K27me3 and H3K27me2

- To identify the effects on H3K27 methylation and the transcriptional landscape of AEBP2 depletion in lymphoma cells
- To evaluate the relative contribution of PRC2.1 and PRC2.2 to H3K27 methylation in lymphoma cells

CHAPTER 2: Materials and Methods

2.1 Cell culture

2.1.1 Culturing conditions

All cell lines were grown at 37 degrees Celsius in 5% v/v CO2.

Human lymphoma cell lines HT, OCI-LY18, Pfeiffer, WSU-DLCL2, SU-DH-L6 and DO-HH2 were cultured in suspension in Roswell Park Memorial Institute medium - RPMI 1640 (Gibco) supplemented with 2mM GlutaMAX (Gibco 61870036) and 10% v/v Heat-Inactivated Foetal Bovine Serum (FBS) (Gibco) and 100U/ml penicillin/streptomycin (Gibco). KARPAS-422 was cultured as above though with 20% v/v Heat-Inactivated FBS. Human lymphoma cell lines OCI-LY1 and OCI-LY7 were cultured in Isocove Modified Dulbecco Media - IMDM (Gibco 12440053) supplemented with 20% v/v Heat-Inactivated FBS and 100U/ml penicillin/streptomycin. Cells were passaged by splitting 8:1 – 12:1 every 2-3 days.

HEK293T, G401 (human malignant rhabdoid tumour) and A673 (human Ewing sarcoma) cell lines were cultured in Dulbecco's Modified Eagle Medium - DMEM high glucose (Sigma D6429) supplemented with 10% v/v FBS (Gibco) and 100U/ml penicillin/streptomycin (Gibco). These cells were maintained on TC-treated culture dishes and passaged every 2-3 days using 0.25% Trypsin-EDTA (Gibco).

TERT immortalised TIG3 (TIG3-T) human fibroblasts were grown in DMEM (Lonza) supplemented with 10% FBS (Gibco), 10% v/v FBS (Gibco) and 100U/ml penicillin/streptomycin (Gibco). B-CPAP thyroid papillary cancer cells were grown in RPMI-1640 (Gibco) with 10% v/v heat-inactivated FBS (Gibso) and 100U/ml penicillin/streptomycin. For serum starvation experiments, fibroblasts and B-CPAP cells were grown until 60-70% confluency. Cells were subjected to serum-free media for 120 hours with media changes at 24 hour intervals until 120 hours.

Mouse embryonic stem cells (mESCs) were maintained on 0.1% gelatine-coated culture dishes and passaged every 2 days using 0.25% Trypsin-EDTA (Gibco 25200056). mESCs were cultured under 2i/LIF conditions in Glasgow Minimum Essential Medium (GMEM; Sigma) supplemented with 20% v/v Heat-Inactivated FBS, 100u/ml penicillin/streptomycin (Gibco), 50μM β-mercaptoethanol (Sigma), 1:100 Glutamax (Gibco), 1:100 non-essential amino acids (Gibco), 1mM sodium pyruvate (Gibco), 1:500 homemade Leukaemia Inhibitory Factor (LIF),

3μM GSK inhibitor CHIRON9902 (Millipore) and 1μM MEK inhibitor PD0325901 (Millipore).

2.1.2 Nucleofection of lymphoma cells by electroporation

Two pairs of sgRNAs were selected targeting intronic DNA either side of AEBP2 exon 2 and cloned into individual pSpCas9 (BB)-2A-eGFP (Addgene, px458). The intended result was excision of AEBP2 exon 2 (shared between all human AEBP2 isoforms) with resultant frame shift and knock-out of AEBP2. Cells were electroporated using a Lonza Amaxa Nucleofector programme X-001. 1.2μg of each paired sgRNA (one sgRNA in intron 1, one sgRNA in intron 2) was added in 10μl deionised nuclease-free H_20 to an Ingenio electroporation cuvette. $1x10^6$ WSU-DLCL2 cells were pelleted by centrifugation at 100g for 3 minutes, washed once in DPBS, pelleted again and all residual supernatant carefully removed. Nucleofection Buffer A (5mM KCl, 15 mM $MgCL_2$, 20mM HEPEPS, 150mM Na_2HPO_4/NaH_2PO_4 pH 7.2) was pre-warmed to 37°C. Pelleted lymphoma cells were resuspended in 100μl of pre-warmed Buffer A and gently mixed with the paired sgRNA mixture in the cuvette. After electroporation, the nucleofection mixture was promptly resuspended in fresh media and returned to the incubator such that time in Buffer A was less than 15 minutes, due to its hyperosmolar nature.

Approximately 24 hours after transfection, GFP-expressing (GFP+) cells were sorted as single cells into 96-well culture plates using a FACSAria Fusion Flow Cytometer operated by Dr Barry Moran at the Trinity Biomedical Sciences Institute Flow Cytometry Facility. Surviving single cell clones were screened at the DNA level for AEBP2 knock-out and positive clones were expanded for validation at the mRNA and protein expression level.

2.1.3 Production of lentivirus

Lentiviral particles were produced using a second generation lentiviral system in HEK393T cells. HEK293T cells were seeded on T75 flasks containing 12 mls DMEM 24 hours prior to intended transfection such that they would be 70-80% confluent on the day of transfection. Following a standard PEI transfection protocol, for HEK293T cells cultured in a T75 culture flask, 4μg of the plasmid of interest, 2μg PAX8 packaging vector and 3μg VSV-G were combined along with 27μg of polyethylenimine (PEI) and 500μl Optimem (Gibco 31985062) and incubated for 20-30 minutes at room temperature. Quantities were scaled linearly as per the surface area of the dish. This mixture was then added drop-wise to the 70-80% confluent

HEK293T cells, which had immediately prior to transfection had media removed and 12mls fresh complete DMEM gently applied. Media supernatant containing viral particles was harvested at 72 hours post-transfection, filtered by passing through a 0.45μm polyethersulfone (PES) filter and stored for if for short-term use at 4°C or frozen at -80°C.

To gauge transfection success, an additional plate of HEK293T cells was transfected with 4 μg of the GFP-expressing vector pGIPZ alone. High PEI transfection efficiency was inferred by the level of visible GFP expression with a blue laser at 24 hours. This plate was then discarded.

2.1.4 Generation of stable cell lines by lentiviral transduction

$1x10^6$ suspension cells per lentiviral infection with one additional pellet for an uninfected negative control were pelleted by centrifugation at 100g for 3 minutes and supernatant media was removed. The pelleted cells were resuspended in lentiviral supernatant (or fresh media for the negative control) supplemented with 1:1000 Polybrene (stock solution 50mg/ml) and transferred to a 6-well plate and sealed with parafilm.

For adherent cells, $7.5x10^5$ adherent cells per lentiviral infection were added to each well of a 6-well plate and incubated for 3 hours or until adherent. Once adherent, the media was removed and lentiviral supernatant supplemented with 1:1000 Polybrene was gently directly applied to the cells and the plates were sealed with parafilm.

The plates were spun at room temperature at 1700 RPM for 2 hours, after which the lentiviral supernatant was removed and replaced with 3-5mls of fresh media in the case of adherent cells, or the cells were resuspended in 3-5 mls of fresh media and transferred to a T25 tissue culture flask for suspension cells.

When a lentiviral vector containing an antibiotic resistance cassette was used, the antibiotic was added at an appropriate concentration to the cells such that a pre-determined final concentration was reached, to allow for selection of clones expressing the desired construct. Cells were grown in culture until complete death of the uninfected negative control cells; thereafter expanded with construct expression confirmed by protein Western blot. When selection using a fluorescent marker was necessary, this was done as detailed in section 2.1.2 above.

2.1.5 Determination of Cas9 efficiency

pXPR_011-sgEGFP lentivirus was generated as described in section 2.1.3. This plasmid expresses enhanced GFP (EGFP) and a sgRNA targeting EGFP, such that GFP is depleted in cells expressing the Cas9 endonuclease over time. Cells surviving Blasticidin selection (having been shown by Western blot to express FLAG-tagged Cas9) as well as their parental cells were seeded on a 12-well tissue culture plate. Increasing volumes of pXPR lentivirus (10µl, 20µl, 50µl, 100µl, 200µl, 400µl) were added with polybrene supplementation to a final concentration of 0.5µg/ml, with 2 additional uninfected wells. The cells were spinoculated at 1700RPM for 2 hours, at which time the viral supernatant was removed and replaced with fresh media. After 24 hours, Puromycin was added to the lentivirally infected wells, including 1 uninfected well, with DMSO added to the other uninfected well. The appropriate dose of Puromycin was previously determined as the lowest dose required to kill uninfected cells at 48 hours (0.5-10µg/ml depending on the cell line).

48 hours after adding puromycin, the cells were trypsinised or resuspended and counted. The infection efficiency was determined by dividing the number of cells per millilitre in lentivirally infected wells by the number of cells in the "uninfected + DMSO" well. Cells with an infection efficiency of 15-30% (chosen such that one lentiviral particle likely incorporated per cell) were seeded forward, such that 4 cell lines were retained (parental and "Cas9" cells with no pXPR infection; and parental and "Cas9" cells + pXPR). Fluorescence-activated cell sorting (FACS) analysis was performed weekly from Day 14 following infection using a BD Accuri C6 flow cytometer with Cas9 activity determined based on the depletion of GFP in cells expressing Cas9 relative to parental cells. Cells with estimated Cas9 activity of 70% or greater were taken forward for PRC2 library screens or sgRNA validation experiments.

2.1.6 PRC2 tiling library CRISPR screen

PRC2 sgRNA library lentivirus was prepared using the ipUSEPR plasmid pool containing a RFP cassette. The PRC2 sgRNA library was designed by Dr Eric Conway and Dr Gerard Brien (Bracken Lab) and generated by Dr Chun-Wei (David) Chen, City of Hope Comprehensive Cancer Center. The library screens in the cell lines PFEIFFER and WSU-DLCL2 were undertaken in collaboration with Dr Eric Conway and in G401 was undertaken by Dr Marlena Mucha. The multiplicity of infection (MOI) was determined by calculating the volume of virus required to result in 10% RFP+ cells as determined by a BD LSRFortessa X-20 flow cytometer.

For this library of ~4000 sgRNAs, to ensure coverage of 1000 cells containing each sgRNA, with the MOI of 10%, 40 million cells were infected with the PRC2 sgRNA library and puromycin added at 24 hours after spinoculation as previously outlined. Given the requirement for pellets for high throughput sequencing for sgRNA quantification at day 3 and day 18, the planned infection was scaled up to 80 million cells, with 4 million cells harvested at Day 3 (10% of 40 million infected cells) and again at Day 18. To allow for technical issues, cell number was scaled up by 20% resulting in 5 million cells harvested per time point, per replicate. Two biological replicates were undertaken and harvested. Pellets were snap frozen in liquid nitrogen until batch processing.

DNA extraction and sequencing were undertaken by Dr Chen's group, but briefly detailed here. Genomic DNA was extracted using the HotSHOT protocol. Cell pellets were lysed in 250µl HotA buffer (0.25mM EDTA, 25mM NaOH: final pH=12) and boiled at 95°C for 30 minutes. DNA was then fragmented by sonication for 15 seconds. 500µl of HotB buffer (40nM Tris-HCl pH 6.8) was added, after which samples were gently vortexed and centrifuged. The purified DNA was then resuspended in DNase/RNase free sigma H_2O. Purified DNA was then amplified by PCR as detailed in Table 2.1 and Table 2.2. Following amplification, PCR products were pooled, run on a 2% agarose gel with excision and purification of the 150bp product band which was subsequently processed for sequencing.

Table 2.1 PCR mixture for gDNA amplification

Component	Stock	Volume
Sample DNA	1µg per 30µl	30µl
DreamTaq HotStart Green 2x MasterMix	2x	50µl
Primer mix (DCF01/DCR03; 5µM each)	5µM each	10µl
ddH20	-	10µl
TOTAL	-	100µl

Primer DCF01: 5'-cttgtggaaaggacgaaacaccg-3'

Primer DCR03: 5'-cctaggaacagcggtttaaaaaagc-3'

Table 2.2 PCR cycle for gDNA amplification

Step	Temperature (°C)	Time (seconds)	
Initial denaturation	95	60	
Denaturation	95	30	35 cycles
Annealing	65	20	
Extension	72	30	
Final extension	72	300	
Hold	4	∞	

2.1.7 sgRNA validation of PRC2 library screen

sgRNAs targeting regions of proteins of interest highlighted by the PRC2 tiling screen were cloned into the ipUSEPR plasmid containing a RFP reporter or LRG2.1 plasmid containing a GFP reporter. Lentivirus was generated for these sgRNAs as described in section 2.1.2 and applied to Cas9-expressing cells for validation, seeded in a 96 well plate. The plates were spun at 1700 rpm for 2 hours and room temperature. Lentiviral media was then removed, fresh media applied and the cells were cultured for a period of 21-45 days. The cells were split every 3 days at an appropriate ratio with RFP or GFP abundance quantified every 3 days using the Guava easyCyte HT system 12 and analysed using FlowJo software.

2.2 DNA methods

2.2.1 sgRNA cloning for PRC2 tiling screen validation

sgRNA expression vectors ipUSEPR (RFP reporter; gift from Dr David Chen) and LRG2.1 (GFP reporter; Addgene 108098) were linearised using the restriction enzyme BsmBI (NEB). The digested reaction was run on a 0.7% agarose gel and the product excised and purified using a QIAquick Gel Extraction Kit (Qiagen 28706). Complementary oligonucleotide primers were ordered with 20 base pair overlap corresponding to the DNA target sequence, with overhangs compatible with the BsmBI-digested backbones. Oligos were annealed and phosphorylated using T4 PNK (NEB M0201S) in a PCR block and ligated using T4 DNA ligase (NEB M0202S). DNA was then transformed into One Shot TOP10 chemically competent *E. coli* (Invitrogen), with several resultant clones prepared, DNA extracted and screened by Sanger sequencing.

2.2.2 Generation of CRISPR-Cas9 targeting plasmid

pSpCas9(BB)-2A-GFP (Addgene PX458) contains *S. pyogenes* Cas9 with a 2A-EGFP marker and a scaffold for sgRNA insertion. sgRNA cloning was undertaken as per the Zhang Lab protocol recommended by Addgene, using sgRNA oligonucleotide primers designed in the GPP web portal from the Broad Institute. The pSpCas9 vector was linearised using the restriction enzyme BbsI (NEB R0539S). DNA was transformed into One Shot TOP10 chemically competent *E. coli* as above and sgRNAs were sequence confirmed.

2.2.3 Generation of AEBP2 and EZH2 wild-type and mutant constructs

The ectopic expression of the 3xHA-tagged wild-type and mutant hEZH2 and hAEBP2 constructs was performed using in-house lentiviral expression vectors derived from pLEX_305 (Addgene 41390) and PLENTI EF1A FLAG/HA (Conway et al., 2018). Human AEBP2-L (NM_001114176.1), AEBP2-S (NM_001267043.2) and EZH2 (NM_001203247.1) ORFs were available in the gateway cloning-compatible entry vector PCR8 (pCR8/GW/TOPO cloning – Invitrogen). Mutant hAEBP2 and hEZH2 ORFs were generated by Q5 Site-Directed Mutagenesis (NEB E0554S) as per the manufacturer's protocol and sequences were confirmed using Sanger sequencing. Expression clones were then generated using Gateway LR Clonase II (ThermoFisher 11791020).

Using similar techniques, codon-optimised hAEBP2-L and hAEBP2-S were ordered as G-blocks from IDT and cloned into a pCR8/GW/TOPO entry vector (Invitrogen K250020). Using Gateway LR Clonase II technology, these constructs were expressed in the expression vector PLEX_305-N-dTAG. This plasmid fuses a $FKBP^{F36V}$ degron tag to the N' terminus of the protein rendering it rapidly degradable upon application of an appropriate PROTAC molecule.

2.2.4 Genotyping of genome-edited cell lines

Single GFP+ cells following nucleofection and single cell sorting (Section 2.1.2) were seeded on 96-well plates. Following numerous population doublings, the plate was split with one plate spared for genotyping and the other for passaging. The cells on the genotyping plate, once confluent, were pelleted by centrifugation at 100g for 5 minutes, washed once with DPBS and resuspended in 20µl of QuickExtract DNA Extraction Solution 1.0 (Lucigen). Cell lysates were transferred to PCR strip tubes using a multichannel pipette, then heated in a thermocycler for

15 minutes at 65°C for 15 minutes, followed by 68°C for 15 minutes and finally 98°C for 10 minutes. As per the manufacturer's protocol, 3µl of "quick extracted" gDNA was added to a mixture of genotyping primers and OneTaq Quick-Load 2X Master Mix with Standard Buffer (NEB M0486). Subsequently, this mixture was PCR amplified and clones were screened using gel electrophoretic analysis.

2.2.5 shRNA generation for targeted RNA interference

98-mer DNA oligonucleotides were designed using the Broad Institute RNAi Consortium GPP Portal and based on previously published shRNA oligonucleotides (Fellmann et al., 2013). The oligonucleotide was diluted in DNAse, RNAse-free H_20 to 0.05ng/µl. As per miRE cloning, overhangs with restriction sites for Xho(5') and EcoRI(3') were added by PCR to the oligonucleotide as per Table 2.3 and run on a thermocycler as per Table 2.4.

Primer miRE_XhoF: TACAATACTCGAGAAGGTATATTGCTGTTGACAGTGAGCG
Primer miRE_EcoRI: TTAGATGAATTCTAGCCCCTTGAAGTCCGAGGCAGTAGGCA

Table 2.3 PCR reaction mixture for miRE cloning

Component	Stock	Volume
5x PCR Buffer	5x	10µl
miRE_Primer mix	10µM each	4µl
dNTP mix (Invitrogen 18427088)	10mM each	1.5µl
Platinum Superfi DNA polymerase (Invitrogen 12351010)	-	0.5µl
ddH20	-	33µl
Sample (oligo DNA)	-	1µl
TOTAL	-	50µl

Table 2.4 PCR cycle for miRE cloning

Step	Temperature (°C)	Time (seconds)	
Initial denaturation	98	30	
Denaturation	98	15	32 cycles
Annealing	72	20	
Final extension	72	300	
Hold	4	∞	

Following completion of the PCR cycle, 5µl of the reaction mixture was run on a 1.5% agarose gel to ensure amplification of a band >100bp in size and the remaining 45µl was digested using EcoRI-HF (NEB R3101) and XhoI (NEB R0146) at 37°C in a thermocycler for 4 hours. The digested reaction was then purified using a QIAquick PCR Purification Kit (Qiagen 28104) and eluted in 30µl of elution buffer.

SGEP (miR-30 variant)-based RNAi plasmid (Addgene 111170) was digested using EcoRI and XhoI as detailed above. The digested plasmid was run on a 1% agarose gel, gel extracted using a QIAquick gel extraction kit (Qiagen 28706) and purified using the QIAquick PCR Purification Kit.

The digested, purified oligonucleotide following miRE PCR and digested, purified SGEP backbone were ligated using T4 DNA ligase (NEB M0202) by incubating at room temperature for 25 minutes. The ligation mixture was immediately transformed in Top10 chemically competent *E. coli* (Invitrogen). Several colonies were prepared and the presence of the correct shRNA sequence was confirmed by Sanger sequencing.

2.2.6 Copy number qPCR of gDNA

Genomic DNA (gDNA) was extracted from lymphoma cell lines using the QiaAMP DNA Blood Minikit (Qiagen 51106) as per manufacturer's protocol. The human haploid genome is estimated by Celera/Human Genome Project to be $3.0x10^9$ base pairs and based on an estimated base pair mass of $1.096x10^{-21}$/bp, the mass of the human genome is estimated to be ($3.0x10^9$ x $1.096x10^{-21}$) = 3.3x10-^{12}g or 3.3pg. Therefore in diploid cells there should be 2 gene copies per 6.6ng of DNA. A standard curve was generated using 660ng, 66ng, 6.6ng, 0.66ng, 0.066ng of gDNA extracted from a known diploid human cell line (Human Mammary Epithelial Cells/HMEC (ATCC). A PCR reaction was set up as per Table 2.5 and analysed by qPCR using SYBR Green I detection chemistry (NEB M3003E) on an Applied Biosystems Quant Studio 3 platform. The copy number of the gene of interest (AEBP2) in 66ng and 6.6ng for each lymphoma cell line was determined using the equation of the line for the standard curve.

Table 2.5 PCR reaction mixture for copy number qPCR

Component	Stock	Volume
SyBR Green I MasterMix	2x	10µl
Sequencing Primers (F+R)	10µM	0.5µl
Sigma H_2O	-	5.5µl
gDNA	-	4µl
TOTAL	-	20µl

2.2.7 Chromatin immunoprecipitation (ChIP)

Cells were counted and normalised cell pellets of equal cell number (up to $50x10^6$ per cell line) were washed twice with DPBS before crosslinking for 10 minutes with 1% formaldehyde (Sigma) in DPBS. The crosslinking reaction was quenched with 125mM glycine for 5 minutes before two further PBS washes. Crosslinked cells were lysed in 6mls of SDS lysis buffer (10mM NaCl, 50mM Tris pH 8.1, 5mM EDTA pH 8.0, 0.5% SDS, 2µg/ml aprotonin, 1µg/ml leupeptin and 1mM PMSF). Chromatin was pelleted by centrifugation at 1200 RPM for 6 minutes at room temperature. The supernatant was discarded and the chromatin was resuspended in 1ml of ChIP buffer (2:1 dilution of SDS lysis buffer : Triton dilution buffer (100mM Tris pH 8.6, 100mM NaCl, 5mM EDTA pH 8.0, 0.02% NaN_3, 5% Triton X-100, 2µg/ml aprotonin, 1µg/ml leupeptin and 1mM PMSF)). Chromatin was sheared to fragments of 200-800bp length by sonication using a Branson Sonifier SFX 150, set for successive pulses of 1 second on, 4 seconds off at 50% amplitude for a total sonication time of 4 minutes. Sonication efficiency was determined by analysing a sample of fragmented DNA on a 1.5% agarose gel. Chromatin was quantified using a Qubit dsDNA High Sensitivity Assay Kit (ThermoFisher Q32854). 1% input samples were taken from well-sonicated chromatin as an appropriate quantity of chromatin was added to respective antibodies and incubated overnight whilst rotating at 4°C.

After the overnight incubation, 40µl of equilibrated Protein G/A Dynabeads (Invitrogen) were added to the respective chromatin-antibody mixes and left to rotate for 2-4 hours at 4°C. After this, all beads were washed three times in mixed micelle wash buffer (150mM NaCl, 20mM Tris pH 8.1, 5mM EDTA pH 8.0, 5.2% Sucrose, 1% Triton X-100, 0.2% SDS), twice with buffer 500 (0.1% sodium deoxycholate, 1mM EDTA pH 8.0, 50mM HEPES pH 7.5, 1% Triton X-100), twice with LiCl detergent wash (0.5% sodium deoxycholate, 1mM EDTA pH 8.0,

250mM LiCl, 0.5% NP-40, 10mM Tris pH 8.0) and finally once with TE (10mM Tris pH 8.0, 1mM EDTA pH 8.0). Immunoprecipitated material was eluted from the magnetic beads with elution buffer (0.1 M $NaHCO_3$, 1% SDS) while shaking for 1 hour at 65°C. This supernatant was retained and de-crosslinked alongside input samples overnight, shaking at 65°C.

The following day, these samples were treated with RNaseA (ThermoFisher) at 37°C for 1 hour and Proteinase K (Sigma) at 55°C for 2 hours prior to column-based DNA fragment purification (Qiagen or ThermoFisher). ChIP enrichment was established by qPCR using the SYBR Green I detection system on an Applied Biosystems Quant Studio 3 platform.

Due to lack of enrichment for AEBP2 and FLAG/HA-tagged exogenous AEBP2 on ChIP qPCR, additional crosslinking for 1 hour at room temperature using 2mM EGS (ethylene glycol bis – succinimidyl succinate) prior to standard 1% formaldehyde crosslinking for 10 minutes was utilised. Additional sonication steps were required to yield DNA fragments within the desired size range. Ultimately this approach did not yield greater enrichments for these antibodies in lymphoma cell lines.

2.2.8 Quantitative chromatin immunoprecipitation relative to an exogenous reference genome (ChIP-Rx)

Quantitative chromatin immunoprecipitation relative to a reference exogenous genome (ChIP-Rx) coupled with massively parallel DNA sequencing was performed for genome-wide mapping of histone post-translational modifications and SUZ12, as previously described (Orlando et al., 2014). E14 wild-type mouse embryonic stem cells were processed as the spike-in reference genome for all lymphoma cell line ChIPs. Spike-in chromatin was added to well-sonicated human lymphoma cell line chromatin at a ratio of 1:9 prior to overnight incubation with antibody. Purified DNA at the end of the ChIP protocol (section 2.2.6) was quantified using the Qubit dsDNA High Sensitivity Assay Kit. ChIP-Rx sequencing libraries were prepared using the NEBNext Ultra II DNA Library Kit for Illumina (NEB E7645) and NEBNext Multiplex Oligos for Illumina (Index Primer Sets 1, 2 and 4; NEB E7335, E7500 and E7730) as per the manufacturer's protocol. Input DNA was standardised per ChIP antibody (range 1-50ng). Following adaptor ligation, DNA was PCR amplified for 4-8 cycles depending on input DNA amount. PCR-amplifed DNA was purified using AMPure XP beads (Beckman Coulter A63881) and warmed to room temperature. The quality of DNA libraries was

examined on a High Sensitivity D1000 Screen Tape (Agilent). The libraries were then used for cluster generation and sequencing using an Illumina NextSeq 500, with 75bp length. Reads were aligned to the human genome hg38 and mouse reference genome mm10 using Bowtie v2.10 (Langmead & Salzberg, 2012). A normalisation factor was generated by establishing the number of human reads relative to spike-in mouse genome. Ambiguous reads aligning to more than one reference genome and duplicated reads were removed.

Bioinformatic analyses were performed by Darragh Nimmo and Dr Craig Monger (EZH2/AEBP2 shRNA ChIP-Rx) and Dr Cheng Wang (isogenic system ChIP-Rx). Bigwig files were generated at 10bp resolution using the bamCoverage utility from the deepTools suite (Ramírez et al., 2016) and the data was visualised using the UCSC genome browser. Peaks were called using MACS2 with FDR <0.05 (Yong Zhang et al., 2008) and annotated using HOMER (Heinz et al., 2010).

2.3 RNA methods

2.3.1 RNA preparation for RT-qPCR analysis

5 million cells per replicate were harvested, washed twice in PBS, snap frozen in liquid nitrogen and stored at -80°C until processing. Total RNA was extracted from cells using the RNeasy kit (Qiagen) as per the manufacturer's protocol. cDNA was synthesised from 1µg of input RNA by reverse transcription PCR using the High-Capacity cDNA Reverse Transcription Kit with RNase Inhibitor (Applied Biosystems 4374966) with 1Oligo-$dT_{(18)}$ primers. Relative RNA abundance was determined by SYBR Green I detection chemistry (NEB M3003E) on the Applied Biosystems QuantStudio 3 Real-Time PCR System. Rplp0 mRNA was used as a quantitative normaliser.

2.3.2 QuantSeq 3' mRNA sequencing for RNA quantification

RNA was purified from 5 million human lymphoma cells per condition and per replicate as detailed in section 2.3.1 using the RNeasy kit (Qiagen). cDNA was generated from this RNA for quantification by sequencing using the QuantSeq 3' mRNA-Seq Library Prep FWD Kit for Illumina (Lexogen) using 500ng total RNA as input. The optimal number of PCR cycles for endpoint PCR was determined by qPCR assay using the PCR Add-on Kit for Illumina

(Lexogen Cat. No. 020). Individual i7 indexing primers were amplified by PCR with synthesised cDNA and purified. The quality of DNA libraries was examined on a High Sensitivity D1000 Screen Tape (Agilent). The libraries were subsequently used for cluster generation and sequenced using an Illumina NextSeq500 (ID: NB501524), with single end 75bp read length.

Raw sequencing reads were aligned to the human genome (hg38) using HISAT2 (Pertea et al., 2016) and the aligned files were converted to bigwig files using bamcoverage (Ramírez et al., 2014). Sequence reads were aggregated into a count for each gene using featurecounts (Liao et al., 2014) and differentially expressed genes were identified using DESeq2 (Love et al., 2014). Volcano plots of differentially expressed genes were generated using EnhancedVolcano (Blighe et al., 2019).

2.4 Protein methods

2.4.1 Preparation of whole cell protein lysates and western blotting

Suspension cells were harvested by centrifugation and pelleting, while adherent cells were harvested by scraping or trypsinisation. They were washed twice in cold PBS and either snap frozen in liquid nitrogen and stored at -20°C until processing or lysed immediately in cold High salt buffer (50mM Tris-HCl pH 7.2, 300mM NaCl, 0.5% (v/v) NP-40, 1mM EDTA pH 7.4, 2µg/mL Aprotinin, 1µg/mL Leupeptin, 1mM PMSF). Cells were sonicated (continuous mode for 10 seconds at 40% amplitude), incubated with rotation at 4°C for 20 minutes and then clarified by centrifugation at 21,000g for 20 minutes at 4°C. Bradford Assays were performed to determine the concentration of protein lysates and samples were normalised to the same concentration. Denatured protein lysates were separated on SDS-PAGE (in-house) or Bolt Bis-Tris (Invitrogen) gels alongside a Chameleon Duo Pre-Stained Protein Ladder (Li-COR) and transferred to nitrocellulose (0.2µM, Amersham) membranes. Membranes were blocked against nonspecific binding and then incubated with the relevant primary antibody either overnight at 4°C or for one hour at room temperature for certain primary antibodies. Secondary antibodies were applied for one hour at room temperature. Subsequently, relative protein levels were determined by chemiluminescence or infrared fluorescence detection on a Li-COR Odyssey FC.

2.4.2 Cellular fractionation

Cells were harvested and washed twice with cold PBS. The pellet was lysed in 2-3 pellet volumes of Buffer A (25mM HEPES pH 7.6, 5mM $MgCL_2$, 25mM KCl, 0.05mM EDTA, 10% Glycerol, 0.1% NP-40, 1mM DTT, 2µg/mL Aprotinin, 1µg/mL Leupeptin, 1mM PMSF) and incubated on ice for 15 minutes. The suspension was then transferred to a dounce homogeniser and douced 8 times with a type A (loose) pestle to break the cell membrane. Lysates were centrifuged at 500rcf for 5 minutes in a 4°C centrifuge and the supernatant collected and labelled as the cytoplasmic fraction.

The pellet was washed once with Buffer A, centrifuged at 500 RCP for 5 minutes at 4°C and the supernatant carefully but completely discarded. The pellet was resuspended in 1ml of buffer S1 (120mM NaCl, 20mM HEPES pH 7.6, 1.5mM $MgCl_2$, 0.2mM EDTA, 10% Glycerol, 1mM DTT, 2µg/mL Aprotinin, 1µg/mL Leupeptin, 1mM PMSF), transferred into a dounce homogeniser and dounced 15 times with a type B (tight) pestle to break the nuclear membrane. The lysate was centrifuged at 21000g for 15 minutes at 4°C, the supernatant was collected and labelled as the nuclear soluble fraction.

The samples were centrifuged again and all residual supernatant removed. The samples were resuspended in 2-3 pellet volumes of buffer S2 (420mM NaCl, 20mM HEPES pH 7.6, 1.5mM $MgCl_2$, 0.2mM EDTA, 10% Glycerol, 1mM DTT, 2µg/mL Aprotinin, 1µg/mL Leupeptin, 1mM PMSF) and incubated for 30 minutes at 4°C with rotation. An equal volume of buffer D (25mM HEPES pH 7.6, 5mM $MgCl_2$, 0.2mM EDTA, 1mM DTT, 2µg/mL Aprotinin, 1µg/mL Leupeptin, 1mM PMSF) was then added to the samples to dilute the buffer S2. Benzonase nuclease (Sigma E1014) was added to each sample at a final concentration of 0.15 U/µl and incubated for 1.5 hours at 4°C with rotation. The samples were then centrifuged at 21000g for 30 minutes to separate the insoluble fraction from the chromatin-bound protein extract. The supernatant was collected containing the chromatin-bound protein fraction. The protein content of all three fractions (cytoplasmic, nuclear soluble and chromatin-bound) was then quantified by Bradford assay and the samples were processed for Western blot as above (section 2.4.1).

2.4.3 HA/FLAG immunoprecipitation

Snap frozen cells were thawed on ice and lysed in 650µl of high salt buffer (50mM Tris pH 7.2, 300mM NaCl, 1mM EDTA pH 7.4, 0.5% NP-40, 2µg/mL Aprotinin, 1µg/mL Leupeptin, 1mM PMSF). The lysates were then sonicated for 10 seconds at 40% amplitude and incubated for 20 minutes at 4°C with rotation. Lysates were then diluted with 650µl of no salt buffer (50mM Tris pH 7.2, 1mM EDTA pH 7.4, 0.5% NP-40, 2µg/mL Aprotinin, 1µg/mL Leupeptin, 1mM PMSF) and clarified by centrifugation at 21000g for 20 minutes at 4°C. Pierce magnetic Anti-HA beads for HA-IP (ThermoFisher 88836) and mouse IgG-coupled beads (Sigma) were washed 4 times for 5 minutes each in 1ml of PBS-T (PBS supplemented with 0.1% tween) with one final wash in wash buffer (1:1 ratio of high salt buffer : no salt buffer). For FLAG-IP, FLAG beads were washed as above (beads gift from Dr. Claudio Ciferri, Genentech, San Francisco).

The lysate protein was quantified by Bradford assay with normalisation to the lowest concentration lysate. The lysates were equilibrated with mouse IgG beads for 1 hour at 4°C with rotation. The mouse IgG beads were removed by centrifugation. 5-20% input samples were taken and the immunoprecipitation was set up with 20µl packed anti-HA or anti-FLAG. beads added to each sample (with 1µg of protein per IP). Benzonase nuclease was added to each IP to a final concentration of 2.5U/ml and the samples were incubated overnight at 4°C with rotation. HA-tagged complexes were then eluted from the anti-HA beads in 60µl of Elution buffer (1:50 dilution of Influenza Haemagglutinin (HA) peptide (Sigma I2149) in wash buffer to a final concentration of 1mg/ml) by incubating at 37°C for 10 minutes on a shaking incubator. Similarly, FLAG-tagged complexes were eluted by addition of competitive 3xFLAG peptide (Sigma F1804). The eluates were then denatured and processed for Western blot.

2.4.4 Endogenous immunoprecipitation

Cell lines were harvested as previously described, washed twice in ice-cold PBS and washed pellets were resuspended in 10mls of Buffer A (25mM HEPES pH 7.6, 5mM $MgCl_2$, 25mM KCl, 0.05M EDTA, 10% (v/v) Glycerol, 0.1% NP-40, 1mM DTT, 2µg/mL Aprotinin, 1µg/mL Leupeptin, 1mM PMSF). Samples were incubated for 10 minutes at 4°C with rotation. Nuclei were then pelleted by spinning at 500rcf for 10 minutes in a 4°C centrifuge. Nuclear pellets were resuspended in 4.5mls of Buffer C (10mM HEPES pH 7.6, 3mM MgCl2, 100mM KCl,

0.5mM EDTA, 10% (v/v) Glycerol, 1mM DTT, 2µg/mL Aprotinin, 1µg/mL Leupeptin, 1mM PMSF). 1/10 volume 3M Ammonium Sulphate $(NH_4)_2SO_4$ made in Buffer C was then added to each sample and they were incubated on ice for 20 minutes. Lysates were transferred into 5ml Beckman Coulter ultracentrifuge tubes (Beckman Coulter 344057) compatible with swinging bucket SW 55 Ti and spun for 15 minutes at 4°C at 350,000rcf. The lysates were transferred to new 15ml tubes and nuclear extracts were precipitated by adding 300mg $(NH_4)_2SO_4$ per 1ml lysate to each tube. Samples were incubated on ice for 20 minutes, transferred to fresh ultracentrifuge tubes and spun at 350,000rcf for 15 minutes at 4°C. The supernatant was removed and the protein pellet was resuspended in 1ml of IP buffer (300mM NaCl, 50mM Tris-HCl pH 7.5, 1mM EDTA, 1% Triton X-100, 1mM DTT, 2µg/mL Aprotinin, 1µg/mL Leupeptin, 1mM PMSF). At this time, a Bradford assay was performed to quantify the total protein yield. 500µg of protein was diluted to a total volume of 500µl of IP buffer. A 5-10% input sample was retained at this time. 1µl of Benzonase nuclease was added alongside 1µg of primary antibody to the IP samples and the mixture was incubated overnight at 4°C with rotation. Protein G magnetic Dynabeads (Invitrogen) were washed 5 times in IP buffer. 20µl of packed beads was added to each IP and the bead-IP mixture was incubated for 2 hours at 4°C with rotation, followed by bead collection on a magnetic rack and removal of the supernatant. The beads were then washed five times with 1ml of 4°C IP buffer (each wash for 5 minutes at 4°C with rotation). The samples were eluted in 50µl of Bolt loading dye sample buffer (Biosciences B0008) and incubated at 95°C on a shaking incubator for 5 minutes. The beads were removed and the samples brought forward for Western blot analysis.

2.5 EZH2 and EZH1 staining of paraffin-embedded lymph node biopsies

Professor Elisabeth Vandenberghe identified two well-matched patients with histological grade 2A follicular lymphoma with available material in the St James' Hospital lymphoma bio-bank (ethical approval 2020-09-(01)) which was then analysed as follows for assessment of EZH1 and EZH2 expression by Aoibhinn Mooney (histopathology laboratory scientist) and Professor Richard Flavin (Consultant Histopathologist).

2.5.1 Assessment of EZH2 expression using immunohistochemical analysis

Patient slides were loaded onto the Ventana Benchmark Ultra Autostainer (Roche Diagnostics, Risch-Rotkreuz, Switzerland). The following protocol was used; slides were deparaffinised at 72ºC, followed by a pre-treatment step (antigen retrieval), using Cell conditioning 1 (CC1) (Roche Diagnostics) for 32 min at 100ºC. Slides were incubated with anti-EZH2 rabbit monoclonal concentrate primary antibody (D2C9) (Cell signaling) at a dilution of 1:150 for 24min at 36ºC. These working solutions were made using the Roche Diagnostics antibody diluent. The bound primary antibody was then visualized using the OptiView detection kit (Roche Diagnostics) with 3,3'- diaminobenzidine tetrahydrochloride (DAB) chromogen, as per the manufacturer's instructions. Slides were counterstained in Heamatoxylin II for 4 min and post counterstained with bluing reagent for 4 min. Once staining was completed, the slides were unloaded from the autostainer and immersed in a mild detergent to remove the liquid coverslip (LCS). The slides were then dehydrated in alcohol, cleared in xylene and cover-slipped using the Tissue-Tek® Glas™ Cover slipper (Sakura®, The Netherlands).

2.5.2 Assessment of EZH1 expression using RNA in-situ hybridisation

Patient slides were deparaffinised with two changes of xylene for 5 min each, followed by two changes of 100% alcohol for 1 min each, and air-dried for 5 min at RT. RISH was performed manually using an EZH1 probe (RNAscope® Probe – Hs-EZH1, ACD Biotechne®, Newark, USA) in conjunction with the RNAscope® 2.5 HD Reagent Kit – RED (ACD Biotechne®), as per manufacturer's instructions. Briefly samples were pre-treated with 5-8 drops of hydrogen peroxide for 10 min at RT, followed by washing 3 times in distilled water. Target retrieval was performed by boiling slides in RNAscope® 1X Target Retrieval Reagent for 20 min. The slides were rinsed with distilled water, followed by a wash with 100% alcohol, and allowed to air dry. A barrier was drawn around the tissue sections using the Immedge™ hydrophobic barrier pen. Once the barrier was dry, the slides were placed on a HybEZ™ Slide Rack and 5 drops of RNAscope® Protease Plus was added to each slide. The HybEZ™ Slide Rack was placed in the pre-warmed HybEZ™ Humidity Control Tray. The lid was closed, sealed and the tray was inserted back into the HybEZ™ oven at 40ºC and incubated for 30 min. The slides were removed and washed 3 times in distilled water. Following pre-treatment, the RNAscope® assay was performed. Four drops of the EZH1 probe – Hs-EZH1 (Cat no: 528941) was applied to all slides, ensuring the probe entirely covered each section. The lid was placed on the HybEZ™ Humidity Control Tray and placed in the oven at 40ºC for 2 hours to hybridize. The

HybEZ™ Humidity Control Tray was then removed from the oven and the slides were washed in two changes of 1X Wash Buffer at RT for 2 min each. Next, the slides were hybridized in the same means at 40ºC with 4 drops of AMP 1 for 30 min, AMP 2 for 15 min. AMP 3 for 30 min and AMP 4 for 15 min. The slides were hybridized in the same manner at RT with 4 drops of AMP 5 for 60 min and AMP 6 for 15 min. The slides were washed between each AMP reagent with two changes of 1X Wash Buffer at RT for 2 min each. To detect the target mRNA signals, a RED working solution was prepared using a 1:60 ratio of Fast RED-B to Fast RED-A and 120µl red solution was pipetted onto each slide in the HybEZ™ Slide Rack. The HybEZ™ Slide Rack was placed in the HybEZ™ Humidity Control Tray. The lid was sealed and the slides were incubated at RT for 10 min. Following incubation, the HybEZ™ Slide Rack was removed from the HybEZ™ Humidity Control Tray and the slides were rinsed with tap water. The slides were then counterstained with 50% Gills Heamatoxylin for 2 min at RT, and dried in a 60ºC oven for 15 min. Subsequently, the slides were placed into fresh xylene and cover slipped using the Tissue-Tek® Glas™ Cover slipper.

2.6 Evolutionary conservation analysis

AEBP2 and SUZ12 sequences from selected named species were collected from the UniProt database (Bateman et al., 2021) (Figure 4.12). Alignment was performed by the EMBL-EBI high speed multiple sequence alignment programme MAFFT (Katoh & Standley, 2013; Madeira et al., 2019). Protein alignment data was analysed using Jalview Desktop software (version 2.11.2.4; Waterhouse et al., 2009).

2.7 Primers and Oligonucleotides

Table 2.6 ChIP-qPCR primers

PCR Primer	Forward	Reverse
h*CcnA2* promoter	TGACGTCATTCAAGGCGA	GCTCAGTTTCCTTTGGTTTAC
h*Atf3* promoter	TGTTTTTTCTTTTGCGTTTGGC	TCGTGGCAACCAAATCTAAACAG
h*Flt3* promoter	TCTCTTAAGGATGCGCGTCAC	CCCCTTCCACTTTGCACCAG
h*Olig2* promoter	AGCCACGGCCATCTCCTAGAC	CAGGCACAAAGTCCCCACTATC
h*RarB* promoter	CATCCCAGTCCTCAAACAGCTC	GGGTCTATTCTTTGCCAAAGGG
h*MYC* enhancer	AGGAGCCCACCTTCTCATTT	ACATTGCAAGAGTGGCTGTG
h*ActinB* gene body	CCCAGATTGGGGACAAAGGAAG	CGACCAGTGTTTGCCTTTTATGG

Table 2.7 CRISPR knockout genotyping primers

PCR Primer	Forward	Reverse
hAEBP2_intron2seq	AGGTCAACAAGTGATTTGCAGAG	CAAACTAAAATCCAGCACATACCC

Table 2.8 RT-qPCR primers

PCR Primer	Forward	Reverse
m*RPLPO*	TTCATTGTGGGAGCAGAC	CAGCAGTTTCTCCAGAGC
h*AEBP2_exon5*	CACGGCCACATGATTTCTTC	CACGGCCACATGATTTCTTC
h*EZH2*	GCCAGACTGGGAAGAAATCTGAGAA	AGCTGTCTCAGTCGCATGTACTCTGA
h*MTF2*	CCAGAAAAAGAACGCGTACAGG	CTTCTCCGCAAATGTGGTATTG
h*IRF4*	AGAAGAGCATCTTCCGCATC	CCTTTAAACAGTGCCCAAGC
h*PRDM1*	CTACCCTTATCCCGGAGAGC	GCTCGGTTGCTTTAGACTGC
h*CDKN1A*	GGAAGACCATGTGGACCTGT	TAGGGCTTCCTCTTGGAGAA
h*CD138/SDC1*	GAGCAGGACTTCACCTTTGA	TTCGTCCTTCTTCTTCATGC
h*CD38*	CAACTCTGTCTTGGCGTCAGT	CCCATACACTTTGGCAGTCTACA
h*JCHAIN*	TCCTGGCGGTTTTTATTAAGGC	AGTAATCCGGGCACACTTACAT
h*IL16*	ACGAAGCTACTTGACGAAAAGAC	GTTTCAGCAGAACCATTTGCAG
h*DLX1*	TGCCAGAAAGTCTCAACAGCC	CGAGTGTAAACAGTGCATGGA

Table 2.9 sgRNA target sequences

sgRNA	Target Sequence	PAM sequence (hg38)
hRPA3	GATGAATTGAGCTAGCATGC	CGG
ROSA	GAAGATGGGCGGGAGTCTTC	N/A
NTC	GTAGCGAACGTGTCCGGCGT	N/A
h*EZH2_sg1*	TTATCAGAAGGAAATTTCCG	AGG
h*EZH2_sg2*	TTATGATGGGAAAGTACACG	GGG
h*EED_sg1*	AAGAGAATGATCCATACCAC	AGG
h*EED_sg2*	ACAAACACGCCAAATGCACC	TGG
h*SUZ12_sg1*	GAGACTCTCTGAATTTCTAG	TGG
h*SUZ12_sg2*	GGAGACTATTCTTGATGGGA	AGG
h*AEBP2_ZF1_sg1*	AGTTGAAGCAAGCCTGGCAC	TGG
h*AEBP2_ZF1_sg2*	GGCTAGAGTTGAAGCAAGCC	TGG
h*AEBP2_ZF2_sg1*	AACCAACTTTGACTGGTAGA	TGG
h*AEBP2_ZF2_sg2*	CCTTTGTAACCAACTTTGAC	TGG
h*AEBP2_ZF3_sg1*	CAGTGGAGACAAACCTTTCA	AGG
h*AEBP2_ZF3_sg2*	ACATGCATCCTTACCTTGAA	AGG
h*AEBP2_ZF3_sg3*	GCCAGCTTTGCTTCTCAGGG	AGG
h*AEBP2_KRM*	AAGCTGGAATGAACAAAAGG	AGG
h*AEBP2_SBH_sg1*	CTTTCATTCACCCACACATC	AGG
h*AEBP2_SBH_sg2*	TTCATAGTCTGCCTGATGTG	TGG
h*JARID2_UIM_sg1*	ACCACCCGTTCTTCTGACCA	CGG
h*JARID2_UIM_sg2*	GGATTCCGTGGTCAGAAGAA	CGG
h*JARID2_UIM_sg3*	TCCGTGGTCAGAAGAACGGG	TGG
h*JARID2_PIM_sg1*	CTTACCTCGAAGGCAGAGAA	AGG
h*JARID2_PIM_sg2*	CTTACCTTTCTCTGCCTTCG	AGG
h*JARID2_PIM_sg3*	GTTGCAAAGTCTTACCTCGA	AGG
h*JARID2_PIM_sg4*	TTGGGCAGCGCAGGAGAACC	TGG
h*MTF2_sg1*	ATGGTTATATGTGACAAGTG	TGG
h*MTF2_sg2*	GCAGACATTACCCTATAGTG	TGG
h*AEBP2ko_Intron1_sg1*	GTTACTATGCTTTGTTCACA	TGG
h*AEBP2ko_Intron1_sg2*	GATGTGATAAGCTGTGTGTG	GGG
h*AEBP2ko_Intron2_sg3*	TAATAAAACTAACGAAAACA	GGG
h*AEBP2ko_Intron2_sg4*	TTAATTTATAATTGCTAGTT	AGG

Table 2.10 Q5 site-directed mutagenesis primers

Mutant	Forward	Reverse
h*AEBP2_H281A*	TCTGGCAGATGCCATCCGTTCCATAC	TCTGGGCTAGAGTTGAAG
h*AEBP2_I282D*	GGCAGATCACGACCGTTCCATAC	AGATCTGGGCTAGAGTTG
h*AEBP2_C302A*	ATGGAAAGGTGCTAAAGTATATAACACT CCATC	AAGCAAACAAATACCCCTC
h*AEBP2_M319D*	ACAAAGGCATGATCTGACACACAGTGG	AACCAACTTTGACTGGTAG
h*AEBP2_K329D*	CAAACCTTTCGATTGTGTTGTTGGTG	TCTCCACTGTGTGTCAGC
h*AEBP2_Q342K*	CTTTGCTTCTAAGGGAGGGCTAG	CTGGCATTGCAGCCACCA
h*AEBP2_H348A*	GCTAGCTCGTGCTGTACCCACAC	CCTCCCTGAGAAGCAAAG
h*AEBP2_KRM_1*	GCTGCATTAAAGAACAAAAGACGACG	TGCTGCGTTCATTCCAGCTTTAGAAG
h*AEBP2_KRM_2*	GCAGCGTCATTACCACGGCCACAT	GGCGGCGTTCTTTAATGCAGCTGCTG
h*AEBP2_W451A*	TTTGCTTCATGCGATGCCTGAAG	AGTTTGATCTTCCCAGAATC
h*AEBP2_W461A*	GCCTGATGTGGCGGTGAATGAAAG	AGAATGTCTTCAGGCATC
h*EZH2_Y111D*	ACCCATAATGGATTCTTGGTCTC	ACTGAAGCAACTGCATTC
h*EZH2_A677G*	GTGGTGGATGGAACCCGCAAG	AAAATCATTGTTCAAGTTGAACAG AAAGC

Table 2.11 shRNA sequences

shRNA ID	Target	98-mer oligonucleotide (target sequence underlined)
sh*RENILLA*	Non-human	TGCTGTTGACAGTGAGCGCAGGAATTATAATGCTTATCTATAGTGAAGCC ACAGATGTATAGATAAGCATTATAATTCCTATGCCTACTGCCTCGGA
sh*EZH2_1*	Exon	TGCTGTTGACAGTGAGCGCCAGGATGGTACTTTCATTGAATAGTGAAGCC ACAGATGTATTCAATGAAAGTACCATCCTGATGCCTACTGCCTCGGA
sh*EZH2_2*	Exon	TGCTGTTGACAGTGAGCGCCAGCAGAAGAACTAAAGGAAATAGTGAAGC CACAGATGTATTTCCTTTAGTTCTTCTGCTGTTGCCTACTGCCTCGGA
sh*EZH2_3*	Exon	TGCTGTTGACAGTGAGCGAAGCAGAAGAACTAAAGGAAAATAGTGAAG CCACAGATGTATTTTCCTTTAGTTCTTCTGCTGTGCCTACTGCCTCGGA
sh*EZH2_4*	Exon	TGCTGTTGACAGTGAGCGATCGGTGTCAAACACCAATAAATAGTGAAGC CACAGATGTATTTATTGGTGTTTGACACCGAGTGCCTACTGCCTCGGA
sh*EZH2_5*	Exon	TGCTGTTGACAGTGAGCGAACCAATAAAGATGAAGCCAAATAGTGAAGC CACAGATGTATTTGGCTTCATCTTTATTGGTGTGCCTACTGCCTCGGA
sh*EZH2_6*	Exon	TGCTGTTGACAGTGAGCGAAGGGAAAGTGTATGATAAATATAGTGAAGC CACAGATGTATATTTATCATACACTTTCCCTCTGCCTACTGCCTCGGA
sh*AEBP2_1*	Stop codon/3' UTR	TGCTGTTGACAGTGAGCGAAACGACGTTTGCAATCAACTATAGTGAAGC CACAGATGTATAGTTGATTGCAAACGTCGTTCTGCCTACTGCCTCGGA
sh*AEBP2_2*	3' UTR	TGCTGTTGACAGTGAGCGCAGGGACTATGTACTACTGTTATAGTGAAGCC ACAGATGTATAACAGTAGTACATAGTCCCTTTGCCTACTGCCTCGGA
sh*AEBP2_3*	3' UTR	TGCTGTTGACAGTGAGCGCAAGGTGTTTGTGAGATATAAATAGTGAAGC CACAGATGTATTTATATCTCACAAACACCTTATGCCTACTGCCTCGGA
sh*AEBP2_4*	3' UTR	TGCTGTTGACAGTGAGCGAAAGGAGATACTTTGTTTCTAATAGTGAAGCC ACAGATGTATTAGAAACAAAGTATCTCCTTGTGCCTACTGCCTCGGA
sh*AEBP2_5*	3' UTR	TGCTGTTGACAGTGAGCGCAGGGAAGAAATTGTTAGAAAATAGTGAAGC CACAGATGTATTTTCTAACAATTTCTTCCCTTTGCCTACTGCCTCGGA
sh*AEBP2_6*	3' UTR	TGCTGTTGACAGTGAGCGATTCAAGACCAACTTTGGTGCATAGTGAAGC CACAGATGTATGCACCAAAGTTGGTCTTGAAATGCCTACTGCCTCGGA

Table 2.12 List of plasmids

Plasmid	Bacterial Resistance	Mammalian Resistance	Tag	Source
pLENTI FLAG Cas9	Ampicillin	Blasticidin	FLAG	Bracken Lab
pLEX_305	Ampicillin	Puromycin	HA	Addgene 41390
pGIPZ	Ampicillin	Puromycin	GFP	Bracken Lab
pXPR_011_EGFP	Ampicillin	Puromycin	GFP	Bracken Lab
iPUSEPR_EV	Ampicillin	Puromycin	RFP	Dr C. Chen
iPUSEPR_PRC2sgRNAlib	Ampicillin	Puromycin	RFP	Dr C. Chen
LRG2.1	Ampicillin	N/A	GFP	Addgene 108098
SGEP	Ampicillin	Puromycin	GFP	Addgene 111170
pLEX_305-N-dTAG	Chlor/Amp	Puromycin	HA	Addgene 91797
pSpCas9(BB)-2A-GFP (PX458)	Ampicillin	N/A	FLAG/GFP	Addgene 48138
pCR8-hAEBP2-L	Spectinomycin	N/A	N/A	Gift Dr. K Helin
pCR8-hEZH2	Spectinomycin	N/A	N/A	Bracken Lab

Table 2.13 List of primary antibodies

Antibody	Source	Western Blot	IP (µg)	ChIP (µg)
SUZ12	Cell Signalling (3737)	1:2000	1.0	7µl
EZH2	BD43 (Pasini et al., 2004)	1:10	-	-
EZH2	AC22 (Bracken et al., 2006)	-	1.0	-
EED	Cell Signalling (51673S)	1:500	-	-
BMI1	DC9 (Bracken et al., 2007)	1:20	-	-
AEBP2	Cell Signalling (D7C6X)	1:500	-	20 µl
JARID2	Cell Signalling (D6M9X)	1:500	-	-
EPOP	Active Motif (61753)	1:1000	-	-
PHF1	Proteintech (15663-1-AP)	1:500	-	-
MTF2	Proteintech (16208-1-AP)	1:500	-	-
PHF19	Brien et al., 2015	1:500	-	-
Histone H3	Abcam (ab1791)	1:50000	-	-
H3K27ac	Abcam (ab4729)	1:1000	-	2.0 µg
H3K27me1	Active Motif (0321)	1:2000	-	-
H3K27me2	Cell Signalling (9728S)	1:2000	-	2.25 µg
H3K27me3	Cell Signalling (Custom)	-	-	1.0 µg
H3K27me3	Active Motif (0323)	1:2500	-	-
H3K36me2	Abcam (ab9049)	1:2500	-	5 µg
H3K36me3	Abcam (ab9050)	1:2500	-	5 µg
HA	Cell Signalling (3724)	1:500	-	-

FLAG	Sigma-Aldrich (clone M2)	1:1000	-	-
BETA-ACTIN	Proteintech (60008-1-Ig)	1:5000	-	-
GAPDH	Proteintech (60004-1-Ig)	1:5000	-	-
VINCULIN	Cell Signalling (4650)	1:2500	-	-
CyclinA2	Cell Signalling (BF683)	1:500	-	-
MOUSE IgG	Millipore (12-371)	-	2.5	2.0-2.5 µg
RABBIT IgG	Millipore (12-370)	-	2.5	2.0-2.5 µg

Table 2.14 List of secondary antibodies

Antibody	Source	Western Blot
IRDye 800CW Goat anti-Mouse IgG	Li-COR	1:10,000
IRDye 800CW Goat anti-Rabbit IgG	Li-COR	1:10,000
IRDye 680RD Goat anti-Mouse IgG	Li-COR	1:10,000
IRDye 680RD Goat anti-Rabbit IgG	Li-COR	1:10,000
IRDye 680LT Goat anti-Mouse IgG	Li-COR	1:20,000
IRDye 680LT Goat anti-Rabbit IgG	Li-COR	1:20,000
Goat anti-Mouse IgG	Merck (401253)	1:5,000 - 1:10,000
Goat anti-Rabbit IgG	Merck (A0545)	1:5,000 - 1:10,000

CHAPTER 3: Mapping disrupted K27 methylation in EZH2 mutant lymphoma and the differential effects of PRC2 enzymatic inhibition and PRC2 degradation

3.1 Introduction

EZH2 is the enzymatic subunit of Polycomb Repressive Complex 2 (PRC2) and mediates transcriptional repression by catalysing all degrees of lysine methylation at position 27 on the N-terminal tail of histone H3 (Cao & Zhang, 2004). EZH2 is highly expressed in B-cell lymphoid progenitors and deficiency of EZH2 results in defects early in lymphopoiesis including defective V(D)J recombination and the inability to form lymphoid germinal centres (Béguelin et al., 2013; Su et al., 2003). EZH2 expression peaks bi-modally in the life cycle of the B-cell; peaking first in Pre-B stage lymphocytes before declining in resting naïve B cells and peaking once more when B-cells receive antigen stimulation and with T-cell help, enter the lymphoid germinal centre (GC) reaction (van Galen et al., 2004; Velichutina et al., 2010).

Recurrent heterozygous missense mutations in EZH2 at hotspot residues Y646 and less commonly A682 and A692, are well-described and present in up to one quarter of cases of follicular lymphoma and germinal centre-derived diffuse large B-cell lymphoma (GCB-DLBCL)(Bödör et al., 2013; McCabe, Ott, et al., 2012; Morin et al., 2010; Okosun et al., 2014). Y646X (Y646F/Y646S/Y646H/Y646N) mutations are approximately 15-20 times more common than mutations at A682 and A692 in patients. Henceforth in this thesis when referring to "mutant EZH2", I specifically refer to EZH2 with the above mentioned mutations and not to putative "loss-of-function" EZH2 mutations as found in myeloid malignancies and the congenital disorder marked by overgrowth and intellectual disability – Weaver syndrome (Deevy & Bracken, 2019; Ernst et al., 2010; Nikoloski et al., 2010; Tatton-Brown et al., 2013).

Initially understood to confer a loss of function phenotype due to the impaired ability of purified mutant EZH2 to monomethylate a biotinylated peptide (Morin et al., 2010), further work revealed that mutant EZH2 is actually significantly more efficient that wild-type EZH2 at higher order methylation (di- and tri-methylation) of H3K27 (Sneeringer et al., 2010; Yap et al., 2011). Thus, this mutation is often characterised as "gain-of-function" or perhaps more accurately "change-of-function" as a small portion of genomic loci lose H3K27me3 in the presence of this mutation (Souroullas et al., 2016). Mutated EZH2 requires an intact wild-type EZH2 allele to perform mono-methylation of nucleosomal H3 substrate before the mutant allele rapidly catalyses di- and tri-methylation of H3K27me1. *In vitro* analyses revealed that wild-type EZH2 has a preference for H3 substrate with less methylation, with a H3K27me0:me1:me2 k_{cat}:K_m (reflecting catalytic activity of a given substrate) of 9:6:1.

However, the EZH2 Y646F and A682G alleles have H3K27me0:me1:me2 k_{cat}:K_m of 1:2:13 and 1.1:0.6:1 respectively, resulting in aberrant accumulation of the H3K27me3 mark in cell lines carrying these mutations (McCabe, Graves, et al., 2012; Sneeringer et al., 2010). This intriguing work also revealed that the uncommon A682G mutant does not require a wild-type EZH2 allele for its activity and as a methyltransferase is just as active at H3K27 trimethylation as the Y646F mutant.

Hyper-trimethylation at H3K27 is advantageous for lymphoma cells for a number of reasons. Lymphoma cells bearing elevated H3K27me3 have a proliferative advantage, resulting in enlarged, hyperplastic germinal centres and the amassing of cells in the GC light zone, due at least in part to aberrant silencing of numerous tumour suppressor genes including CDKN1A/p21 and Sestrin1 (Béguelin et al., 2013, 2020; Oricchio et al., 2017). In fact, aberrant spreading of H3K27me3 in the lymphoma EZH2 mutant context results in the silencing of de novo H3K27me3-marked topologically associating domains (TADs) including some containing tumour suppressor genes (Donaldson-Collier et al., 2019). These TADs can be reactivated by treatment with the EZH2 enzymatic inhibitor Tazemetostat. Furthermore, it was revealed that promoters marked bivalently by H3K4me3 and H3K27me3 in GC B-cells are preferentially bound by EZH2 and these bivalent genes (enriched for gene sets associated with exit from the germinal centre and terminal differentiation) are more highly repressed in the presence of the EZH2 mutant (Béguelin et al., 2013). Although the presence of the EZH2 mutation does correlate with reduced expression of genes essential for the B-cell terminal differentiation programme, this does not correlate with a reduction in long-lived Memory B-cells or antibody-producing plasma cells (Béguelin et al., 2020). Instead, the EZH2 mutation results in a significant increase in dividing centrocytes in the light zone of the GC as well as significant down-regulation of cellular pro-apoptotic signals (Béguelin et al., 2020).

The altered landscape of H3K27 methylation marks conferred by mutant EZH2 is not simply due to its hyper-trimethylation activity. Indeed, ChIP-Seq in melanoma and lymphoma cell lines expressing mutant EZH2 has demonstrated that while most genomic loci gain H3K27me3, a smaller number actually lose this mark (Souroullas et al., 2016). Arising from this data was the understanding that mutant EZH2 results in global redistribution of the H3K27me3 mark, from highly focal peaks in $EZH2^{WT/WT}$ cells to a larger number of broad but less focal peaks in $EZH2^{Y646X/WT}$ cells. ChIP-Rx of $EZH2^{WT}$ and $EZH2^{Y646F}$ murine non-malignant centroblasts and centrocytes revealed that *de novo* H3K27me3-marked promoters in

EZH2 mutant cells tended to be adjacent to H3K27me3 peaks in wild-type cells, inferring spreading of the mark. Concomitant RNA-Seq demonstrated that in the EZH2 mutant context, downregulated genes were usually just upstream or downstream of wild-type H3K27me3 peaks, whilst upregulated genes did not contain H3K27me3 peaks and surrounding TSSs had a more modest gain in H3K27me3 (Béguelin et al., 2020). Surprisingly, quantitative chromatin immunoprecipitation relative to an exogenous reference genome (ChIP-Rx) of H3K27me2 and H3K27me3 in an EZH2-mutant lymphoma has not yet been published.

Knockdown of EZH2 by siRNA and shRNA, as well as EZH2 enzymatic inhibition, have been shown to block GC lymphocyte proliferation and reduce H3K27me3 levels in lymphoma cells (Béguelin et al., 2013; Knutson et al., 2014; McCabe, Ott, et al., 2012; Qi et al., 2012; Velichutina et al., 2010). More recently, EED allosteric inhibition and PRC2-directed PROTAC (proteolysis targeting chimera) drugs targeting EED have also been demonstrated a strong antiproliferative phenotype while reducing H3K27me3 in lymphoma cells (Y. He et al., 2017; J. H. R. Hsu et al., 2020; Potjewyd et al., 2020).

Although the natural history of follicular and other indolent non-Hodgkin lymphomas is understood to consist of inexorable relapses and remissions, a population of patients once diagnosed never require treatment for their disease or can be monitored clinically on a "watch and wait" approach before needing any therapy, often for years (Advani et al., 2004; Armitage & Longo, 2016; Horning, 1993; Rosenberg, 1985). This subset of clinically very indolent cases, as well as the inevitability of relapse in treated patients, alludes to the presence of a population of likely chemotherapy-resistant, non-proliferative or minimally proliferative, "cancer stem cells": a potential reservoir for relapse but often undetectable by standard molecular or immunophenotypic diagnostic techniques. Unpublished data from the Bracken Lab has identified in serum-starved, non-proliferating cells, the preponderance of a "G0" PRC2 complex lacking EZH2 but containing EZH1, EED, SUZ12 and the substoichiometric component PHF1/PCL1. This supports previous work demonstrating the greater abundance of EZH1 over EZH2 in non-proliferating cells, notable also for the effects of EZH1 on chromatin compaction (Bracken et al., 2003; Grau et al., 2021; Margueron et al., 2008; Wassef et al., 2019). Additionally, EZH1-PRC2 is a much weaker methyltransferase than EZH2-PRC2 *in vitro* (Lavarone et al., 2019; Margueron et al., 2008). Considering these observations, it is likely that EZH1 exerts its activities in non-proliferating cells by means other than its methyltransferase activity, and likely relating to its effects on chromatin compaction. This

could potentially be a useful insight in the context of indolent lymphomas as EZH1 may demarcate non-proliferating, indolent cells which would not be targeted by PRC2 methyltransferase inhibitors due to the function of EZH1 in these cells being uncoupled from its methyltransferase activity.

Clinical responses to EZH2 inhibitor drugs in lymphoma (as a monotherapy) are not durable, with clinical data regarding combination therapies incorporating EZH2 inhibitors keenly awaited (Italiano et al., 2018; Izutsu et al., 2021; Morschhauser et al., 2020; Song et al., 2022). Mechanisms of disease progression in patients have not yet been described. Models of lymphoma progression upon treatment with EZH2 inhibitor drugs in cell lines have proposed hotspot mutations in EZH2 preventing drug binding, EZH2 CXC domain deletions resulting in enhanced methyltransferase activity, upregulated secondary pathways including PI3K and MAPK and downregulated apoptotic genes (Baker et al., 2015a; Bisserier & Wajapeyee, 2018; Brooun et al., 2016a; Gibaja et al., 2016a; Kwok et al., 2022; Qi et al., 2017). The presence of a population of cells not targetable by EZH2 inhibitor therapy may also provide part of the mechanism for disease progression in patients. This population of cells may be targetable by a dEED PROTAC drug destabilising PRC2 by degrading one of its components; EED.

In this chapter, I describe using ChIP-Rx the altered landscape of the H3K27 methylation marks H3K27me2 and H3K27me3 in an isogenic system consisting of an EZH2 wild-type GC lymphoma cell line overexpressing either EZH2 wild-type or EZH2 with a gain-of-function mutation ($EZH2^{Y646F}$). I will demonstrate using some unpublished Bracken lab data (under revisions for Molecular Cell – Healy, McCole, Nolan et al 2022) that an EZH1-PRC2 complex is more abundant than EZH2-PRC2 in quiescent cells expressing mutant EZH2 and is present in lymphoma biopsy samples from patients with follicular lymphoma. I also generate a lympoma model whereby dEED can overcome acquired resistance to Tazemetostat. Using a PRC2 enzymatic inhibitor (Tazemetostat) and a PRC2 degrader drug targeting EED (UNC7700), I will illustrate using ChIP-Rx and RNA-Sequencing the differential effects of these means of targeting PRC2 on the landscape of H3K27me2 and H3K27me3 across the genome and their effects on gene transcription.

3.2 Results

3.2.1 Mapping the H3K27 di- and tri-methylation landscape in an isogenic lymphoma cell line expressing a gain-of-function EZH2 mutation

As outlined in section 3.1, recurrent heterozygous gain-of-function mutations in EZH2 affecting hotspot residues Y646, A682 and A692 (NCBI reference sequence NM_004456.4) are present in approximately 25% of cases of follicular lymphoma and GCB-DLBCL. These mutations function in concert with a wild-type allele of EZH2 to dramatically increase the overall levels of H3K27me3 in cells harbouring the mutation. A DLBCL cell line OCI-LY7 (gift from Professor Diego Pasini, European Institute of Oncology, Milan) was lentivirally transduced using a pCAG-FLAG-AVI plasmid with puromycin selection to express FLAG-tagged EZH2^{WT}, FLAG-EZH2^{Y646F} or FLAG-EZH2^{Y646N} (Figure 3.1A). Successful expression of the constructs was confirmed using western blot analysis (Figure 3.1B). Immunoblotting for FLAG-EZH2 confirmed that OCI-LY7 expressing FLAG-EZH2^{WT} and FLAG-EZH2^{Y646F} were more highly expressed at the protein level than FLAG-EZH2^{Y646N}. Correspondingly, the expected phenotype of elevated H3K27me3 compared to parental cells, with reduced H3K27me2 was more apparent in the cell line with greater expression of the mutant construct. There was no significant change in H3K27me1 as expected. Concurrent blotting for substoichiometric components from PRC2.1 and PRC2.2 showed that expression of additional EZH2 either wild-type or mutant had no significant effect on their expression (Figure 3.1C). I was unable to successfully blot PALI1 or PALI2 in these cells.

As FLAG-EZH2^{WT} and FLAG-EZH2^{Y646F} were expressed equally by western blot analysis, these cells were brought forward for chromatin immunoprecipitation followed by qPCR (ChIP-qPCR), followed by quantitative ChIP relative to an reference genome (ChIP-Rx), using E14 wild-type mouse embryonic stem cells mESCs as a 10% reference genome spike-in. Based on previously published ChIP-Seq (ChIP coupled with massively parallel DNA sequencing) data in lymphoma cell lines and ChIP-Rx data in mouse centrocytes and centroblasts expressing mutant EZH2 (Béguelin et al., 2013, 2020; Donaldson-Collier et al., 2019; Souroullas et al., 2016), I expected that I would see a genome-wide redistribution of the H3K27 di- and tri-methyl modifications. I hypothesised that SUZ12 binding at Polycomb target genes may be reduced in the EZH2 mutant context due to mutant EZH2 writing the H3K27me3 mark

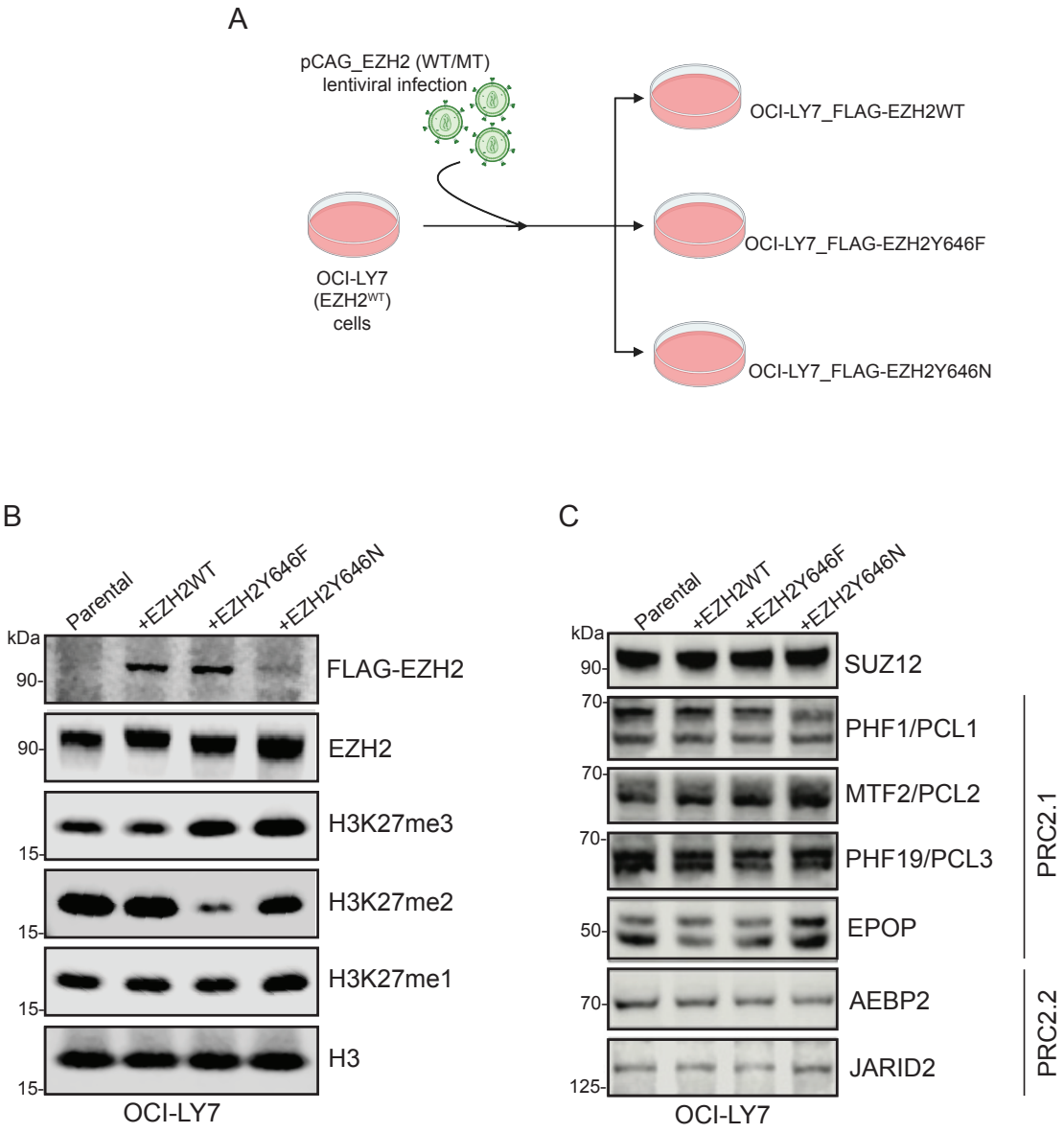

Figure 3.1 Generation of an isogenic model of mutant EZH2 using an EZH2 wild-type lymphoma cell line

A. Schematic of experimental design for generation of isogenic model.

B. Western blot analysis examining the expression of $EZH2^{WT}$, $EZH2^{Y646F}$ and $EZH2^{Y646N}$ constructs and their effects on methylation at H3K27.

C. Western blot analysis of PRC2 core component SUZ12 and PRC2.1 and PRC2.2 subcomplex assembly components to examine for differential expression in the presence of EZH2 wild-type and mutant constructs.

genome-wide, instead of primarily at Polycomb-target promoters. Due to the gain in H3K27me3, I predicted that I may also see a small reduction in H3K27 acetylation.

I performed ChIP-qPCRs at a number of human genomic loci, using antibodies against IgG (to help ascertain signal versus background enrichment), SUZ12, H3K27me2, H3K27me3 and H3K27ac in OCI-LY7 cells expressing FLAG-EZH2^{WT} and FLAG-EZH2^{Y646F} (Figure 3.2A-B). This demonstrated a gain of H3K27me3 at each examined locus, with no significant change of SUZ12 and H3K27ac. H3K27me2 is a low-abundance modification usually distributed usually genome-wide without detectable "peaks" and thus its distribution is best appreciated on a larger scale.

To gain a more comprehensive view and appreciation of subtle changes in the genomic distribution of the H3K27me2, H3K27me3 and H3K27ac post-translational modifications resulting from the presence of gain-of-function mutant EZH2, as well as to examine the localisation of SUZ12 in this context, I performed ChIP-Rx. As expected, parsing the genome into 10kb bins and examining the abundance of H3K27me3 and H3K27me2 genome-wide reflected a gain of H3K27me3 and loss of H3K27me2 (Figure 3.2C-D). SUZ12 peaks appeared to be of marginally lower amplitude upon examination of the UCSC genome browser view generated from the ChIP-Rx. H3K27me3 peaks were less defined due to spreading of the H3K27me3 mark, while H3K27me2 was of lower amplitude genome-wide (Figure 3.3A). There was no clear change to H3K27ac distribution. Polycomb target gene promoters were defined by the presence of SUZ12 peaks in the EZH2 wild-type context: SUZ12 being used as a surrogate for core PRC2 localisation. Examination of Polycomb target gene promoters revealed that spread of the H3K27me3 mark in the EZH2 mutant was more marked upstream (5-prime) of the SUZ12 peak, although H3K27me3 was also elevated 3-prime of the peak. Correspondingly, loss of H3K27me2 at these sites showed a reciprocal pattern (Figure 3.3B). This pattern suggests that H3K27me2 is being converted to H3K27me3 at these sites by mutant EZH2 with increased catalytic efficiency for H3K27me2 compared to the wild-type context, consistent with previous histone methyltransferase assay work (McCabe, Graves, et al., 2012; Sneeringer et al., 2010). Additionally, it is likely that SUZ12 has a lower residency time at Polycomb target genes in the EZH2 mutant context due to its increased activity elsewhere, as reflected by the smaller SUZ12 peaks in this ChIP-Rx.

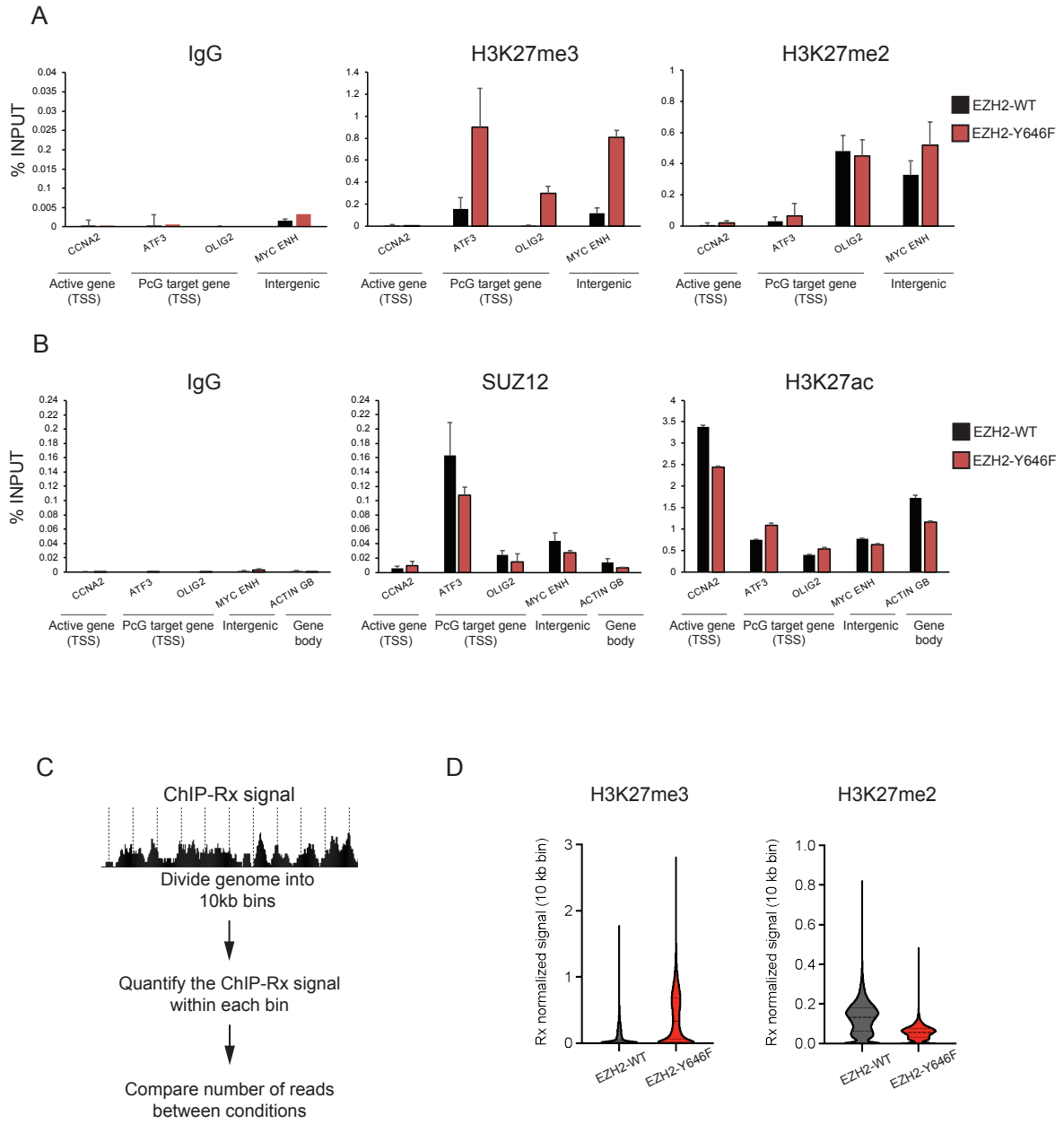

Figure 3.2 ChIP-qPCR and quantitative analysis of overall genome-wide abundance of H3K27me2 and H3K27me3 marks in an isogenic system expressing mutant EZH2

A-B. ChIP-qPCR analyses at various genomic loci for the indicated antibodies in the EZH2 wild-type cell line ectopically expressing EZH2-wild type and EZH2^{Y646F}.

C. Schematic representation of quantitative analysis of ChIP-Rx signal genome-wide.

D. Violin plots demonstrating genome-wide overall increase in the abundance of H3K27me3 and decrease in H3K27me2 in the EZH2 mutant context as compared with the EZH2 wild-type context.

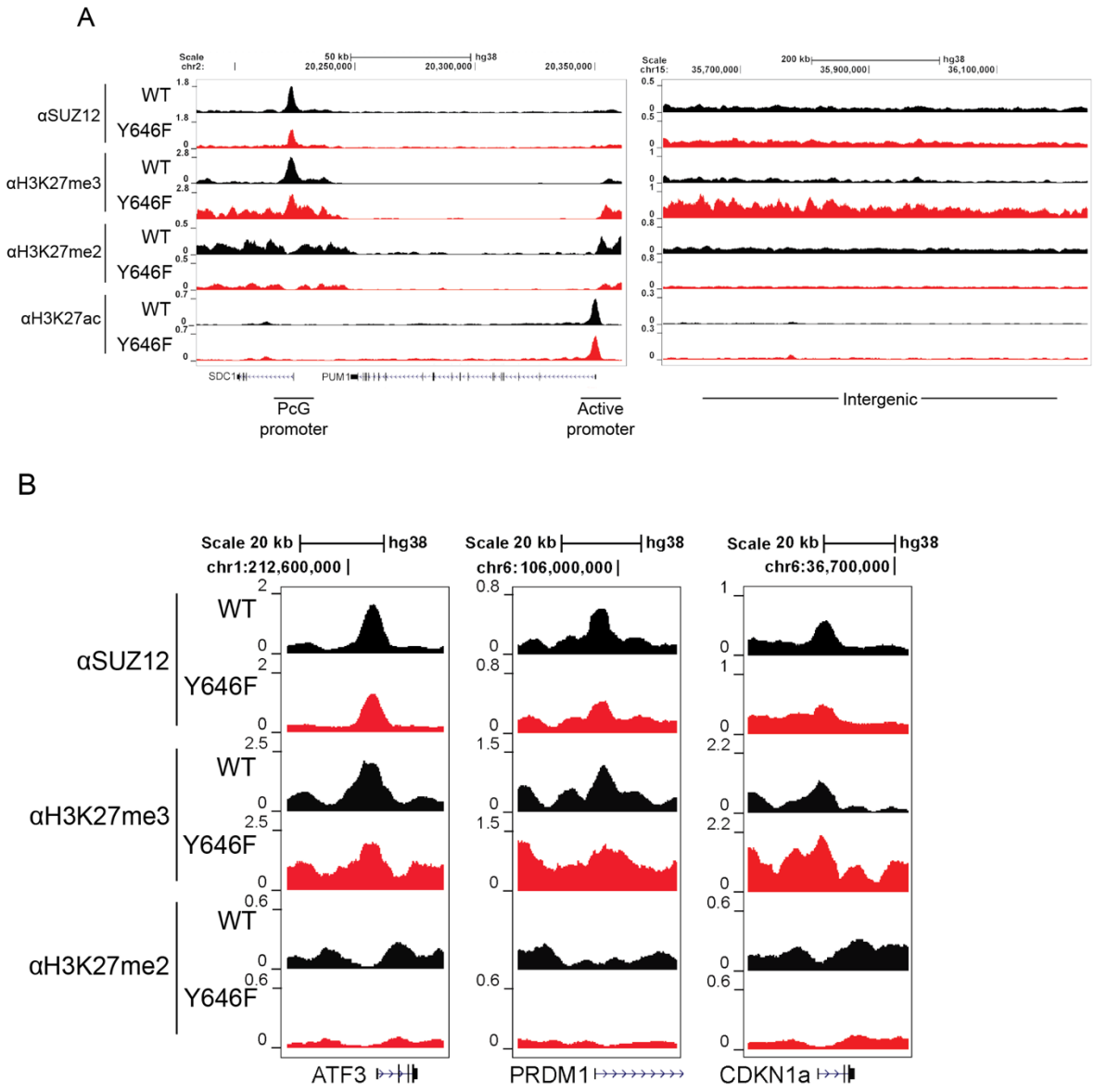

Figure 3.3 UCSC genome browser tracks demonstrate reciprocal loss of H3K27me2 and gain of H3K27me3 in lymphoma cells expressing mutant EZH2

A. UCSC genome browser representations of ChIP-Rx for indicated antibodies at a representative polycomb target gene promoter (SDC1/CD138), a gene expressed in terminally differentiated B-cells, an active gene promoter as defined by H3K27ac peak at its TSS (PUM1) and at an intergenic location.

B. UCSC genome browser representation of Polycomb target gene promoters demonstrating a relatively greater gain of H3K27me3 mark immediately 5-prime of a SUZ12-defined polycomb target gene promoters.

3.2.2 Describing the genomic pattern of loss of H3K27me2 and gain of H3K27me3 in isogenic lymphoma cells expressing mutant EZH2^{Y646F}.

Although the clear trend from this data is that H3K27me3 is primarily gained across the genome and H3K27me2 lost in the presence of mutant EZH2, I wished to better define these patterns of gain and loss respectively. In order to do this, using 10kb genomic bins, the abundance of H3K27me3 and H3K27me2 in each bin were directly compared between the EZH2 wild-type and mutant contexts. This demonstrated that over 90% of genomic bins gain H3K27me3 in mutant EZH2 compared to wild-type, and lose H3K27me2 in mutant EZH2 compared to wild-type (Figure 3.4A). On a chromosome-wide scale, comparing the fold change of ChIP signal abundance for EZH2 mutant compared to EZH2 wild-type lymphoma cells, in 100kb bins along chromosome 8, both SUZ12 and H3K27me3 appear to gain abundance in the mutant context, while H3K27me2 is depleted (Figure 3.4B). More precisely comparing the status of H3K27 di- and tri-methylation in the same bin between the contexts, the log2 fold-change of H3K27me3 comparing mutant and wild-type was plotted directly against the log2 fold-change of H3K27me2 showing that the majority of bins that lose H3K27me2 simultaneously gain H3K27me3 (Figure 3.4C). Gain of H3K27me3 correlates also with gain of SUZ12 at a majority of genomic loci (Figure 3.4D), reflecting that catalysation of H3K27me3 requires more stable association of PRC2 than H3K27me2. Consistent with previous ChIP-Seq data (Souroullas et al., 2016), a small portion of sites retain more H3K27me3 in the wild-type context, reflecting that the EZH2^{Y646F} mutant neo-functionalises the complex with redistribution of H3K27 methylation marks, rather than simply converting H3K27me2 to H3K27me3 genome-wide.

Distinct patterns of alteration can be observed on average plots across the genome (Figure 3.4E). Polycomb target genes were defined by the presence of SUZ12 peaks in the EZH2 wild-type context. Active genes were defined by the presence of H3K27ac peaks in the EZH2 wild-type context. Intergenic sites were non-genic regions further than 5kb from transcriptional start sites (TSS) or transcriptional termination sites (TTS). Average plots demonstrated again that at Polycomb target genes, less SUZ12 is stably bound in the EZH2 mutant context, with a marginal but clear increase in abundance intergenically, consistent with my hypothesis that SUZ12 is leached from Polycomb target genes and writing higher order H3K27 methylation across the genome. Starkly, intergenic loci are predominantly carpeted by H3K27me3 in the presence of the EZH2 mutant, where H3K27me2 does so in the wild-type context.

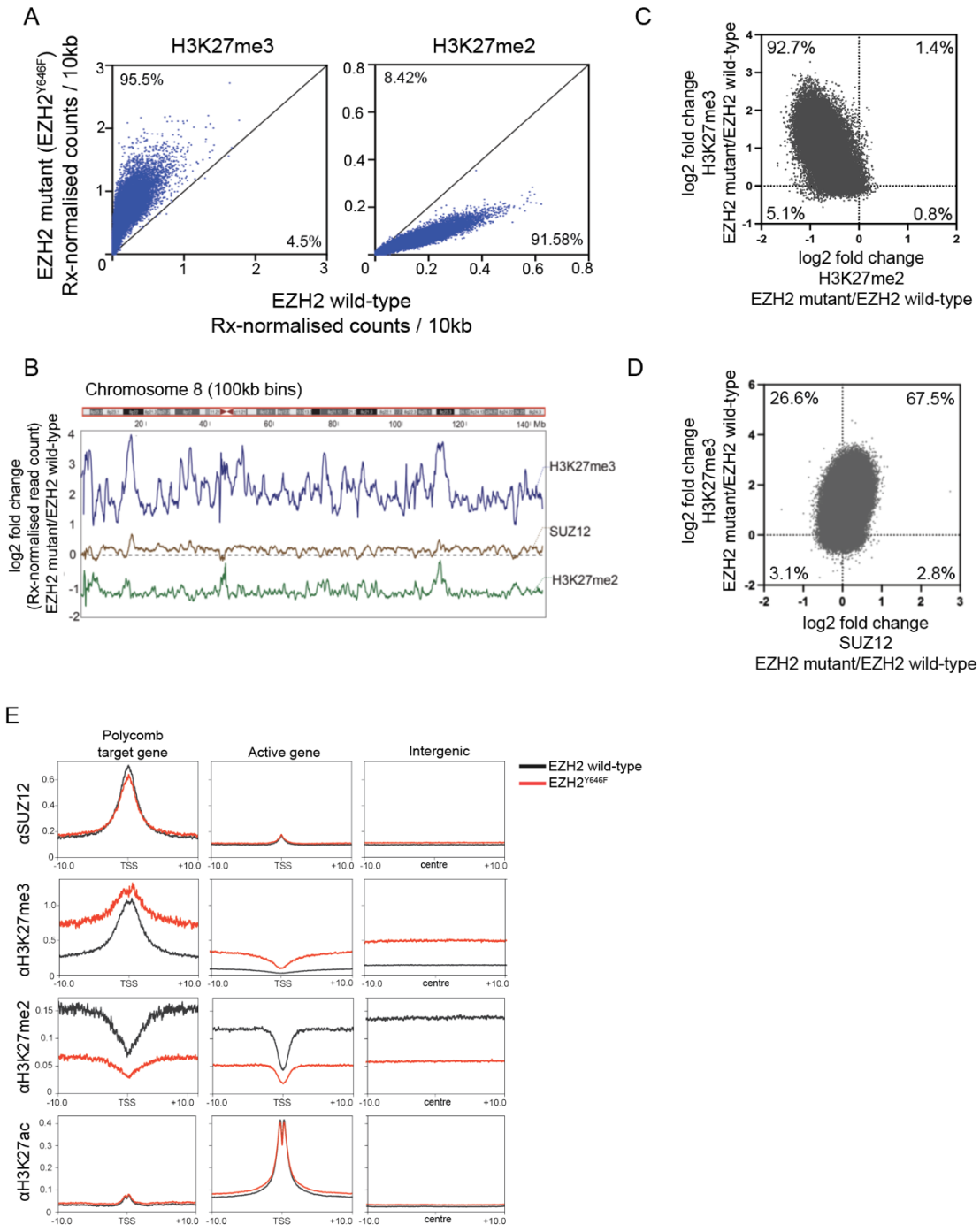

Figure 3.4 Mutant EZH2 neo-functionalises PRC2 with gain of H3K27me3 and loss of H3K27me2 in most bins, but differential H3K27me3 gain in a portion of genomic loci

A. Genome-wide correlation of H3K27me3 and H3K27me2 signal within 10kb bins between EZH2 wild-type and mutant cell lines. Each dot represents one 10kb bin.

B. Ideogram of Chromosome 8 plotting Log_2 fold change of Rx-normalised reads (EZH2 mutant/EZH2 wild-type) for H3K27me3, H3K27me2 and SUZ12.

C. Density plot directly comparing log2 fold change of H3K27me3 and H3K27me2 between EZH2 wild-type and mutant contexts. Each dot represents one 10kb bin.

D. Density plot directly comparing log2 fold change of H3K27me3 and SUZ12 between EZH2 wild-type and mutant contexts. Each dot represents one 10kb bin.

E. Average ChIP-Rx signal profiles of SUZ12, H3K27me3, H3K27me2 and H3K27ac at their peaks (+/-10kb) in the indicated cell lines.

3.2.3 Non-dividing cells are resistant to EZH2 inhibitor therapy and can be targeted by PROTAC-mediated degradation of EZH1-PRC2.

As discussed in section 3.1, EZH1 is expressed ubiquitously in cells while EZH2 expression is known to be attenuated in non-dividing cells. It has been proposed that EZH1, although a much less efficient methyltransferase enzyme than EZH2, maintains H3K27 methylation in these quiescent/non-dividing cells while also mediating transcriptional repression by mediating long-range interactions resulting in chromatin compaction (Lavarone et al., 2019; Margueron et al., 2008). Furthermore, B-cell activation results in an increase in global acetylation coupled with chromatin decompaction (Kieffer-Kwon et al., 2017). A paper from the Bracken Lab currently under revision following initial review entitled "A non-catalytic role of EZH2-PRC2 to promote canonical PRC1 recruitment in quiescent cells" (Healy, McCole, et al. 2022) has again demonstrated this predominance of EZH1-PRC2 over EZH2-PRC2 in quiescent cells. Follicular lymphoma; an indolent non-Hodgkin lymphoma is an appealing model for testing this hypothesis, in that tumours can remain stable without meeting criteria for therapy for many years, although once treated invariably relapse in due course. This could reflect the presence of non-proliferating cells remaining stable for a period of time in a measurable tumour, and/or acting as a reservoir for future disease relapses or even transformation to more aggressive disease.

I attempted to culture several lymphoma cell lines in serum-free media to induce cellular quiescene, as has previously been published in several cellular contexts (Legesse-Miller et al., 2012; Yao, 2014). However, tested lymphoma cell lines did not survive sufficiently rigorous serum starvation for testing this hypothesis, possibly reflecting a reliance on quiescent lymphoma cells on their microenvironment for survival. HA-EZH2^{WT} and HA-EZH2^{Y641F} were stably expressed by lentiviral infection in TERT-immortalised human fibroblasts (Tig3-T cells) (Figure 3.5A). Parental Tig3-T cells and Tig3-T cells expressing these EZH2 constructs were then either passaged in normal media or serum-free media for serum starvation for 96 hours. Thereafter, serum-starved (quiescent) and cycling cells were treated for 72 hours with either DMSO or 10 μM GSK-343 (an EZH2 enzymatic inhibitor) (Verma et al., 2012) and harvested for western blot analysis (Figure 3.5B). Western blot for CyclinA2 confirmed successful serum starvation and induction of cellular quiescence in serum starved cells. As expected, GSK-343 had no effect on H3K27me2 and H3K27me3 levels in quiescent cells but did significantly reduce the levels of both marks in cycling cells.

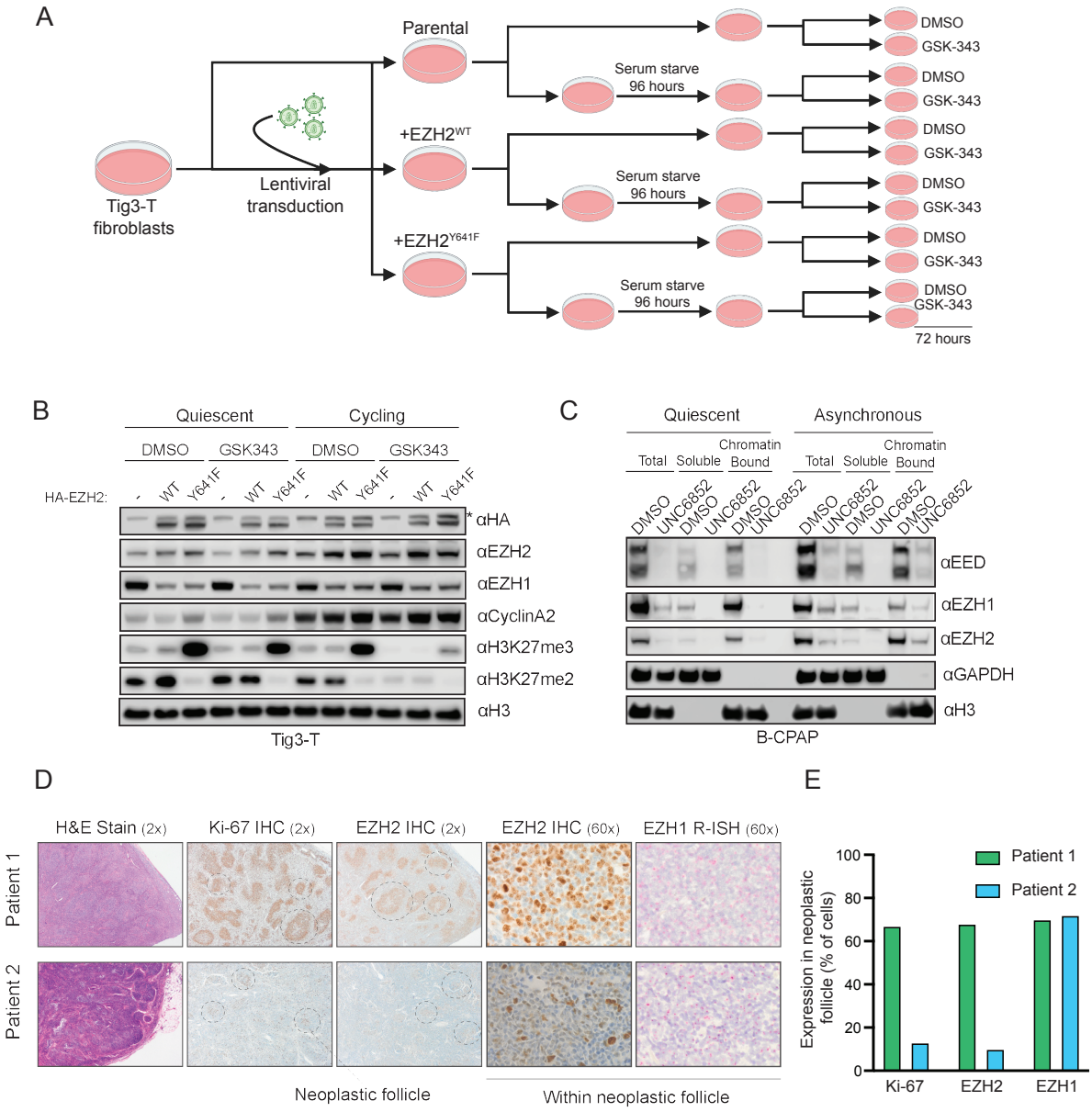

Figure 3.5 EZH1-PRC2 is abundant in quiescent cells and is refractory to PRC2 enzymatic inhibition, but is targetable by PRC2 degradation

A. Experimental schematic representing generation of Tig3-T fibroblasts expressing EZH2 constructs, subsequent serum starvation and drug treatment.
B. Western blot analysis of quiescent and cycling Tig3-T fibroblasts ectopically expressing wild-type and mutant EZH2, treated by DMSO or GSK-343. Asterisk (*) indicates non-specific background band.
C. Western blot analysis of B-CPAP thyroid cancer cell line demonstrating degradation of PRC2 in quiescent and cycling cells using an EED PROTAC UNC6852.
D. H&E (haematoxylin and eosin) staining, Ki-67 and EZH2 immunohistochemistry and EZH1 R-ISH (RNA in situ hybridisation) of two lymph node biopsy samples from patients with histological grade 2A follicular lymphoma.
E. Quantification of Ki-67, EZH2 and EZH1 expression for lymph node biopsy samples.

Additionally, EZH1 was more expressed in quiescent than cycling cells: the corollary of EZH2 expression.

Using the human papillary thyroid cancer cell line B-CPAP, cellular quiescence was induced using serum starvation for 96 hours and both quiescent and cycling cells were treated with either DMSO or the UNC6852 EED-degrading PROTAC for 72 hours, followed by harvesting of these cells for cellular fractionation (Figure 3.5C). This PROTAC and its quality control were first published by the laboratory of a collaborator for this project, Professor Lindsey James (Potjewyd et al., 2020). GAPDH was absent from the chromatin-bound fraction and Histone H3 absent from the soluble fraction, confirming successful fractionation. EED and PRC2 components EZH1 and EZH2 were robustly depleted in both quiescent and cycling cells upon treatment with the EED PROTAC, confirming successful targeting of PRC2 even in non-proliferating cells.

To examine the hypothesis that EZH1-PRC2 is highly expressed in follicular lymphoma but refractory to enzymatic inhibition, tissue blocks were first drawn from the St. James' Hospital lymphoma biobank (ethical approval 2020-09-(01)) and examined by Aoibhinn Mooney (histopathology laboratory scientist) and Professor Richard Flavin (Consultant Histopathologist). Ki-67 is a nuclear protein associated with cellular proliferation but absent in G0, that has been explored as a biomarker in indolent lymphoma, with higher expression understood to relate to more aggressive disease (Broyde et al., 2009; Hooghe et al., 2008; Hoster et al., 2008; Klapper et al., 2009; Shirendeb et al., 2009). For this small scale study, Ki-67 and EZH2 immunohistochemistry were used to identify more rapidly proliferating tumours, with high expression reflecting active proliferation (Figure 3.5D-E). EZH1 immunohistochemistry failed to stain nuclei and therefore EZH1 R-ISH was utilised instead, successfully staining a portion of nuclei. Patient 1 has multiply relapsed follicular lymphoma, rapidly requiring therapy following this biopsy. Patient 2 presented with a right inguinal mass and stage 3A disease, though did not require therapy for 14 years from the time of this biopsy. Interestingly, while both patients harbour abundant EZH1-positive cells (approximately 60% of cells within neoplastic follicle), only patient 1 whose tumour expressed abundant EZH2 and Ki-67 had clinically active disease requiring therapy. Although this requires validation in a larger series, these cases illustrate the presence of lymphoma cells in both patients likely to be refractory to PRC2 enzymatic inhibitors but potentially targetable by PRC2 degradation with a PROTAC molecule.

3.2.4 Lymphoma cells with acquired resistance to EZH2 inhibitor treatment remain sensitive to PROTAC-mediated EED degradation.

In vivo analyses in lymphoma cell lines have revealed a number of recurrent mutations in EZH2 capable of conferring acquired resistance to EZH2 inhibitors in previously sensitive B-NHL cell lines (Baker et al., 2015b; Bisserier & Wajapeyee, 2018; Gibaja et al., 2016b; Qi et al., 2017) (Figure 3.6B). These mutations arise in either the enzymatic SET domain of EZH2, or in a ten-residue helix near the C-terminus of EZH2 annotated the "activation loop", that upon activation of EZH2 interacts with the SET domain (Brooun et al., 2016). In the case of the more common oncogenic $EZH2^{Y646X}$ mutant, biallelic resistant mutations are required in lymphoma cell lines to confer resistance (Gibaja et al., 2016b; Qi et al., 2017), whereas in the case of $EZH2^{A682X}$ mutation, mutation of either the mutant or wild-type allele drug confers resistance (Baker et al., 2015b). Contact mediated through Tyrosine Y111 in the activation loop of EZH2 with Y661 in the SET domain creates a ligand-binding cavity for EZH2 inhibitors, as modelled in Figure 3.6A using structure 5IJ8 (Brooun et al., 2016a) (NCBI EZH2 reference sequence NM_001203247.1). However, mutation of either residue can result in steric hinderance, preventing drug binding. Similar mechanisms for acquired resistance to other drugs have been demonstrated in patients with lymphoma, exemplified by the example of acquired C481S mutations in Bruton's Tyrosine Kinase preventing covalent binding of the BTK inhibitor drug Ibrutinib, resulting in disease progression (Woyach et al., 2014). Despite non-durable responses to Tazemetostat reported in patients treated with this drug in clinical trials, mechanisms for disease progression arising from acquired resistance to Tazemetostat have not yet been described in patients (Italiano et al., 2018; Izutsu et al., 2021; Morschhauser et al., 2020; Song et al., 2022).

Previously published work demonstrated that ectopic expression of an EZH2 allele in the $EZH2^{A682}$ mutant cell line Pfeiffer, containing both the oncogenic A677G/A682G mutant and the putative hotspot resistant mutant Y111D resulted in acquired resistance to EZH2 inhibitor treatment (Baker et al., 2015). Pfeiffer is usually exquisitely sensitive to EZH2 inhibitor drugs (McCabe et al., 2012). Please note that this paper utilised the 746 residue EZH2 isoform (NM_001203247.1) rather than the 751 residue EZH2 isoform referenced elsewhere in this thesis (NM_004456.4). These isoforms differ by the exchange of H297-P298 in the shorter isoform for H297-RKCYN-S303 in the longer isoform. Accordingly, the mutation A677G in the shorter isoform corresponds with A682G in the longer isoform and Y641X corresponds

with Y646X, while N-terminus substitutions such as Y111D are consistent between isoforms. An EZH2 mutant allele containing in cis mutants A677G and Y111D was generated and expressed using a PLENTI lentiviral vector (incorporating HA and FLAG tags) in the lymphoma cell line Pfeiffer (Figure 3.6C). Despite multiple replicates and rounds of lentiviral infection, expression of wild-type EZH2 did not reach the same expression level as $EZH2^{Y111D/A677G}$. One possible explanation is that cells given a higher dose of mutant EZH2 had a proliferative advantage in the mixed cellular proliferation, as evidenced by Pfeiffer cells ectopically expressing $EZH2^{Y111D/A677G}$ having a marginally shorter doubling time than parental cells (Figure 3.6D). Using CellTiter Glo® to measure ATP as a surrogate marker for cellular viability, IC50 experiments were undertaken to ascertain the concentration of Tazemetostat (EPZ-6438) to inhibit proliferation by 50% at day 6 of treatment (Figure 3.6E). This assay confirmed that the lymphoma cell line expressing $EZH2^{Y111D/A677G}$ had acquired resistance to Tazemetostat compared to both parental Pfeiffer and Pfeiffer expressing wild-type EZH2. Treating Pfeiffer parental and $EZH2^{Y111D/A677G}$ cells with the IC50 dose of Tazemetostat for the parental context revealed that H3K27me3 was markedly reduced in the parental context only, whereas a 10μM dose of the second generation EED-degrading PROTAC from Professor Lindsey James (first generation published (Potjewyd et al., 2020)) ablated H3K27me3 and degraded PRC2 in both cell lines (Figure 3.6F). This second generation EED PROTAC is currently in press by the James lab. There were no viable cells in UNC7700-treated cells by Day 6. Outside of the context of acquired EZH2 inhibitor resistance, this molecule was also tested against a Day 3 IC50 dose of Tazemetostat in the EZH2 mutant cell line WSU-DLC2, similarly destabilising core PRC2 and ablating the H3K27me3 mark to a similar extent (Figure 3.6G). Given that Tazemetostat therapy singly affects PRC2 enzymatic activity, the ability of PRC2 degradation achieve the same effect as shown here is an appealing prospect in overcoming acquired drug resistance.

Whilst both approaches reduced the levels of H3K27me3 in the cells, I decided to examine whether PRC2 degradation resulted in any additional changes to the genomic localisation of H3K27me2 and H3K27me3 in lymphoma cells, or exerted any differential effect on the transcriptional landscape compared to PRC2 enzymatic inhibition. This was motivated by work previously discussed in sections 3.1 and 3.2.3 reflecting the potential role for PRC2 (containing EZH1) in mediating long-range interactions resulting in chromatin compaction, independently of its role in writing H3K27 methylation marks.

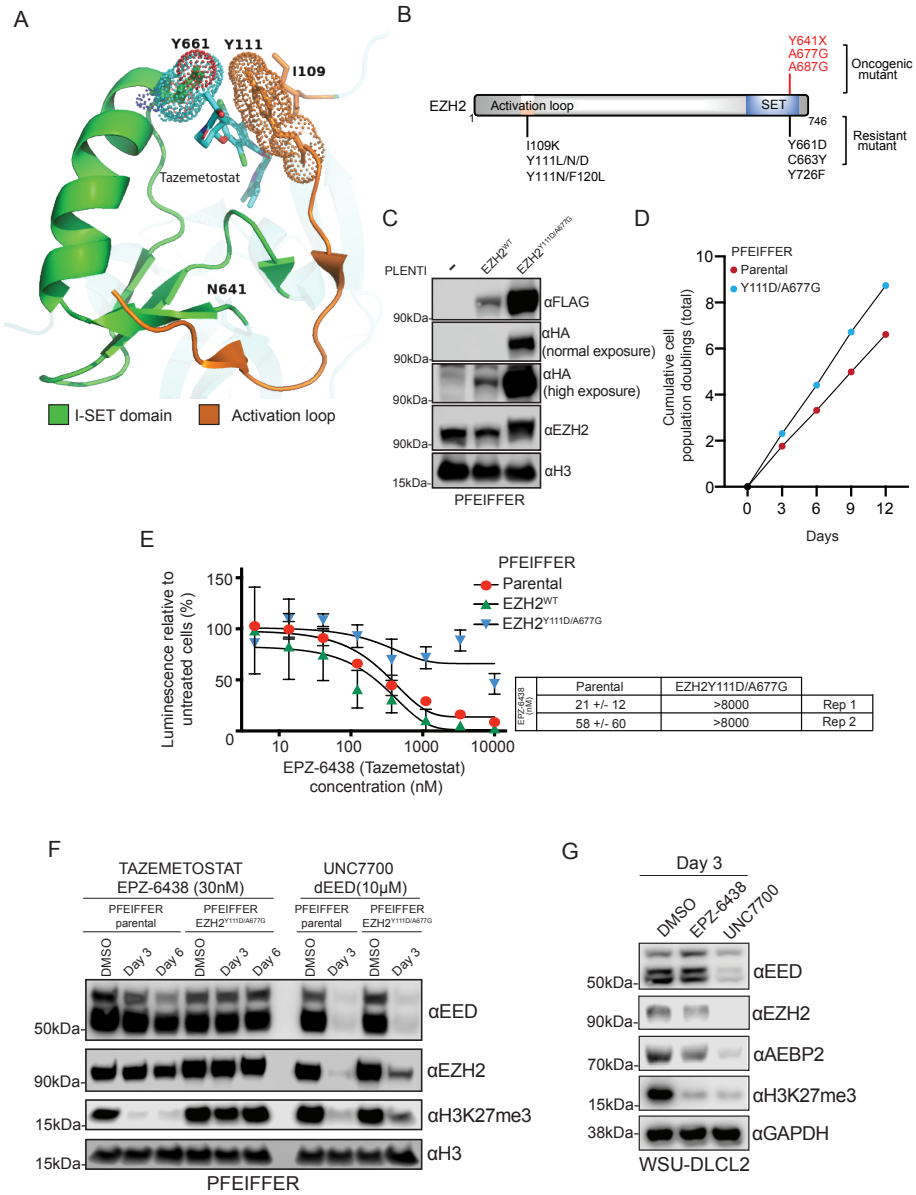

Figure 3.6 Acquired resistance to EZH2 enzymatic inhibition can be overcome by PRC2 degradation

A. Modelling of PRC2 enzymatic inhibitor drug binding in a pocket between EZH2 residues Y111 in the activation loop and Y661 in the I-SET domain (indicated by dots), with residues known to confer drug resistance when mutated and EZH2 oncogenic mutant Y641N highlighted (PDB structure ID 5IJ8).

B. Schematic representation of EZH2 with hotspot oncogenic mutations and hotspot mutations conferring drug resistance in lymphoma cell lines highlighted.

C. Western blot analysis demonstrating ectopic expression of wild-type and mutant EZH2 in the EZH2 mutant cell line Pfeiffer.

D. Proliferation assay measuring cumulative cell doublings over a 12 day period.

E. Cellular viability assay measuring ATP concentration in cell lines treated with various doses of Tazemetostat for 6 days.

F. Western blot analysis of Pfeiffer parental and Pfeiffer EZH2$^{Y111D/A677G}$ cells treated with PRC2 enzymatic inhibitor drug Tazemetostat and PRC2 PROTAC UNC7700.

G. Western blot analysis of EZH2 mutant cell line WSU-DLCL2 treated with DMSO, 100nM Tazemetostat or 10μM UNC7700 for 3 days.

3.2.5 PRC2 enzymatic inhibitor Tazemetostat and EED-degrading PROTAC UNC7700 reduce the level of H3K27me3 in lymphoma cells

To compare the effects of PRC2 enzymatic inhibition with degradation of PRC2, a dose was established in the EZH2 mutant cell line WSU-DLCL2 for each drug such that H3K27me3 would be depleted by approximately 90% after 3 days of treatment (Figure 3.6G). Firstly, I wished to examine the differential changes resulting from both methods of targeting PRC2 on the genomic localisation of H3K27me2 and H3K27me3 in those cells (Figure 3.7A). Initial ChIP-qPCRs (Figure 3.7B) demonstrated that as expected, H3K27me3 was reduced at numerous genomic loci compared to the DMSO treatment. As this is an EZH2 mutant cell line, H3K27me2 is present at very low levels and this antibody failed to enrich over IgG by qPCR. H3K27me2 and H3K27me3 were ChIPs were taken forward for ChIP-Rx as changes in these marks would best be illustrated on a genome-wide scale, using E14 wild-type mouse embryonic stem cells for the exogenous reference genome spike-in for normalisation.

The genome was parsed into 10kb bins and the signal for ChIP antibodies H3K27me2 and H3K27me3 was quantified within each bin relative to the 10% mouse reference genome spike-in. Plotting ChIP antibody signal along chromosome 9 (chosen as a sample chromosome for large global analysis) revealed that on a global level, both UNC7700 and Tazemetostat robustly depleted H3K27me3. Intriguingly, at this day 3 timepoint, I observed that H3K27me2 was slightly increased in the UNC7700-treated context compared to DMSO, whereas H3K27me2 was reduced in the Tazemetostat-treated context compared to DMSO treatment (Figure 3.7C). However, the mark was present in all conditions at very low abundance. Directly comparing the three treatment conditions against each other, both UNC7700 and Tazemetostat depleted H3K27me3 compared to DMSO in over 85% of bins genome-wide, with Tazemetostat doing so marginally more effectively when comparing the two PRC2 drugs directly (Figure 3.7D-E). A comparable analysis for H3K27me2 revealed that this mark actually increased marginally in UNC7700 treated cells compared to DMSO in over 50% of bins, while it was depleted by Tazemetostat in over 50% of bins.

Polycomb target gene promoters were defined by the presence of SUZ12 peaks in a previous ChIP-Rx in this cell line carried out in the Bracken lab (data not shown here). Approximately 3000 Polycomb target gene promoters were identified. Intergenic regions were defined as regions >5kb from the nearest annotated gene. Further analysis of the data revealed that small

H3K27me3 peaks were retained at Polycomb target gene promoters with Tazemetostat treatment, whereas these were lost with UNC7700 (dEED treatment). This likely reflects the mark being written at sites of CpG-rich promoters of Polycomb target genes where PRC2 is most stably bound. This stability is disrupted by degradation of the complex, resulting in additional loss of H3K27me3 at these sites (Figure 3.8A-E). I propose that more intergenic H3K27me3 is retained with dEED treatment than Tazemetostat treatment because the portion of PRC2 not destabilised by dEED is not enzymatically inhibited, whereas all PRC2 should be enzymatically inhibited with the EZH2 inhibitor drug Tazemetostat. The observation that the low abundance mark H3K27me2 is marginally gained with UNC7700 treatment compared to DMSO at day 3 should be examined with a longer course of treatment and additional replicates.

3.2.6 PRC2-mediated transcriptional repression is mediated by its enzymatic activity

Given that both UNC7700 and Tazemetostat robustly depleted H3K27me3 levels in the EZH2 mutant cell line WSU-DLCL2 after 3 days of treatment, I wished to examine whether the drugs would have a differential effect on gene expression at that time point. I hypothesised that as UNC7700 results in degradation of PRC2, it may result in additional de-repression by disrupting any potential role PRC2 is playing in chromatin compaction or other long range interactions.

Using QuantSeq 3' mRNA sequencing (Moll et al., 2014) of three biological replicates for each condition: DMSO, UNC7700 and Tazemetostat treatment of lymphoma cells for three days, I generated libraries for next generation sequencing. RNA-sequencing analysis revealed that Tazemetostat de-repressed significantly more genes than UNC7700 treatment, with most genes de-repressed in UNC7700 overlapping with genes de-repressed in Tazemetostat treatment (Figure 3.9A-B). Similarly, most genes down-regulated by UNC7700 overlapped with those down-regulated by Tazemetostat. Gene Ontology analysis for genes up-regulated and down-regulated compared to DMSO-treated cells, revealed similar enriched terms (Figure 3.10B-C). Examination of specific genes of interest demonstrated that similar genes of interest were de-repressed by treatment with both UNC7700 and Tazemetostat, though to a greater extent by Tazemetostat treatment, likely reflecting its greater effect on H3K27me3 levels.

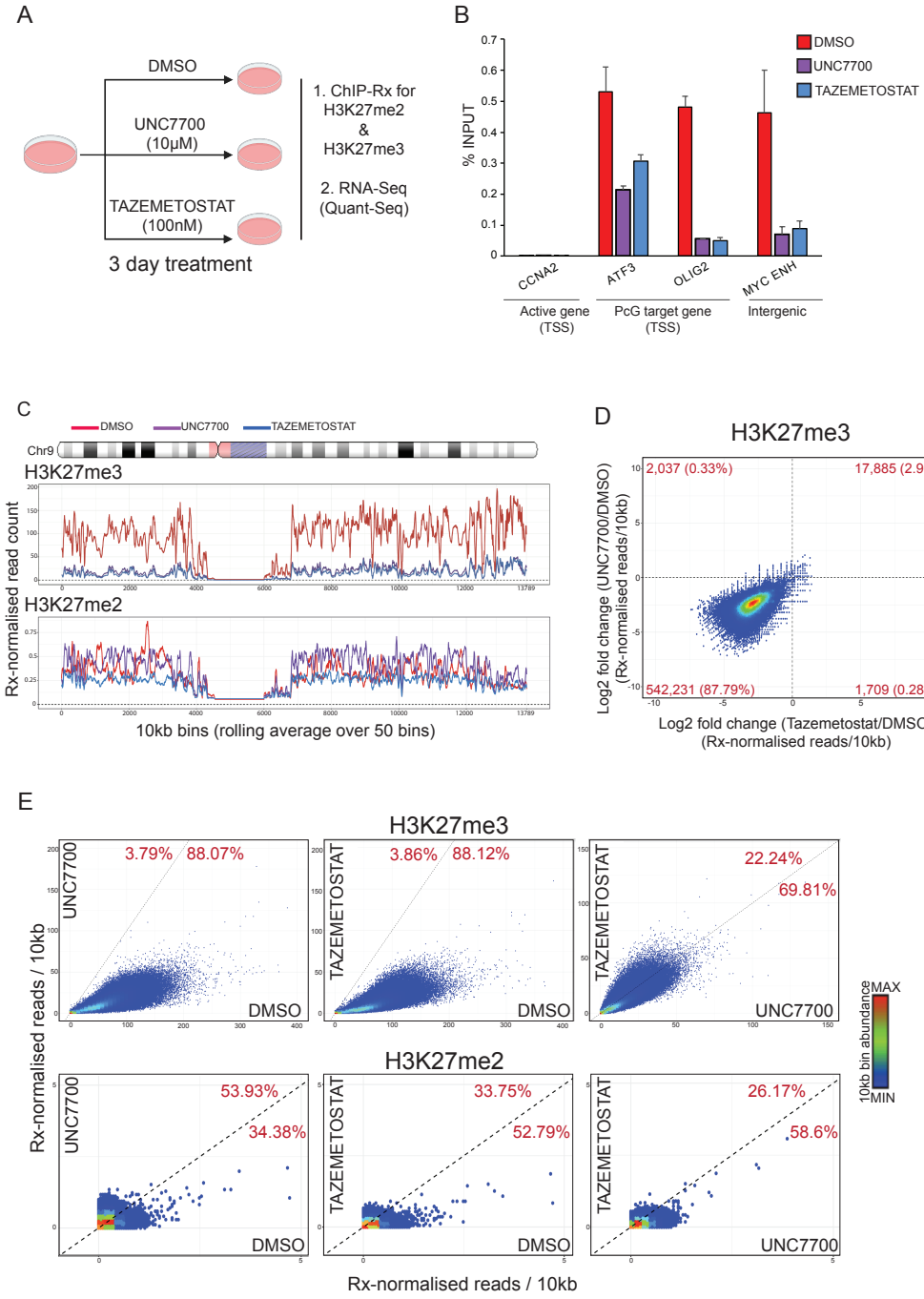

Figure 3.7 PRC2 enzymatic inhibition and degradation globally reduce the level of H3K27me3 in EHZ2 mutant lymphoma cells

A. Schematic representation of experimental design for ChIP-Rx and RNA-Seq in lymphoma cells treated with EZH2 enzymatic inhibition and PRC2 PROTAC drug.
B. ChIP-qPCRs at various genomic loci for H3K27me3 mark.
C. Ideogram of Chromosome 9 with plots of H3K27me3 and H3K27me2 in each condition quantified in 0.5Mb bins.
D. Composite plot comparing pattern H3K27me3 loss/gain within each 10kb bin between UNC7700/DMSO and Tazemetostat/DMSO. Each dot represents one 10kb bin.
E. Genome-wide correlation of H3K27me3 signal within 10kb bins between UNC7700-treated and TAZ-treated cells, compared to signal in DMSO treatment. Each dot represents one 10kb bin.

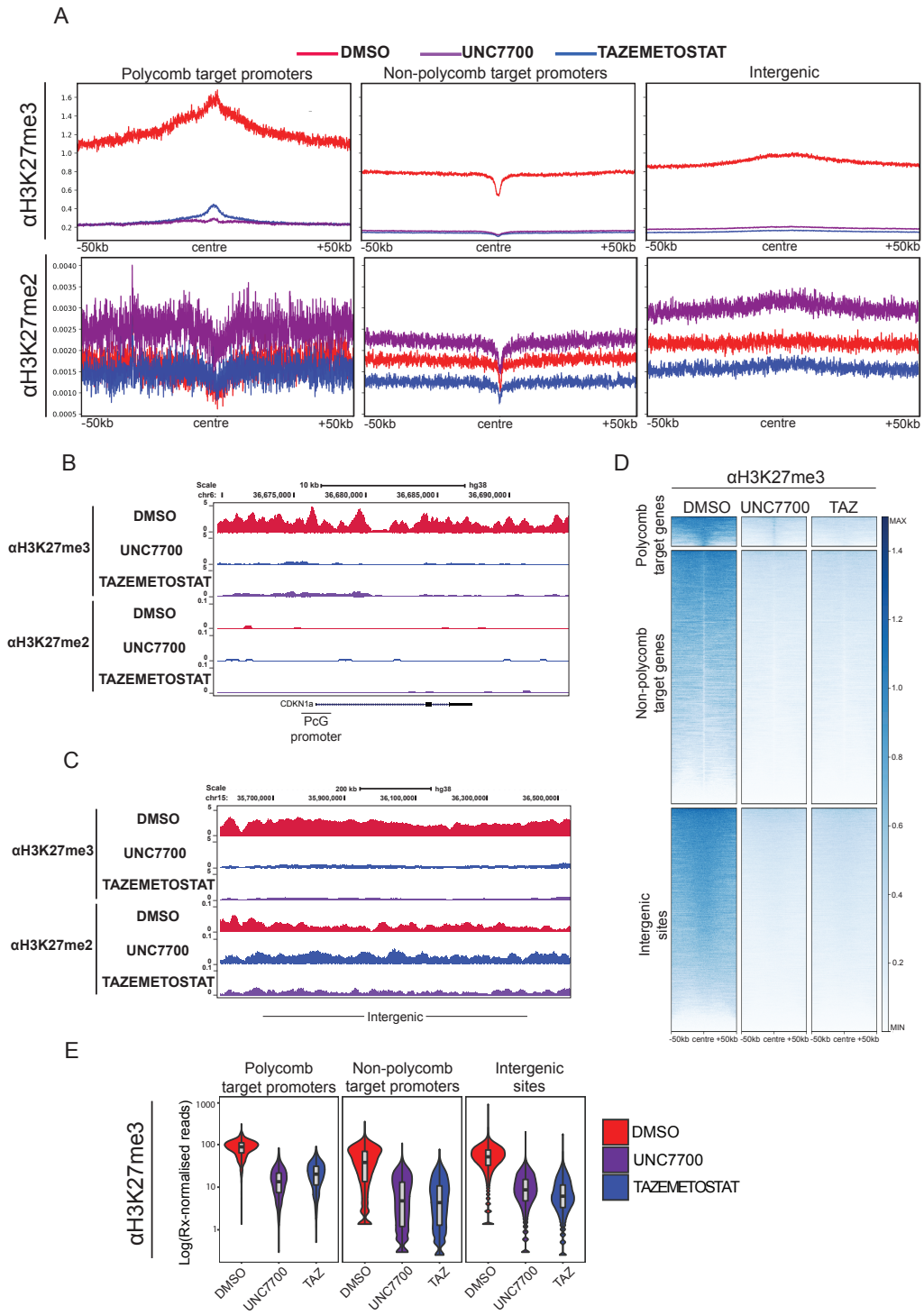

Figure 3.8 UNC7700 reduces H3K27me3 more effectively than Tazemetostat at Polycomb target genes

A. Average ChIP-Rx signal for H3K27me3 and H3K27me3 at polycomb target promoters, non-polycomb target promoters and intergenic regions in DMSO, UNC7700 and Tazemetostat treated lymphoma cells.

B-C. UCSC genome browser view of H3K27me2 and H3K27me3 in all treatment conditions at Polycomb target gene CDKN1a and a sample intergenic region.

D-E. Quantification by heat map (D) and as violin plots (E) of H3K27me3 signal at Polycomb target gene promoters, non-Polycomb promoters and intergenic regions in cells in all conditions.

CDKN1a, previously shown to be de-repressed by EZH2 inhibitor therapy, was similarly enriched here (Béguelin et al., 2013). Other sample genes of interest including Sestrin 1, (previously shown to be a target of mutant EZH2), as well as IRF4/MUM1 and Jchain, genes important for the plasma cell terminal differentiation programme, were also shown to be derepressed (Figure 3.10A) (Mlynarczyk et al., 2019; Nutt et al., 2015; Oricchio et al., 2017; Pasqualucci, Trifonov, et al., 2011; A. Q. Xu et al., 2020).

Taken together, given that PRC2 enzymatic inhibition by Tazemetostat resulted in a greater number of gene expression changes than the EED PROTAC UNC7700, these data suggest that PRC2 enzymatic function is the key mechanism underlying PRC2-mediated transcriptional repression in this EZH2 mutant lymphoma cell line. It would be interesting to examine whether this is direct, or indirect via recruitment of cPRC1 to chromatin.

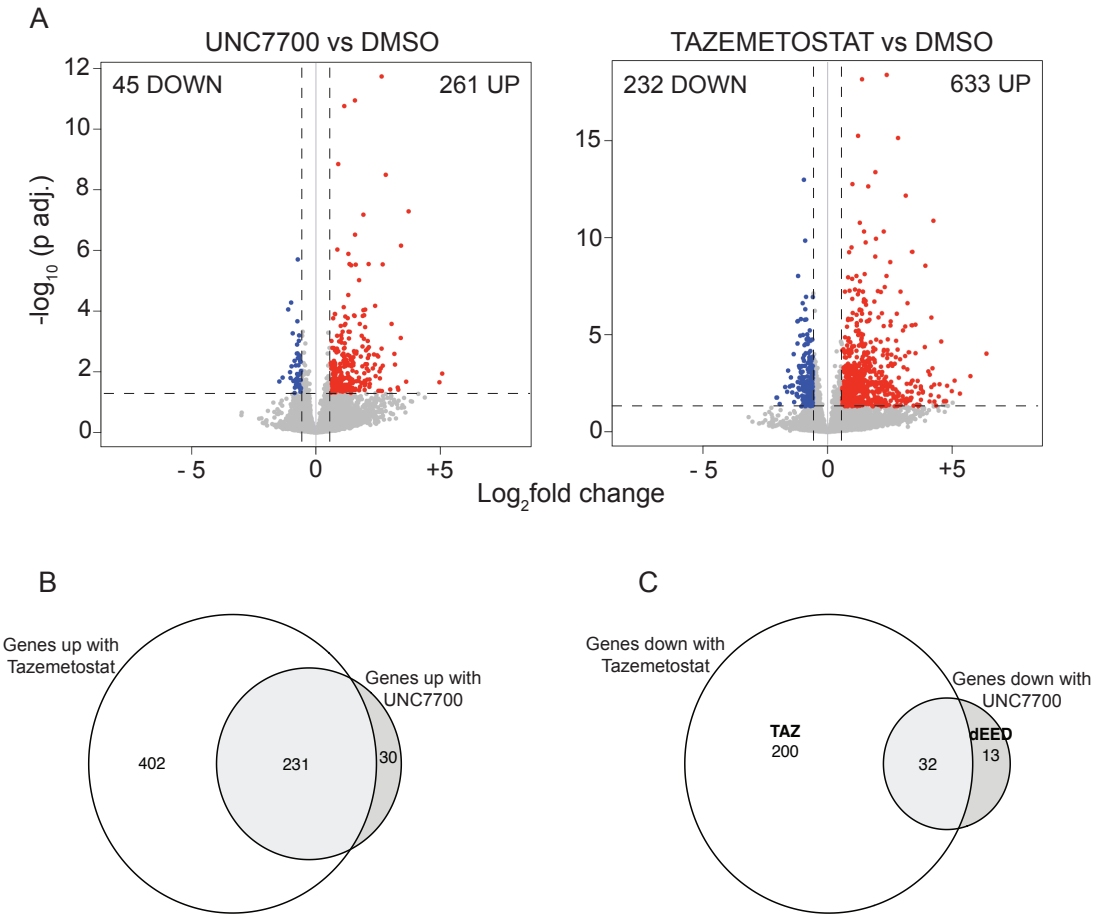

Figure 3.9 PRC2 enzymatic inhibition results in greater gene expression changes than PRC2 degradation

A. Volcano plots of RNA-sequencing representing the $\log_2$ fold change in gene expression in cells treated with UNC7700 compared to DMSO (left) and Tazemetostat compared with DMSO (right). $-\text{Log}_{10}$ of the adjusted p value is represented on the Y-axis.

B-C. Venn diagrams demonstrating that most genes upregulated or downregulated by treatment with UNC7700 compared to DMSO, overlap with those upregulated or downregulated by treatment with Tazemetostat.

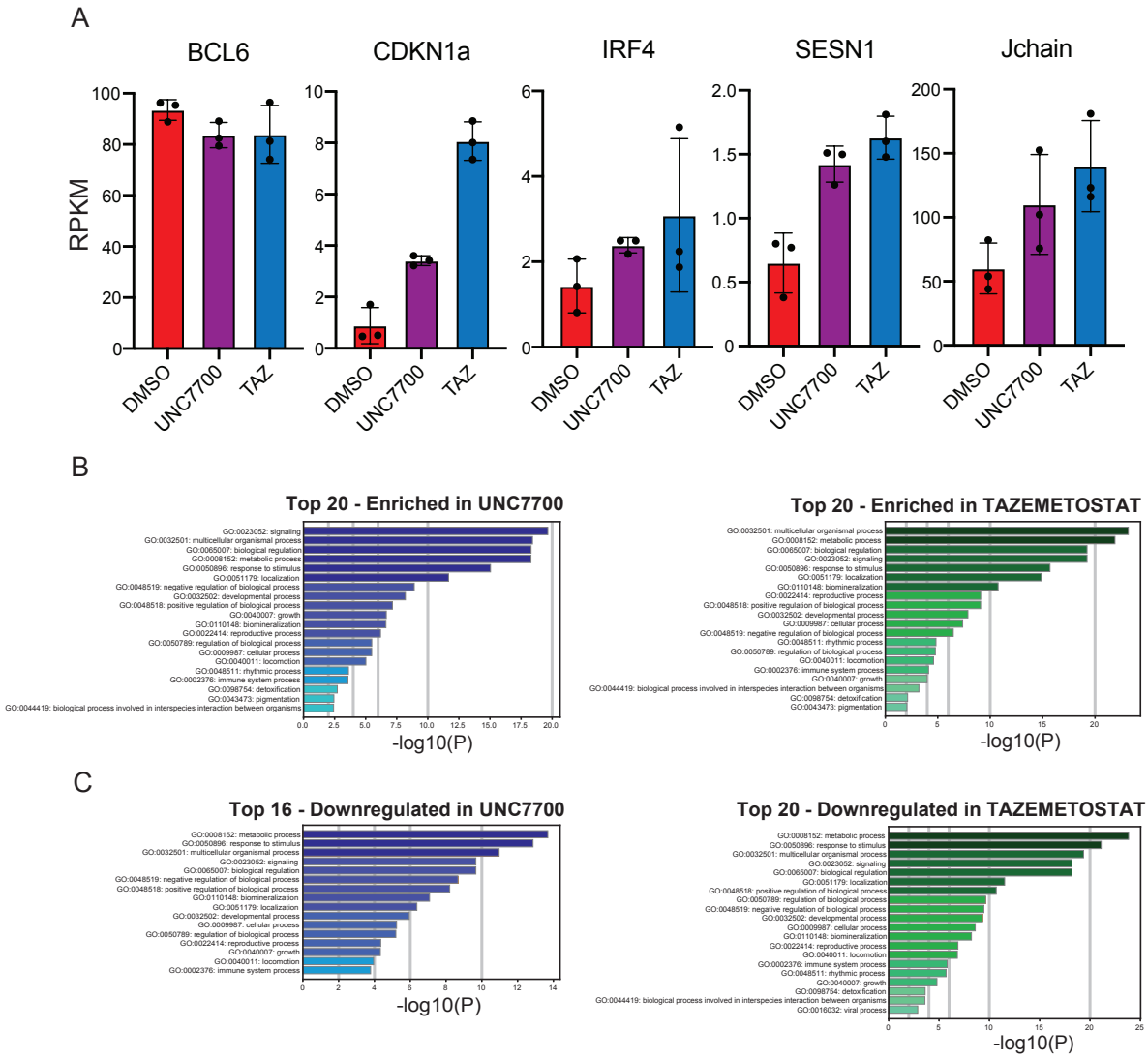

Figure 3.10 Gene expression changes resulting from PRC2 enzymatic inhibition and degradation share gene ontology terms

A. Graphical representation of selected genes demonstrating de-repression by both UNC7700 and Tazemetostat treatment, though greater de-repression by Tazemetostat.

B-C. The top 20 Gene ontology (GO) terms for genes upregulated (B) and downregulated (C) upon treatment with UNC7700 and Tazemetostat based on p-value. Note: only 16 terms significantly derepressed with UNC7700 treatment. GO obtained using the Metascape database [http://metascape.org]

3.3 Discussion

Although it well described that the nett effect of the gain/change-of-function EZH2 mutation in lymphoma is massive gain of H3K27me3 and reduction in H3K27me2, previously published ChIP-Seq data was not normalised to an exogenous reference genome for quantification, with the result that subtle dynamic changes in this epigenomic profile could be underappreciated (Orlando et al., 2014). The isogenic model of an EZH2 wild-type GCB-DLBCL cell line expressing either wild-type EZH2 or EZH2^{Y646F} will provide a useful point of reference for those working in the lymphoma field. The subtle increase in SUZ12 binding genome-wide in the mutant context at the expense of slightly less SUZ12 binding at Polycomb target genes suggests that PRC2 is leached away from these sites and has increased occupancy time genome-wide writing H3K27 tri-methylation, where it normally writes di-methylation via transient hit-and-run interactions that do not require stable binding of the complex (Conway et al., 2015; Ferrari et al., 2014; Youmans et al., 2018). Furthermore, we have described with greater comprehensiveness than previously published the well-known pattern of H3K27me3 gain and H3K27me2 conferred by the presence of mutant EZH2. Indeed, over 90% of genomic loci (as parsed into 10kb bins), gain H3K27me3 while losing H3K27me2. Mutant EZH2 results in broader, more poorly defined H3K27me3 peaks at Polycomb target promoters, with marginally higher H3K27me3 5-prime than 3-prime to the peak. Although RNA-Sequencing was not undertaken in this isogenic system, it would be interesting in dissecting the neo-functionalisation of mutant EZH2 by examining transcriptional changes resulting from the rare sites losing H3K27me3.

This isogenic system does not address, however, potential differential binding of PRC2 subcomplex assemblies genome-wide. PRC2.2 has been demonstrated to interact with H2AK119ub across the genome (S. Cooper et al., 2016; Glancy et al., 2021; Kalb et al., 2014; Kasinath et al., 2020), although PRC2.1 has been shown to also have a role in intergenic H3K27me3 deposition (Conway et al., 2021; Healy et al., 2019; Jonas Westergaard Højfeldt et al., 2019). It is as yet undefined if a particular PRC2 subcomplex assembly is responsible for the intergenic accumulation of H3K27me3 in EZH2 mutant lymphoma. This could be addressed by additional ChIP-Rx analyses for substoichiometric components.

An unconventional PRC1 complex comprising PRC1-CBX8-BCOR has been proposed, that binds bivalent Polycomb target gene promoters in lymphoma cells (Béguelin et al., 2016). CBX8 has lower affinity than the other CBX subunits for H3K27me3, only binding meta-stably (Kaustov et al., 2011). Potentially, this subunit may, in the abundance of genome-wide H3K27me3 in the EZH2 mutant context, still play a role in chromatin compaction. Chromatin mass spectrometry of PRC1 components in this isogenic system with and without tazemetostat treatment, although not planned at this time, could potentially shed light on differential binding of PRC1 resulting from the genome-wide increase in H3K27me3. Additionally, it would be interesting to examine the effects of the EZH2 mutation on the landscape of H3K36 methylation marks. It has previously been reported that while H3K36me2 and H3K27me2 commonly co-localise on nucleosomes *in cis* (Streubel et al., 2018), H3K36 methylation inhibits allosteric activation of PRC2 and resultantly its methyltransferase activity, without inhibiting binding of the complex to chromatin (Finogenova et al., 2020; Jani et al., 2019; Klymenko & Jürg, 2004; Schmitges et al., 2011; Streubel et al., 2018; Yuan et al., 2011). Although negative regulation by H3K36 methylation marks on PRC2 activity is well-described, it is unclear whether the reciprocal would also hold to be true. However in a BAP1-deleted mouse ESC model with resultant elevation of intergenic H2AK119ub1 and H3K27me3, reduced levels of intergenic H3K36me2 were observed (Conway et al., 2021). Should H3K36me2/3 be reduced by the increased abundance of H3K27me3 in EZH2 mutant lymphomas, perhaps inhibiting the demethylase for H3K36me2/3 could be an interesting avenue to pursue. Indeed, PRC2-PHF19 has been shown to recruit the H3K36me3 demethylase NO66 and could be contributing to altered H3K36 methylation states in this context (Brien et al., 2012; Kooistra & Helin, 2012a).

Although small-scale and preliminary, our study demonstrating the presence of EZH1-PRC2 within representative neoplastic follicles of well-matched patients with follicular lymphoma is a fascinating prospect. The EZH2 mutational status of these patients is not known, however, mutant EZH2 is not known to alter the expression levels of EZH1 or EZH2 in lymphoma cells. EZH1-PRC2 could be demarcating non-dividing cells, not targetable by PRC2 enzymatic inhibition and likely also to be refractory to chemotherapy if not actively cell cycling (A. J. Cole et al., 2020; Xie et al., 2022). Indeed, loss of function mutations of EZH2 have been attributed to chemoresistance in acute myeloid leukaemia (Göllner et al., 2017; Kempf et al., 2021), albeit that there was no evidence to suggest that cells in this AML context were quiescent. Targeting EZH1-PRC2 via degradation of this complex could be a useful approach

in targeting non-dividing tumours. Furthermore, in a model of acquired resistance to PRC2 inhibitor therapy, PRC2 degradation via EED-targeting PROTAC resulted in a loss of H3K27me3 of similar magnitude to that of PRC2 enzymatic inhibition, likely thereby overcoming acquired resistance, given that the only direct effect of PRC2 enzymatic inhibition is a reduction in H3K27 methylation marks.

PRC2 methyltransferase activity appears to hold the key to the oncogenic function of EZH2 in DLBCL cell lines. Upon treatment with Tazemetostat, all PRC2 enzymatic activity is inhibited to some degree, whereas while PRC2 degradation degrades PRC2 to a large extent, the remaining undegraded complex is not enzymatically inhibited. As a result, in the cell line examined here, Tazemetostat resulted in a greater loss of H3K27me3 genome-wide than UNC7700, albeit that UNC7700 resulted in a greater loss of H3K27me3 at Polycomb-target gene promoters. It is likely that given that PRC2 is most stably bound at these sites, most H3K27me3 is retained there in Tazemetostat-treated cells. However, that was not reflected by the RNA-Sequencing at Day 3, wherein Tazemetostat brought about significantly greater effects on the transcriptional landscape than UNC7700. One tantalising though unproven prospect is that the marginally elevated levels of H3K27me2 in UNC7700-treated cells are maintaining greater repression in this context, or else the intergenic H3K27me3 which is also marginally higher in this treatment compared to Tazemetostat. Despite the less marked effect of UNC7700 on the transcriptional landscape at Day 3, it should not be forgotten that few cells survive as long as day 6 of treatment with a 10μM, which could indicate that there are dramatic transcriptional changes at some time point between day 3 and day 6, or another directly toxic effect of the compound. However, at lower concentrations of drug, the degradation of PRC2 was not robust. Further iterations of improved compounds may go towards improving this understanding. Additionally, it would be interesting to examine whether destabilisation of PRC2 influences the localisation of PRC1. Indeed, as previously discussed, the hierarchical model of Polycomb recruitment to chromatin reflects CBX subunits in cPRC1 binding the H3K27me3 mark and mediating chromatin compaction via oligomerisation of its PHC subunits (Blackledge et al., 2020; Fursova et al., 2019; Kyo-ichi Isono et al., 2005). PRC2 degradation offers an opportunity to interfere with PRC2 enzymatic activity due to lower abundance of the methyltransferase complex, to degrade EZH1-PRC2 in non-proliferating cells and also to disrupt cPRC1 binding due to ablation of the H3K27me3 mark.

Work detailed in Chapters 4 and 5 begins to examine the contribution of substoichiometric components of PRC2 to the mechanism of action of the EZH2 oncogene.

Chapter 4: A CRISPR tiling screen of PRC2 components in germinal centre B-cell lymphoma reveals AEBP2 as a specific genetic dependency

4.1 Introduction

Ectopic expression of the Cas9 endonuclease, the enzymatic component of type II CRISPR (clustered regularly interspaced palindromic repeats) and a single guide RNA (sgRNA) can generate a double-strand break (DSB) at a specific region of interest in the genome (Cong et al., 2013). Non-homologous end joining following these DSBs is error-prone, with the potential to generate an array of short deletion, insertion or frameshift mutations in the vicinity of the sgRNA recognition site. CRISPR/Cas9-mediated gene editing is an extremely useful and precise tool for genetic loss-of-function screening, representing an improvement over RNA interference, the utility of which is limited by incomplete protein depletion and confounding off-target effects (Echeverri et al., 2006; Jackson et al., 2006; Shalem et al., 2014). Cells transduced with sgRNAs targeting functionally important domains are outcompeted by non-transduced cells in culture, indicating negative selection attributable to perturbation of an essential gene or domain (J. Shi et al., 2015). This technology has been utilised also to identify novel genetic dependencies in a number of diseases including cancer and sickle cell disease, as well as to identify potential novel domains or dependencies within known genes (Brien et al., 2018; Grevet et al., 2018; J. Shi et al., 2015). CRISPR/Cas9-mediated gene editing is also scalable and can be done in a massively parallel fashion, whereby a pool or "library" of sgRNAs is simultaneously transduced into a population of cells, which when sequenced at an early and late timepoint can identify sgRNAs which have been negatively selected either by causing cell death or by being out-competed, over the time course of the experiment (Burgess, 2020).

CRISPR was first described within the realm of the bacterial adaptive immune system (Ishino et al., 1987; Terns & Terns, 2011; Wiedenheft et al., 2012). The discovery that it could be repurposed to induce targeted genome edits in other cellular contexts by exogenous transduction of a gRNA molecule (comprising crRNA – CRISPR RNA with sequence homology for the DNA target sequence and tracrRNA – transactivating CRISPR RNA, providing a scaffold) and a suitable endonuclease enzyme, ultimately earned Professor Jennifer Doudna and Professor Emmanuelle Charpentier the Nobel Prize in Chemistry 2020 (Cong et al., 2013; Jinek et al., 2012). Since that time, numerous iterative improvements have honed the efficiency and specificity of this system, including the development of novel endonucleases with enhanced on-target and reduced off-target effects (Bravo et al., 2022; Strecker et al., 2019; Tsai et al., 2015). Off-target effects remain an issue for CRISPR and are increasingly

recognised, with issues arising due to promiscuous gRNA activity at alternative PAM sites and genomic regions with incomplete sequence homology (Doench et al., 2016; P. D. Hsu et al., 2013). The availability of a suitable Protospacer Adjacent Motif (PAM) sequence, essential for activity of the endonuclease at its target site, can be another rate-limiting step. Clinical trials involving CRISPR-based cellular therapy in human patients are recently reporting preliminary results. One example is the use of CRISPR/Cas9-mediated gene editing therapy for patients with monogenic red cell disorders such as Sickle Cell Anaemia and β-thalassaemia. Normal adult haemoglobin A comprises a globulin tetramer of 2 α-globulin and 2 β-globulin chains (α2β2). Sickle cell anaemia and β-thalassaemia are characterised by a pathologically missense mutated β-globin gene and a deficiency of β-globin respectively. Restoration of foetal haemoglobin F (α2γ2) by targeting the enhancer of the transcription factor BCL11a using CRISPR/Cas9 in autologously harvested CD34+ haematopoietic stem cells has shown positive early data and rendered a population of patients transfusion-independent and significantly less debilitated by their illness (Frangoul et al., 2021).

In 2020, the EZH2 selective small molecule enzymatic inhibitor Tazemetostat (EPZ-6438) received accelerated approval from the US FDA (Food and Drink Administration) for the treatment of EZH2-mutant lymphoma beyond second line, relapsed/refractory EZH2-wild type lymphoma where no suitable alternative exists, and for unresectable INI1/SMARB1 deficient epithelioid sarcoma and other SMARCB1 deficient soft tissue sarcomas (FDA 2020 reference ID 4627347). As previously discussed in Chapter 3 sections 3.1 and 3.2.4, de novo EZH2 mutations conferring acquired resistance to EZH2 inhibitor therapy have been demonstrated in lymphoma cell lines and are anticipated to account for acquired resistance and secondary progression amongst initial responders to Tazemetostat in human patients with lymphoma. This is a strong motivator to identify additional vulnerabilities associated with the oncogene EZH2 in lymphoma.

The primary aim of this chapter was to perform a large-scale CRISPR tiling screen utilising every available PAM sequence within all known components of PRC2, to uncover any novel genetic dependencies in PRC2 in the context of EZH2 mutant lymphoma. Secondary aims were to uncover any candidate substoichiometric components that might contribute to the mechanism of action of the EZH2 oncogene and to validate any findings arising from the CRISPR tiling screen.

4.2 Results

4.2.1 Preparation of lymphoma cell lines for PRC2 tiling CRISPR screen

Prior to optimisation of lymphoma cell lines for transduction with a PRC2 tiling library, I examined publicly available data from Project Achilles: a compendium of genome-wide CRISPR data from over 1000 cell lines (Meyers et al., 2017). This identified that SUZ12, EED and EZH2 were predicted genetic dependencies in both EZH2 wild-type and mutant germinal centre B-cell lymphoma cell lines, with no clear signal in terms of genetic dependencies among the substoichiometric PRC2 components (Figure 4.1A). Western blot analyses were performed across a panel of lymphoma cell lines to examine the relative expression of different PRC2 components (Figure 4.1B). This revealed that in EZH2 mutant cell lines, the PRC2.2 component JARID2 was more weakly expressed than in EZH2 wild type cell lines. PRC2.1 component PALI1 was weakly expressed in KARPAS-422, while EPOP was not visibly expressed in Pfeiffer. EZH2 mutant cell lines demonstrated the expected pattern of elevated H3K27me3 and reduced H3K27me2 as compared with EZH2 wild-type lymphoma cell lines (Figure 4.1C).

In collaboration with Dr Chun-Wei Chen (Beckman Research Institute, City of Hope, California), Dr Eric Conway (Bracken lab) designed a fully saturated sgRNA library utilising every available PAM sequence targeting exonic regions of genes encoding core and auxiliary components of PRC2, as well as numerous positive and negative controls. The library comprises approximately 4000 sgRNAs (Figure 4.2A-B). EZHIP was not included in the screen as at the time of library design it was not established as a PRC2 component, and reassuringly is not known to be expressed in haematopoietic cells in any case (Ragazzini et al., 2019). The sgRNA library was cloned into an iPUSEPR plasmid, containing a sgRNA scaffold and RFP reporter. Rigorous optimisation by Dr Chen ensured equal representation of sgRNAs within the library.

Briefly, the pipeline for optimisation of cell lines for this CRISPR library was as follows. Firstly, FLAG-tagged *Strep. pyogenes* Cas9 endonuclease was stably expressed in cells by lentiviral transduction followed by blasticidin selection (10 μg/ml) (Figure 4.2C).

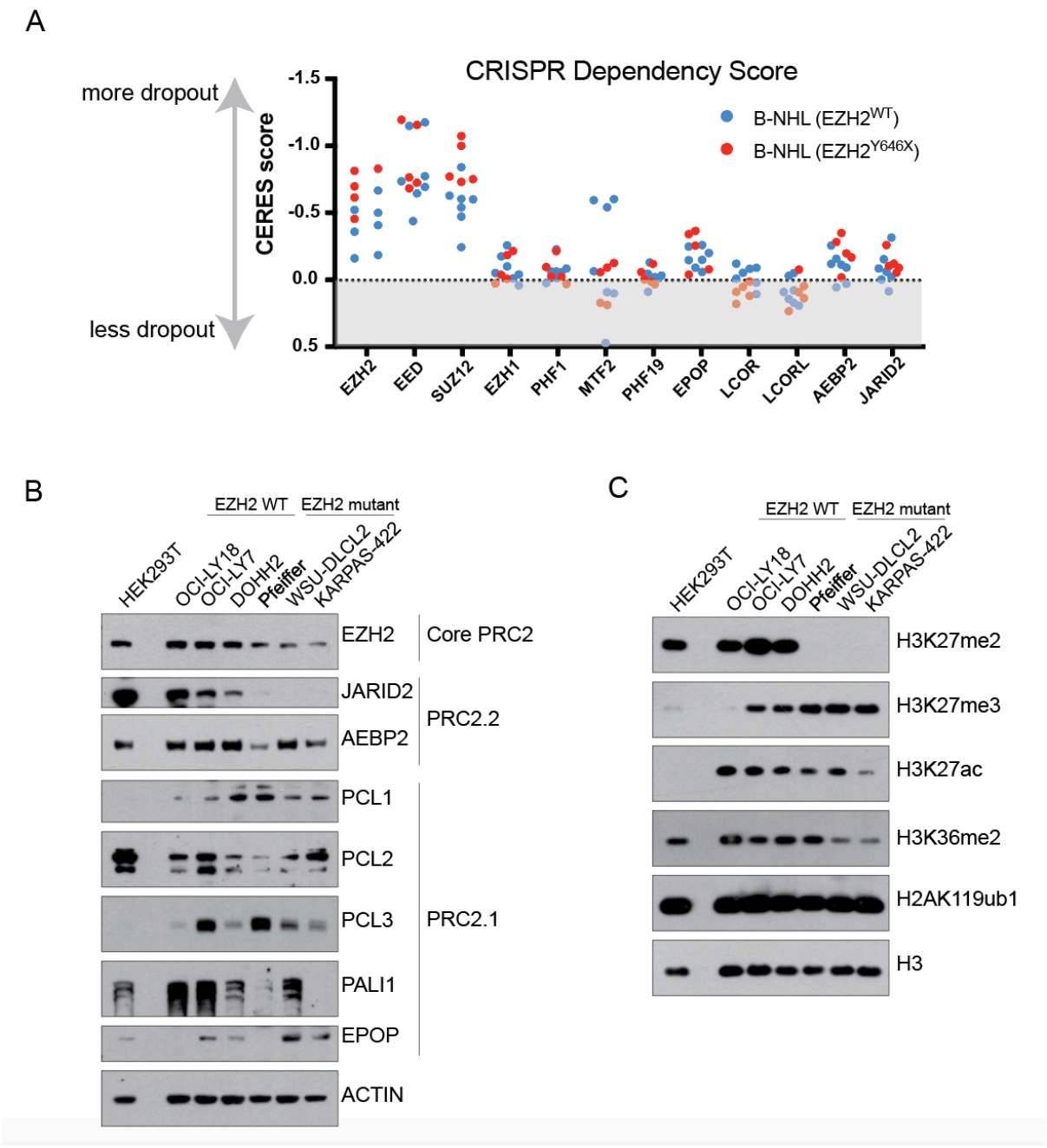

Figure 4.1 Predicted vulnerabilities of B-cell NHL cell lines to disruption of PRC2 components and baseline whole cell western blots

A. Project Achilles data illustrating perturbation effects of sgRNAs targeting PRC2 components (6 sgRNAs per gene) from genome-wide screen in lymphoma cell lines (EZH2 mutant and wild-type as indicated). Data downloaded from depmap.org (21q4 data set).

B. Western blot analysis of EZH2 and PRC2.1/PRC2.2 subcomplex components in EZH2 mutant and wild-type lymphoma cell lines with HEK293T included for reference. Note: CRISPR screen performed in Pfeiffer and WSU-DLCL2 EZH2 mutant cell lines.

C. Western blot analysis of histone post-translational modifications in EZH2 wild-type and mutant cell lines with histone H3 as loading control.

Cells surviving blasticidin treatment were harvested for western blot analysis, to confirm FLAG-Cas9 expression. The cutting efficiency of Cas9-expressing cells was determined using a Cas9 activity assay modified for suspension cells (Chapter 2 section 2.1.5) (Figure 4.2D). Cell lines with Cas9 efficiency ≥70% were suitable for transduction with the PRC2 lentiviral library and were also suitable for use in subsequent validation work detailed later in this chapter. Aiming for a multiplicity of infection of 10-25% such that only one sgRNA would be transduced per cell, the sgRNA library was lentivirally transduced, with 5 million pelleted cells harvested at the first and final timepoints for each biological replicate and subsequent processing for genomic DNA extraction and high-throughput sequencing as detailed in section 2.1.6. Fold changes in sgRNA abundance between the first and final timepoint demonstrate sgRNAs negatively selected/outcompeted over the time course of the experiment (Figure 4.2F).

A number of germinal centre lymphoma cell lines were optimised and reached the desired cutting efficiency of ≥70% by Day 14-21 of the PXPR protocol (Figure 4.2E), although several cell lines required multiple rounds of infection to do so (OCI-LY1, HT). We chose to proceed with the cell lines Pfeiffer and WSU-DLCL2 for the CRISPR PRC2 tiling screen, as representative EZH2 mutant cell lines with the 2 most common EZH2 mutations: $EZH2^{A682G}$ (Pfeiffer) and $EZH2^{Y646F}$ (WSU-DLCL2). Dr Eric Conway and I performed these screens. Two biological replicates were completed with pellets harvested at Day 3 and Day 18 following library transduction. Harvested cell pellets were frozen in liquid nitrogen and processed by Dr Chun-Wei Chen, as detailed in Chapter 2, section 2.1.6.

4.2.2 PRC2-focussed CRISPR tiling screen reveals AEBP2 and core PRC2 components EZH2, EED and SUZ12 as genetic dependencies in germinal centre B-cell lymphoma

Next generation sequencing data was returned from Dr Chen's group, with quality control indicating that over 90% of library guides were represented in the sequenced pool at the day 3 timepoint for each lymphoma cell line and replicate. Given that the library was designed to be saturated for every possible PAM sequence targeting coding regions in PRC2, numerous guides within the library had high off-target probability CFD (Cutting Frequency Determination) scores and were filtered out at this point, reducing the size of the library from 3973 to 3532 sgRNAs (Doench et al., 2016). Furthermore, guides present at low coverage (<10 reads per

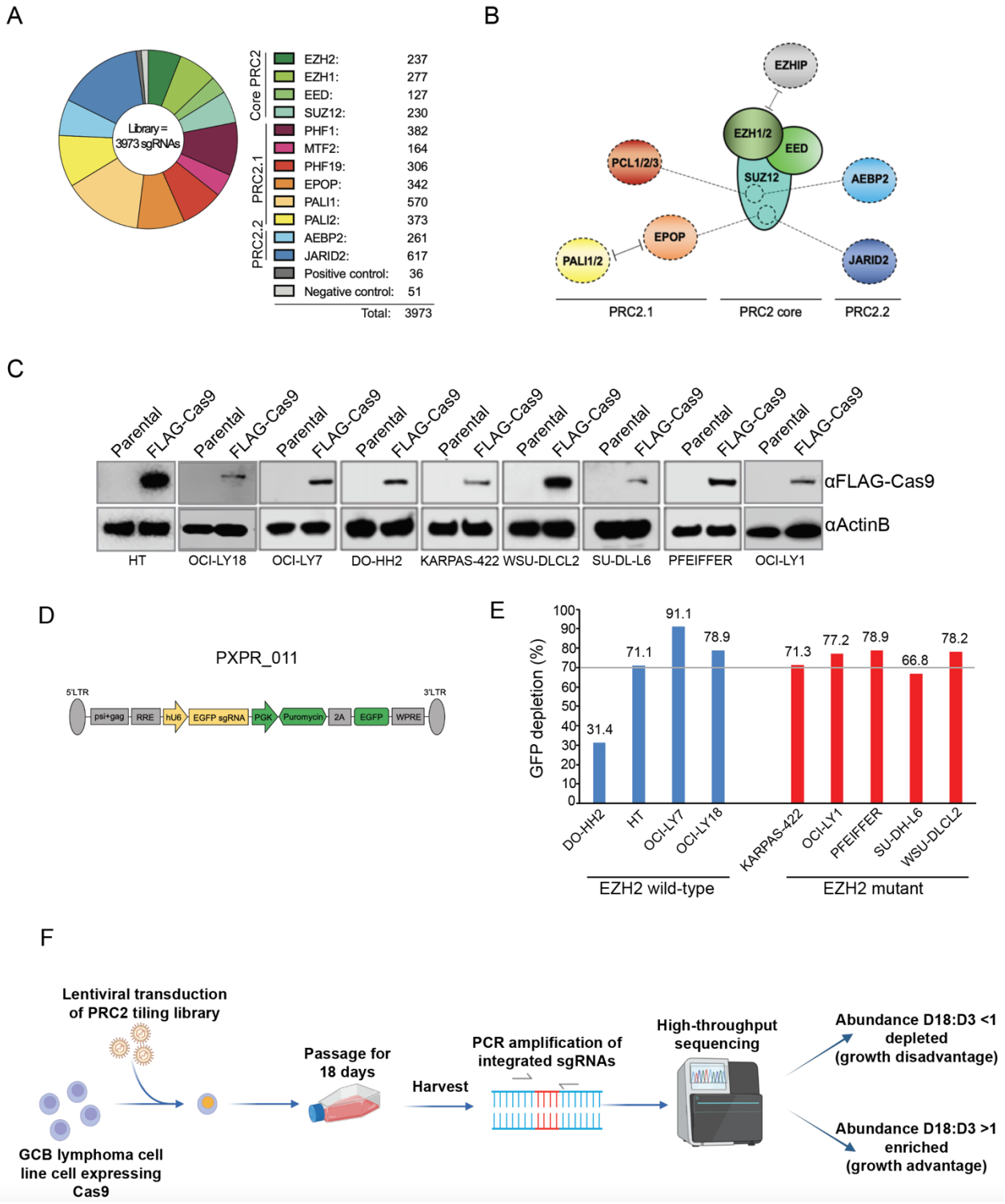

Figure 4.2 Generation and optimisation of lymphoma cell lines for CRISPR screen

A-B: Schematic representation of PRC2 and guide representation in saturated PRC2 tiling library.
C: Western blot analyses using indicated antibodies to demonstrate FLAG-Cas9 expression.
D: Schematic of pXPR_011 plasmid containing EGFP and sgRNA targeting EGFP.
E: Bar chart representation of GFP depletion measured using a BD Accuri flow cytometer to determine Cas9 cutting efficiency at Day 14-21 following infection with pXPR_011 lentivirus.
F: Schematic of CRISPR tiling screen work-flow.

million reads) at day 3 for each cell line were removed from analysis for that cell line, to reduce the likelihood of small artefactual changes being interpreted as biologically relevant. Therefore the final analysed PRC2 library with predicted off-target and low coverage guides removed consisted of 3070 guides for WSU-DLCL2 and 3067 guides for Pfeiffer respectively (Figure 4.3A).

The results of the PRC2 tiling library are displayed in figure 4.3B-C with the median value for sgRNAs targeting a particular gene and the interquartile range represented (i.e. 50% of sgRNAs fall within the indicated range). This graphic displays the $\log_2$ fold change for each sgRNA across two biological replicates. The positive control sgRNAs depleted well for each cell line and in the lymphoma cell lines the negative control sgRNAs either did not deplete or were enriched.

In the EZH2 mutant lymphoma cell lines WSU-DLCL2 and Pfeiffer, core PRC2 components EZH2, EED and SUZ12 depleted robustly. Pfeiffer, a much more slow-growing cell line than WSU-DLCL2, was likely harvested at too early a time-point to see maximal depletion of sgRNAs and highlight genes of interest. As previously discussed, EED and EZH2 are known to be targetable dependencies in B-cell lymphoma and have been inhibited enzymatically in numerous studies using various molecules to date. It follows that SUZ12 would also be a dependency given that it comprises an indispensable part of core PRC2 alongside EED and EZH2. However, one surprising and very interesting finding was that AEBP2 was the only substoichiometric component where over 50% of sgRNAs depleted in both lymphoma cell lines, with WSU-DLCL2 outperforming Pfeiffer likely due to Pfeiffer cells being harvested at too early a final timepoint. As seen in western blots from these cell lines in Figure 4.1B, AEBP2 is strongly expressed. JARID2, the other component of PRC2.2, is weakly expressed in these cell lines on western blot and did not deplete in this CRISPR screen.

I subsequently went on to validate the findings of this CRISPR tiling screen using more discrete sgRNA and shRNA experiments.

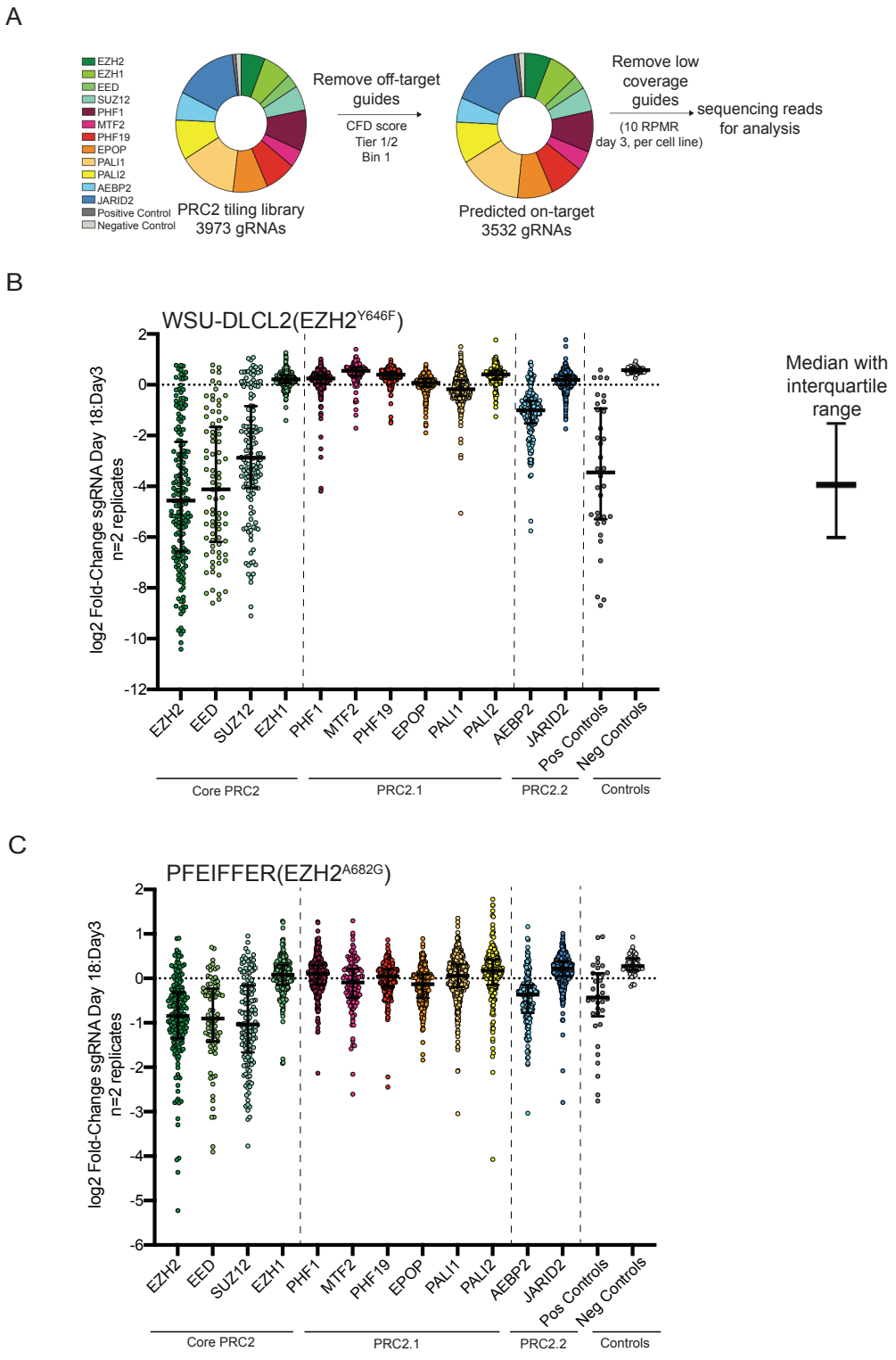

Figure 4.3 PRC2 tiling screen results in EZH2 mutant lymphoma cell lines

A. Schematic representation of post-sequencing filtration of sgRNA library to remove off-target and low coverage sgRNAs.

B-C. PRC2 tiling library results in cell lines WSU-DLCL2 (B) and Pfeiffer (C). Log_2 fold change of sgRNA abundance Day 18:Day3 is shown on the Y axis (n=2 replicates). Median and inter-quartile range sgRNAs targeting each PRC2 gene or positive/negative controls are indicated. Each dot represents one sgRNA.

4.2.3 PRC2.2 component AEBP2, but not JARID2, is a specific genetic dependency in germinal centre B-cell lymphoma.

Having demonstrated in the CRISPR tiling screen that core PRC2 and AEBP2 were candidate genetic dependencies in the EZH2 mutant lymphoma cell lines WSU-DLCL2 and Pfeiffer, I then wished to validate these findings and examine the potential genetic dependency on AEBP2 more closely.

AEBP2 (Adipocyte enhancer binding protein 2) was first identified as a transcriptional repressor at the aP2 gene in mouse cells (G. P. He et al., 1999) and was subsequently co-purified with PRC2 in mass spectrometry in human cells (Cao et al., 2002). Several isoforms of AEBP2 exist in mammals due to the existence of alternative promoters (H. Kim et al., 2009). Differential functions for AEBP2 isoforms have not yet been elucidated, though based on expression patterns it has been proposed that the short isoform of AEBP2 is embryonic-specific while the long isoform is ubiquitous/somatic (H. Kim et al., 2009, 2011). To date, no discrete functions or domains have been ascribed to the N-terminus of AEBP2 (residues 1-216) which is absent from the short isoform.

Three tandem C2H2 zinc finger domains are well-recognised within AEBP2 and have been proposed as interactors with DNA and H2AK119ub1 (Kasinath et al., 2021; H. Kim et al., 2009; Poepsel et al., 2018). Furthermore, a KR-rich motif towards the C-terminus of AEBP2 has been demonstrated to be essential for PRC2 interaction with nucleosomal DNA, with a recent cryo-EM structure demonstrating this interaction (Kasinath et al., 2021; C. H. Lee, Yu, et al., 2018). Additionally, the C-terminus of AEBP2 has been shown to associate with core PRC2 components SUZ12 and RBBP4 (S. Chen et al., 2018, 2020; Ciferri et al., 2012; Kasinath et al., 2021; C. H. Lee, Yu, et al., 2018; Poepsel et al., 2018; Sun et al., 2018).

Based on the PAM sequence utilised by each sgRNA, which should induce a double-stranded break 3 base pairs upstream from the PAM, I mapped sgRNAs targeting AEBP2 to its protein-coding sequence (CDS) (NCBI transcript variant 1 NM_153207.5) (Figure 4.4A). This demonstrated that a number of sgRNAs targeting the N-terminus of AEBP2 depleted, in addition to sgRNAs targeting known functional domains of AEBP2. Literature regarding the N-terminus of AEBP2 long isoform is scarce (manuscript currently in preparation by Dr Marlena Mucha). The N-terminus of AEBP2 is extremely GC-rich, with a calculated GC content in the N-terminus specific region of 74.7%, compared to 42.5% for the remainder of

the CDS (Figure 4.4B). High GC content is concerning in a CRISPR screen given that SpCas9 utilises NGG as its PAM sequence. Although off-target guides were filtered out as per the CFD score as previously described, depleting guides towards the N-terminus of AEBP2 in this screen were invariably directly adjacent to a filtered guide, and given the high GC percentage, I was concerned given high sequence homology and potential alternative PAM usage that many of these sgRNAs may represent off-target effects. Furthermore, the N-terminus is negatively charged and therefore likely to repel negatively charged DNA (Figure 4.4C) and also predicted to be highly unstructured (Figure 4.4D) (Erdos et al., 2021; Ishida & Kinoshita, 2007). To minimise the likelihood of attempting to validate the CRISPR tiling screen results using off-target guides, sgRNAs targeting well-described domains in AEBP2; namely Zinc Fingers 1-3 and AEBP2 KR motif were selected. Additionally, several depleting sgRNAs were identified targeting a helix within the SUZ12-binding region of AEBP2 we have annotated as the "SUZ12-binding helix" (SBH), which I will describe in greater detail in section 4.2.5.

Before examining additional cell lines, I first wished to validate the sgRNA hits from the CRISPR tiling screen in the cell lines WSU-DLCL2 and the SMARCB1$^{-/-}$ malignant rhabdoid tumour cell line G401, which was shown in a similar CRISPR tiling screen performed by Dr Marlena Mucha to be dependent on core PRC2 but not on PRC2 substoichiometric components. A number of sgRNAs targeting EZH2, SUZ12, EED, AEBP2 and JARID2 as well as positive and negative controls were cloned into the CRISPR/Cas9 lentiviral vector LRG2.1 which contains a GFP reporter. The experimental validation schematic and sgRNAs cloned for PRC2.2 components AEBP2 and JARID2 are illustrated in Figure 4.5A-B. Flow cytometry was performed using the Guava easyCyte flow cytometer and resultant data analysed using FlowJo software. This WSU-DLCL2 and G401 validation work was done in collaboration Dr Daniel Angelov (Bracken Lab). Both cell lines depleted for sgRNAs targeting core PRC2, but only WSU-DLCL2 depleted for AEBP2-targeting guides. Both were agnostic to JARID2 disruption. This experiment demonstrated again that the lymphoma cell line WSU-DLCL2 is exquisitely sensitive to sgRNA-mediated disruption of core PRC2 components and AEBP2, but not JARID2 (Figure 4.5C). The malignant rhabdoid tumour cell line G401 was less sensitive to core PRC2 disruption than WSU-DLCL2, though these sgRNAs did significantly deplete (Figure 4.5D). Thus, I validated the findings of the tiling screen in these cell lines and that AEBP2 is a specific dependency in WSU-DLCL2 and not G401.

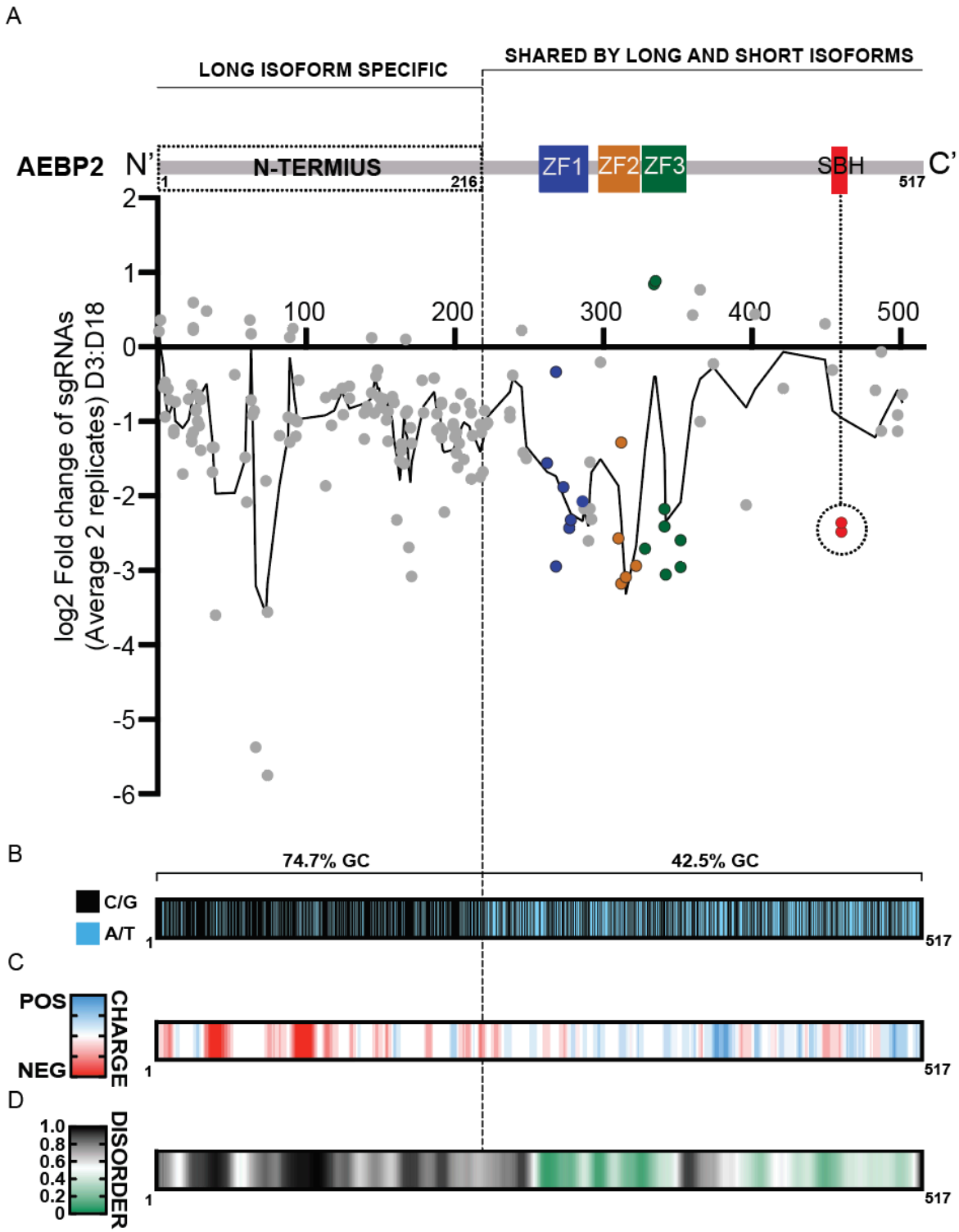

Figure 4.4 sgRNAs targeting AEBP2 N-terminus, Zinc fingers and SUZ12 binding helix (SBH) are negatively selected in the lymphoma cell line WSU-DLCL2

A. Gene scanning view mapping sgRNAs along the AEBP2 gene against their log2 fold-change in the PRC2 CRISPR tiling screen. Each dot represents one sgRNA.

B. AEBP2 N-terminus is significantly more GC-rich than its C-terminus.

C.The N-terminus of AEBP2 has a nett negative charge, with the potential to result in repulsion from negatively-charged DNA.

D. AEBP2 N-terminus is predicted to be intrinsically disordered based on PRDOS score. Values above 0.5 are predicted to be disordered (coloured in black).

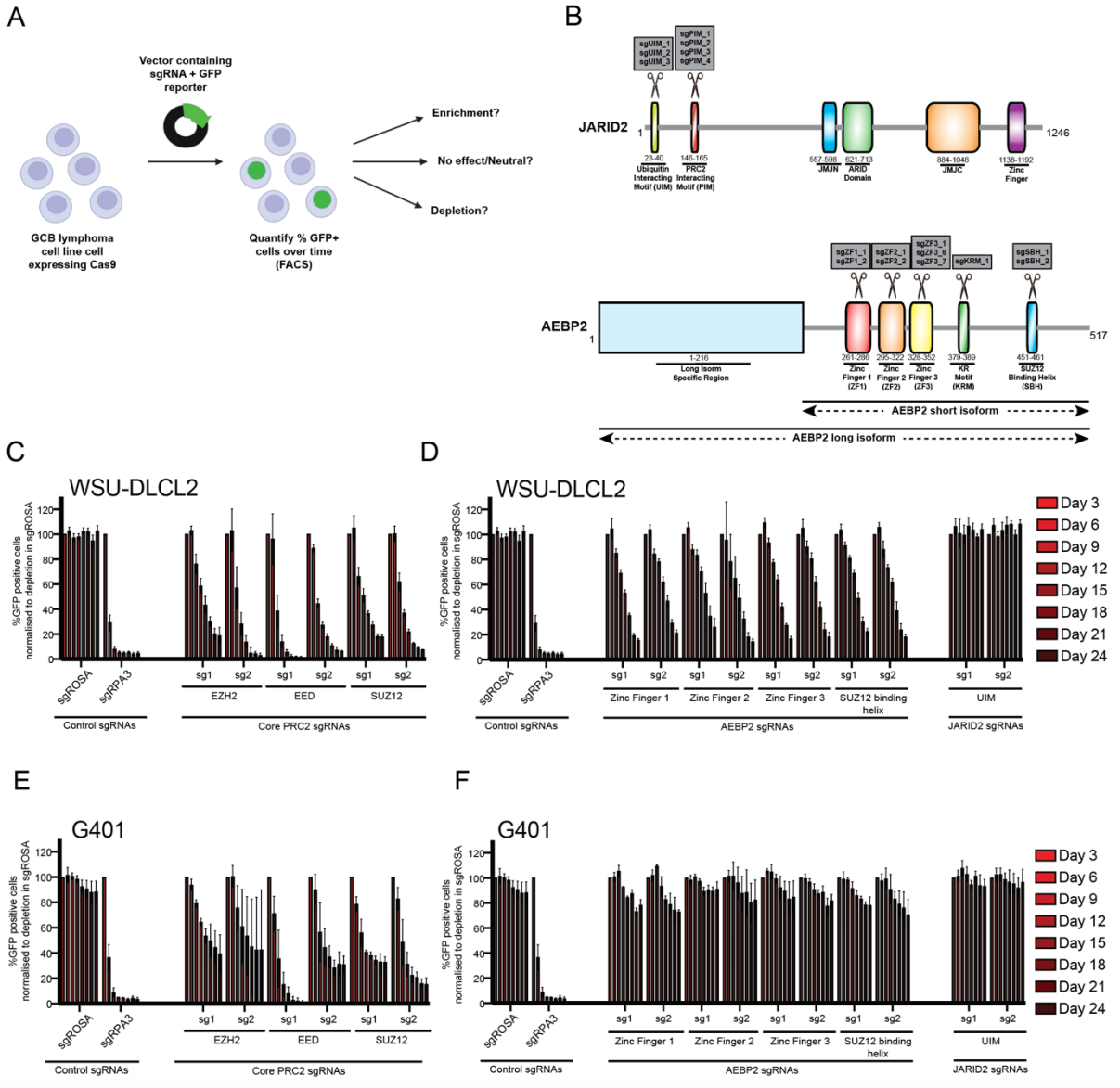

Figure 4.5 PRC2 tiling screen validation in WSU-DLCL2 and G401 confirms AEBP2 sgRNA specificity and AEBP2 genetic dependency in lymphoma

A. Schematic representation of experimental design sgRNA validation.

B. Schematic representation of sgRNAs targeting AEBP2 and JARID2 selected for validation work. Note that annotated domains and selected sgRNAs all target the shared AEBP2 C-terminus, common to all isoforms of AEBP2.

C-D. sgRNA validations utilising control sgRNAs and core PRC2-targeting sgRNAs (C) and PRC2.2 targeting sgRNAs (D) in the lymphoma cell line WSU-DLCL2 (n=4 replicates). Data normalised to Day 3 value and to sgRosa at each time point.

E-F. sgRNA validations utilising control sgRNAs and core PRC2-targeting sgRNAs (E) and PRC2.2 targeting sgRNAs (F) in the malignant rhabdoid tumour cell line G401 (n=4 replicates). Data normalised to Day 3 value and to sgRosa at each time point.

Prior to examining whether AEBP2 was also a dependency in additional germinal centre lymphoma cell lines, I sought first to examine its expression levels in cell lines and patients with germinal centre-derived lymphomas. I performed western blot analysis to examine the expression levels of PRC2.2 components AEBP2 and JARID2 in a number of EZH2 wild-type and mutant lymphoma cell lines (Figure 4.6A). These blots revealed that AEBP2 long isoform was ubiquitously expressed in all cells lines, with weak or absent AEBP2 short isoform expression. JARID2 was variably expressed and absent in a number of EZH2 mutant cell lines. With the assistance of Dr Craig Monger, I examined data from the Sanger Institute Genomics of Drug Sensitivity in Cancer project, which in addition to offering publicly available data regarding drug compounds, offers RNA-Sequencing data for 1000 human cancer cell lines (W. Yang et al., 2013). I analysed RNA-Seq data from B-lymphoid cell lines at various stages of maturation, from extremely immature (B-cell Acute Lymphoblastic Leukaemia) to mature, post-germinal centre neoplasms (Primary Effusion Lymphoma and Multiple Myeloma) (Figure 4.6B). As quality control, I examined genes known to be upregulated at specific times in the B-cell life cycle and suppressed at others; namely TdT (expressed in lymphoblasts), BCL6 (highly expressed in the germinal centre and silenced at lymphocyte exit from the germinal centre) and PRDM1 (involved in the plasma cell terminal differentiation programme). These quality controls were appropriate for putative B-cell stage. The GDSC data confirmed that AEBP2 long isoform is significantly more highly expressed than the short isoform at the RNA level also. Seeking to examine data from patients with lymphoma rather than lymphoma cell lines, I extracted microarray data from a publicly available dataset using Geo2R (Sean & Meltzer, 2007; Shaknovich et al., 2010) (GEO accession entry GSE23967). Concurring with data presented thus far in lymphoma cell lines, this patient-derived data demonstrated that AEBP2 is expressed equally among patients with EZH2 wild-type and mutant GCB-DLBCL (germinal centre-derived diffuse large B-cell lymphoma) and the more mature ABC-DLBCL (activated B-cell DLBCL) (Figure 4.6C).

Motivated by the specific dependency of the B-cell lymphoma cell line WSU-DLCL2 on AEBP2 and the consistent expression of AEBP2 across lymphoid malignancies and in biopsies from patients with lymphoma, I went on to validate AEBP2 as a genetic dependency in additional lymphoma cell lines using sgRNAs in an iPUSEPR backbone containing a red fluorescent protein (RFP) reporter (Figure 4.7). Interestingly, whether or not JARID2 was expressed by western blot, none of the tested cell lines were sensitive to sgRNAs targeting

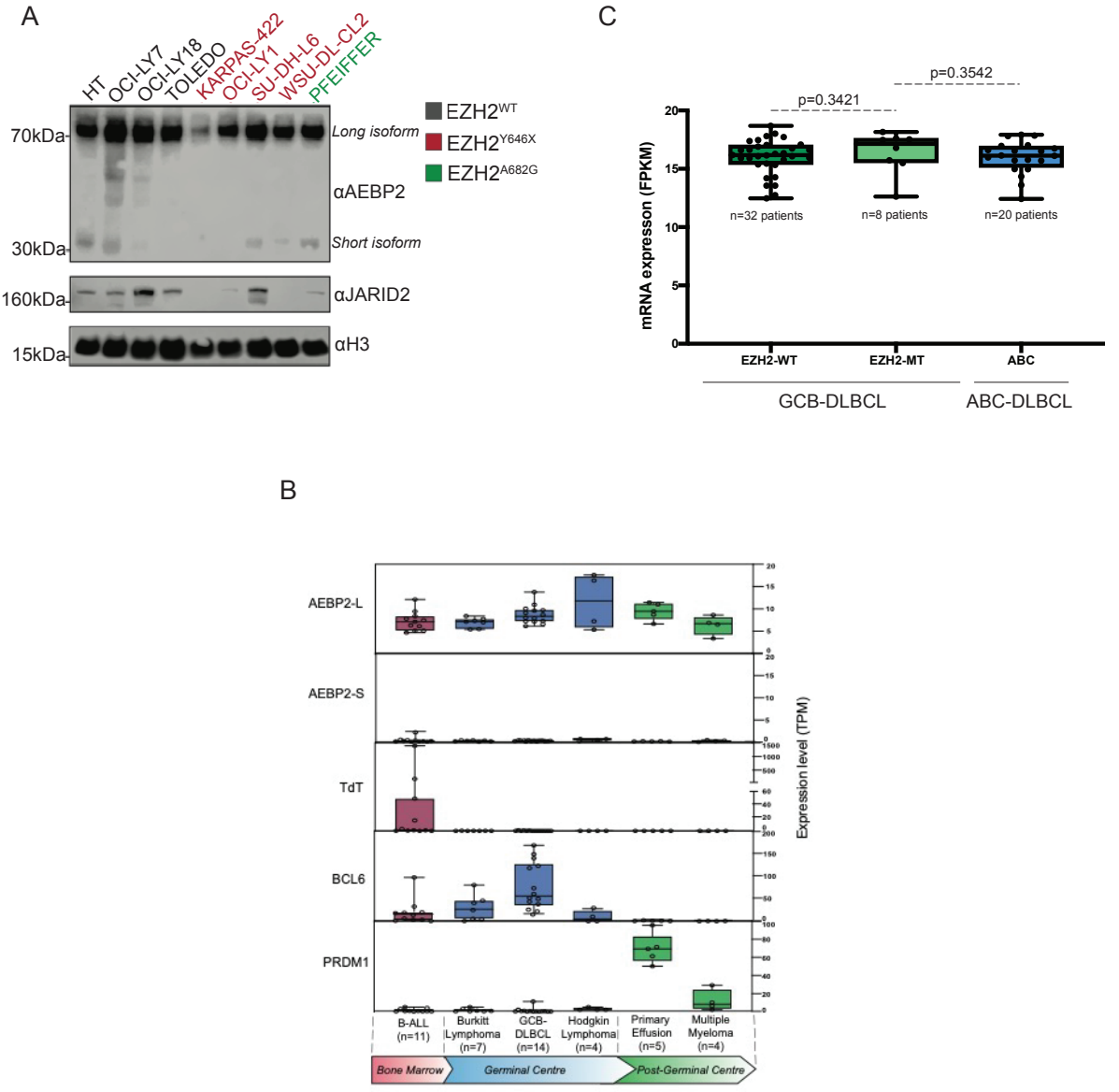

Figure 4.6 AEBP2 long isoform is the predominant AEBP2 isoform in B-lymphoid malignancies

A. Western blot analysis examining AEBP2 and JARID2 expression in B-cell lymphoma cell lines. AEBP2 long isoform (70kDa) is more highly expressed than AEBP2 short isoform (30kDa) in these cell lines.

B. RNA-Sequencing data extracted from Sanger GDSC project demonstrating that AEBP2 long isoform is more highly expressed than AEBP2 short isoform in B-cell neoplasms arising through a spectrum of immaturity to maturity. TdT, BCL6 and PRDM1 included as stage-specific controls. TPM transcripts per million.

C. RNA-sequencing data from patients with EZH2 wild-type and mutant GCB-DLBCL and ABC-DLBCL. Data extracted from (Shaknovich et al., 2010) GEO entry GSE23967. P value calculated using Mann-Whitney test. FPKM fragments per kilobase of exon per million mapped reads.

JARID2, whereas 6 of 7 tested were sensitive to sgRNAs targeting AEBP2 (Figure 4.7A-G). The EZH2 mutant cell line OCI-LY1 was insensitive to AEBP2-targeting sgRNAs. Although this cell line also has frameshift mutations in KMT2D and CREBBP, other cell lines with similar concurrent inactivating mutations (KARPAS-422 and Pfeiffer) remained sensitive to AEBP2 disruption. There was no clear association between AEBP2 dependency and EZH2 mutational status, given that both EZH2 wild-type cell lines (n=3/3) and EZH2 mutant cell lines (n=3/4) were sensitive to loss of AEBP2. The slow growing cell line Pfeiffer from the PRC2 tiling library screen depleted more robustly for AEBP2 in this experiment than in the PRC2 tiling library screen as the experiment was terminated at 36 rather than 18 days.

Next, I decided to examine whether AEBP2 disruption would overcome acquired resistance to EZH2 inhibitor therapy in lymphoma cells. I demonstrated in Chapter 3 Figure 3.6 that ectopic expression of $EZH2^{Y111D/A677G}$ in the EZH2 mutant lymphoma cell line Pfeiffer confers resistance to EZH2 enzymatic inhibition by Tazemetostat, based on previous similar work (Baker et al., 2015a). Given that this mutation is understood to confer resistance by disrupting the Tazemetostat binding pocket in activated EZH2 and not by diminishing its dependency on EZH2, I demonstrated in Chapter 3 that degrading core PRC2 by using the EED PROTAC UNC7700 overcame the acquired resistance to Tazemetostat. Figure 4.8C demonstrates that as would be expected, UNC7700 also results in the intracellular degradation of AEBP2. Utilising sgRNAs expressed in a LRG2.1 vector containing GFP, I performed a GFP depletion assay in Pfeiffer parental cells and Pfeiffer cells with acquired resistance to Tazemetostat, demonstrating that both cell lines are equally dependent on AEBP2 (Figure 4.8A-B). Therefore, I demonstrate that disrupting AEBP2 is a potential mechanism for overcoming acquired resistance to EZH2 inhibitor therapy.

Although AEBP2 has been validated in a number of GCB-DLBCL/transformed follicular lymphoma cell lines as described above, it remains to be evaluated whether AEBP2 may be a dependency in more immature and mature B-cell neoplasms also. I plan to perform sgRNA validation assays in Burkitt lymphoma and ABC-DLBCL cell lines to explore this further.

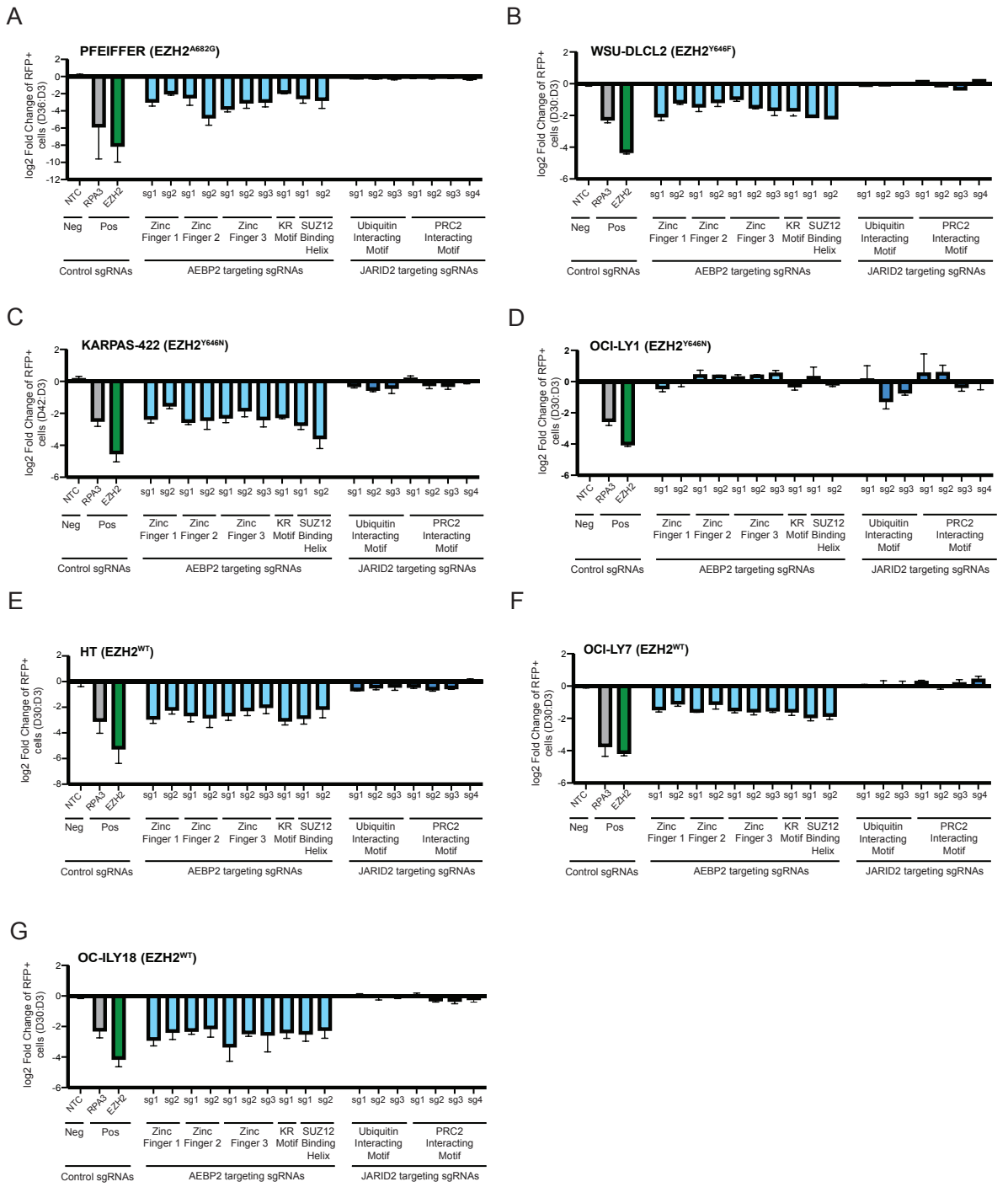

Figure 4.7 Germinal centre lymphoma cell lines are sensitive to AEBP2 and not JARID2 disruption irrespective of their EZH2 mutation status

A-D. sgRNA validations using control, AEBP2 and JARID2-targeting guides in EZH2 mutant cell lines Pfeiffer, WSU-DLCL2, KARPAS-422 and OCI-LY1 (A-D). Log2 fold change of RFP abundance (final timepoint:first timepoint) plotted on Y axis.

E-G. sgRNA validations using control, AEBP2 and JARID2-targeting guides in EZH2 wild-type cell lines HT, OCI-LY7 and OCI-LY18 (E-G). Log2 fold change of RFP abundance (final timepoint:first timepoint) plotted on Y axis.

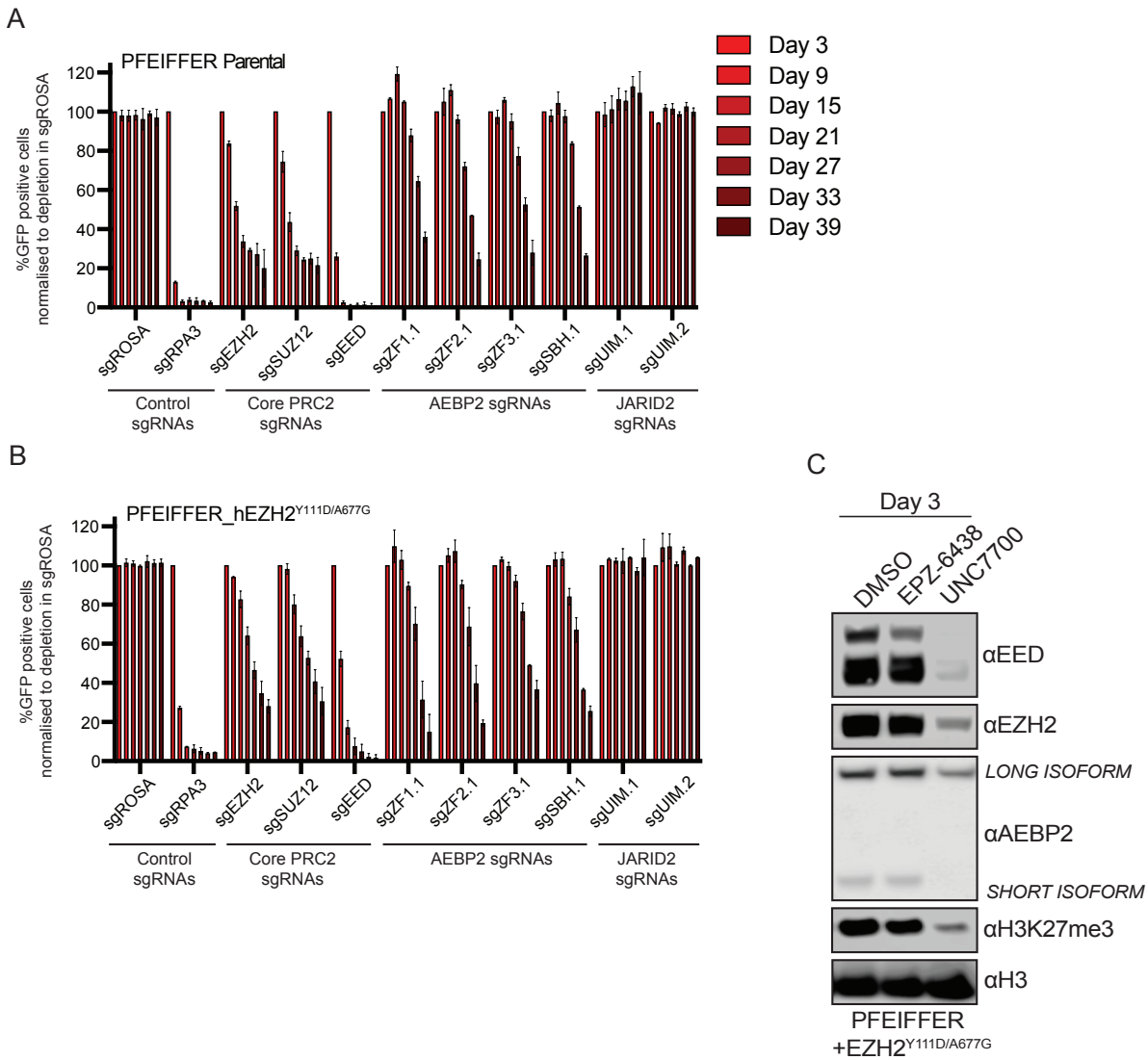

Figure 4.8 AEBP2 depletion overcomes acquired resistance to EZH2 inhibitor drug Tazemetostat

A. GFP depletion assay utilising sgRNAs targeting core PRC2, AEBP2 and JARID2 in Pfeiffer parental cell line (n=4 replicates). GFP measured using Guava easyCyte flow cytometer.

B. GFP depletion assay utilising sgRNAs targeting core PRC2, AEBP2 and JARID2 in Pfeiffer EZH2$^{Y111D/A677G}$ cell line with acquired resistance to EZH2 inhibitor (n=4 replicates). GFP measured using Guava easyCyte flow cytometer.

C. Western blot analysis of EZH2 mutant Pfeiffer cell line expressing ectopic EZH2$^{Y111D/A677G}$, treated with 30nm Tazemetostat or 10μM EED degrader UNC7700, demonstrating disruption of core PRC2 and AEBP2 by EED degradation.

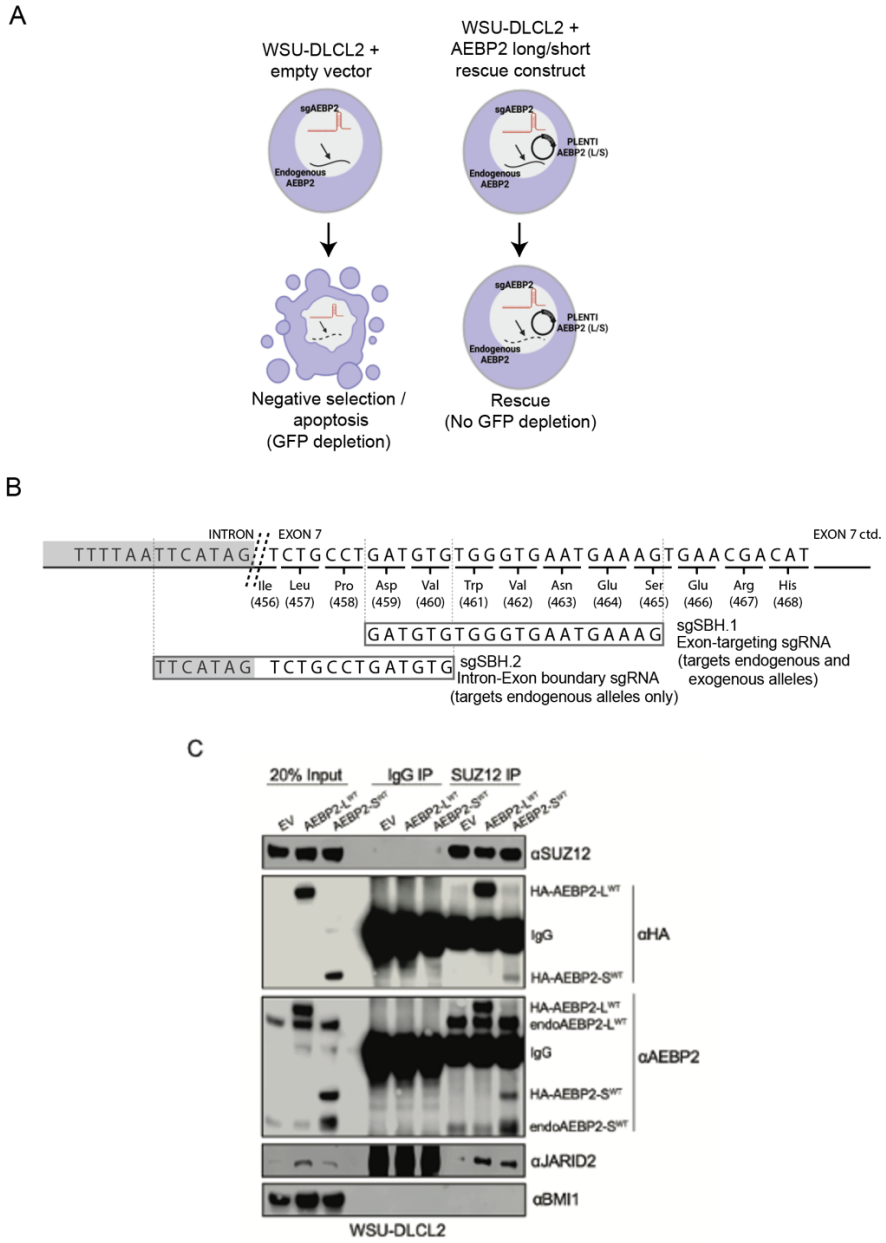

Figure 4.9 Experimental design of AEBP2 rescue and expression of non-targetable wild-type AEBP2 constructs

A. Schematic of AEBP2 rescue experiment in WSU-DLCL2 cells. Cas9-expressing lymphoma cells were lentivirally infected with FLAG/HA-tagged human AEBP2 (long and short isoform respectively) or empty vector, followed by lentiviral infection with an AEBP2-targeting sgRNA. sgRNA abundance was measured at serial timepoints by determining GFP abundance using a Guava easyCyte flow cytometer.

B. Schematic representation of sgRNA choice for rescue experiment. sgSBH.1 represents a sgRNA capable of targeting both exogenous and endogenous AEBP2 in this experiment, whereas sgSBH.2 can only target endogenous AEBP2 due to incomplete sequence homology with the exogenous construct.

C. SUZ12 co-immunoprecipitation followed by western blot analysis in WSU-DLCL2 cell line following infection with empty vector or HA-tagged AEBP2 long/short constructs and puromycin selection. Input consistent with whole cell western blot result.

4.2.4 Ectopic expression of non-targetable human AEBP2 rescues AEBP2 dependency in lymphoma

My comprehensive validation work demonstrated that AEBP2 is a genetic dependency in lymphoma cell lines. However, I wished to ensure that this was specific and not due to off-target effects. To do this, I decided to stably express non-targetable human AEBP2 in the lymphoma cell line WSU-DLCL2 and undertake sgRNA and short hairpin RNA (shRNA) rescue experiments.

The experimental design for this work is outlined in Figure 4.9A. I expressed wild-type AEBP2 long and short isoforms using a PLENTI lentiviral system that contains FLAG and HA tags as well as a puromcyin resistance cassette. These wild-type constructs comprise exclusively exonic DNA, whereas endogenous AEBP2 consists of exonic and intronic DNA. Two sgRNAs targeting AEBP2 were selected with target sequences partially overlapping with intronic DNA. Therefore, these sgRNAs should find sequence homology only with the endogenous AEBP2 sequence, and not the exogenous constructs which lack the intronic sequence partially contained in the sgRNA target. This is illustrated in Figure 4.9B with one of the two selected sgRNAs (sgAEBP2_SBH2) which targets the AEBP2 SUZ12-binding helix (to be discussed in section 4.2.5). Successful and relatively equal expression of AEBP2 long and short wild-type constructs was achieved, with expression similar to that of endogenous AEBP2. Crucially, these constructs were able to co-immunoprecipitate with SUZ12 in the presence of benzonase, indicating that they were in complex with core PRC2 (Figure 4.9C). BMI-1 was used as a negative control, as it is not known to interact with SUZ12

The identified sgRNAs incapable of targeting exogenous AEBP2 - AEBP2_ZF3sg2 and AEBP2_SBHsg2, were used also for validations in figure 4.7 where they were robustly depleted in lymphoma cell lines. These sgRNAs depleted in WSU-DLCL2 empty vector but were rescued by both AEBP2-Long and AEBP2-Short (wild-type) rescue constructs (Figure 4.10A-C), indicating that the AEBP2 dependency in lymphoma cells is both specific and on-target. It was notable that across three biological replicates, although the cell lines were prepared concurrently, depletion for all sgRNAs including positive control sgRNAs targeting RPA3 and EED occurred more slowly, suggesting that the cells with an extra dose of AEBP2 may have had additional fitness or grown more slowly. However, both exogenous AEBP2 long and short isoform constructs clearly rescued cells with disruption of endogenous AEBP2.

I went on to examine whether exogenous AEBP2 long isoform could rescue shRNA-mediated knockdown of AEBP2, given that the long isoform is the most abundant isoform in lymphoma. Utilising the Broad Institute Genetic Perturbation Platform (GPP) and suggested shRNA sequences from (Fellmann et al., 2013), I cloned 6 shRNAs targeting EZH2 (as positive controls) and 6 shRNAs targeting AEBP2 into the shRNA lentivral vector SGEP, which contains a GFP reporter and puromycin resistance cassette. Dr Gerard Brien (Brien Lab, Trinity College Dublin) had previously cloned a non-targeting shRNA: shRenilla. I selected AEBP2-targeting shRNAs that target the 3' UTR (untranslated region) of AEBP2, such that exogenously expressed AEBP2 would not be targetable by these hairpins. Knockdown of AEBP2 was examined on the protein level by whole cell western blot and on the mRNA level by RT-qPCR on Day 7 following lentiviral infection and puromycin selection of the lymphoma cell line WSU-DLCL2 (Figure 4.11A-D). AEBP2 hairpins 2 and 6 reduced AEBP2 expression on the protein level by over 80% at Day 7 and on the mRNA level by 60% and were selected on that basis for the rescue experiment. I observed additionally that H3K27me3 levels appeared to increase with AEBP2 knockdown, although uneven loading was noted. EZH2 hairpins 1 and 5 were selected as they demonstrated the strongest knockdown of EZH2 by protein and mRNA analysis and as expected reduced levels of H3K27me3 in the cells. Notably, by Day 14, endogenous protein levels had partially recovered for all EZH2 hairpins and for AEBP2 hairpin 2 (data not shown), suggesting in a purified population of cells following puromycin selection, cells with less efficient knockdown were outcompeting those with efficient knockdown. However, this would not be the case for growth competition assays in a mixed, unselected population as uninfected cells would retain a growth advantage.

In a growth competition assay using a Guava easyCyte flow cytometer, in WSU-DLCL2 transduced with SGEP empty vector, both EZH2 and AEBP2 hairpins were outcompeted by uninfected cells over time, as illustrated by GFP depletion over time. However, cells expressing the AEBP2 long isoform rescue construct were fully rescued following infection with shAEBP2, but not shEZH2 lentiviruses (Figure 4.11E-F). With both sgRNA and shRNA rescue experiments taken together, exogenous expression of non-targetable AEBP2 fully rescued cellular dropout from endogenous AEBP2 disruption, demonstrating rigorously and comprehensively that AEBP2 is a dependency in germinal centre lymphoma cell lines.

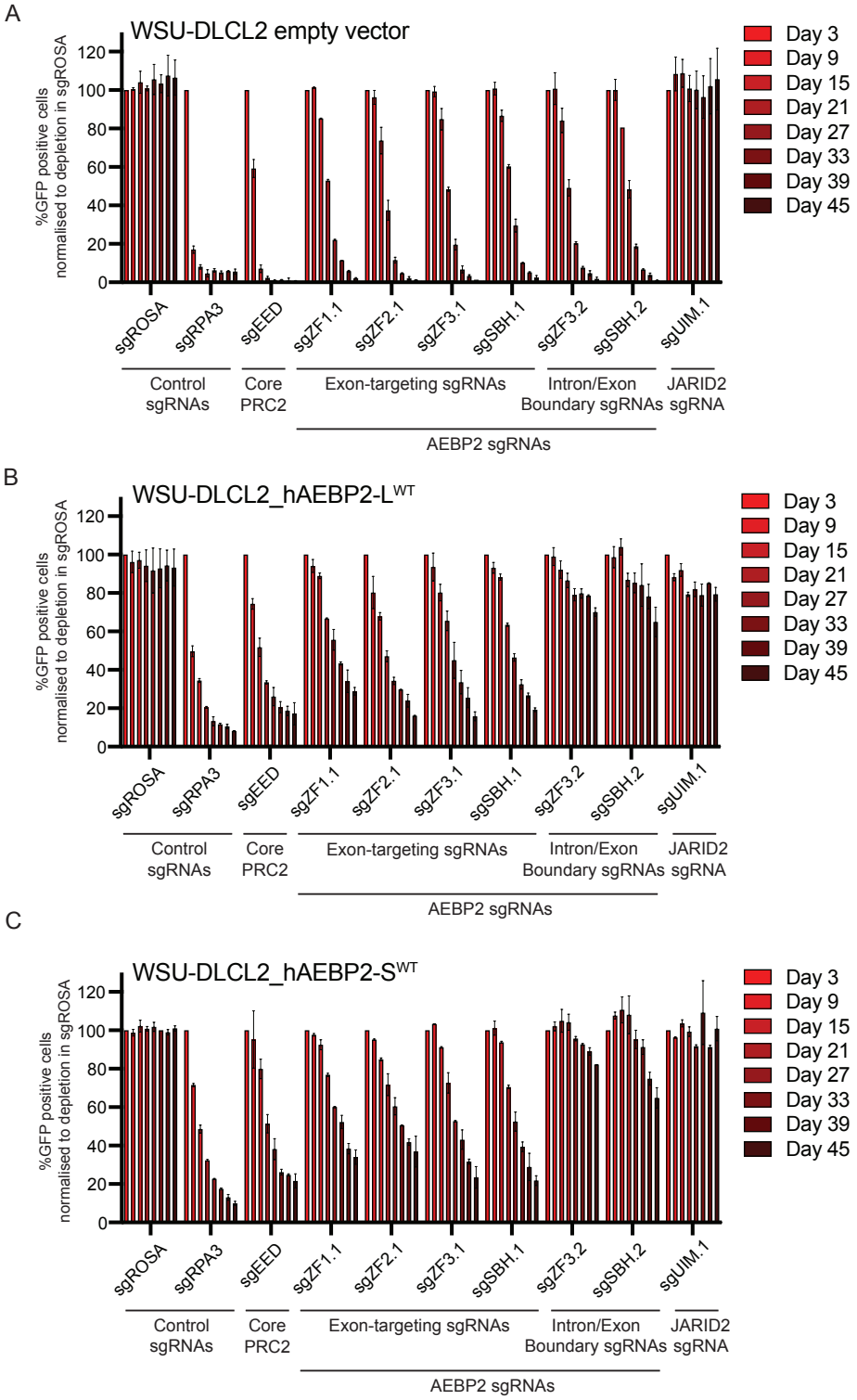

Figure 4.10 Non--targetable AEBP2 rescues AEBP2 sgRNA dropout in lymphoma cells

A-C. CRISPR sgRNA assay measuring GFP depletion in WSU-DLCL2 cells stably expressing (A) empty vector, (B) AEBP2 long isoform and (C) AEBP2 short isoform targeted by control, sgRNAs targeting exonic sequences in AEBP2 (endogenous and exogenous) and intron/exon boundary sgRNAs targeting endogenous AEBP2 only. GFP measured using Guava easyCyte flow cytometer and value normalised to day 3 timepoint and then to depletion in sgRosa.

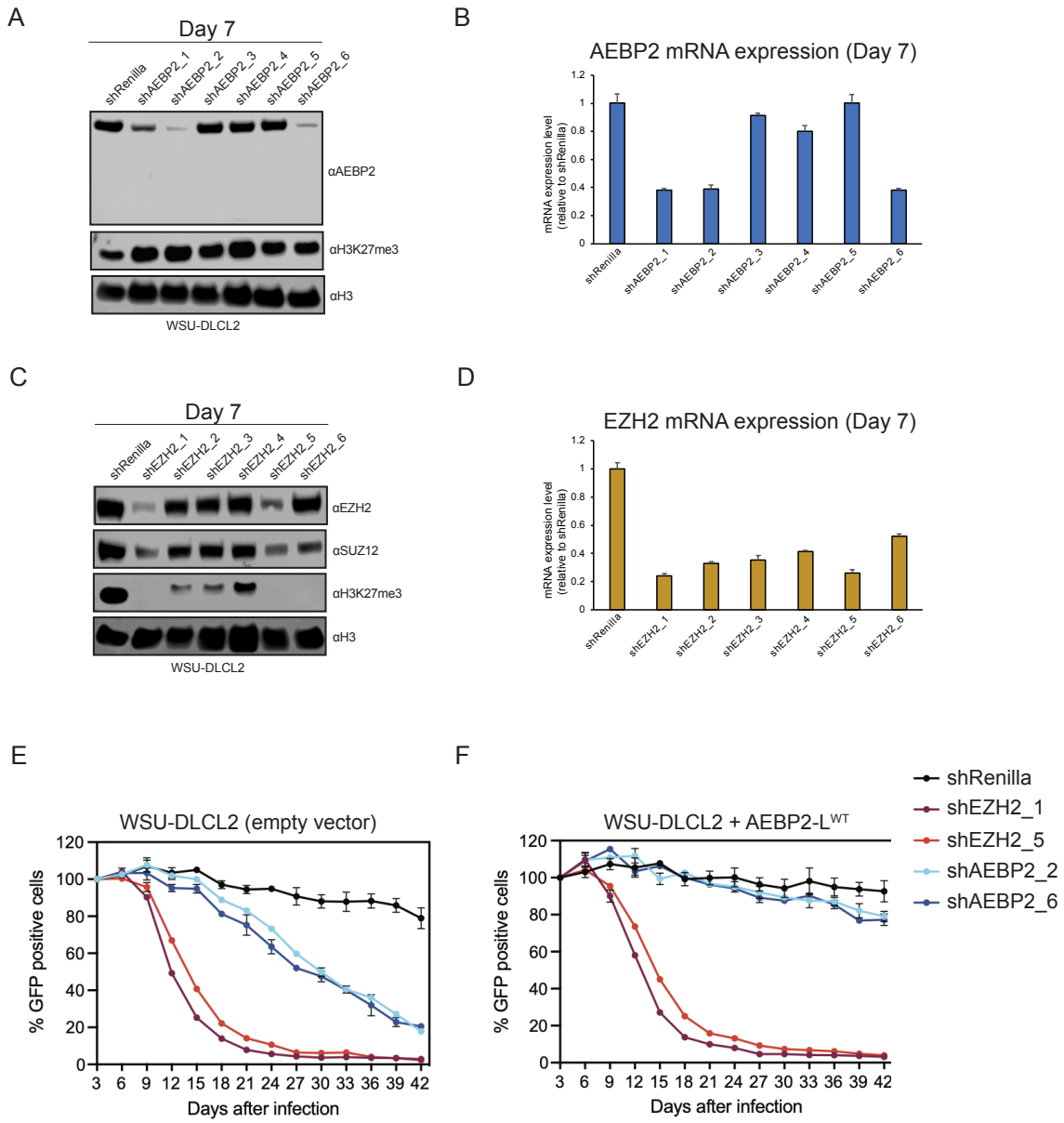

Figure 4.11 AEBP2 long isoform fully rescues AEBP2 knockdown in lymphoma cells.

A-B. AEBP2 expression on protein and mRNA levels by western blot and RT-qPCR at Day 7 following infection and puromycin selection with AEBP2 shRNA lentiviruses.

C-D. EZH2 expression on protein and mRNA levels by western blot and RT-qPCR at Day 7 following infection and puromycin selection with AEBP2 shRNA lentiviruses. SUZ12 included as additional component of core PRC2.

E-F. GFP growth competition assays in (G) WSU-DLCL2 empty vector and (H)WSU-DLCL2 AEBP2 long isoform cells infected with shRenilla and shRNAs targeting EZH2 and AEBP2. GFP measured using Guava easyCyte flow cytometer and calculated as percentage of D3 GFP.

4.2.5 A highly conserved helix in the C-terminus of AEBP2 is essential for the interaction between AEBP2 and SUZ12

Numerous cryogenic electron microscopy (cryo EM) structures have demonstrated putative interactions between AEBP2 and SUZ12, with AEBP2 playing a stabilising role when in complex with PRC2 (S. Chen et al., 2018; Ciferri et al., 2012; Glancy et al., 2021; Kasinath et al., 2021; Poepsel et al., 2018). Due to the intrinsically disordered, unstructured nature of the long isoform AEBP2 N-terminus which could not be resolved using cryo EM, these structures modelled PRC2-AEBP2 +/- JARID2 utilising a short isoform of AEBP2. In these structures, the C2 domain of SUZ12 (SUZ12 residues 150-370) and AEBP2 binding helix (ABH) (residues 81-106) at the N-terminus of SUZ12 had potential interaction interfaces with the C-terminus of AEBP2 (S. Chen et al., 2018, 2020; Ciferri et al., 2012; Kasinath et al., 2021; Poepsel et al., 2018; Youmans et al., 2018). Furthermore, it has previously been demonstrated that the N-terminus of SUZ12, but not the C-terminus can co-immunoprecipitate AEBP2 and that this interaction can be disrupted by mutating SUZ12 residues 95-106 within its ABH (Youmans et al., 2018).

Initially described in the Bracken Lab by Dr Eric Conway and Dr Marlena Mucha, I describe here a small helix in the C-terminus of AEBP2, bound by tryptophan residues, within the previously annotated SUZ12 interacting domain, which we have annotated the SUZ12 binding helix (SBH) of AEBP2. Compared to other amino acids, tryptophan has by far the highest biosynthetic energy cost; requiring more high energy phosphates (ATP/GTP equivalent) than any other residue and is consequently the least abundant amino acid in the cell (Akashi & Gojobori, 2002; Barik, 2020; The Uniprot Consortium, 2019). Examining a structure of PRC2-AEBP2-JARID2 interacting with H2AK119ub (PDB accession 6WKR) (Kasinath et al., 2021), I noted that the SBH is adjacent to a helix in the C2 domain of SUZ12, with close proximity to residues M299 and L311 of SUZ12 (Figure 4.12A). To help determine whether these two motifs within the AEBP2 C-terminus and SUZ12 C2 domain could be functionally important, I obtained the AEBP2 and SUZ12 sequences corresponding to animals representing a number of distinct evolutionary clades from UniProt, aligned them using the Clustal Omega online tool and visualised the alignment using JalView Desktop software. Supporting the hypothesis that these might be functionally important motifs within AEBP2 and SUZ12 respctively, there was a very high degree of conservation observed. For the AEBP2 SBH, tryptophan W451 and W461 (corresponding to the human long isoform) were conserved through all species examined including invertebrates (Figure 4.12C). Mutating either or both of these tryptophans to alanine

residues ablated the interaction between SUZ12 and AEBP2 in HEK293T cells (Figure 4.12B). Examination of the alignment for the motif of interest within SUZ12 revealed that this whole region of SUZ12 is highly conserved throughout all examined mammalian species, with some residues conserved in invertebrate species also (Figure 4.12D). Notably, sgRNAs targeting the AEBP2 SBH robustly depleted in a lymphoma cells, indicating the importance of the interaction between SUZ12 and AEBP2 for lymphoma cell survival (Figures 4.4, 4.5, and 4.7).

Given that sgRNAs targeting the three tandem zinc fingers of AEBP2 also depleted consistently in lymphoma cells, with the benefit of advice from Dr Andrew Flaus (Centre for Chromatin Biology, NUI Galway), I designed and cloned a number of AEBP2 mutants to disrupt these domains (Figure 4.13A). The mutants were generated using the long isoform of AEBP2 as it is the most abundant in lymphoma and cloned using gateway cloning into the expression vector PLEX, containing 3 HA tags and a puromycin resistance cassette. Target residues for mutation are highlighted in red using a Nuclear Magnetic Resonance (NMR) structure of AEBP2 zinc fingers (Figure 4.13B) (PDB accession 5Y0U) (Sun et al., 2018). The AEBP2 constructs were transfected in HEK293T cells for a HA-immunoprecipitation experiment, demonstrating that all constructs could interact with SUZ12 except for the AEBP2 SBH mutant as reported above (Figure 4.13C). The constructs were subsequently stably expressed in the WSU-DLCL2 lymphoma cell line with a view to a sgRNA rescue experiment, which is currently planned.

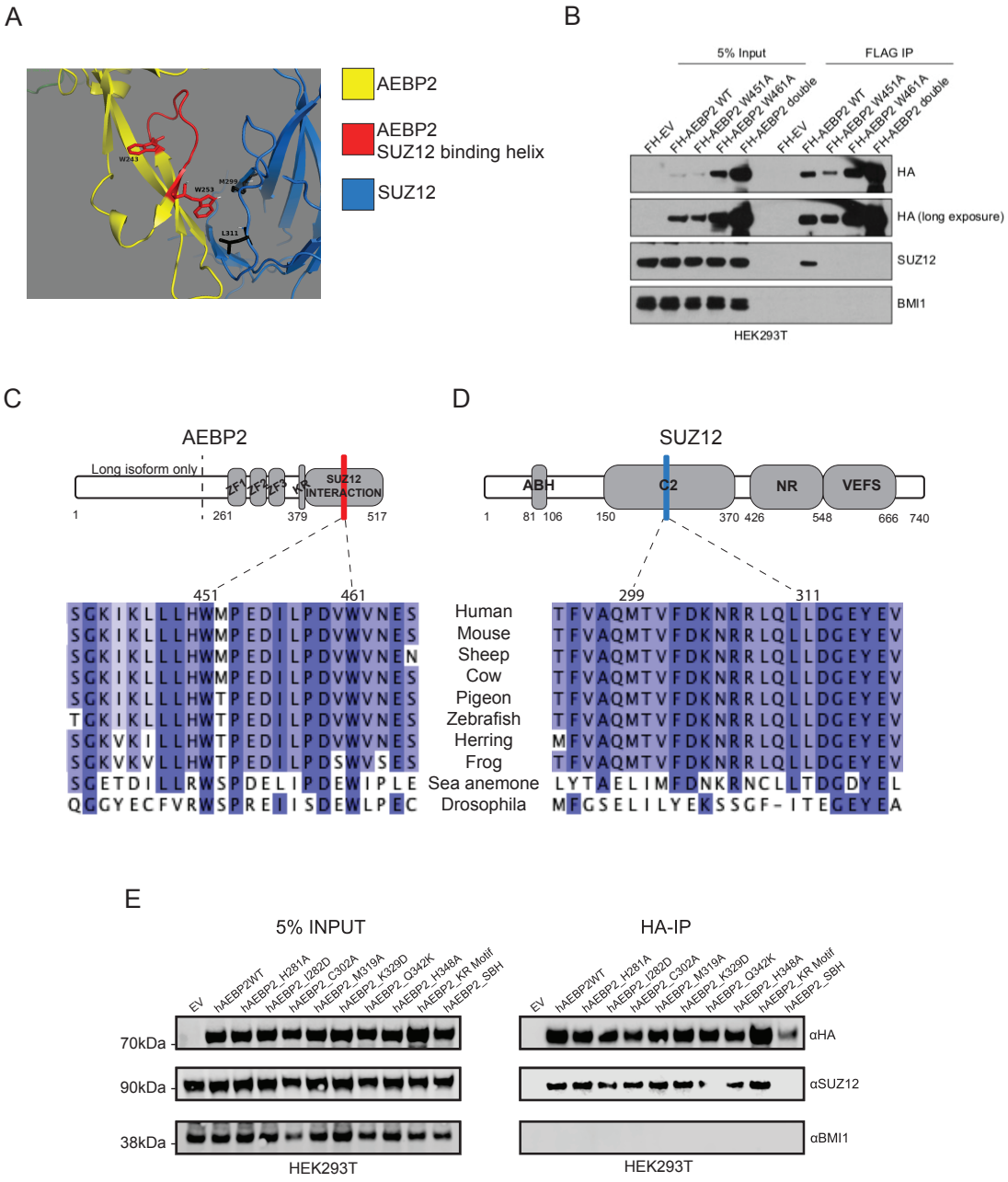

Figure 4.12 A highly conserved SUZ12 binding helix in AEBP2 is essential for interaction with SUZ12

A. Image representing AEBP2 SBH interacting with C2 domain of SUZ12. Generated using PDB 6WKR structure viewed in Pymol. Predicted interacting residues labelled. Note: W243 and W253 correspond with W451 and W461 in AEBP2 long isoform.

B. FLAG immunoprecipitation experiment in HEK293T cells using empty vector (EV), AEBP2 wild-type and SBH mutant constructs. FH = FLAG/HA.

C-D. Cartoon schematics of AEBP2 and SUZ12 with sequence alignment for two potential functional motifs in various species, generated using Jalview software. More conserved residues appear in increasingly dark shades of blue. ZF = zinc finger. KR = KR-rich motif. ABH = AEBP2 binding helix. NR = neck region.

E. HA immunoprecipitation of AEBP2 mutant and wild-type constructs following transfection in HEK293T cells.

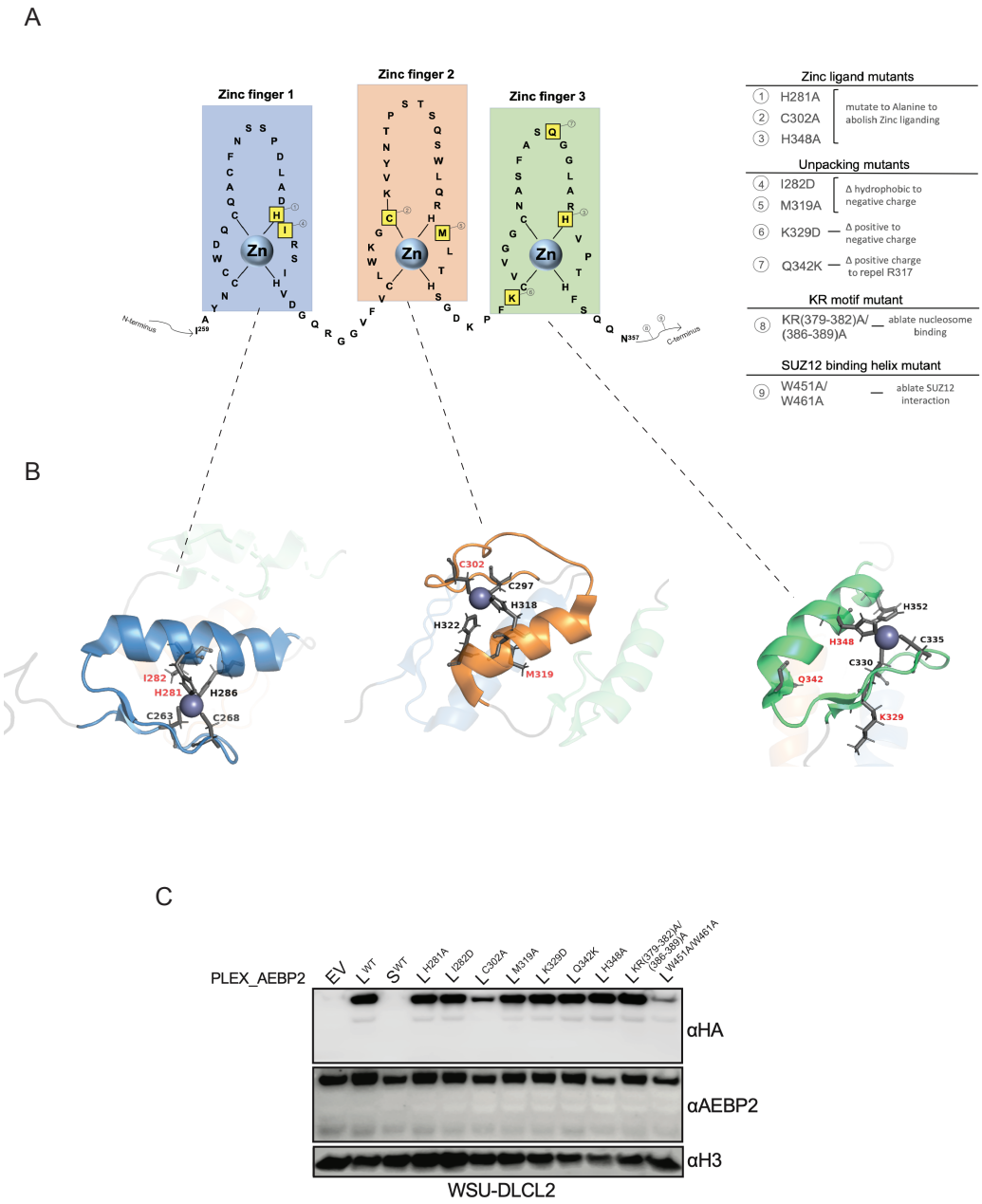

Figure 4.13 Generation of AEBP2 mutant constructs

A. Cartoon schematic of 3 tandem AEBP2 zinc fingers and planned mutations with anticipated perturbation effects.

B. AEBP2 tandem zinc finger models generated using NMR structure of AEBP2 zinc fingers (PDB accession 5Y0U). Red labels denote planned point mutations.

C. Western blot analysis demonstrating expression of AEBP2 mutant constructs in lymphoma cell line WSU-DLCL2. AEBP2 short isoform did not express, but experiment is satisfactorily controlled using AEBP2 long wild-type construct. AEBP2 band for mutant H348A represents only endogenous AEBP2 as the epitope for the selected AEBP2 antibody contains this residue.

4.3 Discussion and future directions

Large scale CRISPR/Cas9 screens have become well established as a powerful tool for exposing novel genetic vulnerabilities in cancer, essential regulators of intracellular processes, novel functional protein domains and even resister genes when undertaken with and without an experimental drug of interest (Brien et al., 2018; Drosos et al., 2022; Grevet et al., 2018; Olivieri et al., 2020; Lu Yang et al., 2021).

The aim of this chapter was to perform a saturated CRISPR screen targeting PRC2 components to uncover novel dependencies in the known PRC2-dependent cancer context GC-derived B-cell non-Hodgkin lymphoma and validate results arising from same. As expected, based on general understanding of the role of EZH2 in lymphoma biology and predicted perturbation effects from publicly available data sets (Figure 4.1), core PRC2 components EZH2, EED and SUZ12 were confirmed to be genetic dependencies in the selected lymphoma cell lines. However, Project Achilles utilises the Avana library, which includes 6 sgRNAs per gene (Sanson et al., 2018); significantly less comprehensive than our approach with a saturated PRC2 tiling library which included almost 4000 sgRNAs in total.

Fascinatingly, I showed PRC2.2 component AEBP2 was shown to be a genetic dependency in both EZH2 wild-type and EZH2 mutant lymphoma cell lines. To my knowledge, this is the first time that a substoichiometric component of PRC2 has been highlighted as a specific dependency in a human cancer context. Furthermore, this dependency is not universal to PRC2-dependent cancer contexts (as evidenced by AEBP2 not being a dependency in the. SMARCB1$^{-/-}$ malignant rhabdoid tumour cell line G401 which is dependent on core PRC2). Curiously, lymphoma cells are entirely agnostic to disruption of the other PRC2.2 component JARID2.

By mapping AEBP2-tiling sgRNAs to their target double-stranded break sites, I identified multiple regions of interest within AEBP2 in the lymphoma context. As previously discussed, the AEBP2 long isoform can be roughly divided into two parts: a 216 amino acid N-terminus which is highly GC-rich, acidic, negatively charged and disordered, and a basic C-terminus transcribed from exons shared with AEBP2 short isoform, which contains all currently known functional domains (Figure 4.4). High GC content rendered it difficult to interpret whether depleting sgRNAs in the AEBP2 N-terminus were real or due to off-target sgRNA activity.

Dissection of potential functions specific to the long isoform of AEBP2 is subject to ongoing work in the Bracken lab by Dr Marlena Mucha. Although AEBP2 short isoform has been demonstrated *in vitro* to enhance methyltransferase activity on chromatinised plasmids and H2AK119ub1-marked nucleosomes, *in vivo* assays and assays examining the long isoform of AEBP2 are lacking (Kasinath et al., 2021; C. H. Lee, Holder, et al., 2018; Poepsel et al., 2018; Xueyin Wang et al., 2017). Seemingly contradictory to this is evidence that loss of AEBP2 in mouse embryonic stem cells results in an increase in H3K27me3 and SUZ12 at polycomb target gene promoters, potentially due to increased activity by PRC2.1 (Conway et al., 2018, 2021; Grijzenhout et al., 2016).

Well-recognised functional domains of AEBP2 were also highlighted by the PRC2 tiling CRISPR screen. I identified that guide depletion is enriched within the three AEBP2 C-terminal tandem zinc fingers. AEBP2 zinc fingers are reported to facilitate PRC2 localisation to chromatin and enhance deposition of H3K27me3 (Kasinath et al., 2021; H. Kim et al., 2009; Poepsel et al., 2018; Xueyin Wang et al., 2017). However, cryo-EM structures of AEBP2 to date have utilised exclusively the short isoform of AEBP2 and have not yet resolved Zinc Finger 3, reflecting that there is much to learn about the role of AEBP2 *in vivo* in PRC2 localisation and activity. Only one PAM sequence was available such that the KR-rich motif of AEBP2 would be targeted and this sgRNA was unfortunately filtered out due to low coverage in the CRISPR tiling screen. However, in validation assays the sgRNA targeting this region did deplete robustly. The KR-rich motif has previously shown to be essential for AEBP2 short isoform interaction with chromatin and to enhance AEBP2 methyltransferase activity *in vitro* (C. H. Lee, Holder, et al., 2018). We also describe here in greater detail a small 11 residue SUZ12 Binding Helix (SBH) in the C-terminal SUZ12 interaction domain of AEBP2 that is necessary for interaction between SUZ12 and AEBP2 (Figure 4.12). sgRNAs targeting this small helix, potentially disrupting the interaction between AEBP2 and SUZ12, significantly depleted in the PRC2 CRISPR screen and validation work.

I have shown that the AEBP2 dependency in lymphoma is specific and not due to off-target sgRNA activity. By ectopically expressing AEBP2 long and short isoforms separately in a lymphoma cell line, the phenotype of sgRNA depletion was rescued. Additionally, ectopic expression of AEBP2 long isoform fully rescued AEBP2 knockdown by two independent AEBP2 shRNAs. This confirms that AEBP2 long isoform, by far the more highly expressed

isoform in lymphoid cells, is a specific genetic dependency in germinal centre B-cell lymphoma (DLBCL/follicular lymphoma).

As yet, no drug or molecule exists for targeting AEBP2 *in vivo*. Given evidence provided here and the current understanding of the functions of AEBP2 in PRC2 biology, theoretical approaches to effectively disrupt AEBP2 in lymphoma cells would either uncouple AEBP2 from its interaction with chromatin (by targeting AEBP2 zinc fingers or KR motif) or uncouple AEBP2 from its PRC2 interaction (by targeting the AEBP2 SUZ12 binding helix). To date, my work on AEBP2 in lymphoma has been in the context of the germinal centre-derived B-cell lymphomas GCB-DLBCL/transformed follicular lymphoma exclusively. I aim to also examine AEBP2 as a functional dependency in a limited number of Burkitt lymphoma (derived from the lymphoid germinal centre dark zone) and ABC-DLBCL (derived from cells that have exited the lymphoid germinal centre) cell lines.

In chapter 5, I will describe in greater detail the mechanism of action for AEBP2 in lymphoma, which will also enhance the understanding of the role of AEBP2 in Polycomb biology more generally.

Chapter 5: AEBP2 disruption in lymphoma leads to PRC2 activation and genome-wide redistribution of H3K27me3 and H3K27me2

5.1 Introduction

I illustrated in chapter 4 that the PRC2.2 component AEBP2 is a specific, novel genetic dependency in B-cell lymphoma cell lines. Highly expressed in B-cell lymphoid malignancies, AEBP2 long isoforms (517aa and 503aa respectively), differing only by 14 residues at their C-terminus, arise due to alterative splicing from a distinct promoter to that of the AEBP2 short isoform (301aa) (Figure 5.1A-B). Long and short isoforms of AEBP2 contain unique first exons but share the remainder of their sequence and all currently annotated domains lie within this common sequence. AEBP2 differential promoter usage was previously described in the paralogous context of the mouse genome in detail, where the short isoform and long isoform were broadly annotated as "embryonic" and "somatic" respectively based on patterns of expression in mouse tissues (Kim et al., 2009, 2015). Consistent with this designation, a long isoform of AEBP2 is more abundant than the short isoform in lymphoma cells (Figure 5.1C).

AEBP2 associates with PRC2 in a subcomplex assembly with JARID2 entitled PRC2.2; mutually exclusive from complexes containing PRC2.1 components PCL1-3, EPOP or PALI1/2 (Conway et al., 2018; Grijzenhout et al., 2016). This association with PRC2 is understood to be mediated by an AEBP2 C-terminal region which interacts with SUZ12 and is situated downstream from the tandem zinc finger domains (S. Chen et al., 2018, 2020; Ciferri et al., 2012; Kasinath et al., 2018, 2021; C. H. Lee, Holder, et al., 2018; Sun et al., 2018). Furthermore, AEBP2 is reported to interact via its zinc finger domains and downstream KR-rich motif with nucleosomal DNA (Ciferri et al., 2012; G. P. He et al., 1999; Kasinath et al., 2021; C. H. Lee, Holder, et al., 2018; Xueyin Wang et al., 2017). An additional interaction has been described between ZnF1-2 of AEBP2 and H2AK119ub1 and the acidic surface of H2A/H2B (Kasinath et al., 2021). Work in mouse embryonic stem cells has demonstrated that loss of JARID2 results in displacement of AEBP2 from chromatin (Healy et al., 2019). Although the presence of AEBP2 has been shown to enhance PRC2 histone methyltransferase activity *in vitro* (Cao & Zhang, 2004; Kasinath et al., 2018; C. H. Lee, Holder, et al., 2018; Xueyin Wang et al., 2017), depletion of AEBP2 *in vivo* results in a mouse ESC context in a moderate gain of H3K27me3 at Polycomb target gene promoters (Grijzenhout et al., 2016). Fascinatingly, AEBP2-deficient mice exhibit transformations in their vertebral skeleton analogous to mice deficient in Trithorax group proteins, which are known to antagonise Polycomb function (Grijzenhout et al., 2016; Ringrose & Paro, 2004; Steffen & Ringrose,

2014). Perhaps these findings allude to AEBP2 inhibiting or antagonising Polycomb function *in vivo*.

The mechanism whereby AEBP2 may inhibit PRC2 activity *in vivo* has not yet been established. As illustrated in figure 4.4, the N-terminus of AEBP2 long isoform is nett negatively charged and acidic compared to the remainder of the protein due to the presence of repetitive patches of consecutive glutamic acid and aspartic acid residues. It has previously been shown that DNA binding proteins generally possess substantial regions of positively electrostatically charged patches at their DNA-binding interface in order to interact with negatively charged DNA, while negatively charged proteins have a lower propensity to interact with DNA (Jones et al., 1999; Marcovitz & Levy, 2011; Stawiski et al., 2003; Szilágyi & Skolnick, 2006). It follows that the presence of significant negative charge at the N-terminus of AEBP2 long isoform may indeed preclude or inhibit the interaction of PRC2-AEBP2 and nucleosomal DNA. Additional possible explanations for the increase in H3K27me3 observed in AEBP2 depleted mouse ESCs could be the formation of hybrid PRC2 complexes containing JARID2 and MTF2/PCL2 that do not occur in the presence of AEBP2, or increased relative activity of PRC2.1 (Conway et al., 2021; Grijzenhout et al., 2016; Healy et al., 2019; Holoch & Margueron, 2017). The varied affinity of AEBP2 isoforms for DNA and their modulatory effects on PRC2 methyltransferase activity is the subject of collaborative work between the Bracken lab and Professor Chen Davidovich at Monash University in Melbourne (Mucha, McKenzie et al., currently in preparation).

Cancer-relevant functions of AEBP2 have rarely been described. One study described in ovarian cancer that genetic depletion of AEBP2 resulted in impaired cellular proliferation and enhanced sensitivity to cisplatin-based chemotherapy (Zhang et al., 2020). Separately, missense mutations in the AEBP2 long isoform N-terminus have been detected at a low variant allele frequency in cases of neurofibromatosis-associated malignant peripheral nerve sheath tumour (M. Zhang et al., 2014), independently of inactivating SUZ12 mutations which are also detected in this context.

In this chapter, I sought to characterise the mechanism whereby AEBP2 is a genetic dependency in B-cell lymphoma. To do this, I used several approaches to generate a system whereby I could acutely deplete AEBP2 and examine the resultant effects on the landscape of H3K27me2 and H3K27me3 and the cellular transcriptional landscape. I also sought to examine the role of other epigenetic regulators in explaining the adverse cellular phenotype resulting from AEBP2 disruption.

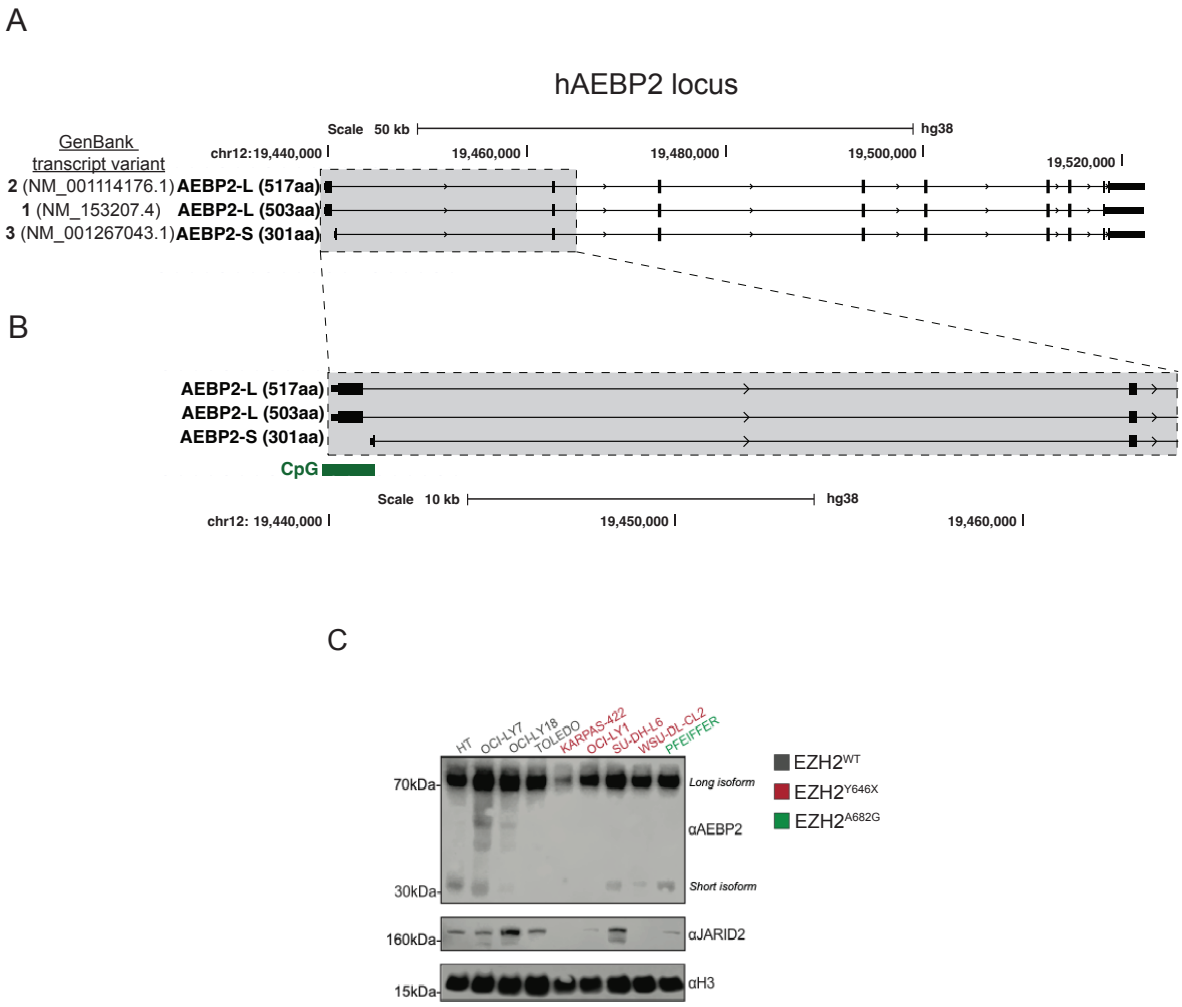

Figure 5.1 Differential promoter usage results in several AEBP2 isoforms

A. UCSC genome browser view of human AEBP2 locus on chromosome 12 illustrating AEBP2 isoforms and allocated GenBank and NCBI transcript variant and reference sequence identifications.

B. Zoom in view of genome browser view of Exon 1, Intron 1 and Exon 2 of human AEBP2 locus. Alternative promoters indicated by small rectangles immediately 5-prime to larger rectangle indicating exon 1. Note that long isoforms have a distinct promoter and exon 1 to the short isoform of AEBP2. Exon 2 is shared by all isoforms.

C. Western blot analysis in lymphoma cell lines demonstrating a greater abundance of AEBP2 long isoform compared to AEBP2 short isoform.

5.2 Results

5.2.1 Examining the effects of acute AEBP2 depletion in lymphoma cells.

Ectopic expression of a degrader tag (dTAG)-fused protein of interest or CRISPR/Cas9-mediated locus-specific knock-in of a dTAG facilitate the study of the acute loss of a protein in real time (Damhofer et al., 2021; Nabet et al., 2018; Woodley et al., 2021). In order to generate a system whereby I could examine the acute effects of AEBP2 depletion on lymphoma cells, I designed an experiment whereby I would ectopically express AEBP2 long and short isoforms in-frame with a fused degradable $FKBP12^{F36V}$ tag, followed by CRISPR/Cas9-mediated excision of exon 2 of endogenous AEBP2 (Figures 5.2A-B). Should the CRISPR/Cas-mediated knockout of endogenous AEBP2 be successful, all remaining AEBP2 would be acutely degradable upon application of a paired PROTAC degrader ligand/drug, thereby facilitating the study of acute depletion of AEBP2 in real time.

Using the gateway cloning compatible PLEX_305-N-dTAG vector, which contains a puromycin resistance cassette as well as N-terminal HA and degrader ($FKBP12^{F36V}$) tags, I lentivirally transduced AEBP2 long and short isoforms (transcript variants 1 and 3) in WSU-DLCL2 EZH2 mutant lymphoma cells (Figure 5.2C). Following confirmation of successful expression of these constructs, I nucleofected paired intron-targeting sgRNAs containing a GFP tag, targeting 5' and 3' of AEBP2 exon 2 (Figure 5.2A) (the first shared exon common to all human AEBP2 isoforms) using a Lonza Amaxa Nucleofector. The codon for a serine residue is divided between Exon 1 and Exon 2 of AEBP2, therefore CRISPR/Cas9-mediated excision of Exon 2 should introduce an early frameshift in AEBP2 resulting in failure to express the protein. 24 hours after electroporation of the cell line with sgRNAs, GFP positive cells were single cell sorted into 96-well tissue culture-treated dishes, such that parental, dTAG-hAEBP2-S and dTAG-hAEBP2-L plates were passaged forward for each pair of sgRNAs. No single cell clones survived passaging on the parental plate, likely reflecting the deleterious effects of AEBP2 loss on lymphoma cells. A small number of clones expressing dTAG-AEBP2-L and dTAG-AEBP2-S survived passaging and were subsequently screened by PCR and western blot for successful knock-out of endogenous AEBP2. An example western blot at day 14 (Figure 5.2D) for dTAG-AEBP2-L expressing clones demonstrated a significant reduction in endogenous AEBP2 levels compared to parental and dTAG-AEBP2-L cells not transduced with sgRNAs. However, these clones when further passaged all recovered

endogenous AEBP2 expression levels by day 21 (Figure 5.2E). Although a 6 hour treatment of cells with 500nm of dTAG-7 ligand successfully degraded the exogenous AEBP2 construct, endogenous levels persisted rendering the cells unsuitable for the intended purpose of studying the acute depletion of AEBP2 (Figure 5.2E). This pattern held true for all clones screened.

Subsequently, I designed codon-optimised constructs of AEBP2-L and AEBP2-S such that they would be resistant to sgRNAs targeting exon 2 and bulk infected cells with sgRNA lentivirus followed by puromycin selection. Once again, despite the initial partial depletion of endogenous AEBP2 by western blot at day 14, at a later time point endogenous levels recovered to 100% of baseline (data not shown here).

To overcome this issue, I then intended to use CRISPR/Cas9-mediated gene editing to knock-in a dTAG on the endogenous AEBP2 c-terminus. Given that in order for this approach to be successful, each allele of AEBP2 would require a dTAG knock-in, I first decided to examine the copy number of AEBP2 in WSU-DLCL2 and other GCB-DLBCL cell lines using copy number qPCR (D'haene et al., 2010). I designed primers flanking exon 2 of AEBP2 and proceeded with the copy-number qPCR as described in Chapter 2 section 2.2.6. Human mammary epithelial cells (HMEC) were used as a diploid cell line for reference and a standard curve was generated for this cell line using a range of input DNA for the PCR. The copy number of the gene of interest (AEBP2) in 66ng (corresponding in a diploid cell line to 20,000 gene copies) for a number of lymphoma cell lines was determined using the equation of the line for the standard curve (Figure 5.2F). This demonstrated that AEBP2 was significantly amplified, with at least 8 copies in each of 6 lymphoma cell lines screened. This finding indicated that it was impractical to pursue knock-in of a dTAG on each AEBP2 allele in these cell lines and instead opted to examine the acute effects of shRNA-mediated AEBP2 knockdown in lymphoma cells.

As previously described in Chapter 4 Figure 4.10, I designed a number of EZH2 and AEBP2 short hairpin RNA vectors (shRNAs) which result in knock-down of AEBP2 and EZH2 on the protein and mRNA levels of 60-80% by Day 7. I decided to utilise these shRNAs in order to examine the effects of AEBP2 knock-down on H3K27me2 and H3K27me3 abundance and distribution by ChIP-Rx and transcriptional changes in lymphoma cells by RNA-Sequencing.

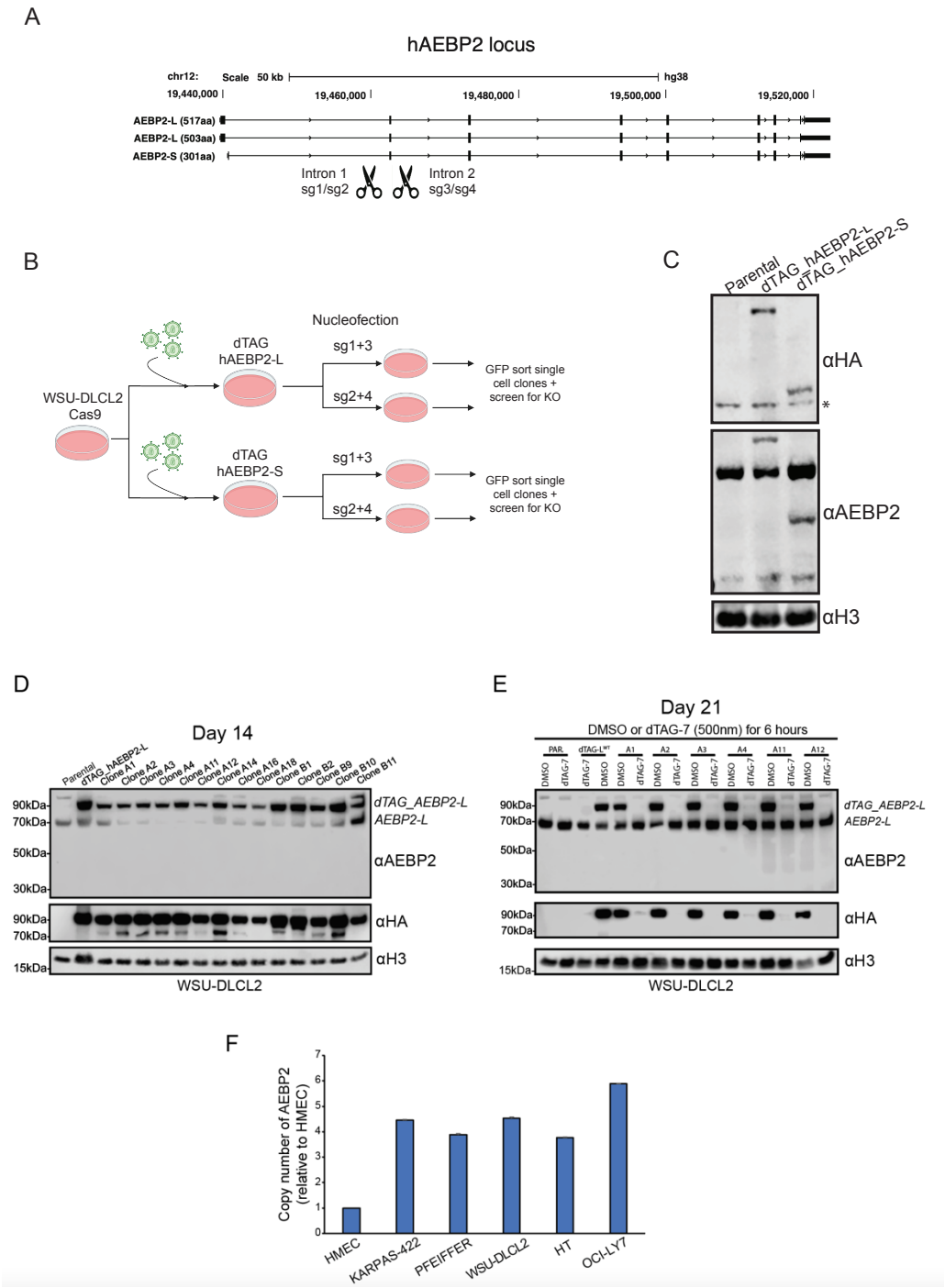

Figure 5.2 Expression of dTAG-AEBP2-Long/Short isoforms in a lymphoma cell line and attempted CRISPR knock-out of endogenous AEBP2

A-B. Experimental schematic for CRISPR knock-out of endogenous AEBP2 by transduction of paired sgRNAs flanking exon 2 and expression of dTAG AEBP2 long and short isoforms.
C. Western blot demonstrating expression of dTAG-AEBP2 long and short constructs.
D. Western blot at Day 14 of single cell clones screened for knockout of endogenous AEBP2.
E. Western blot at Day 21 of single cell clones treated with DMSO or dTAG-7 degrader ligand demonstrating degradation of dTAG-AEBP2 but recovery of endogenous AEBP2 expression.
F. Copy-number qPCR of AEBP2 exon 2 normalised to human mammary epithelial cell (HMEC) line as diploid reference genome, illustrating at least 4-fold amplification of AEBP2 in each tested lymphoma cell line.

5.2.2 AEBP2 and EZH2 knockdown result in genome-wide redistribution of H3K27me3 and H3K27me2 in lymphoma cells

To study the effects of EZH2 and AEBP2 knock-down, I used 2 independent hairpins targeting EZH2 and 2 independent hairpins targeting AEBP2, with shRenilla as a non-targeting control. Hairpins were transduced lentivirally in the EZH2 mutant lymphoma cell line WSU-DLCL2 and western blot analysis was performed at day 7 (Figure 5.3A). Once again, these hairpins resulted in robust knockdown of their target proteins by day 7, with a clear reduction in H3K27me3 in the cells transduced with shEZH2 hairpins. A small increase in H3K27me3 was demonstrated in the shAEBP2 hairpin transduced cells. I performed ChIP-Rx at this day 7 time point for lymphoma cells transduced with all five hairpins for the antibodies H3K27me2 and H3K27me3, with pellets harvested also for RNA-Seq in biological triplicate (Figure 5.3B).

For analysis, the genome was parsed into 10kb bins and the signal for ChIP antibodies H3K27me2 and H3K27me3 was quantified within each bin relative to the 10% mouse reference genome spike-in. Plotting ChIP antibody signal along chromosome 9 (chosen as a sample chromosome for large global analysis) revealed that on a global level, both EZH2 shRNAs depleted H3K27me3 genome-wide, while AEBP2 knockdown by both shRNAs increased H3K27me3 overall genome-wide (Figure 5.4A). Intriguingly, knockdown of both EZH2 and AEBP2 reduced H3K27me2 levels compared to shRenilla. By taking an average of Rx-normalised signal for each antibody for the two EZH2 shRNAs and two AEBP2 shRNAs respectively, I directly compared the three treatment conditions against each other for H3K27me2 and H3K27me3 signal (shRenilla, shEZH2 and shAEBP2) (Figure 5.4B-E). This confirmed that with AEBP2 knockdown, a majority of 10kb bins genome-wide gained H3K27me3 while simultaneously losing H3K27me2 (Figure 5.4C). However, with EZH2 knockdown, reflecting the loss of the catalytic engine of PRC2, a majority of bins lost both H3K27me2 and H3K27me3 (Figure 5.4D). Direct comparison of the effects of EZH2 and AEBP2 knockdown on H3K27me2 revealed that although both EZH2 and AEBP2 knockdown depleted H3K27me2 overall, this mark was lost to a greater degree with AEBP2 knockdown in almost 75% of genomic bins (Figure 5.4E).

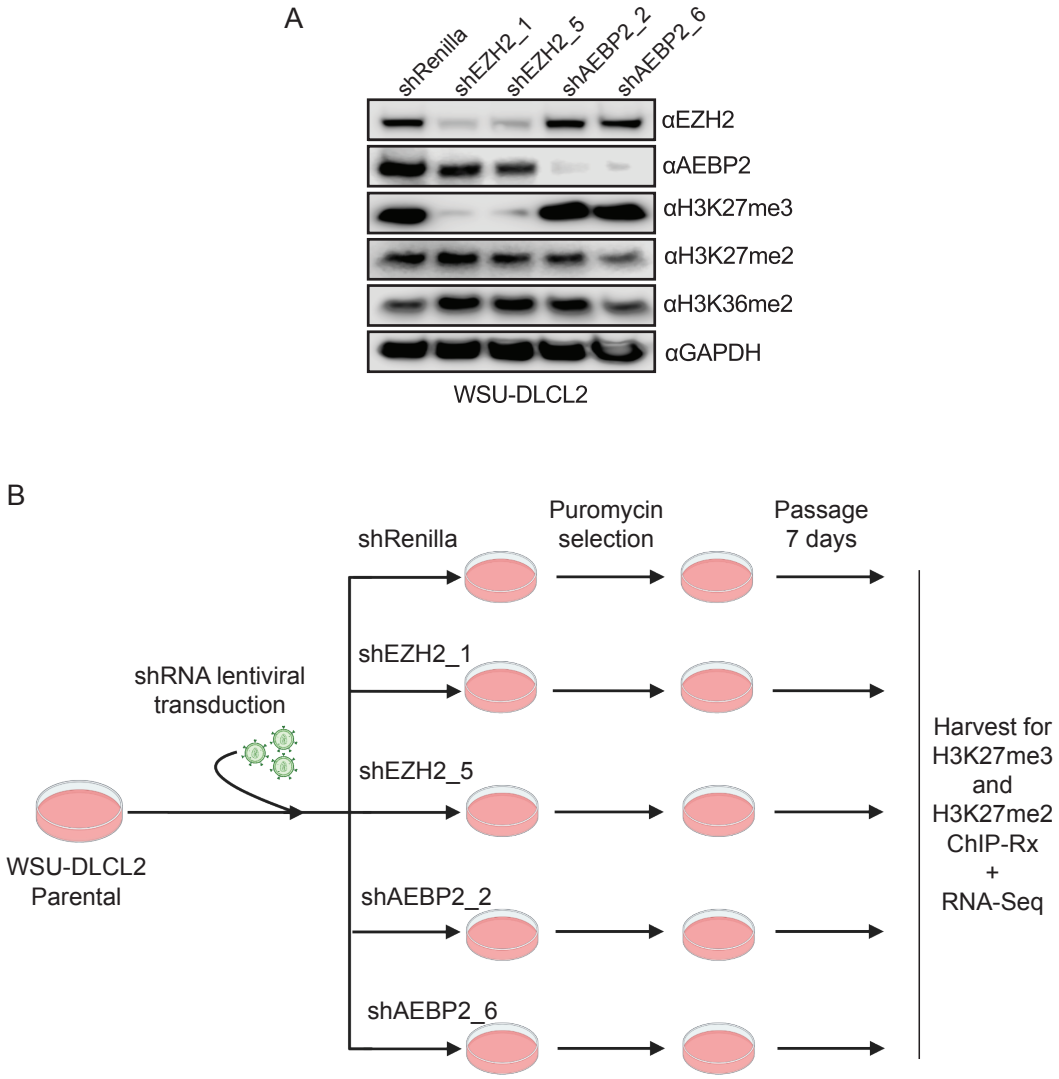

Figure 5.3 Knock-down of AEBP2 and EZH2 using shRNAs and experimental schematic for ChIP-Rx and RNA-Sequencing

A. Western blot analysis of WSU-DLCL2 transduced with shRenilla, shEZH2 or shAEBP2 and passaged for 6 days after puromycin selection, illustrating knockdown of EZH2 and AEBP2 respectively, as well as resultant effects on whole cell levels of selected histone post-translational modifications.

B. Schematic representation of work-flow for ChIP-Rx and RNA-Seq of WSU-DLCL2 lymphoma cell line transduced with indicated shRNAs.

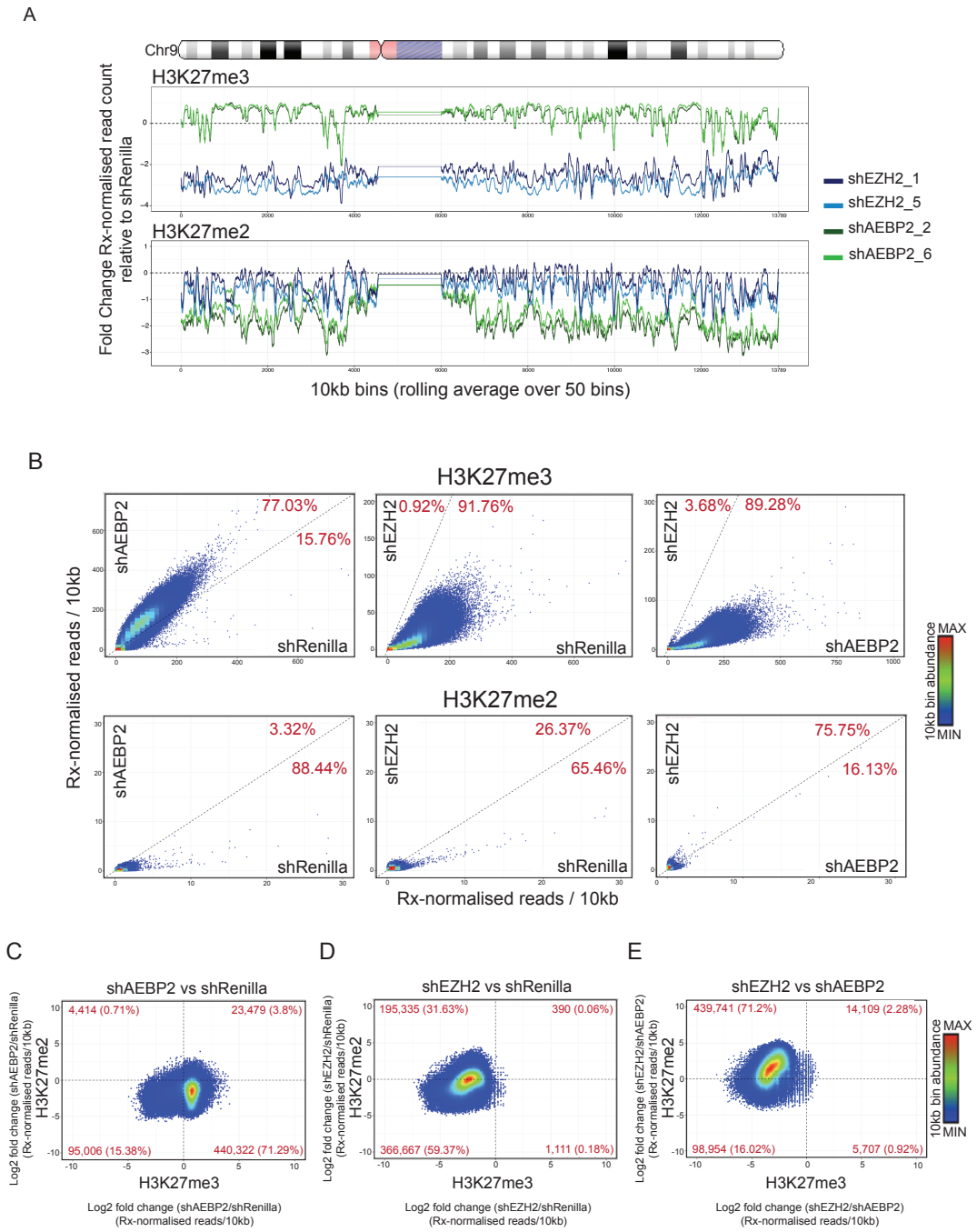

Figure 5.4 AEBP2 and EZH2 knockdown result in divergent effects on H3K27me3 and H3K27me2 genome-wide

A. Ideogram of Chromosome 9 with H3K27me2 and H3K27me3 signal normalised to shRenilla for each EZH2 and AEBP2 knockdown condition, quantified in 0.5Mb bins.

B. Genome-wide correlation of H3K27me3 and H3K27me3 signal within 10kb bins, between AEBP2 knockdown, EZH2 knockdown and shRenilla. Each dot represents one 10kb bin. Average signal of H3K27me2 and H3K27me3 for EZH2 hairpins presented as shEZH2 and AEBP2 hairpins presented as shAEBP2.

C-E. Composite plot comparing pattern of H3K27me2 and H3K27me3 gain/loss between shAEBP2/shRenilla (C), shEZH2/shRenilla (D) and shEZH2/shAEBP2 (E). Each dot represents one 10kb bin.

Polycomb target gene promoters were defined by the presence of SUZ12 peaks in a previous ChIP-Rx in this cell line carried out in the Bracken lab (data not shown here). Approximately 3000 Polycomb target gene promoters were identified. Intergenic regions were defined as regions >5kb from the nearest annotated gene. Knockdown of AEBP2 resulted in gain of H3K27me3 at a majority of Polycomb target gene promoters, as well as non-Polycomb target promoters and intergenically; while H3K27me2 was lost at these sites (Figure 5.5 and 5.6). Knockdown of EZH2 resulted in a loss of H3K27me3 and of H3K27me2. Additional accumulation of H3K27me3 induced by knockdown of AEBP2 was observed promoters and transcriptional start sites of genes essential for the B-cell terminal differentiation transcriptional programme including IRF4/MUM1 and SDC1/CD138 (Figure 5.5B, 5.5D). Notably, in this EZH2 mutant cell line with already dramatically increased intergenic and global H3K27me3, knockdown of AEBP2 increased this hyper-H3K27me3 phenotype even further, at the expense of H3K27me2.

5.2.3 Knockdown of AEBP2 results in few gene expression changes compared to knockdown of EZH2.

I demonstrated using sgRNA and shRNA depletion assays in Chapter 4 that AEBP2 is a genetic dependency in lymphoma. Additionally, in this chapter I have shown that knockdown of AEBP2 results in a moderate genome-wide increase in H3K27me3 in lymphoma cells, while EZH2 knockdown results in a marked genome-wide loss of H3K27me3. I decided to examine whether the respective gene knockdowns resulted in a differential effect on gene expression 7 days after shRNA transduction. To do this, I perform RNA-Sequencing using QuantSeq 3' mRNA sequencing (Moll et al., 2014) for each condition in biological triplicate (shRenilla, 2 EZH2 shRNAs and 2 AEBP2 shRNAs).

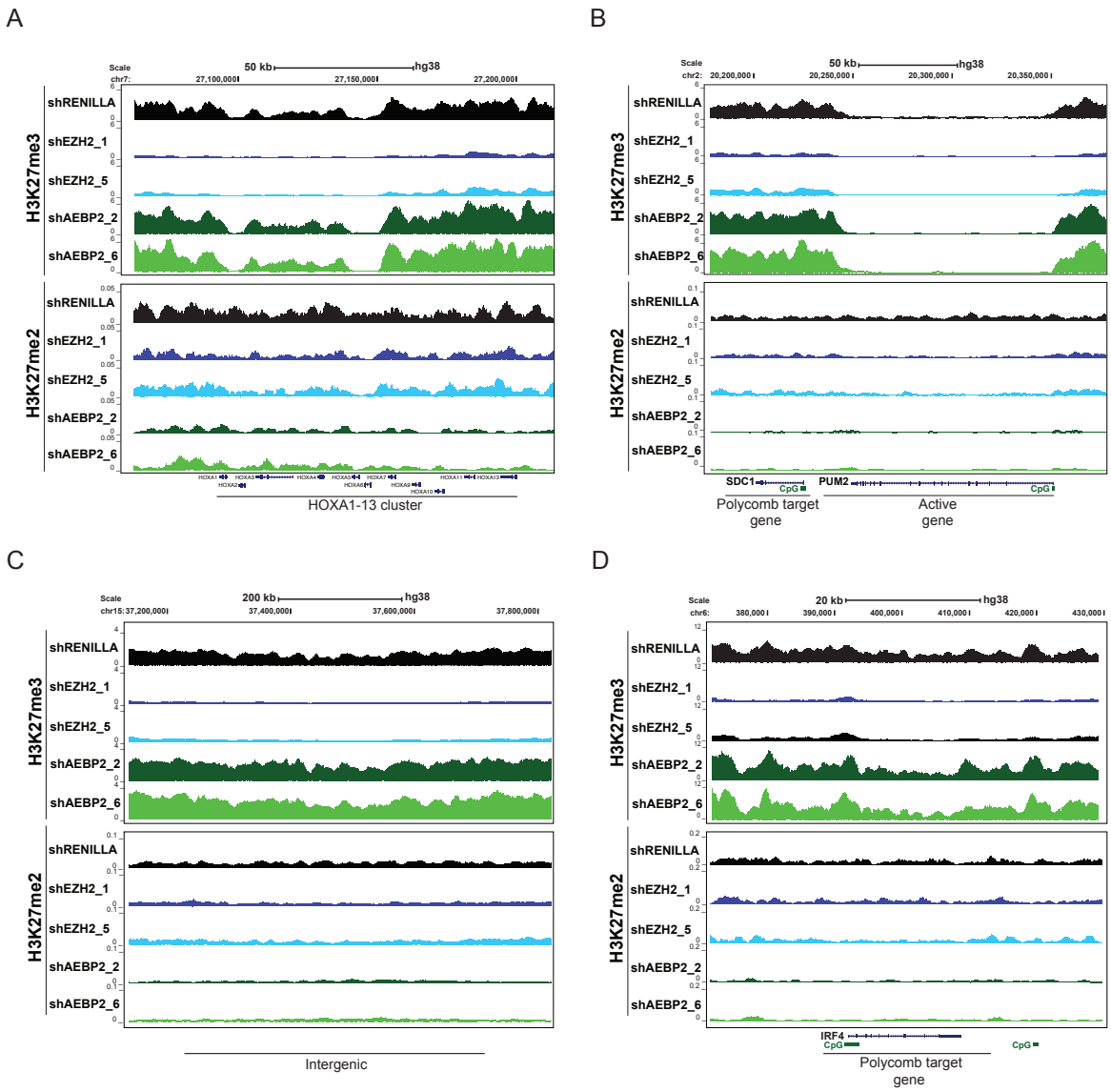

Figure 5.5 AEBP2 knock-down results in broad genome-wide gain of H3K27me3

A-D. UCSC genome browser view of ChIP-Rx normalised reads for H3K27me3 and H3K27me2 in cell lines transduced with shRNAs targeting Renilla, EZH2 and AEBP2 at A) HOXA cluster, B) Polycomb target gene SDC1/CD138 and active gene PUM2, C) intergenic region downstream of Meis2 gene and D) Polycomb target gene IRF4/MUM1.

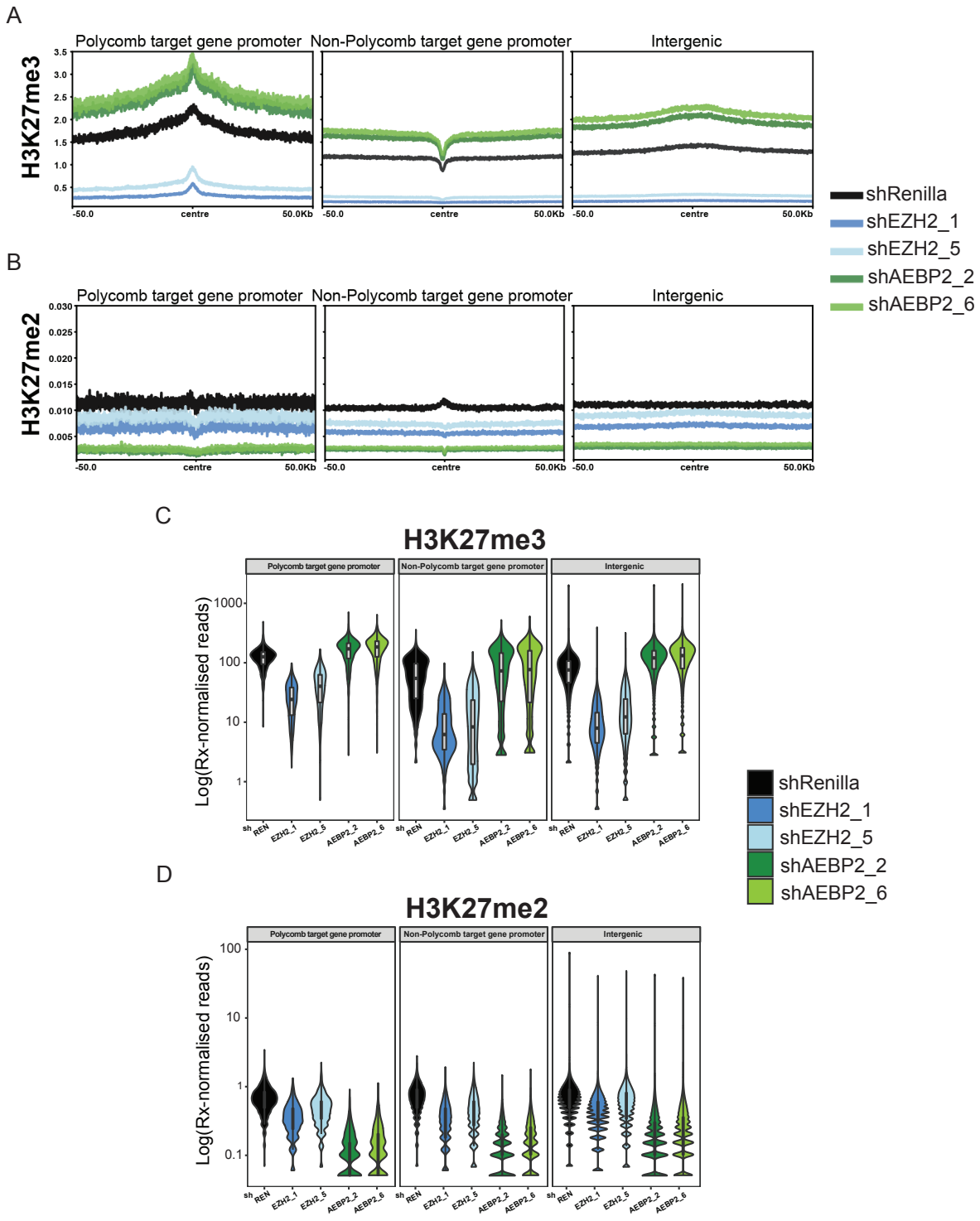

Figure 5.6 AEBP2 knockdown results in increased H3K27me3 at Polycomb target promoters, non-Polycomb target promoters and intergenic regions

A-B. Average ChIP-Rx signal profile of A) H3K27me3 and B) H3K27me2at Polycomb and non-Polycomb target promoters and intergenic sites, in WSU-DLCL2 cell line transduced with indicated shRNAs.

C-D. Violin plot representations of log(Rx-normalised reads) for C) H3K27me3 and D) H3K27me2 at Polycomb target promoters, non-Polycomb target promoters and intergenic sites in WSU-DLCL2 cell line transduced with indicated shRNAs.

Using a cut-off threshold of fold-change 1.5 and adjusted p value <0.05 compared to shRenilla, knockdown of EZH2 resulted at day 7 in up-regulation and down-regulation of hundreds of genes at the mRNA level, with significant overlap between "up" and "down" genes between the two hairpins (76% of genes up-regulated by shEZH2_5 were also up-regulated by shEZH2_1 and 56% of genes down-regulated by shEZH2_5 were also down-regulated by shEZH2_5) (Figure 5.7A-C). In contrast, few genes were up-regulated or down-regulated by AEBP2 knockdown. When combined, 6 genes were up-regulated by both EZH2 and AEBP2 knockdown: Jchain, PDLIM2, STAC3, MCU, CYBA and ISOC2. Other than Jchain, which is known to be involved in the plasma cell gene programme, the other listed genes do not have an established role in lymphoma or normal lymphopoiesis (A. Q. Xu et al., 2020). The small number of transcriptional changes occurring due to AEBP2 knockdown at Day 7 was initially a surprising finding given the strong phenotype of lymphoma cell line dependency on AEBP2 demonstrated by sgRNA and shRNA depletion in Chapter 4. Depletion of cells with AEBP2 knockdown consistently occurs at a later timepoint compared to cells with EZH2 knockdown (Chapter 4 Figure 4.10B) and given the opposing effects of knockdown of these genes on H3K27me3 levels, perhaps it should not be surprising that their effects on the transcriptional landscape are also different.

Given the elevated levels of H3K27me3 in the context of AEBP2 knockdown, I wished to examine whether mRNA levels from transcriptionally repressed genes in lymphoma cells were even lower with AEBP2 knockdown at day 14 than day 7. To examine this hypothesis, I harvested shRenilla and shAEBP2 cells at Day 7 and Day 14 and performed RT-qPCR analysis at a number of gene loci (Figure 5.7D). On the mRNA level, AEBP2 was robustly reduced by both AEBP2 hairpins at days 7 and 14 of the experiment. MTF2, known to compete for the C2 domain of SUZ12 with AEBP2 in order to interact with core PRC2 (S. Chen et al., 2018), was slightly increased or unchanged at the mRNA level by AEBP2 knockdown. Jchain was up-regulated on the mRNA level by both AEBP2 hairpins, corresponding with the results of the RNA-Sequencing experiment in this cell line.. Interestingly, in AEBP2 knockdown cells at the day 14 timepoint, mRNA transcripts from Polycomb target genes CD138/SDC1, PRDM1 and DLX1 were reduced compared to Day 7. This suggests that transcriptional changes resulting from AEBP2 knockdown are likely to be more apparent at a later timepoint than day 7 and also that global increases in H3K27me3 likely result in further repression of already repressed genes in this cell line.

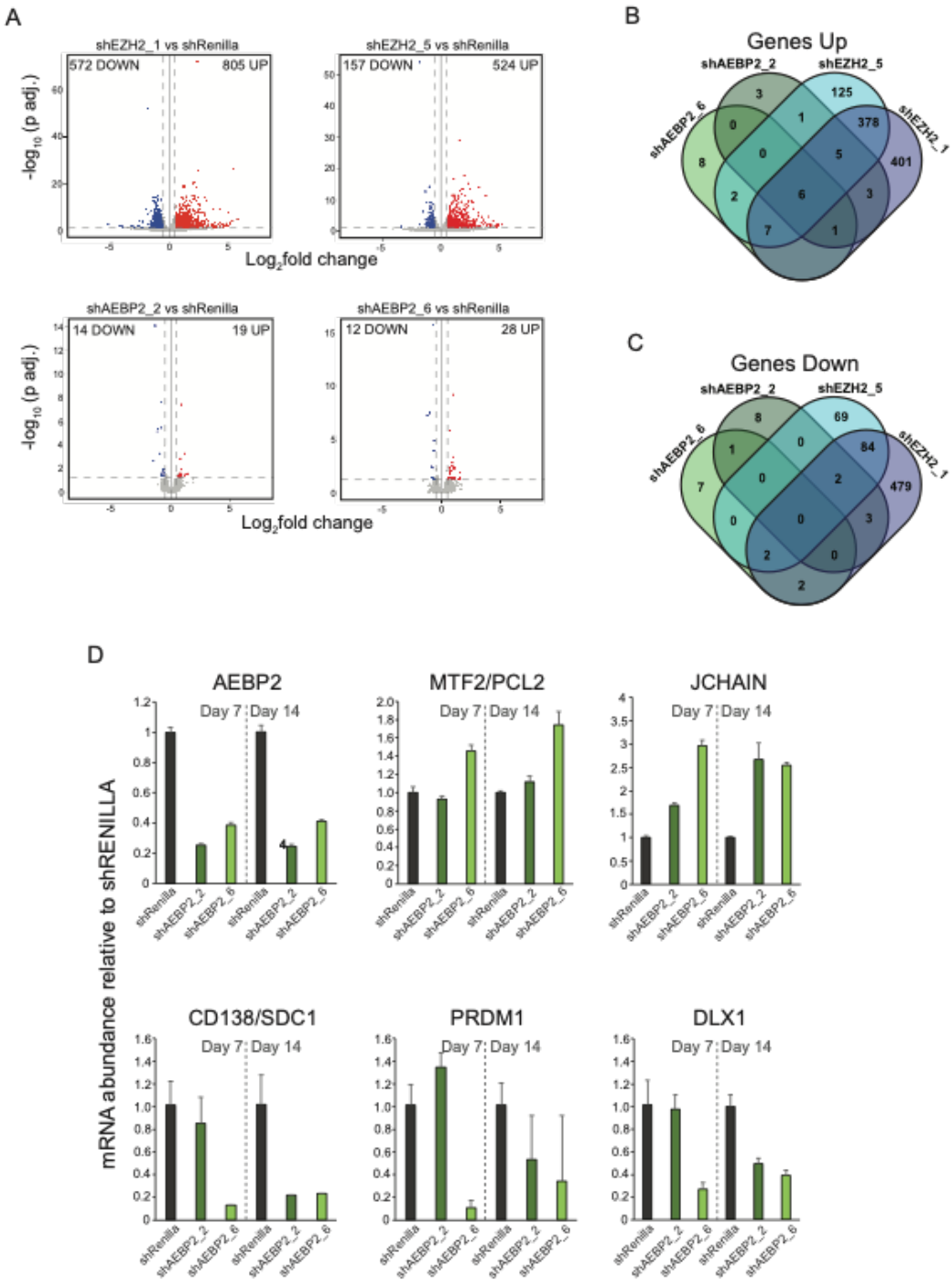

Figure 5.7 Few transcriptional changes result from AEBP2 knock-down in lymphoma cells compared to EZH2 knock-down

A. Volcano plots of RNA-sequencing data representing $\log_2$ fold change in gene expression in cells transduced with shEZH2 or shAEBP2 compared to shRenilla as indicated. $-\text{Log}_{10}$ of the adjusted p value is represented on the Y-axis. (n=3 replicates)

B-C. Venn diagrams representing overlap in genes upregulated (B) and downregulated (C) by EZH2 and AEBP2 knockdown.

D. Grapical representation of RT-qPCR of selected genes normalised to shRenilla at each time point demonstrating differential expression between day 7 and day 14 timepoints.

As AEBP2 knockdown in lymphoma cells results in a broad gain of H3K27me3 genome-wide, I hypothesise that cells with AEBP2 knockdown will exhibit a global decrease in total mRNA transcript abundance, due to a loss of transcription from both intergenic and genic sites. To test this hypothesis, I intend to perform spike-in normalised high-depth RNA sequencing at days 7 and 14 of AEBP2 knockdown, which would have the power to detect focal signal changes in the context of altered global changes (K. Chen et al., 2016; Fursova et al., 2021). This would overcome the potential issue of a reduction in transcripts from a gene of interest being masked by a global reduction in transcripts due to global hyper-trimethylation at H3K27 and also facilitate mapping of transcript abundance from intergenic and genic regions respectively.

5.3.4 AEBP2 depletion hyper-activates PRC2.1 in EZH2 mutant lymphoma.

Given that depletion of AEBP2 results in globally elevated levels of H3K27me3 on a background of already elevated H3K27me3 due to the presence of mutant EZH2, I wished to examine mechanistically which form of PRC2 is writing the additional H3K27me3 in this context.

Several roles have been described for Polycomb-like proteins 1-3 (PCL1-3; aliases PHF1, MTF2 and PHF19) in PRC2 recruitment to chromatin. PCL proteins contained extended helix domains which link PRC2 to CpG island DNA, increase PRC2 affinity for DNA and residency time on chromatin (Ballaré et al., 2012; Cao et al., 2008; Choi et al., 2017; Glancy et al., 2021; Healy et al., 2019; Haojie Li et al., 2017; Nekrasov et al., 2007; Perino et al., 2018; Youmans et al., 2021; Q. Zhang et al., 2019). Furthermore, biochemical assays have demonstrated that the Tudor domains of PCLs recognise and bind to the H3K36me2/3 mark, potentially recruiting H3K36 demethylases (Ballaré et al., 2012; Brien et al., 2012; Cai et al., 2013; Musselman et al., 2012).

Given that PCL proteins compete with AEBP2 for the C2 domain of SUZ12 (S. Chen et al., 2018; Youmans et al., 2018), I first wanted to test if in the context of AEBP2 depletion, more PCL proteins will form stable PRC2.1 complexes due to diminished competition for SUZ12 from AEBP2. Furthermore, I wished to examine whether the increased spreading of H3K27me3 in AEBP2 knockdown disrupts H3K36me2/H3K36me3 levels.

Firstly, I generated lentivirus using the CRISPR/Cas9 compatible vector LRG2.1 containing sgRNAs targeting mouse ROSA26 (non-targeting control), AEBP2 exon 2 and MTF2. This vector contains an EGFP reporter. I lentivirally transduced these sgRNAs in the EZH2 mutant lymphoma cell line WSU-DLCL2 and 24 hours later, GFP+ cells were bulk sorted using a FACSAria Fusion Flow Cytometer operated by Dr Barry Moran at Trinity Biomedical Sciences Institute Flow Cytometry Facility. Although limited by low cell number at Day 7, I intended to perform endogenous SUZ12 and IgG immunoprecipitations in the three cell lines. The IP was not successful due to low protein input, but western blot analysis of the 20% input for the experiment confirmed that AEBP2 depletion using a sgRNA significantly increased the MTF2 expression, while MTF2 depletion also increased AEBP2 expression (Figure 5.8A). AEBP2 knock-out in mouse embryonic stem cells has been shown to result in the formation of novel hybrid PRC2 complexes containing JARID2 and MTF2 (Grijzenhout et al., 2016). In lymphoma cells knockdown of AEBP2 displayed no increase in overall levels of JARID2 or the PRC2.1 component EPOP (Figure 5.8B). While this needs more rigorous analysis, this data suggests that upon depletion of AEBP2, more Polycomb-like protein containing PRC2.1 complexes exist in lymphoma cells.

To test if the increased levels of both H3K27me3 and PRC2.1 complexes effected methylation levels at H3K36, I performed ChIP-qPCR for antibodies H3K36me2 and H3K36me3 using WSU-DLCL2 cells transduced with shRNAs targeting Renilla (negative control), EZH2 and AEBP2, as previously used for H3K27me2 and H3K27me3 ChIP-Rx. Overall, knockdown of AEBP2 was associated with a reduction in levels of H3K36me2 and H3K36me3 at a number of genomic loci (Figure 5.8C). Although more rigorous analysis is needed, these data suggest that the increase in H3K27me3 and PRC2.1 activity resulting from AEBP2 depletion leads to a decrease in H3K36 methylation. I intend to test this observation with additional biological replicates and ChIP-Rx, including antibodies for MTF2 (to examine whether MTF2 binding on chromatin is increased with AEBP2 knockdown) and RNA polymerase II to examine the effects of the redistribution of H3K27 and H3K36 methylation marks on the localisation of cellular transcriptional machinery.

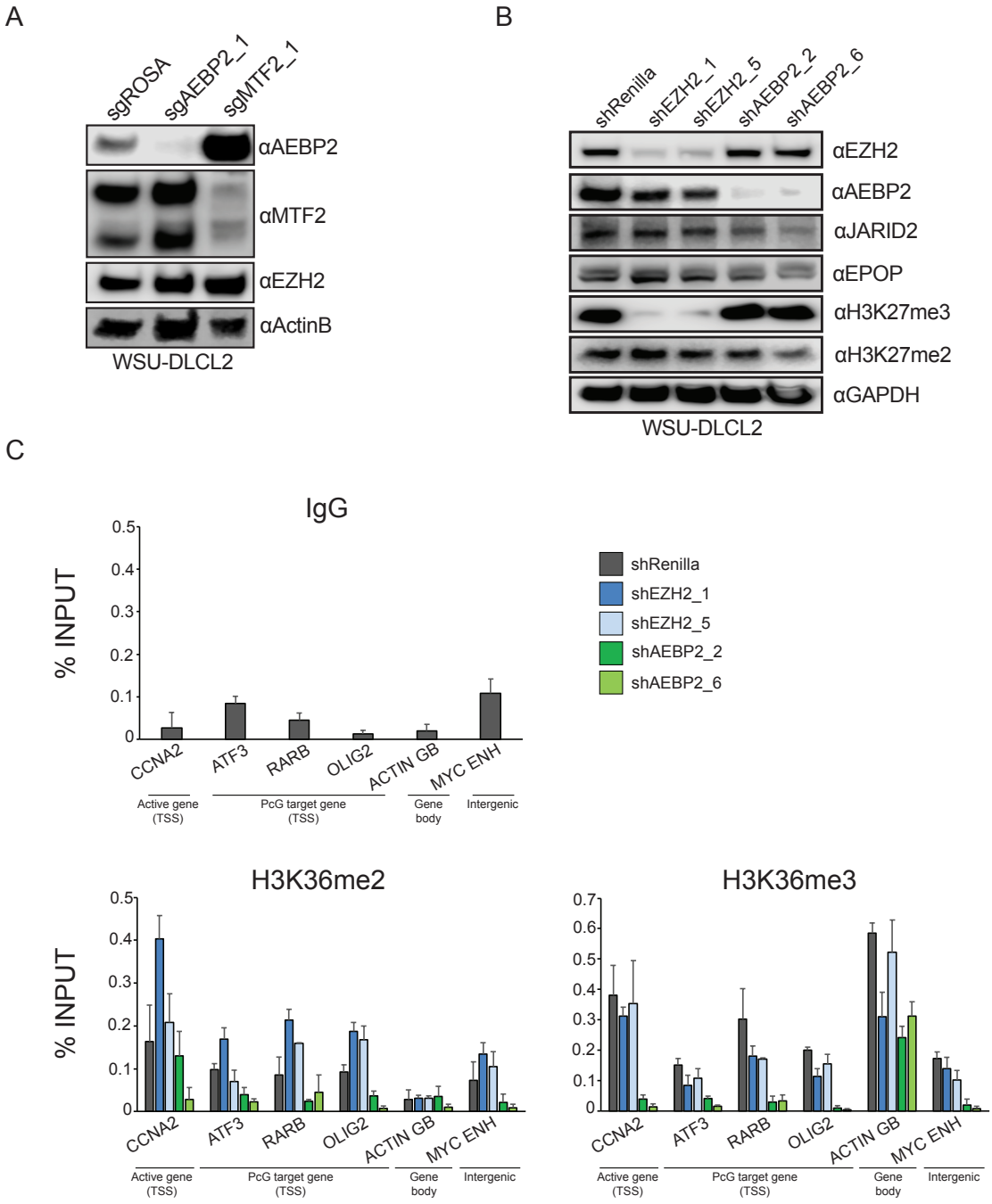

Figure 5.8 AEBP2 knockdown results in increased levels of PRC2 complexes containing MTF2 and a reduction in levels of H3K36me2 and H3K36me3 marks

A. Western blot analysis in lymphoma cells subjected to CRISPR/Cas9-mediated depletion of ROSA, AEBP2 or MTF2, demonstrating reciprocal increase in AEBP2 expression with depletion of MTF2 and vice versa.
B. Western blot analysis in lymphoma cells subjected to EZH2 or AEBP2 knockdown demonstrating that AEBP2 knockdown does not result in an increase in JARID2 levels.
C. ChIP-qPCR analyses at various genomic loci for H3K36me2 and H3K36me3 in EZH2 mutant lymphoma cell line WSU-DLCL2 with shRENILLA or EZH2/AEBP2 knockdown.

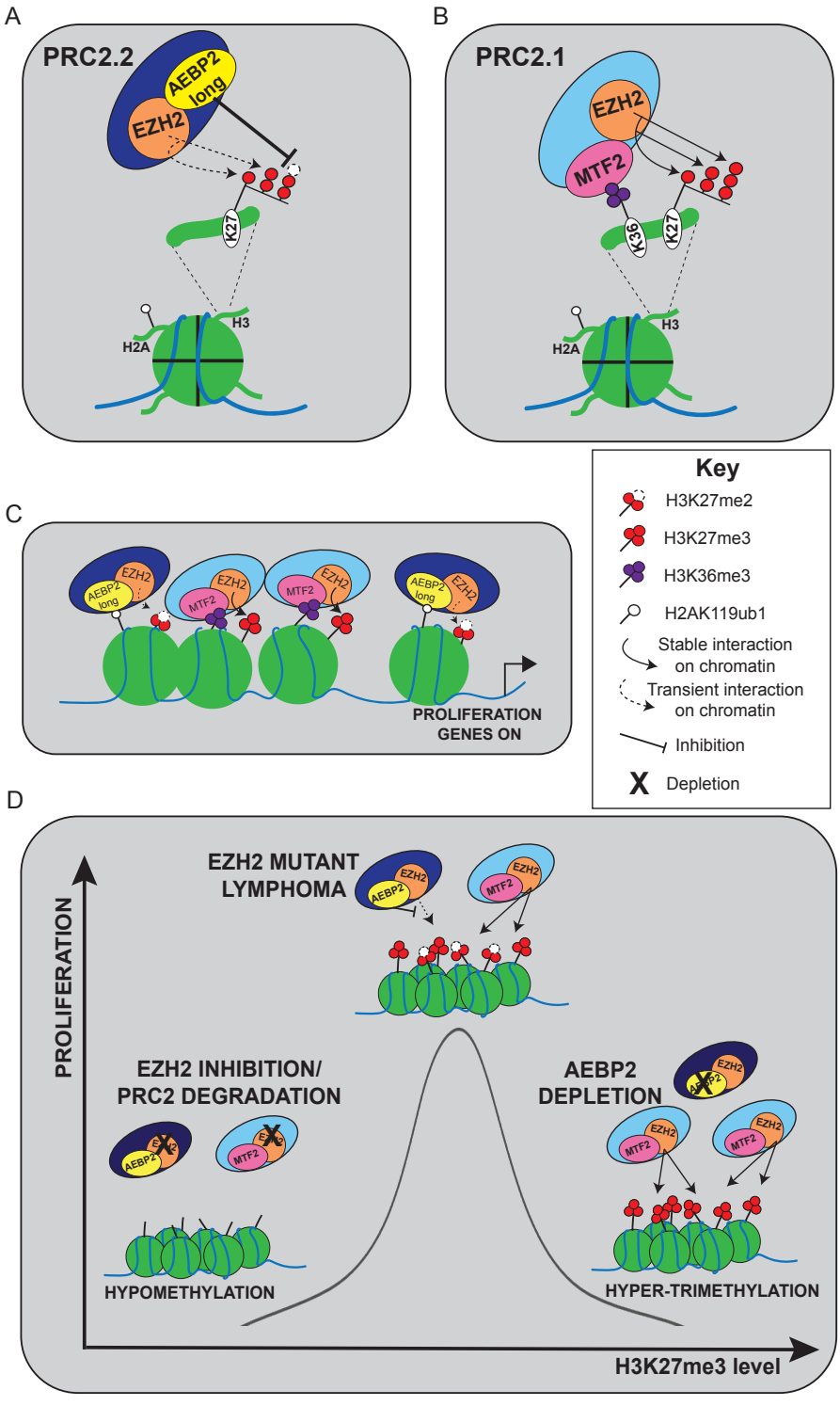

Figure 5.9 AEBP2 antagonism of PRC2-mediated H3K27me3 is essential for EZH2 mutant lymphoma proliferation

A-B. PRC2.2-AEBP2 antagonises PRC2 methyltransferase activity *in vivo*, resulting in impaired H3K27me3, whereas PRC2.1 performs all degrees of H3K27 methylation.

C. Balance of PRC2.1 and PRC2.2 activity cooperatively maintains optimal H3K27 methylation status for lymphoma cellular proliferation.

D. Perturbation of H3K27me3 by PRC2 inhibition or hyperactivation by AEBP2 depletion and resultant increased PRC2.1 activity adversely effects EZH2 mutant lymphoma cells.

5.3 Discussion and future directions

The pathogenic role of the driver oncogene EZH2 in germinal centre B-cell lymphoma is increasingly well understood, with mechanisms of action including a pro-proliferative signal, aberrant repression of tumour suppressor genes and terminal differentiation genes, impaired immune surveillance and impaired apoptosis (Béguelin et al., 2013, 2016, 2020; Bödör et al., 2013; Donaldson-Collier et al., 2019; Morin et al., 2011; Oricchio et al., 2017; Yap et al., 2011). All of these mechanisms have been evidentially linked to the ability of mutant EZH2 to act in concert with a wild-type EZH2 allele to generate abnormally high levels of H3K27me3 and furthermore have been shown to be reversible with EZH2 enzymatic inhibition. Furthermore, the first *in vivo* studies to demonstrate acquired resistance to EZH2 inhibitor therapy (in cell lines, as these mechanisms have yet to be described in patients) share the common end result of lymphoma cells restoring pathologically elevated H3K27me3 levels, which is clearly advantageous for their survival (Baker et al., 2015a; Bisserier & Wajapeyee, 2018; Brooun et al., 2016a; Gibaja et al., 2016a; Qi et al., 2017). In chapter 3, I demonstrated that PRC2 depletion via PROTAC-mediated degradation of EED, one of its obligatory core components, did not result in any additional transcriptional changes beyond that of the EZH2 enzymatic inhibitor Tazemetostat: supporting evidence that EZH2 enzymatic activity underlies its oncogenic function.

Using biochemical assays and mouse embryonic stem cells as models, AEBP2 has been ascribed conflicting roles in its modulation of PRC2 methyltransferase activity: *in vitro*, AEBP2 increases PRC2 methyltransferase activity, while depletion of AEBP2 *in vivo* increases H3K27me3 levels (Cao & Zhang, 2004; Conway et al., 2018, 2021; Grijzenhout et al., 2016; Jonas W. Højfeldt et al., 2018; Kasinath et al., 2018; C. H. Lee, Holder, et al., 2018; Xueyin Wang et al., 2017). In keeping with previously published *in vivo* data, in EZH2 mutant lymphoma cells, two independent short hairpin RNAs targeting AEBP2 resulted in a global increase in H3K27me3 and loss of H3K27me2. This is a surprising finding, considering these cells already harbour abnormally elevated H3K27me3 levels due to the presence of oncogenic mutant EZH2. Furthermore, AEBP2 is a genetic dependency for six of seven tested lymphoma cell lines (Chapter 4 Figure 4.7). This suggests that beyond a ceiling level of H3K27me3, additional H3K27me3 is detrimental for lymphoma cells. Another group has demonstrated a similar phenomenon, whereby SETD2 inhibition resulting in reduced H3K36me3 and

subsequent spreading of H3K36me3 was detrimental for EZH2 mutant lymphoma cells (Kwok et al., 2022). This publication supports the concept that PRC2 hyperactivation is a potential avenue for targeting EZH2 mutant lymphoma and should be explored in other PRC2-dependent cancer contexts (Figure 5.9D).

The mechanism whereby AEBP2 is a genetic dependency in lymphoma and the effects of PRC2 hyperactivation via depletion of AEBP2 require further exploration. RNA-Sequencing in the context of AEBP2 knockdown revealed few changes in gene expression changes at day 7. RT-qPCR analyses performed at day 14 demonstrated that mRNA transcripts from Polycomb target genes are somewhat reduced. Thus, I hypothesise that the global levels of mRNA from cells with PRC2 hyperactivation will be reduced, thereby potentially masking discrete changes in transcript levels. To address this issue, I intend to perform spike-in RNA-Sequencing in lymphoma cells using a *Drosophila* cell spike-in, such that with a constant cell-number, overall changes in RNA abundance can be more clearly identified, including more sensitive detection of changes in mRNA transcripts from specific genomic loci (K. Chen et al., 2016; Fursova et al., 2021).

As previously discussed, PRC2.1 and PRC2.2 are well-described as defining mutually exclusive PRC2 subcomplex assemblies. AEBP2 and PCL proteins compete for the same region of SUZ12 in order to stably associate with core PRC2 (S. Chen et al., 2018, 2020; Youmans et al., 2018). I propose that this antagonistic interplay between PRC2.1 and PRC2.2 subcomplex assemblies provides an essential balance for germinal centre B-cell lymphoma cells, whereby AEBP2 negatively regulates PRC2 activity to maintain elevated H3K27me3 within its narrow optimal window (Figure 5.9). In support of this hypothesis, I have demonstrated with preliminary data that MTF2 expression increases at the protein level with AEBP2 depletion. The reciprocal also holds to be true. AEBP2 long isoform contains a nett negative charge at its N-terminus, likely resulting in a reduced propensity to interact with negatively-charged DNA (Jones et al., 1999; Marcovitz & Levy, 2011; Stawiski et al., 2003; Szilágyi & Skolnick, 2006). This is in sharp contrast to PCL proteins which increase PRC2 residency time on chromatin (Choi et al., 2017; Youmans et al., 2021). Therefore, it is likely that in AEBP2-depleted lymphoma cells, PCL proteins more stably associate with SUZ12, resulting in additional H3K27me3 due to increased overall PRC2 affinity for and residency on chromatin, genome-wide (Figure 5.9A-C). I intend to examine this with MTF2 ChIP-Rx in the context of non-targeting shRNA (shRenilla) and two independent AEBP2 shRNAs. PCL

proteins have been shown via their Tudor domains to associate with H3K36me2 and H3K36me3 marks (Ballaré et al., 2012; Brien et al., 2012; Cai et al., 2013; Musselman et al., 2012). In a mouse embryonic stem cell model, this interaction recruited the H3K36me3 demethylase to stem cell genes during differentiation (Brien et al., 2012; Musselman et al., 2012). Should this mechanism hold to be true in the lymphoma context, it may explain why H3K36 methylation marks would be lost in the context of increased PRC2.1 activity.

Indeed, a mutual antagonism between H3K36 methylation and H3K27 methylation is well recognised. H3K36 methylation inhibits allosteric activation of PRC2 and resultantly its methyltransferase activity, without inhibiting binding of the complex to chromatin (Finogenova et al., 2020; Jani et al., 2019; Klymenko & Jürg, 2004; Schmitges et al., 2011; Streubel et al., 2018; Yuan et al., 2011). Conversely, the H3K36M mutant oncohistone present in ~95% of chondroblastomas, wherein H3M36 cannot be methylated, results in an intergenic increase in H3K27me3 (Behjati et al., 2013; Klein et al., 2018; Lu et al., 2016). Furthermore, inhibition/depletion of NSD1/2-mediated H3K36me2 and SETD2-mediated H3K36me3 have been shown to result in an increase in intergenic H3K27me3 levels (Drosos et al., 2022; Kwok et al., 2022; Streubel et al., 2018). I show here preliminary data that in AEBP2 knockdown lymphoma cells, H3K36me2/H3K36me3 marks are reduced and intend to examine this on a genome-wide scale using ChIP-Rx for H3K36me2, H3K36me3 and RNAPol II. This reduction in H3K36 methylation marks which normally antagonise H3K27 di- and tri-methylation may contribute to the phenotype of elevated H3K27me3 genome-wide upon AEBP2 knockdown in lymphoma cells. I demonstrated in Chapter 4 that EZH2 wild-type lymphoma cell lines are also sensitive to AEBP2 depletion. I intend to examine the effects of AEBP2 knock-down on H3K27 and H3K36 methylation status in this context also.

Therefore, my short-term work will be towards examining the hypothesis that knockdown of AEBP2 impairs lymphoma proliferation by:

- Global gain of H3K27me3 and loss of H3K27me2 as supported by ChIP-Rx
- Reduced transcription from Polycomb target genes (supported by RT-qPCR) and potentially globally reduced transcription due to bystander and proliferation genes being silenced by broad repressive H3K27me3 blanket
- Increased activity of PRC2.1 resulting in increased H3K27me3 and reduced H3K36me2/H3K36me3 (supported by elevated MTF2 on protein level upon AEBP2 knockdown and ChIP-qPCR of H3K36me2/H3K36me3).

Chapter 6: General discussion

6.1 Discussion

6.1.1 Summary of findings

In chapter 3, using an isogenic lymphoma cell line expressing wild-type and mutant EZH2 (EZH2^{Y646F}), I describe using ChIP-Rx the genome-wide redistribution of the repressive marks H3K27me2 and H3K27me3 resulting from the presence of this mutation. In this experiment, I demonstrate the well-described phenotype of genome-wide gain of H3K27me3 and loss of H3K27me2, with the caveat that a small portion of genomic loci lose H3K27me3 as was previously ascribed to neo-functionalisation of PRC2 by mutant EZH2 (Souroullas et al., 2016). Additionally, I demonstrate that core PRC2 (represented by SUZ12 in this experiment) is leached from Polycomb target gene promoters by mutant EZH2 and marginally increased genome-wide, reflecting the more stable interaction with chromatin required to write the H3K27me3 mark. As EZH2 inhibitor drugs begin to find a place in treatment algorithms for patients with relapsed/refractory B-cell lymphoma and SMARBC1 deficient sarcomas, the mechanisms for initial and acquired resistance to these therapies are clinically very important. We demonstrate in human fibroblast and thyroid cancer cell lines and patient-derived lymph node biopsies from patients with follicular lymphoma that PRC2-EZH1 defines quiescent, non-proliferating cells which are resistant to EZH2 enzymatic inhibition but sensitive to PRC2 degradation via an EED-targeting PROTAC molecule. Moreover, I demonstrate that PRC2 degradation overcomes acquired resistance to EZH2 enzymatic inhibition arising due to acquired hotspot mutations in EZH2 that preclude EZH2 inhibitor drug binding. Dissection of the differential effects of PRC2 enzymatic inhibition (EZH2 inhibitor Tazemetostat) and PRC2 degradation (EED degrader UNC7700), reveals broadly similar effects on the distribution of H3K27me3 and mostly overlapping gene expression changes. In this experiment, Tazemetostat was more effective in reducing H3K27me2 and H3K27me3 than UNC7700, likely because residual undegraded PRC2 in UNC7700-treated cells was not enzymatically inhibited; with the result that Tazemetostat treatment resulted in greater gene expression changes at day 3 of treatment than UNC7700. Overall, this work describes in greater detail than previously published the disrupted genomic localisation and activity of PRC2 containing mutant EZH2 in lymphoma and identifies PRC2 degradation as a means of overcoming numerous mechanisms of resistance to EZH2 enzymatic inhibition.

In chapter 4, in collaboration with Dr Eric Conway I performed a PRC2-directed CRISPR tiling library utilising almost 4000 sgRNAs targeting PRC2 core and substoichiometric components in the EZH2 mutant lymphoma cell lines WSU-DLCL2 and Pfeiffer. This work reveals that the core PRC2 components EZH2, EED and SUZ12 as well as the PRC2.2 component AEBP2 are genetic dependencies in these cell lines. The other PRC2.2 component JARID2 is not a dependency. Previous work in the Bracken lab utilising this PRC2 tiling library had revealed the SMARCBI$^{-/-}$ malignant rhabdoid tumour cell line G401 to be genetically dependent on core PRC2. Validation work confirms that six of seven tested lymphoma cell lines are genetically dependent on AEBP2 and not JARID2, but G401 is not dependent on either PRC2.2 component. AEBP2 depletion also overcomes acquired resistance to Tazemetostat. Examining numerous lymphoma cell lines and utilising publicly available data from cancer cell lines and patients with DLBCL, I illustrate that AEBP2 is highly expressed in all stages of B-cell maturation and that AEBP2 long isoform is the predominant form of AEBP2 expressed in these cells. Arising from the PRC2 tiling CRISPR screen and subsequent validation work, I identify that the previously annotated AEBP2 Zinc Finger and KR-rich motifs are functionally important in lymphoma. Additionally, I highlight sgRNAs targeting a small, previously undescribed AEBP2 motif annotated the SUZ12 binding helix (SBH) that deplete in lymphoma cell lines. I show that this highly conserved motif is essential for AEBP2 interaction with SUZ12. I demonstrate that ectopic expression of AEBP2 long isoform fully rescues sgRNA and shRNA-mediated depletion of AEBP2 in lymphoma cells, indicating that the more abundant long isoform is functional and underlies the AEBP2 oncogenic dependency in lymphoma. Taken together, this research is the first evidence that a substoichiometric PRC2 component is a dependency in a cancer context. AEBP2 long isoform was shown to be by far the most abundant isoform in lymphoma, as well as being functionally important.

In chapter 5, I examine the effects of AEBP2 disruption on the genomic localisation and abundance of H3K27me3 and H3K27me2 in lymphoma cells and the ensuing effects on the transcriptional landscape, using two independent shRNAs targeting AEBP2. This reveals that H3K27me3 is increased even in the EZH2 mutant lymphoma cellular context which already has dramatically elevated H3K27me3 levels. H3K27me3 gain is evident genome-wide, with marked changes evident intergenically and at Polycomb target gene promoters. At day 7, few transcriptional changes were demonstrated using RNA-Seq, however at a day 14 time point, there is a reduction in mRNA transcripts from Polycomb target genes including genes essential for B-cell maturation. I predict that overall mRNA transcripts are reduced due to elevated

H3K27me3 and that spike-in of Drosophila cells followed by RNA-Sequencing performed at a day 14 time point will reveal hitherto cryptic transcriptional changes. I show that with reduced competition from AEBP2 for interaction with SUZ12, PRC2.1-MTF2 levels increase in lymphoma cells, which likely represents the engine for hyper-trimethylation at H3K27 seen in AEBP2 knockdown EZH2 mutant lymphoma cells. I also provide preliminary evidence that elevated H3K27me3 levels mediated by AEBP2 knock-down result in reduced H3K36me2 and H3K36me3 at numerous genomic loci. Overall, the work in this chapter reveals clues to the mechanism of action for AEBP2 in lymphoma cells, and potentially in Polycomb biology more generally. Highlighted here also is the contribution of disrupted interplay between PRC2.1 and PRC2.2 subcomplex assemblies to H3K27 methylation upon AEBP2 knockdown in lymphoma.

6.1.2 EZH2 oncogenic function is mediated by its enzymatic function

Polycomb group proteins are highly expressed in germinal centre-derived DLBCL and moreover have been shown to be essential for lymphoid germinal centre formation (Béguelin et al., 2013; Van Kemenade et al., 2001). Recurrent hotspot mutations in EZH2, detected in up to 25% of GCB-subtype DLBCL and follicular lymphoma, result in an altered substrate preference of mutant EZH2 for di-methylated H3K27, resulting in pathologically elevated H3K27me3 levels intergenically and genome-wide (Bödör et al., 2013; McCabe, Graves, et al., 2012; Morin et al., 2011; Okosun et al., 2014; Sneeringer et al., 2010; Souroullas et al., 2016). Interestingly, mutant EZH2 generates approximately 2800 *de novo* H3K27me3 peaks in mouse germinal centre lymphocytes (Béguelin et al., 2020). Targeting this hypermethylation utilising EZH2 enzymatic inhibition has shown clinical utility in lymphomas harbouring mutant EZH2 (Italiano et al., 2018; Izutsu et al., 2021; Knutson et al., 2014; Morschhauser et al., 2020). In chapter 3, in an isogenic lymphoma model expressing wild-type or mutant EZH2, SUZ12 co-localises with increased H3K27me3 genome-wide. However, in an EZH2 mutant cell line, PRC2 degradation using the EED-degrading PROTAC UNC7700 did not result in any additional transcriptional changes compared to the EZH2 inhibitor Tazemetostat, despite its additional effect of destabilising PRC2. Taken together, these data suggest that the oncogene EZH2 exerts its effects via deposition of repressive H3K27 methylation marks and not necessary due to nucleation of PRC2 itself. However, potential roles for canonical PRC1-mediated chromatin compaction via recognition of this excessive H3K27me3 should be explored and evaluated, with possible therapeutic potential.

6.1.3 AEBP2 is a potential therapeutic target in cancer

Large-scale CRISPR screens have emerged as a useful tool in unveiling essential regulators of cellular processes and key players in cancer biology. I utilised this technology to comprehensively screen PRC2 core and substoichiometric components in order to detect proteins or domains within proteins essential for a proliferative advantage in lymphoma cell lines. Moreover, I wished to identify novel targets relating to the oncogene EZH2 in B-cell lymphoma. Core PRC2 components EZH2, EED and SUZ12 as well as PRC2.2 component AEBP2, but not JARID2 emerged as dependencies in both screened EZH2 mutant lymphoma cell lines. Subsequent validation work in numerous additional EZH2 mutant and wild-type lymphoma cell lines revealed this dependency on AEBP2 to be specific and on-target, with complete sgRNA and shRNA rescue by exogenous wild-type AEBP2 constructs. Furthermore, an additional PRC2-dependent cancer context (SMARB1$^{-/-}$ malignant rhabdoid tumour) was agnostic to AEBP2 depletion. Although the long isoform of AEBP2 is by far the most abundant isoform in B-lymphoid malignancies, the PRC2 tiling screen identified domains common to all AEBP2 isoforms as being critical dependencies in lymphoma: Zinc Fingers 1-3, KR-rich motif and a small motif we denote the SUZ12 binding helix within a broad C-terminal previously annotated SUZ12 interaction domain. Therefore, if a molecule were to be developed to target AEBP2 specifically, it should either degrade AEBP2 or disrupt its interaction with either SUZ12 (via the SUZ12 binding helix) or with nucleosomal DNA (via its Zinc Fingers or KR motif). Indeed, based on these findings, we are currently working with a collaborator (Dr Oliver Bell, University of Southern California) to identify a molecule capable of targeting AEBP2 in mouse embryonic stem cells using a modified TetOperator/TetRepressor system as described in (Yelagandula et al., 2021).

6.1.4 AEBP2 and EED depletion can overcome acquired resistance to EZH2 enzymatic inhibition

Numerous mechanisms for acquired resistance to EZH2 inhibitor therapy have been described in lymphoma cell lines models, including the acquisition of EZH2 point mutations excluding Tazemetostat from its binding pocket in EZH2, EZH2 CXC domain hypermorphic mutations resulting in increased EZH2 methyltransferase activity and Tazemetostat addiction and upregulation of secondary signalling pathways (Baker et al., 2015a; Bisserier & Wajapeyee, 2018; Brooun et al., 2016a; Gibaja et al., 2016a; Kwok et al., 2022). However, mechanisms of tumour escape in patients have yet to be described. Additionally, we describe using human fibroblasts and thyroid cancer cell lines and lymph node biopsies from patients with follicular

lymphoma, the predominance in quiescent, non-proliferating cells of a PRC2 complex containing EZH1 and lacking EZH2, which is refractory to EZH2 enzymatic inhibition *in vivo*. In Chapters 3 and 4, I demonstrate that AEBP2 depletion and PRC2 degradation via an EED-degrading PROTAC drug UNC7700 overcome several mechanisms of acquired resistance to Tazemetostat. The utility of these approaches will be tested when mechanisms of tumour escape in patients are described. Durations of response amongst initial responders to Tazemetostat monotherapy in relapsed/refractory B-cell lymphoma patients are relatively modest, with a median duration of 1 year (Morschhauser et al., 2020). Re-biopsy of patients progressing on Tazemetostat and determination of the mechanism(s) giving rise to acquired resistance to Tazemetostat will yield crucial information guiding further therapeutic options and whether PRC2 remains a viable genetic dependency for these tumours.

6.1.5 AEBP2 depletion in lymphoma cells results in a gain of H3K27me3 and loss of H3K27me2

AEBP2 knockdown by two independent shRNAs in an EZH2 mutant lymphoma cell line resulted in further gain of H3K27me3; an impressive feat given the already elevated levels of H3K27me3 genome-wide resulting from the presence of the EZH2 oncogenic mutant in this context. Although at day 7 few discrete resultant transcriptional changes were evident, downregulation of lymphoma-relevant Polycomb target genes became more apparent at a day 14 timepoint. Transcriptional changes will likely be best appreciated using spike-in RNA-sequencing with a fixed ratio of spike-in *Drosophila* to lymphoma cells. Given the opposing phenotype of H3K27 methylation changes upon knockdown of AEBP2 compared with EZH2 knockdown, it is likely that the resultant transcriptional changes will also differ: EZH2 knockdown results in mainly transcriptional derepression, whereas AEBP2 knockdown will likely result in a repressive transcriptional signature.

I propose that EZH2 mutant lymphoma is dependent on a synergy between PRC2-AEBP2 and PRC2.1 complexes. AEBP2 long isoform, the predominant isoform expressed in lymphoma cells, likely inhibits PRC2 activity due to electrostatic repulsion of DNA via its negatively charged N-terminus. This repulsion likely either results in impaired interaction with DNA, or reduced residency time facilitating lower order H3K27 methylation, whilst also competing with PCL proteins for interaction with their SUZ12 binding site. Depletion of AEBP2 thereby results in the formation of more PRC2.1 complexes and also the loss of the inhibitory effect of AEBP2

on H3K27 methylation, resulting in a further gain of H3K27me3 beyond that which confers a proliferative advantage to lymphoma cells: i.e. PRC2 activation. This is supported by evidence of increased expression of PCL protein MTF2 upon knockdown of AEBP2, though will require further investigation using ChIP-Rx and SUZ12 co-immunoprecipitation in lymphoma cells.

Importantly, while I have demonstrated that AEBP2 is an oncogenic dependency in EZH2 wild-type lymphoma cell lines, I have not yet examined the effects of AEBP2 knockdown on H3K27 methylation status and result transcriptional changes in this context, but intend to do so in the short term.

6.1.6 AEBP2 may be a useful target in other cancer contexts with increased levels of H3K27me3

Analogous to PRC2 activation by depletion of AEBP2 as proposed in this thesis, PRC2 activation via inhibition of SETD2-mediated H3K36me3 was also recently proposed as a means of therapeutically harnessing hyperactive EZH2 in EZH2 mutant lymphoma (Kwok et al., 2022). Interestingly, by ChIP-qPCR I observed a reduction in H3K36me2 and H3K36me3 marks upon knockdown of AEBP2 in EZH2 mutant lymphoma cells also and intend to follow this up with ChIP-Rx for these marks and RNAPol II to examine whether localisation of transcriptional machinery is also altered. I propose that there may be a cancer epigenetic signature, whereby tumours with elevated intergenic (or global) H3K27me3 levels may be sensitive to PRC2 activation via AEBP2 disruption or an alternative means of PRC2 activation (i.e. disruption of other factors that normally inhibit PRC2 activity, such as UTX/UTY and H3K36me2/me3 methyltransferase enzymes). I outline here several such cancer contexts.

Loss of function mutations in the H3K27me2/3 demethylase gene KDM6A(UTX) have been detected in up to 10% of cases of multiple myeloma, T-cell acute lymphoblastic leukaemia and numerous solid cancer contexts including oesophageal cancer, small cell lung cancer, renal cell carcinoma and colorectal cancer (Ezponda et al., 2017; Ho et al., 2013; Van Der Meulen et al., 2014, 2015; Van Haaften et al., 2009). Deficiency of UTX in these tumours is characterised by elevated H3K27me3 at certain genomic with resultant gene repression, which is reversible by reintroduction of UTX or treatment with EZH2 inhibitor drugs. It would be interesting to explore the effects of PRC2 activation on these tumours. Additionally, UTX/UTY inhibition could be an interesting avenue for induction of PRC2 activation.

Loss or inhibition of NSD1/2-mediated H3K36me2 and SETD2-mediated H3K36me3 have been shown to increase H3K27me3 levels genome-wide, with most marked change observed intergenically, where H3K27me3 is normally found in low abundance (Drosos et al., 2022; Kwok et al., 2022; Streubel et al., 2018). Loss of function mutations in NSD1 have been detected in 10% of patients with *Human Papilloma Virus* negative head and neck squamous cell carcinomas (HNSCC) and less commonlya in squamous cell lung cancer (Brennan et al., 2017; Bui et al., 2018). NSD1 deficiency in HNSCC results in CpG hypomethylation, due to loss of H3K36me2, which along with H3K36me3 recruits DNMT3a and DNMT3b via their PWWP domains to chromatin (Bui et al., 2018; T. Chen et al., 2004; Deevy & Bracken, 2019; Dhayalan et al., 2010; Ge et al., 2004). In support of this, in HNSCC cell lines, loss of NSD1-mediated H3K36me2 has been shown to correlate with DNA hypomethylation and marked intergenic gain of H3K27me3 (Farhangdoost et al., 2021). Inactivating mutations in the H3K36me3 methyltransferase enzyme SETD2 are found in approximately 3% of cases of renal cell carcinoma and 15% and 8% of cases of paediatric and adult high-grade glioma respectively (Dalgliesh et al., 2010; Fontebasso et al., 2013). Given that enzymatic inhibition of SETD2-mediated H3K36me3 results in lymphoma cells in genome-wide gain of H3K27me3 (Kwok et al., 2022), it would be interesting to examine if this is also the case in tumours with loss of function mutations in SETD2 and furthermore if this could be exploited using PRC2 activation. A similar phenomenon of intergenic H3K27me3 gain due to loss of H3K36 methylation has been observed in the presence of the H3.3K36M oncohistone, which is present in 95% of cases of chondroblastoma (Lu et al., 2016).

Deletion or loss of function mutations of the PR-DUB component BAP1, the H2AK119ub1 deubiquitylase enzyme are found in over a quarter of cases of malignant mesothelioma, uveal melanoma, cholangiocarcinoma and renal clear cell carcinoma (Carbone et al., 2013; Cerami et al., 2012; J. Gao et al., 2013). Loss of BAP1 has been shown in mouse embryonic stem cells to result in a genome-wide gain of H2AK119ub1, with subsequent leaching of PRC2 from polycomb target genes and intergenic gain of H3K27me3 (Conway et al., 2021; Fursova et al., 2021; Tamburri et al., 2020). Loss of H2AK119ub1 in mouse embryonic stem cells displaces AEBP2 from chromatin (Tamburri et al., 2020). Should BAP1 deficient cancer contexts also be characterised by elevated intergenic H3K27me3, it would be interesting to examine whether depletion of AEBP2 further increases H3K27me3 to deleterious levels due to ablation of the inhibitory effect on methyltransferase activity conferred by AEBP2 long isoform.

6.1.7 Future directions

In the research chapters of this thesis, I have presented strong data describing the importance of EZH2 methyltransferase activity in mediating its oncogenic effects in germinal centre lymphoma and also identifying AEBP2 as a genetic dependency in lymphoma. The AEBP2 dependency was shown to be specific, on-target and present in numerous EZH2 mutant and wild-type lymphoma cell lines. However, I have not yet examined the dependency of other lymphoma contexts on AEBP2. Given that AEBP2 long isoform is similarly highly expressed in another germinal-centre derived lymphoma – Burkitt Lymphoma, and also in activated B-cell subtype (ABC) DLBCL, I intend to perform sgRNA depletion assays in these contexts also. Perhaps AEBP2 dependency in lymphoma is not confined to GCB-DLBCL and follicular lymphoma.

Mechanistically, I demonstrated that AEBP2 depletion leads to genome-wide gain of H3K27me3 and loss of H3K27me2. This supports previous work demonstrating that AEBP2 knock-out in mouse ESCs results in gain of H3K27me3 and may allude to specific functions of the AEBP2 long isoform in inhibiting PRC2 activity *in vivo*. Although I have shown in an EZH2 mutant lymphoma context the effects of AEBP2 perturbation on H3K27me2 and H3K27me3 localisation, I plan to examine this in an EZH2 wild-type lymphoma context, given that EZH2 wild-type cell lines were also shown to be genetically dependent on AEBP2. I also plan to perform further ChIP-Rx analyses to examine as previously discussed the effects of AEBP2 depletion on MTF2 localisation, H3K36me2/3 levels, RNAPol II localisation and PRC1 localisation (RING1A/1B). Furthermore, as previously mentioned I plan to perform spike-in RNA-sequencing to better describe transcriptional changes resulting from this elevation in H3K27me3 levels. It would also be interesting to explore whether or not this elevation in H3K27me3 affects chromatin accessibility or chromatin compaction via ATAC-Seq and Hi-C.

6.2 Conclusions

The data presented in this thesis support the following conclusions:

- The EZH2 gain-of-function mutation EZH2^{Y646F} in lymphoma results in genome-wide redistribution of H3K27me3, H3K27me2 and SUZ12 with broad gain of H3K27me3 and loss of H3K27me2.
- PRC2-EZH1 is upregulated and highly expressed in quiescent cells and is targetable by an EED-degrading PROTAC.
- EZH2 enzymatic inhibition and EED degradation result in similar transcriptional effects in B-cell lymphoma.
- PRC2.2 component AEBP2 and not JARID2 is a specific genetic dependency in B-cell lymphoma.
- AEBP2 long isoform is the predominant isoform in B-cell lymphoma.
- AEBP2 zinc finger domains, KR-rich motif and SUZ12 binding helix are functionally important in lymphoma.
- Depletion of AEBP2 or core PRC2 can overcome acquired resistance to EZH2 enzymatic inhibition.
- AEBP2 depletion results in genome-wide gain of H3K27me3 and loss of H3K27me2, with increased activity by PRC2.1.

References

Adler, P. N., Martin, E. C., Charlton, J., & Jones, K. (1991). Phenotypic consequences and genetic interactions of a null mutation in the Drosophila posterior Sex Combs gene. *Developmental Genetics*. https://doi.org/10.1002/dvg.1020120504

Advani, R., Rosenberg, S. A., & Horning, S. J. (2004). Stage I and II follicular non-Hodgkin's lymphoma: Long-term follow-up of no initial therapy. *Journal of Clinical Oncology*. https://doi.org/10.1200/JCO.2004.10.086

Agger, K., Cloos, P. A. C., Christensen, J., Pasini, D., Rose, S., Rappsilber, J., Issaeva, I., Canaani, E., Salcini, A. E., & Helin, K. (2007). UTX and JMJD3 are histone H3K27 demethylases involved in HOX gene regulation and development. *Nature*. https://doi.org/10.1038/nature06145

Akasaka, T., van Lohuizen, M., van der Lugt, N., Mizutani-Koseki, Y., Kanno, M., Taniguchi, M., Vidal, M., Alkema, M., Berns, A., & Koseki, H. (2001). Mice doubly deficient for the polycomb group genes Mel18 and Bmi1 reveal synergy and requirement for maintenance but not initiation of Hox gene expression. *Development*.

Akasaka, Takeshi, Kanno, M., Balling, R., Mieza, M. A., Taniguchi, M., & Koseki, H. (1996). A role for mel-18, a Polycomb group-related vertebrate gene, during the anteroposterior specification of the axial skeleton. *Development*.

Akashi, H., & Gojobori, T. (2002). Metabolic efficiency and amino acid composition in the proteomes of Escherichia coli and Bacillus subtilis. *Proceedings of the National Academy of Sciences of the United States of America*. https://doi.org/10.1073/pnas.062526999

Alabert, C., Barth, T. K., Reverón-Gómez, N., Sidoli, S., Schmidt, A., Jensen, O., Imhof, A., & Groth, A. (2015). Two distinct modes for propagation of histone PTMs across the cell cycle. *Genes and Development*. https://doi.org/10.1101/gad.256354.114

Alekseyenko, A. A., Gorchakov, A. A., Kharchenko, P. V., & Kuroda, M. I. (2014). Reciprocal interactions of human C10orf12 and C17orf96 with PRC2 revealed by BioTAP-XL cross-linking and affinity purification. *Proceedings of the National Academy of Sciences of the United States of America*. https://doi.org/10.1073/pnas.1400648111

Armitage, J. O., & Longo, D. L. (2016). Is watch and wait still acceptable for patients with low-grade follicular lymphoma? *Blood*. https://doi.org/10.1182/blood-2015-11-632745

Asmar, F., Punj, V., Christensen, J., Pedersen, M. T., Pedersen, A., Nielsen, A. B., Hother, C., Ralfkiaer, U., Brown, P., Ralfkiaer, E., Helin, K., & Grønbæk, K. (2013). Genome-wide profiling identifies a DNA methylation signature that associates with TET2 mutations in diffuse large B-cell lymphoma. *Haematologica*. https://doi.org/10.3324/haematol.2013.088740

Baker, T., Nerle, S., Pritchard, J., Zhao, B., Rivera, V. M., Garner, A., & Gonzalvez, F. (2015a). Acquisition of a single EZH2 D1 domain mutation confers acquired resistance to EZH2-targeted inhibitors. *Oncotarget*. https://doi.org/10.18632/oncotarget.5066

Baker, T., Nerle, S., Pritchard, J., Zhao, B., Rivera, V. M., Garner, A., & Gonzalvez, F. (2015b). Acquisition of a single EZH2 D1 domain mutation confers acquired resistance to EZH2-targeted inhibitors. *Oncotarget*, *6*(32), 32646–32655. https://doi.org/10.18632/oncotarget.5066

Baker, T., Nerle, S., Pritchard, J., Zhao, B., Rivera, V. M., Garner, A., & Gonzalvez, F. (2015c). Acquisition of a single EZH2 D1 domain mutation confers acquired resistance to EZH2-targeted inhibitors. *Oncotarget*. https://doi.org/10.18632/oncotarget.5066

Baliñas-Gavira, C., Rodríguez, M. I., Andrades, A., Cuadros, M., Álvarez-Pérez, J. C., Álvarez-Prado, Á. F., de Yébenes, V. G., Sánchez-Hernández, S., Fernández-Vigo, E.,

Muñoz, J., Martín, F., Ramiro, A. R., Martínez-Climent, J. A., & Medina, P. P. (2020). Frequent mutations in the amino-terminal domain of BCL7A impair its tumor suppressor role in DLBCL. *Leukemia*. https://doi.org/10.1038/s41375-020-0919-5

Ballaré, C., Lange, M., Lapinaite, A., Martin, G. M., Morey, L., Pascual, G., Liefke, R., Simon, B., Shi, Y., Gozani, O., Carlomagno, T., Benitah, S. A., & Di Croce, L. (2012). Phf19 links methylated Lys36 of histone H3 to regulation of Polycomb activity. *Nature Structural and Molecular Biology*. https://doi.org/10.1038/nsmb.2434

Bannister, A. J., Zegerman, P., Partridge, J. F., Miska, E. A., Thomas, J. O., Allshire, R. C., & Kouzarides, T. (2001). Selective recognition of methylated lysine 9 on histone H3 by the HP1 chromo domain. *Nature*. https://doi.org/10.1038/35065138

Barik, S. (2020). The uniqueness of tryptophan in biology: Properties, metabolism, interactions and localization in proteins. In *International Journal of Molecular Sciences*. https://doi.org/10.3390/ijms21228776

Basso, K., & Dalla-Favera, R. (2010). BCL6. master regulator of the germinal center reaction and key oncogene in B Cell lymphomagenesis. In *Advances in Immunology*. https://doi.org/10.1016/S0065-2776(10)05007-8

Basso, K., & Dalla-Favera, R. (2015). Germinal centres and B cell lymphomagenesis. *Nature Reviews Immunology*. https://doi.org/10.1038/nri3814

Basso, K., Klein, U., Niu, H., Stolovitzky, G. A., Tu, Y., Califano, A., Cattoretti, G., & Dalla-Favera, R. (2004). Tracking CD40 signaling during germinal center development. *Blood*. https://doi.org/10.1182/blood-2003-12-4291

Bateman, A., Martin, M. J., Orchard, S., Magrane, M., Agivetova, R., Ahmad, S., Alpi, E., Bowler-Barnett, E. H., Britto, R., Bursteinas, B., Bye-A-Jee, H., Coetzee, R., Cukura, A., da Silva, A., Denny, P., Dogan, T., Ebenezer, T. G., Fan, J., Castro, L. G., … Teodoro, D. (2021). UniProt: the universal protein knowledgebase in 2021. *Nucleic Acids Research*. https://doi.org/10.1093/nar/gkaa1100

Batlevi, C. L., Park, S. I., Nastoupil, L., Phillips, T., Amengual, J. E., Andorsky, D., Campbell, P., McKay, P., Pagel, J. M., Leonard, J. P., Yang, J., O'Connor, H., Hamlett, A., Adib, D., & Morschhauser, F. (2021). Interim Analysis of the Randomized Phase 1b/3 Study Evaluating the Safety and Efficacy of Tazemetostat Plus Lenalidomide and Rituximab in Patients with Relapsed/Refractory Follicular Lymphoma. *Blood*. https://doi.org/10.1182/blood-2021-148199

Baylin, S. B., & Jones, P. A. (2016). Epigenetic determinants of cancer. *Cold Spring Harbor Perspectives in Biology*. https://doi.org/10.1101/cshperspect.a019505

Beà, S., Valdés-Mas, R., Navarro, A., Salaverria, I., Martín-Garcia, D., Jares, P., Giné, E., Pinyol, M., Royo, C., Nadeu, F., Conde, L., Juan, M., Clot, G., Vizán, P., Di Croce, L., Puente, D. A., López-Guerra, M., Moros, A., Roue, G., … Campo, E. (2013). Landscape of somatic mutations and clonal evolution in mantle cell lymphoma. *Proceedings of the National Academy of Sciences of the United States of America*. https://doi.org/10.1073/pnas.1314608110

Bednar, J., Garcia-Saez, I., Boopathi, R., Cutter, A. R., Papai, G., Reymer, A., Syed, S. H., Lone, I. N., Tonchev, O., Crucifix, C., Menoni, H., Papin, C., Skoufias, D. A., Kurumizaka, H., Lavery, R., Hamiche, A., Hayes, J. J., Schultz, P., Angelov, D., … Dimitrov, S. (2017). Structure and Dynamics of a 197 bp Nucleosome in Complex with Linker Histone H1. *Molecular Cell*. https://doi.org/10.1016/j.molcel.2017.04.012

Béguelin, W., Popovic, R., Teater, M., Jiang, Y., Bunting, K. L., Rosen, M., Shen, H., Yang, S. N., Wang, L., Ezponda, T., Martinez-Garcia, E., Zhang, H., Zheng, Y., Verma, S. K., McCabe, M. T., Ott, H. M., VanAller, G. S., Kruger, R. G., Liu, Y., … Melnick, A. M. (2013). EZH2 Is Required for Germinal Center Formation and Somatic EZH2 Mutations Promote Lymphoid Transformation. *Cancer Cell*.

https://doi.org/10.1016/j.ccr.2013.04.011
Béguelin, W., Teater, M., Gearhart, M. D., Calvo Fernández, M. T., Goldstein, R. L., Cárdenas, M. G., Hatzi, K., Rosen, M., Shen, H., Corcoran, C. M., Hamline, M. Y., Gascoyne, R. D., Levine, R. L., Abdel-Wahab, O., Licht, J. D., Shaknovich, R., Elemento, O., Bardwell, V. J., & Melnick, A. M. (2016). EZH2 and BCL6 Cooperate to Assemble CBX8-BCOR Complex to Repress Bivalent Promoters, Mediate Germinal Center Formation and Lymphomagenesis. *Cancer Cell*. https://doi.org/10.1016/j.ccell.2016.07.006
Béguelin, W., Teater, M., Meydan, C., Hoehn, K. B., Phillip, J. M., Soshnev, A. A., Venturutti, L., Rivas, M. A., Calvo-Fernández, M. T., Gutierrez, J., Camarillo, J. M., Takata, K., Tarte, K., Kelleher, N. L., Steidl, C., Mason, C. E., Elemento, O., Allis, C. D., Kleinstein, S. H., & Melnick, A. M. (2020). Mutant EZH2 Induces a Pre-malignant Lymphoma Niche by Reprogramming the Immune Response. *Cancer Cell*. https://doi.org/10.1016/j.ccell.2020.04.004
Behjati, S., Tarpey, P. S., Presneau, N., Scheipl, S., Pillay, N., Van Loo, P., Wedge, D. C., Cooke, S. L., Gundem, G., Davies, H., Nik-Zainal, S., Martin, S., McLaren, S., Goodie, V., Robinson, B., Butler, A., Teague, J. W., Halai, D., Khatri, B., … Flanagan, A. M. (2013). Distinct H3F3A and H3F3B driver mutations define chondroblastoma and giant cell tumor of bone. *Nature Genetics*. https://doi.org/10.1038/ng.2814
Bejar, R., Lord, A., Stevenson, K., Bar-Natan, M., Pérez-Ladaga, A., Zaneveld, J., Wang, H., Caughey, B., Stojanov, P., Getz, G., Garcia-Manero, G., Kantarjian, H., Chen, R., Stone, R. M., Neuberg, D., Steensma, D. P., & Ebert, B. L. (2014). TET2 mutations predict response to hypomethylating agents in myelodysplastic syndrome patients. *Blood*. https://doi.org/10.1182/blood-2014-06-582809
Békés, M., Langley, D. R., & Crews, C. M. (2022). PROTAC targeted protein degraders: the past is prologue. In *Nature Reviews Drug Discovery*. https://doi.org/10.1038/s41573-021-00371-6
Beketova, E., Owens, J. L., Asberry, A. M., & Hu, C. D. (2022). PRMT5: a putative oncogene and therapeutic target in prostate cancer. In *Cancer Gene Therapy*. https://doi.org/10.1038/s41417-021-00327-3
Bensberg, M., Rundquist, O., Selimovic, A., Lagerwall, C., Benson, M., Gustafsson, M., Vogt, H., Lentini, A., & Nestor, C. E. (2021). TET2 as a tumor suppressor and therapeutic target in T-cell acute lymphoblastic leukemia. *Proceedings of the National Academy of Sciences of the United States of America*. https://doi.org/10.1073/pnas.2110758118
Berek, C., Berger, A., & Apel, M. (1991). Maturation of the immune response in germinal centers. *Cell*. https://doi.org/10.1016/0092-8674(91)90289-B
Bereshchenko, O. R., Gu, W., & Dalla-Favera, R. (2002). Acetylation inactivates the transcriptional repressor BCL6. *Nature Genetics*. https://doi.org/10.1038/ng1018
Beringer, M., Pisano, P., Di Carlo, V., Blanco, E., Chammas, P., Vizán, P., Gutiérrez, A., Aranda, S., Payer, B., Wierer, M., & Di Croce, L. (2016). EPOP Functionally Links Elongin and Polycomb in Pluripotent Stem Cells. *Molecular Cell*. https://doi.org/10.1016/j.molcel.2016.10.018
Bernstein, B. E., Mikkelsen, T. S., Xie, X., Kamal, M., Huebert, D. J., Cuff, J., Fry, B., Meissner, A., Wernig, M., Plath, K., Jaenisch, R., Wagschal, A., Feil, R., Schreiber, S. L., & Lander, E. S. (2006). A Bivalent Chromatin Structure Marks Key Developmental Genes in Embryonic Stem Cells. *Cell*. https://doi.org/10.1016/j.cell.2006.02.041
Beroukhim, R., Mermel, C. H., Porter, D., Wei, G., Raychaudhuri, S., Donovan, J., Barretina, J., Boehm, J. S., Dobson, J., Urashima, M., McHenry, K. T., Pinchback, R. M., Ligon, A. H., Cho, Y. J., Haery, L., Greulich, H., Reich, M., Winckler, W., Lawrence, M. S., …

Meyerson, M. (2010). The landscape of somatic copy-number alteration across human cancers. *Nature*. https://doi.org/10.1038/nature08822
Bevington, S., & Boyes, J. (2013). Transcription-coupled eviction of histones H2A/H2B governs V(D)J recombination. *EMBO Journal*. https://doi.org/10.1038/emboj.2013.42
Bintu, L., Kopaczynska, M., Hodges, C., Lubkowska, L., Kashlev, M., & Bustamante, C. (2011). The elongation rate of RNA polymerase determines the fate of transcribed nucleosomes. *Nature Structural and Molecular Biology*. https://doi.org/10.1038/nsmb.2164
Bird, A. P., & Taggart, M. H. (1980). Variable patterns of total DNA and rDNA methylation in animals. *Nucleic Acids Research*. https://doi.org/10.1093/nar/8.7.1485
Bisserier, M., & Wajapeyee, N. (2018). Mechanisms of resistance to ezh2 inhibitors in diffuse large b-cell lymphomas. *Blood*. https://doi.org/10.1182/blood-2017-08-804344
Bitoun, E., Oliver, P. L., & Davies, K. E. (2007). The mixed-lineage leukemia fusion partner AF4 stimulates RNA polymerase II transcriptional elongation and mediates coordinated chromatin remodeling. *Human Molecular Genetics*. https://doi.org/10.1093/hmg/ddl444
Blackledge, N. P., Fursova, N. A., Kelley, J. R., Huseyin, M. K., Feldmann, A., & Klose, R. J. (2020). PRC1 Catalytic Activity Is Central to Polycomb System Function. *Molecular Cell*. https://doi.org/10.1016/j.molcel.2019.12.001
Blackledge, N. P., & Klose, R. J. (2021). The molecular principles of gene regulation by Polycomb repressive complexes. In *Nature Reviews Molecular Cell Biology*. https://doi.org/10.1038/s41580-021-00398-y
Blackledge, N. P., Rose, N. R., & Klose, R. J. (2015). Targeting Polycomb systems to regulate gene expression: Modifications to a complex story. *Nature Reviews Molecular Cell Biology*. https://doi.org/10.1038/nrm4067
Blighe, K., Rana, S., & Lewis, M. (2019). EnhancedVolcano: Publication-ready volcano plots with enhanced colouring and labelin. In *R-Package*.
Bödör, C., Grossmann, V., Popov, N., Okosun, J., O'Riain, C., Tan, K., Marzec, J., Araf, S., Wang, J., Lee, A. M., Clear, A., Montoto, S., Matthews, J., Iqbal, S., Rajnai, H., Rosenwald, A., Ott, G., Campo, E., Rimsza, L. M., … Jude, F. (2013). EZH2 mutations are frequent and represent an early event in follicular lymphoma. *Blood*. https://doi.org/10.1182/blood-2013-04-496893
Bondarev, A. D., Attwood, M. M., Jonsson, J., Chubarev, V. N., Tarasov, V. V., & Schiöth, H. B. (2021). Recent developments of HDAC inhibitors: Emerging indications and novel molecules. In *British Journal of Clinical Pharmacology*. https://doi.org/10.1111/bcp.14889
Bonev, B., & Cavalli, G. (2016). Organization and function of the 3D genome. In *Nature Reviews Genetics*. https://doi.org/10.1038/nrg.2016.112
Bourc'his, D., Xu, G. L., Lin, C. S., Bollman, B., & Bestor, T. H. (2001). Dnmt3L and the establishment of maternal genomic imprints. *Science*. https://doi.org/10.1126/science.1065848
Bouska, A., Zhang, W., Gong, Q., Iqbal, J., Scuto, A., Vose, J., Ludvigsen, M., Fu, K., Weisenburger, D. D., Greiner, T. C., Gascoyne, R. D., Rosenwald, A., Ott, G., Campo, E., Rimsza, L. M., Delabie, J., Jaffe, E. S., Braziel, R. M., Connors, J. M., … Chan, W. C. (2017). Combined copy number and mutation analysis identifies oncogenic pathways associated with transformation of follicular lymphoma. *Leukemia*. https://doi.org/10.1038/leu.2016.175
Boyer, L. A., Plath, K., Zeitlinger, J., Brambrink, T., Medeiros, L. A., Lee, T. I., Levine, S. S., Wernig, M., Tajonar, A., Ray, M. K., Bell, G. W., Otte, A. P., Vidal, M., Gifford, D. K., Young, R. A., & Jaenisch, R. (2006). Polycomb complexes repress developmental regulators in murine embryonic stem cells. *Nature*. https://doi.org/10.1038/nature04733

Brach, D., Johnston-Blackwell, D., Drew, A., Lingaraj, T., Motwani, V., Warholic, N. M., Feldman, I., Plescia, C., Smith, J. J., Copeland, R. A., Keilhack, H., Chan-Penebre, E., Knutson, S. K., Ribich, S. A., Raimondi, A., & Thomenius, M. J. (2017). EZH2 inhibition by tazemetostat results in altered dependency on B-cell activation signaling in DLBCL. *Molecular Cancer Therapeutics*. https://doi.org/10.1158/1535-7163.MCT-16-0840

Bracken, A. P., Dietrich, N., Pasini, D., Hansen, K. H., & Helin, K. (2006). Genome-wide mapping of polycomb target genes unravels their roles in cell fate transitions. *Genes and Development*. https://doi.org/10.1101/gad.381706

Bracken, A. P., & Helin, K. (2009). Polycomb group proteins: Navigators of lineage pathways led astray in cancer. In *Nature Reviews Cancer*. https://doi.org/10.1038/nrc2736

Bracken, A. P., Kleine-Kohlbrecher, D., Dietrich, N., Pasini, D., Gargiulo, G., Beekman, C., Theilgaard-Mönch, K., Minucci, S., Porse, B. T., Marine, J. C., Hansen, K. H., & Helin, K. (2007). The Polycomb group proteins bind throughout the INK4A-ARF locus and are disassociated in senescent cells. *Genes and Development*. https://doi.org/10.1101/gad.415507

Bracken, A. P., Pasini, D., Capra, M., Prosperini, E., Colli, E., & Helin, K. (2003). EZH2 is downstream of the pRB-E2F pathway, essential for proliferation and amplified in cancer. *EMBO Journal*. https://doi.org/10.1093/emboj/cdg542

Bravo, J. P. K., Liu, M. Sen, Hibshman, G. N., Dangerfield, T. L., Jung, K., McCool, R. S., Johnson, K. A., & Taylor, D. W. (2022). Structural basis for mismatch surveillance by CRISPR–Cas9. *Nature*. https://doi.org/10.1038/s41586-022-04470-1

Brennan, K., Shin, J. H., Tay, J. K., Prunello, M., Gentles, A. J., Sunwoo, J. B., & Gevaert, O. (2017). NSD1 inactivation defines an immune cold, DNA hypomethylated subtype in squamous cell carcinoma. *Scientific Reports*. https://doi.org/10.1038/s41598-017-17298-x

Brien, G. L., Bressan, R. B., Monger, C., Gannon, D., Lagan, E., Doherty, A. M., Healy, E., Neikes, H., Fitzpatrick, D. J., Deevy, O., Grant, V., Marqués-Torrejón, M. A., Alfazema, N., Pollard, S. M., & Bracken, A. P. (2021). Simultaneous disruption of PRC2 and enhancer function underlies histone H3.3-K27M oncogenic activity in human hindbrain neural stem cells. *Nature Genetics*. https://doi.org/10.1038/s41588-021-00897-w

Brien, G. L., Gambero, G., O'Connell, D. J., Jerman, E., Turner, S. A., Egan, C. M., Dunne, E. J., Jurgens, M. C., Wynne, K., Piao, L., Lohan, A. J., Ferguson, N., Shi, X., Sinha, K. M., Loftus, B. J., Cagney, G., & Bracken, A. P. (2012). Polycomb PHF19 binds H3K36me3 and recruits PRC2 and demethylase NO66 to embryonic stem cell genes during differentiation. *Nature Structural and Molecular Biology*. https://doi.org/10.1038/nsmb.2449

Brien, G. L., Remillard, D., Shi, J., Hemming, M. L., Chabon, J., Wynne, K., Dillon, E. T., Cagney, G., Van Mierlo, G., Baltissen, M. P., Vermeulen, M., Qi, J., Fröhling, S., Gray, N. S., Bradner, J. E., Vakoc, C. R., & Armstrong, S. A. (2018). Targeted degradation of BRD9 reverses oncogenic gene expression in synovial sarcoma. *ELife*. https://doi.org/10.7554/eLife.41305

Brooun, A., Gajiwala, K. S., Deng, Y. L., Liu, W., Bolaños, B., Bingham, P., He, Y. A., Diehl, W., Grable, N., Kung, P. P., Sutton, S., Maegley, K. A., Yu, X., & Stewart, A. E. (2016a). Polycomb repressive complex 2 structure with inhibitor reveals a mechanism of activation and drug resistance. *Nature Communications*. https://doi.org/10.1038/ncomms11384

Brooun, A., Gajiwala, K. S., Deng, Y. L., Liu, W., Bolaños, B., Bingham, P., He, Y. A.,

Diehl, W., Grable, N., Kung, P. P., Sutton, S., Maegley, K. A., Yu, X., & Stewart, A. E. (2016b). Polycomb repressive complex 2 structure with inhibitor reveals a mechanism of activation and drug resistance. *Nature Communications*, *7*, 11384. https://doi.org/10.1038/ncomms11384

Broyde, A., Boycov, O., Strenov, Y., Okon, E., Shpilberg, O., & Bairey, O. (2009). Role and prognostic significance of the Ki-67 index in non-Hodgkin's lymphoma. *American Journal of Hematology*. https://doi.org/10.1002/ajh.21406

Bui, N., Huang, J. K., Bojorquez-Gomez, A., Licon, K., Sanchez, K. S., Tang, S. N., Beckett, A. N., Wang, T., Zhang, W., Shen, J. P., Kreisberg, J. F., & Ideker, T. (2018). Disruption of NSD1 in head and neck cancer promotes favorable chemotherapeutic responses linked to hypomethylation. *Molecular Cancer Therapeutics*. https://doi.org/10.1158/1535-7163.MCT-17-0937

Burgess, D. J. (2020). CRISPR screens beyond Cas9. In *Nature Reviews Genetics*. https://doi.org/10.1038/s41576-020-0232-1

Burkhardt, B., Michgehl, U., Rohde, J., Erdmann, T., Berning, P., Reutter, K., Rohde, M., Borkhardt, A., Burmeister, T., Dave, S., Tzankov, A., Dugas, M., Sandmann, S., Fend, F., & Finger, J. (2022). Burkitt lymphoma differs according to age. *Nature Communications*, *13*(2022), 1–12. https://doi.org/10.1038/s41467-022-31355-8

Caganova, M., Carrisi, C., Varano, G., Mainoldi, F., Zanardi, F., Germain, P. L., George, L., Alberghini, F., Ferrarini, L., Talukder, A. K., Ponzoni, M., Testa, G., Nojima, T., Doglioni, C., Kitamura, D., Toellner, K. M., Su, I. H., & Casola, S. (2013). Germinal center dysregulation by histone methyltransferase EZH2 promotes lymphomagenesis. *Journal of Clinical Investigation*. https://doi.org/10.1172/JCI70626

Cai, L., Rothbart, S. B., Lu, R., Xu, B., Chen, W. Y., Tripathy, A., Rockowitz, S., Zheng, D., Patel, D. J., Allis, C. D., Strahl, B. D., Song, J., & Wang, G. G. (2013). An H3K36 Methylation-Engaging Tudor Motif of Polycomb-like Proteins Mediates PRC2 Complex Targeting. *Molecular Cell*. https://doi.org/10.1016/j.molcel.2012.11.026

Campagne, A., Lee, M. K., Zielinski, D., Michaud, A., Le Corre, S., Dingli, F., Chen, H., Shahidian, L. Z., Vassilev, I., Servant, N., Loew, D., Pasmant, E., Postel-Vinay, S., Wassef, M., & Margueron, R. (2019). BAP1 complex promotes transcription by opposing PRC1-mediated H2A ubiquitylation. *Nature Communications*. https://doi.org/10.1038/s41467-018-08255-x

Cao, R., Tsukada, Y. I., & Zhang, Y. (2005). Role of Bmi-1 and Ring1A in H2A ubiquitylation and hox gene silencing. *Molecular Cell*. https://doi.org/10.1016/j.molcel.2005.12.002

Cao, R., Wang, H., He, J., Erdjument-Bromage, H., Tempst, P., & Zhang, Y. (2008). Role of hPHF1 in H3K27 Methylation and Hox Gene Silencing. *Molecular and Cellular Biology*. https://doi.org/10.1128/mcb.01589-07

Cao, R., Wang, L., Wang, H., Xia, L., Erdjument-Bromage, H., Tempst, P., Jones, R. S., & Zhang, Y. (2002). Role of histone H3 lysine 27 methylation in polycomb-group silencing. *Science*. https://doi.org/10.1126/science.1076997

Cao, R., & Zhang, Y. (2004). The functions of E(Z)/EZH2-mediated methylation of lysine 27 in histone H3. In *Current Opinion in Genetics and Development*. https://doi.org/10.1016/j.gde.2004.02.001

Carbone, M., Yang, H., Pass, H. I., Krausz, T., Testa, J. R., & Gaudino, G. (2013). BAP1 and cancer. *Nature Reviews Cancer*. https://doi.org/10.1038/nrc3459

Casanova, M., Preissner, T., Cerase, A., Poot, R., Yamada, D., Li, X., Appanah, R., Bezstarosti, K., Demmers, J., Koseki, H., & Brockdorff, N. (2011). Polycomblike 2 facilitates the recruitment of PRC2 Polycomb group complexes to the inactive X chromosome and to target loci in embryonic stem cells. *Development*.

https://doi.org/10.1242/dev.053652
Cattoretti, G., Pasqualucci, L., Ballon, G., Tam, W., Nandula, S. V., Shen, Q., Mo, T., Murty, V. V., & Dalla-Favera, R. (2005). Deregulated BCL6 expression recapitulates the pathogenesis of human diffuse large B cell lymphomas in mice. *Cancer Cell*. https://doi.org/10.1016/j.ccr.2005.03.037
Cerami, E., Gao, J., Dogrusoz, U., Gross, B. E., Sumer, S. O., Aksoy, B. A., Jacobsen, A., Byrne, C. J., Heuer, M. L., Larsson, E., Antipin, Y., Reva, B., Goldberg, A. P., Sander, C., & Schultz, N. (2012). The cBio Cancer Genomics Portal: An open platform for exploring multidimensional cancer genomics data. *Cancer Discovery*. https://doi.org/10.1158/2159-8290.CD-12-0095
Chapuy, B., Stewart, C., Dunford, A. J., Kim, J., Kamburov, A., Redd, R. A., Lawrence, M. S., Roemer, M. G. M., Li, A. J., Ziepert, M., Staiger, A. M., Wala, J. A., Ducar, M. D., Leshchiner, I., Rheinbay, E., Taylor-Weiner, A., Coughlin, C. A., Hess, J. M., Pedamallu, C. S., … Shipp, M. A. (2018). Molecular subtypes of diffuse large B cell lymphoma are associated with distinct pathogenic mechanisms and outcomes. *Nature Medicine*. https://doi.org/10.1038/s41591-018-0016-8
Chen, C. W., Koche, R. P., Sinha, A. U., Deshpande, A. J., Zhu, N., Eng, R., Doench, J. G., Xu, H., Chu, S. H., Qi, J., Wang, X., Delaney, C., Bernt, K. M., Root, D. E., Hahn, W. C., Bradner, J. E., & Armstrong, S. A. (2015). DOT1L inhibits SIRT1-mediated epigenetic silencing to maintain leukemic gene expression in MLL-rearranged leukemia. *Nature Medicine*. https://doi.org/10.1038/nm.3832
Chen, K., Hu, Z., Xia, Z., Zhao, D., Li, W., & Tyler, J. K. (2016). The Overlooked Fact: Fundamental Need for Spike-In Control for Virtually All Genome-Wide Analyses. *Molecular and Cellular Biology*. https://doi.org/10.1128/mcb.00970-14
Chen, S., Jiao, L., Liu, X., Yang, X., & Liu, X. (2020). A Dimeric Structural Scaffold for PRC2-PCL Targeting to CpG Island Chromatin. *Molecular Cell*. https://doi.org/10.1016/j.molcel.2019.12.019
Chen, S., Jiao, L., Shubbar, M., Yang, X., & Liu, X. (2018). Unique Structural Platforms of Suz12 Dictate Distinct Classes of PRC2 for Chromatin Binding. *Molecular Cell*. https://doi.org/10.1016/j.molcel.2018.01.039
Chen, T., Tsujimoto, N., & Li, E. (2004). The PWWP Domain of Dnmt3a and Dnmt3b Is Required for Directing DNA Methylation to the Major Satellite Repeats at Pericentric Heterochromatin. *Molecular and Cellular Biology*. https://doi.org/10.1128/mcb.24.20.9048-9058.2004
Cheutin, T., McNairn, A. J., Jenuwein, T., Gilbert, D. M., Singh, P. B., & Misteli, T. (2003). Maintenance of stable heterochromatin domains by dynamic HP1 binding. *Science*. https://doi.org/10.1126/science.1078572
Chiron, D., Di Liberto, M., Martin, P., Huang, X., Sharman, J., Blecua, P., Mathew, S., Vijay, P., Eng, K., Ali, S., Johnson, A., Chang, B., Ely, S., Elemento, O., Mason, C. E., Leonard, J. P., & Chen-Kiang, S. (2014). Cell-cycle reprogramming for Pi3K inhibition overrides a relapse-specific C481s BTK mutation revealed by longitudinal functional genomics in mantle cell lymphoma. *Cancer Discovery*. https://doi.org/10.1158/2159-8290.CD-14-0098
Chittock, E. C., Latwiel, S., Miller, T. C. R., & Müller, C. W. (2017). Molecular architecture of polycomb repressive complexes. In *Biochemical Society Transactions*. https://doi.org/10.1042/BST20160173
Choi, J., Bachmann, A. L., Tauscher, K., Benda, C., Fierz, B., & Müller, J. (2017). DNA binding by PHF1 prolongs PRC2 residence time on chromatin and thereby promotes H3K27 methylation. *Nature Structural and Molecular Biology*. https://doi.org/10.1038/nsmb.3488

Ci, W., Polo, J. M., Cerchietti, L., Shaknovich, R., Wang, L., Shao, N. Y., Ye, K., Farinha, P., Horsman, D. E., Gascoyne, R. D., Elemento, O., & Melnick, A. (2009). The BCL6 transcriptional program features repression of multiple oncogenes in primary B cells and is deregulated in DLBCL. *Blood*. https://doi.org/10.1182/blood-2008-12-193037

Ci, W., Polo, J. M., & Melnick, A. (2008). B-cell lymphoma 6 and the molecular pathogenesis of diffuse large B-cell lymphoma. In *Current Opinion in Hematology*. https://doi.org/10.1097/MOH.0b013e328302c7df

Ciferri, C., Lander, G. C., Maiolica, A., Herzog, F., Aebersold, R., & Nogales, E. (2012). Molecular architecture of human polycomb repressive complex 2. *ELife*. https://doi.org/10.7554/eLife.00005

Clapier, C. R., Iwasa, J., Cairns, B. R., & Peterson, C. L. (2017). Mechanisms of action and regulation of ATP-dependent chromatin-remodelling complexes. In *Nature Reviews Molecular Cell Biology*. https://doi.org/10.1038/nrm.2017.26

Cole, A. J., Iyengar, M., Panesso-Gómez, S., O'Hayer, P., Chan, D., Delgoffe, G. M., Aird, K. M., Yoon, E., Bai, S., & Buckanovich, R. J. (2020). NFATC4 promotes quiescence and chemotherapy resistance in ovarian cancer. *JCI Insight*. https://doi.org/10.1172/JCI.INSIGHT.131486

Cole, H. A., Ocampo, J., Iben, J. R., Chereji, R. V., & Clark, D. J. (2014). Heavy transcription of yeast genes correlates with differential loss of histone H2B relative to H4 and queued RNA polymerases. *Nucleic Acids Research*. https://doi.org/10.1093/nar/gku1013

Cong, L., Ran, F. A., Cox, D., Lin, S., Barretto, R., Habib, N., Hsu, P. D., Wu, X., Jiang, W., Marraffini, L. A., & Zhang, F. (2013). Multiplex genome engineering using CRISPR/Cas systems. *Science*. https://doi.org/10.1126/science.1231143

Conway, E., Healy, E., & Bracken, A. P. (2015). PRC2 mediated H3K27 methylations in cellular identity and cancer. In *Current Opinion in Cell Biology*. https://doi.org/10.1016/j.ceb.2015.10.003

Conway, E., Jerman, E., Healy, E., Ito, S., Holoch, D., Oliviero, G., Deevy, O., Glancy, E., Fitzpatrick, D. J., Mucha, M., Watson, A., Rice, A. M., Chammas, P., Huang, C., Pratt-Kelly, I., Koseki, Y., Nakayama, M., Ishikura, T., Streubel, G., … Bracken, A. P. (2018). A Family of Vertebrate-Specific Polycombs Encoded by the LCOR/LCORL Genes Balance PRC2 Subtype Activities. *Molecular Cell*. https://doi.org/10.1016/j.molcel.2018.03.005

Conway, E., Rossi, F., Fernandez-Perez, D., Ponzo, E., Ferrari, K. J., Zanotti, M., Manganaro, D., Rodighiero, S., Tamburri, S., & Pasini, D. (2021). BAP1 enhances Polycomb repression by counteracting widespread H2AK119ub1 deposition and chromatin condensation. *Molecular Cell*. https://doi.org/10.1016/j.molcel.2021.06.020

Cooper, D. N., & Krawczak, M. (1989). Cytosine methylation and the fate of CpG dinucleotides in vertebrate genomes. *Human Genetics*. https://doi.org/10.1007/BF00286715

Cooper, S., Grijzenhout, A., Underwood, E., Ancelin, K., Zhang, T., Nesterova, T. B., Anil-Kirmizitas, B., Bassett, A., Kooistra, S. M., Agger, K., Helin, K., Heard, E., & Brockdorff, N. (2016). Jarid2 binds mono-ubiquitylated H2A lysine 119 to mediate crosstalk between Polycomb complexes PRC1 and PRC2. *Nature Communications*. https://doi.org/10.1038/ncomms13661

D'haene, B., Vandesompele, J., & Hellemans, J. (2010). Accurate and objective copy number profiling using real-time quantitative PCR. In *Methods*. https://doi.org/10.1016/j.ymeth.2009.12.007

Dalgliesh, G. L., Furge, K., Greenman, C., Chen, L., Bignell, G., Butler, A., Davies, H., Edkins, S., Hardy, C., Latimer, C., Teague, J., Andrews, J., Barthorpe, S., Beare, D.,

Buck, G., Campbell, P. J., Forbes, S., Jia, M., Jones, D., … Futreal, P. A. (2010). Systematic sequencing of renal carcinoma reveals inactivation of histone modifying genes. *Nature*, *463*(7279), 360–363. https://doi.org/10.1038/nature08672

Damhofer, H., Radzisheuskaya, A., & Helin, K. (2021). Generation of locus-specific degradable tag knock-ins in mouse and human cell lines. *STAR Protocols*. https://doi.org/10.1016/j.xpro.2021.100575

Daou, S., Hammond-Martel, I., Mashtalir, N., Barbour, H., Gagnon, J., Iannantuono, N. V. G., Nkwe, N. Sen, Motorina, A., Pak, H., Yu, H., Wurtele, H., Milot, E., Mallette, F. A., Carbone, M., & Affar, E. B. (2015). The BAP1/ASXL2 histone H2A deubiquitinase complex regulates cell proliferation and is disrupted in cancer. *Journal of Biological Chemistry*. https://doi.org/10.1074/jbc.M115.661553

Deevy, O., & Bracken, A. P. (2019). PRC2 functions in development and congenital disorders. In *Development (Cambridge)*. https://doi.org/10.1242/dev.181354

Dhayalan, A., Rajavelu, A., Rathert, P., Tamas, R., Jurkowska, R. Z., Ragozin, S., & Jeltsch, A. (2010). The Dnmt3a PWWP domain reads histone 3 lysine 36 trimethylation and guides DNA methylation. *Journal of Biological Chemistry*. https://doi.org/10.1074/jbc.M109.089433

Di Croce, L., & Helin, K. (2013). Transcriptional regulation by Polycomb group proteins. In *Nature Structural and Molecular Biology*. https://doi.org/10.1038/nsmb.2669

Dias, S., Månsson, R., Gurbuxani, S., Sigvardsson, M., & Kee, B. L. (2008). E2A Proteins Promote Development of Lymphoid-Primed Multipotent Progenitors. *Immunity*. https://doi.org/10.1016/j.immuni.2008.05.015

Dixon, J. R., Selvaraj, S., Yue, F., Kim, A., Li, Y., Shen, Y., Hu, M., Liu, J. S., & Ren, B. (2012). Topological domains in mammalian genomes identified by analysis of chromatin interactions. *Nature*. https://doi.org/10.1038/nature11082

Doench, J. G., Fusi, N., Sullender, M., Hegde, M., Vaimberg, E. W., Donovan, K. F., Smith, I., Tothova, Z., Wilen, C., Orchard, R., Virgin, H. W., Listgarten, J., & Root, D. E. (2016). Optimized sgRNA design to maximize activity and minimize off-target effects of CRISPR-Cas9. *Nature Biotechnology*. https://doi.org/10.1038/nbt.3437

Donaldson-Collier, M. C., Sungalee, S., Zufferey, M., Tavernari, D., Katanayeva, N., Battistello, E., Mina, M., Douglass, K. M., Rey, T., Raynaud, F., Manley, S., Ciriello, G., & Oricchio, E. (2019). EZH2 oncogenic mutations drive epigenetic, transcriptional, and structural changes within chromatin domains. *Nature Genetics*. https://doi.org/10.1038/s41588-018-0338-y

Drosos, Y., Myers, J. A., Xu, B., Mathias, K. M., Beane, E. C., Radko-Juettner, S., Mobley, R. J., Larsen, M. E., Piccioni, F., Ma, X., Low, J., Hansen, B. S., Peters, S. T., Bhanu, N. V., Dhanda, S. K., Chen, T., Upadhyaya, S. A., Pruett-Miller, S. M., Root, D. E., … Roberts, C. W. M. (2022). NSD1 mediates antagonism between SWI/SNF and polycomb complexes and is required for transcriptional activation upon EZH2 inhibition. *Molecular Cell*, *82*(13), 2472-2489.e8. https://doi.org/10.1016/j.molcel.2022.04.015

Duan, R., Du, W., & Guo, W. (2020). EZH2: A novel target for cancer treatment. In *Journal of Hematology and Oncology*. https://doi.org/10.1186/s13045-020-00937-8

Dura, J. M., Randsholt, N. B., Deatrick, J., Erk, I., Santamaria, P., Freeman, J. D., Freeman, S. J., Weddell, D., & Brock, H. W. (1987). A complex genetic locus, polyhomeotic, is required for segmental specification and epidermal development in D. melanogaster. *Cell*. https://doi.org/10.1016/0092-8674(87)90106-1

Echeverri, C. J., Beachy, P. A., Baum, B., Boutros, M., Buchholz, F., Chanda, S. K., Downward, J., Ellenberg, J., Fraser, A. G., Hacohen, N., Hahn, W. C., Jackson, A. L., Kiger, A., Linsley, P. S., Lum, L., Ma, Y., Mathey-Prévôt, B., Root, D. E., Sabatini, D.

M., … Bernards, R. (2006). Minimizing the risk of reporting false positives in large-scale RNAi screens. *Nature Methods*. https://doi.org/10.1038/nmeth1006-777

Ennishi, D., Takata, K., Béguelin, W., Duns, G., Mottok, A., Farinha, P., Bashashati, A., Saberi, S., Boyle, M., Meissner, B., Ben-Neriah, S., Woolcock, B. W., Telenius, A., Lai, D., Teater, M., Kridel, R., Savage, K. J., Sehn, L. H., Morin, R. D., … Steidl, C. (2019). Molecular and genetic characterization of MHC deficiency identifies ezh2 as therapeutic target for enhancing immune recognition. *Cancer Discovery*. https://doi.org/10.1158/2159-8290.CD-18-1090

Erdos, G., Pajkos, M., & Dosztányi, Z. (2021). IUPred3: Prediction of protein disorder enhanced with unambiguous experimental annotation and visualization of evolutionary conservation. *Nucleic Acids Research*. https://doi.org/10.1093/nar/gkab408

Ernst, T., Chase, A. J., Score, J., Hidalgo-Curtis, C. E., Bryant, C., Jones, A. V., Waghorn, K., Zoi, K., Ross, F. M., Reiter, A., Hochhaus, A., Drexler, H. G., Duncombe, A., Cervantes, F., Oscier, D., Boultwood, J., Grand, F. H., & Cross, N. C. P. (2010). Inactivating mutations of the histone methyltransferase gene EZH2 in myeloid disorders. *Nature Genetics*. https://doi.org/10.1038/ng.621

Ezponda, T., Dupéré-Richer, D., Will, C. M., Small, E. C., Varghese, N., Patel, T., Nabet, B., Popovic, R., Oyer, J., Bulic, M., Zheng, Y., Huang, X., Shah, M. Y., Maji, S., Riva, A., Occhionorelli, M., Tonon, G., Kelleher, N., Keats, J., & Licht, J. D. (2017). UTX/KDM6A Loss Enhances the Malignant Phenotype of Multiple Myeloma and Sensitizes Cells to EZH2 inhibition. *Cell Reports*. https://doi.org/10.1016/j.celrep.2017.09.078

Fang, R., Barbera, A. J., Xu, Y., Rutenberg, M., Leonor, T., Bi, Q., Lan, F., Mei, P., Yuan, G. C., Lian, C., Peng, J., Cheng, D., Sui, G., Kaiser, U. B., Shi, Y., & Shi, Y. G. (2010). Human LSD2/KDM1b/AOF1 regulates gene transcription by modulating intragenic H3K4me2 Methylation. *Molecular Cell*. https://doi.org/10.1016/j.molcel.2010.07.008

Farcas, A. M., Blackledge, N. P., Sudbery, I., Long, H. K., McGouran, J. F., Rose, N. R., Lee, S., Sims, D., Cerase, A., Sheahan, T. W., Koseki, H., Brockdorff, N., Ponting, C. P., Kessler, B. M., & Klose, R. J. (2012). KDM2B links the polycomb repressive complex 1 (PRC1) to recognition of CpG islands. *ELife*. https://doi.org/10.7554/eLife.00205

Farhangdoost, N., Horth, C., Hu, B., Bareke, E., Chen, X., Li, Y., Coradin, M., Garcia, B. A., Lu, C., & Majewski, J. (2021). Chromatin dysregulation associated with NSD1 mutation in head and neck squamous cell carcinoma. *Cell Reports*. https://doi.org/10.1016/j.celrep.2021.108769

Fellmann, C., Hoffmann, T., Sridhar, V., Hopfgartner, B., Muhar, M., Roth, M., Lai, D. Y., Barbosa, I. A. M., Kwon, J. S., Guan, Y., Sinha, N., & Zuber, J. (2013). An optimized microRNA backbone for effective single-copy RNAi. *Cell Reports*. https://doi.org/10.1016/j.celrep.2013.11.020

Feng, Q., Wang, H., Ng, H. H., Erdjument-Bromage, H., Tempst, P., Struhl, K., & Zhang, Y. (2002). Methylation of H3-lysine 79 is mediated by a new family of HMTases without a SET domain. *Current Biology*. https://doi.org/10.1016/S0960-9822(02)00901-6

Ferrari, K. J., Scelfo, A., Jammula, S. G., Cuomo, A., Barozzi, I., Stützer, A., Fischle, W., Bonaldi, T., & Pasini, D. (2014). Polycomb-Dependent H3K27me1 and H3K27me2 Regulate Active Transcription and Enhancer Fidelity. *Molecular Cell*. https://doi.org/10.1016/j.molcel.2013.10.030

Ferrero, S., Rossi, D., Rinaldi, A., Bruscaggin, A., Spina, V., Eskelund, C. W., Evangelista, A., Moia, R., Kwee, I., Dahl, C., Di Rocco, A., Stefoni, V., Diop, F., Favini, C., Ghione, P., Mahmoud, A. M., Schipani, M., Kolstad, A., Barbero, D., … Gaidano, G. (2020). KMT2D mutations and TP53 disruptions are poor prognostic biomarkers in mantle cell

lymphoma receiving high-dose therapy: A FIL study. *Haematologica*. https://doi.org/10.3324/haematol.2018.214056

Filipovski, M., Soffers, J. H. M., Vos, S. M., & Farnung, L. (2022). Structural basis of nucleosome retention during transcription elongation. *Science*, *376*(6599), 1313–1316. https://doi.org/10.1126/science.abo3851

Finogenova, K., Bonnet, J., Poepsel, S., Schäfer, I. B., Finkl, K., Schmid, K., Litz, C., Strauss, M., Benda, C., & Müller, J. (2020). Structural basis for prc2 decoding of active histone methylation marks h3k36me2/3. *ELife*. https://doi.org/10.7554/eLife.61964

Fischle, W., Wang, Y., Jacobs, S. A., Kim, Y., Allis, C. D., & Khorasanizadeh, S. (2003). Molecular basis for the discrimination of repressive methyl-lysine marks in histone H3 by polycomb and HP1 chromodomains. *Genes and Development*. https://doi.org/10.1101/gad.1110503

Flavahan, W. A., Drier, Y., Liau, B. B., Gillespie, S. M., Venteicher, A. S., Stemmer-Rachamimov, A. O., Suvà, M. L., & Bernstein, B. E. (2016). Insulator dysfunction and oncogene activation in IDH mutant gliomas. *Nature*. https://doi.org/10.1038/nature16490

Fodor, B. D., Kubicek, S., Yonezawa, M., O'Sullivan, R. J., Sengupta, R., Perez-Burgos, L., Opravil, S., Mechtler, K., Schotta, G., & Jenuwein, T. (2006). Jmjd2b antagonizes H3K9 trimethylation at pericentric heterochromatin in mammalian cells. *Genes and Development*. https://doi.org/10.1101/gad.388206

Foglizzo, M., Middleton, A. J., Burgess, A. E., Crowther, J. M., Dobson, R. C. J., Murphy, J. M., Day, C. L., & Mace, P. D. (2018). A bidentate Polycomb Repressive-Deubiquitinase complex is required for efficient activity on nucleosomes. *Nature Communications*. https://doi.org/10.1038/s41467-018-06186-1

Fontebasso, A. M., Schwartzentruber, J., Khuong-Quang, D. A., Liu, X. Y., Sturm, D., Korshunov, A., Jones, D. T. W., Witt, H., Kool, M., Albrecht, S., Fleming, A., Hadjadj, D., Busche, S., Lepage, P., Montpetit, A., Staffa, A., Gerges, N., Zakrzewska, M., Zakrzewski, K., … Majewski, J. (2013). Mutations in SETD2 and genes affecting histone H3K36 methylation target hemispheric high-grade gliomas. *Acta Neuropathologica*. https://doi.org/10.1007/s00401-013-1095-8

Frangoul, H., Altshuler, D., Cappellini, M. D., Chen, Y.-S., Domm, J., Eustace, B. K., Foell, J., de la Fuente, J., Grupp, S., Handgretinger, R., Ho, T. W., Kattamis, A., Kernytsky, A., Lekstrom-Himes, J., Li, A. M., Locatelli, F., Mapara, M. Y., de Montalembert, M., Rondelli, D., … Corbacioglu, S. (2021). CRISPR-Cas9 Gene Editing for Sickle Cell Disease and β-Thalassemia. *New England Journal of Medicine*. https://doi.org/10.1056/nejmoa2031054

Fursova, N. A., Blackledge, N. P., Nakayama, M., Ito, S., Koseki, Y., Farcas, A. M., King, H. W., Koseki, H., & Klose, R. J. (2019). Synergy between Variant PRC1 Complexes Defines Polycomb-Mediated Gene Repression. *Molecular Cell*. https://doi.org/10.1016/j.molcel.2019.03.024

Fursova, N. A., Turberfield, A. H., Blackledge, N. P., Findlater, E. L., Lastuvkova, A., Huseyin, M. K., Dobrinic, P., & Klose, R. J. (2021). BAP1 constrains pervasive H2AK119ub1 to control the transcriptional potential of the genome. *Genes and Development*. https://doi.org/10.1101/GAD.347005.120

Gao, J., Aksoy, B. A., Dogrusoz, U., Dresdner, G., Gross, B., Sumer, S. O., Sun, Y., Jacobsen, A., Sinha, R., Larsson, E., Cerami, E., Sander, C., & Schultz, N. (2013). Integrative analysis of complex cancer genomics and clinical profiles using the cBioPortal. *Science Signaling*. https://doi.org/10.1126/scisignal.2004088

Gao, X., Burris III, H. A., Vuky, J., Dreicer, R., Sartor, A. O., Sternberg, C. N., Percent, I. J., Hussain, M. H. A., Rezazadeh Kalebasty, A., Shen, J., Heath, E. I., Abesada-Terk, G.,

Gandhi, S. G., McKean, M., Lu, H., Berghorn, E., Gedrich, R., Chirnomas, S. D., Vogelzang, N. J., & Petrylak, D. P. (2022). Phase 1/2 study of ARV-110, an androgen receptor (AR) PROTAC degrader, in metastatic castration-resistant prostate cancer (mCRPC). *Journal of Clinical Oncology*. https://doi.org/10.1200/jco.2022.40.6_suppl.017

Gao, Z., Zhang, J., Bonasio, R., Strino, F., Sawai, A., Parisi, F., Kluger, Y., & Reinberg, D. (2012). PCGF Homologs, CBX Proteins, and RYBP Define Functionally Distinct PRC1 Family Complexes. *Molecular Cell*. https://doi.org/10.1016/j.molcel.2012.01.002

Ge, Y. Z., Pu, M. T., Gowher, H., Wu, H. P., Ding, J. P., Jeltsch, A., & Xu, G. L. (2004). Chromatin targeting of de novo DNA methyltransferases by the PWWP domain. *Journal of Biological Chemistry*. https://doi.org/10.1074/jbc.M312296200

Georgopoulos, K., Bigby, M., Wang, J. H., Molnar, A., Wu, P., Winandy, S., & Sharpe, A. (1994). The ikaros gene is required for the development of all lymphoid lineages. *Cell*. https://doi.org/10.1016/0092-8674(94)90407-3

Gibaja, V., Shen, F., Harari, J., Korn, J., Ruddy, D., Saenz-Vash, V., Zhai, H., Rejtar, T., Paris, C. G., Yu, Z., Lira, M., King, D., Qi, W., Keen, N., Hassan, A. Q., & Chan, H. M. (2016a). Development of secondary mutations in wild-type and mutant EZH2 alleles cooperates to confer resistance to EZH2 inhibitors. *Oncogene*. https://doi.org/10.1038/onc.2015.114

Gibaja, V., Shen, F., Harari, J., Korn, J., Ruddy, D., Saenz-Vash, V., Zhai, H., Rejtar, T., Paris, C. G., Yu, Z., Lira, M., King, D., Qi, W., Keen, N., Hassan, A. Q., & Chan, H. M. (2016b). Development of secondary mutations in wild-type and mutant EZH2 alleles cooperates to confer resistance to EZH2 inhibitors. *Oncogene*, *35*(5), 558–566. https://doi.org/10.1038/onc.2015.114

Gitlin, A. D., Shulman, Z., & Nussenzweig, M. C. (2014). Clonal selection in the germinal centre by regulated proliferation and hypermutation. *Nature*. https://doi.org/10.1038/nature13300

Glancy, E., Ciferri, C., & Bracken, A. P. (2021). Structural basis for PRC2 engagement with chromatin. In *Current Opinion in Structural Biology*. https://doi.org/10.1016/j.sbi.2020.10.017

Göllner, S., Oellerich, T., Agrawal-Singh, S., Schenk, T., Klein, H. U., Rohde, C., Pabst, C., Sauer, T., Lerdrup, M., Tavor, S., Stölzel, F., Herold, S., Ehninger, G., Köhler, G., Pan, K. T., Urlaub, H., Serve, H., Dugas, M., Spiekermann, K., … Müller-Tidow, C. (2017). Loss of the histone methyltransferase EZH2 induces resistance to multiple drugs in acute myeloid leukemia. *Nature Medicine*. https://doi.org/10.1038/nm.4247

Gounder, M., Schöffski, P., Jones, R. L., Agulnik, M., Cote, G. M., Villalobos, V. M., Attia, S., Chugh, R., Chen, T. W. W., Jahan, T., Loggers, E. T., Gupta, A., Italiano, A., Demetri, G. D., Ratan, R., Davis, L. E., Mir, O., Dileo, P., Van Tine, B. A., … Stacchiotti, S. (2020). Tazemetostat in advanced epithelioid sarcoma with loss of INI1/SMARCB1: an international, open-label, phase 2 basket study. *The Lancet Oncology*. https://doi.org/10.1016/S1470-2045(20)30451-4

Grau, D., Zhang, Y., Lee, C. H., Valencia-Sánchez, M., Zhang, J., Wang, M., Holder, M., Svetlov, V., Tan, D., Nudler, E., Reinberg, D., Walz, T., & Armache, K. J. (2021). Structures of monomeric and dimeric PRC2:EZH1 reveal flexible modules involved in chromatin compaction. *Nature Communications*. https://doi.org/10.1038/s41467-020-20775-z

Green, M. R. (2018). Chromatin modifying gene mutations in follicular lymphoma. In *Blood*. https://doi.org/10.1182/blood-2017-08-737361

Greenberg, M. V. C., & Bourc'his, D. (2019). The diverse roles of DNA methylation in mammalian development and disease. In *Nature Reviews Molecular Cell Biology*.

https://doi.org/10.1038/s41580-019-0159-6
Greger, V., Passarge, E., Höpping, W., Messmer, E., & Horsthemke, B. (1989). Epigenetic changes may contribute to the formation and spontaneous regression of retinoblastoma. *Human Genetics*. https://doi.org/10.1007/BF00286709
Grembecka, J., He, S., Shi, A., Purohit, T., Muntean, A. G., Sorenson, R. J., Showalter, H. D., Murai, M. J., Belcher, A. M., Hartley, T., Hess, J. L., & Cierpicki, T. (2012). Menin-MLL inhibitors reverse oncogenic activity of MLL fusion proteins in leukemia. *Nature Chemical Biology*. https://doi.org/10.1038/nchembio.773
Grevet, J. D., Lan, X., Hamagami, N., Edwards, C. R., Sankaranarayanan, L., Ji, X., Bhardwaj, S. K., Face, C. J., Posocco, D. F., Abdulmalik, O., Keller, C. A., Giardine, B., Sidoli, S., Garcia, B. A., Chou, S. T., Liebhaber, S. A., Hardison, R. C., Shi, J., & Blobel, G. A. (2018). Domain-focused CRISPR screen identifies HRI as a fetal hemoglobin regulator in human erythroid cells. *Science*. https://doi.org/10.1126/science.aao0932
Grijzenhout, A., Godwin, J., Koseki, H., Gdula, M. R., Szumska, D., McGouran, J. F., Bhattacharya, S., Kessler, B. M., Brockdorff, N., & Cooper, S. (2016). Functional analysis of AEBP2, a PRC2 polycomb protein, reveals a trithorax phenotype in embryonic development and in ESCs. *Development (Cambridge)*. https://doi.org/10.1242/dev.123935
Guenther, M. G., Lawton, L. N., Rozovskaia, T., Frampton, G. M., Levine, S. S., Volkert, T. L., Croce, C. M., Nakamura, T., Canaani, E., & Young, R. A. (2008). Aberrant chromatin at genes encoding stem cell regulators in human mixed-lineage leukemia. *Genes and Development*. https://doi.org/10.1101/gad.1741408
Harms, P. W., Hristov, A. C., Kim, D. S., Anens, T., Quist, M. J., Siddiqui, J., Carskadon, S., Mehra, R., Fullen, D. R., Johnson, T. M., Chinnaiyan, A. M., & Palanisamy, N. (2014). Activating mutations of the oncogene EZH2 in cutaneous melanoma revealed by next generation sequencing. *Human Pathology: Case Reports*. https://doi.org/10.1016/j.ehpc.2014.07.002
Hashwah, H., Schmid, C. A., Kasser, S., Bertram, K., Stelling, A., Manz, M. G., & Müller, A. (2017). Inactivation of CREBBP expands the germinal center B cell compartment, down-regulates MHCII expression and promotes DLBCL growth. *Proceedings of the National Academy of Sciences of the United States of America*. https://doi.org/10.1073/pnas.1619555114
Hauri, S., Comoglio, F., Seimiya, M., Gerstung, M., Glatter, T., Hansen, K., Aebersold, R., Paro, R., Gstaiger, M., & Beisel, C. (2016). A High-Density Map for Navigating the Human Polycomb Complexome. *Cell Reports*. https://doi.org/10.1016/j.celrep.2016.08.096
He, G. P., Kim, S., & Ro, H. S. (1999). Cloning and characterization of a novel zinc finger transcriptional repressor. A direct role of the zinc finger motif in repression. *Journal of Biological Chemistry*. https://doi.org/10.1074/jbc.274.21.14678
He, Y., Selvaraju, S., Curtin, M. L., Jakob, C. G., Zhu, H., Comess, K. M., Shaw, B., The, J., Lima-Fernandes, E., Szewczyk, M. M., Cheng, D., Klinge, K. L., Li, H. Q., Pliushchev, M., Algire, M. A., Maag, D., Guo, J., Dietrich, J., Panchal, S. C., … Pappano, W. N. (2017). The EED protein-protein interaction inhibitor A-395 inactivates the PRC2 complex. *Nature Chemical Biology*. https://doi.org/10.1038/nchembio.2306
Healy, E., Mucha, M., Glancy, E., Fitzpatrick, D. J., Conway, E., Neikes, H. K., Monger, C., Van Mierlo, G., Baltissen, M. P., Koseki, Y., Vermeulen, M., Koseki, H., & Bracken, A. P. (2019). PRC2.1 and PRC2.2 Synergize to Coordinate H3K27 Trimethylation. *Molecular Cell*. https://doi.org/10.1016/j.molcel.2019.08.012
Heinz, S., Benner, C., Spann, N., Bertolino, E., Lin, Y. C., Laslo, P., Cheng, J. X., Murre, C.,

Singh, H., & Glass, C. K. (2010). Simple Combinations of Lineage-Determining Transcription Factors Prime cis-Regulatory Elements Required for Macrophage and B Cell Identities. *Molecular Cell*. https://doi.org/10.1016/j.molcel.2010.05.004

Heise, N., de Silva, N. S., Silva, K., Carette, A., Simonetti, G., Pasparakis, M., & Klein, U. (2014). Germinal center B cell maintenance and differentiation are controlled by distinct NF-κB transcription factor subunits. *Journal of Experimental Medicine*. https://doi.org/10.1084/jem.20132613

Helming, K. C., Wang, X., Wilson, B. G., Vazquez, F., Haswell, J. R., Manchester, H. E., Kim, Y., Kryukov, G. V., Ghandi, M., Aguirre, A. J., Jagani, Z., Wang, Z., Garraway, L. A., Hahn, W. C., & Roberts, C. W. M. (2014). ARID1B is a specific vulnerability in ARID1A-mutant cancers. *Nature Medicine*. https://doi.org/10.1038/nm.3480

Heward, J., Konali, L., D'Avola, A., Close, K., Yeomans, A., Philpott, M., Dunford, J., Rahim, T., Al Seraihi, A. F., Wang, J., Korfi, K., Araf, S., Iqbal, S., Bewicke-Copley, F., Kumar, E., Barisic, D., Calaminici, M., Clear, A., Gribben, J., … Fitzgibbon, J. (2021). KDM5 inhibition offers a novel therapeutic strategy for the treatment of KMT2D mutant lymphomas. *Blood*. https://doi.org/10.1182/blood.2020008743

Hnisz, D., Weintrau, A. S., Day, D. S., Valton, A. L., Bak, R. O., Li, C. H., Goldmann, J., Lajoie, B. R., Fan, Z. P., Sigova, A. A., Reddy, J., Borges-Rivera, D., Lee, T. I., Jaenisch, R., Porteus, M. H., Dekker, J., & Young, R. A. (2016). Activation of proto-oncogenes by disruption of chromosome neighborhoods. *Science*. https://doi.org/10.1126/science.aad9024

Ho, A. S., Kannan, K., Roy, D. M., Morris, L. G. T., Ganly, I., Katabi, N., Ramaswami, D., Walsh, L. A., Eng, S., Huse, J. T., Zhang, J., Dolgalev, I., Huberman, K., Heguy, A., Viale, A., Drobnjak, M., Leversha, M. A., Rice, C. E., Singh, B., … Chan, T. A. (2013). The mutational landscape of adenoid cystic carcinoma. *Nature Genetics*. https://doi.org/10.1038/ng.2643

Hodis, E., Watson, I. R., Kryukov, G. V., Arold, S. T., Imielinski, M., Theurillat, J. P., Nickerson, E., Auclair, D., Li, L., Place, C., Dicara, D., Ramos, A. H., Lawrence, M. S., Cibulskis, K., Sivachenko, A., Voet, D., Saksena, G., Stransky, N., Onofrio, R. C., … Chin, L. (2012). A landscape of driver mutations in melanoma. *Cell*. https://doi.org/10.1016/j.cell.2012.06.024

Hoffman, G. R., Rahal, R., Buxton, F., Xiang, K., McAllister, G., Frias, E., Bagdasarian, L., Huber, J., Lindeman, A., Chen, D., Romero, R., Ramadan, N., Phadke, T., Haas, K., Jaskelioff, M., Wilson, B. G., Meyer, M. J., Saenz-Vash, V., Zhai, H., … Jagani, Z. (2014). Functional epigenetics approach identifies BRM/SMARCA2 as a critical synthetic lethal target in BRG1-deficient cancers. *Proceedings of the National Academy of Sciences of the United States of America*. https://doi.org/10.1073/pnas.1316793111

Højfeldt, Jonas W., Laugesen, A., Willumsen, B. M., Damhofer, H., Hedehus, L., Tvardovskiy, A., Mohammad, F., Jensen, O. N., & Helin, K. (2018). Accurate H3K27 methylation can be established de novo by SUZ12-directed PRC2. *Nature Structural and Molecular Biology*. https://doi.org/10.1038/s41594-018-0036-6

Højfeldt, Jonas Westergaard, Hedehus, L., Laugesen, A., Tatar, T., Wiehle, L., & Helin, K. (2019). Non-core Subunits of the PRC2 Complex Are Collectively Required for Its Target-Site Specificity. *Molecular Cell*. https://doi.org/10.1016/j.molcel.2019.07.031

Holliday, R., & Grigg, G. W. (1993). DNA methylation and mutation. *Mutation Research - Fundamental and Molecular Mechanisms of Mutagenesis*. https://doi.org/10.1016/0027-5107(93)90052-H

Holoch, D., & Margueron, R. (2017). Mechanisms Regulating PRC2 Recruitment and Enzymatic Activity. In *Trends in Biochemical Sciences*. https://doi.org/10.1016/j.tibs.2017.04.003

Hooghe, B., Hulpiau, P., van Roy, F., & De Bleser, P. (2008). ConTra: a promoter alignment analysis tool for identification of transcription factor binding sites across species. *Nucleic Acids Research*. https://doi.org/10.1093/nar/gkn195

Horning, S. J. (1993). Natural history of and therapy for the indolent non-Hodgkin's lymphomas. In *Seminars in Oncology*.

Hoster, E., Dreyling, M., Klapper, W., Gisselbrecht, C., Van Hoof, A., Kluin-Nelemans, H. C., Pfreundschuh, M., Reiser, M., Metzner, B., Einsele, H., Peter, N., Jung, W., Wörmann, B., Ludwig, W. D., Dührsen, U., Eimermacher, H., Wandt, H., Hasford, J., Hiddemann, W., & Unterhalt, M. (2008). A new prognostic index (MIPI) for patients with advanced-stage mantle cell lymphoma. *Blood*, *111*(2), 558–565. https://doi.org/10.1182/blood-2007-06-095331

Hsu, J. H. R., Rasmusson, T., Robinson, J., Pachl, F., Read, J., Kawatkar, S., O' Donovan, D. H., Bagal, S., Code, E., Rawlins, P., Argyrou, A., Tomlinson, R., Gao, N., Zhu, X., Chiarparin, E., Jacques, K., Shen, M., Woods, H., Bednarski, E., … Bloecher, A. (2020). EED-Targeted PROTACs Degrade EED, EZH2, and SUZ12 in the PRC2 Complex. *Cell Chemical Biology*. https://doi.org/10.1016/j.chembiol.2019.11.004

Hsu, P. D., Scott, D. A., Weinstein, J. A., Ran, F. A., Konermann, S., Agarwala, V., Li, Y., Fine, E. J., Wu, X., Shalem, O., Cradick, T. J., Marraffini, L. A., Bao, G., & Zhang, F. (2013). DNA targeting specificity of RNA-guided Cas9 nucleases. *Nature Biotechnology*. https://doi.org/10.1038/nbt.2647

Hu, C. C. A., Dougan, S. K., McGehee, A. M., Love, J. C., & Ploegh, H. L. (2009). XBP-1 regulates signal transduction, transcription factors and bone marrow colonization in B cells. *EMBO Journal*. https://doi.org/10.1038/emboj.2009.117

Huang, Y., & Rao, A. (2014). Connections between TET proteins and aberrant DNA modification in cancer. In *Trends in Genetics*. https://doi.org/10.1016/j.tig.2014.07.005

Hübner, J. M., Müller, T., Papageorgiou, D. N., Mauermann, M., Krijgsveld, J., Russell, R. B., Ellison, D. W., Pfister, S. M., Pajtler, K. W., & Kool, M. (2019). EZHIP/CXorf67 mimics K27M mutated oncohistones and functions as an intrinsic inhibitor of PRC2 function in aggressive posterior fossa ependymoma. *Neuro-Oncology*. https://doi.org/10.1093/neuonc/noz058

Ikawa, T., Kawamoto, H., Wright, L. Y. T., & Murre, C. (2004). Long-term cultured E2A-deficient hematopoietic progenitor cells are pluripotent. *Immunity*. https://doi.org/10.1016/S1074-7613(04)00049-4

Ingham, P. W. (1983). Differential expression of bithorax complex genes in the absence of the extra sex combs and trithorax genes. *Nature*. https://doi.org/10.1038/306591a0

Ingham, P. W. (1985). Genetic control of the spatial pattern of selector gene expression in Drosophila. *Cold Spring Harbor Symposia on Quantitative Biology*. https://doi.org/10.1101/SQB.1985.050.01.026

Ishida, T., & Kinoshita, K. (2007). PrDOS: Prediction of disordered protein regions from amino acid sequence. *Nucleic Acids Research*. https://doi.org/10.1093/nar/gkm363

Ishino, Y., Shinagawa, H., Makino, K., Amemura, M., & Nakatura, A. (1987). Nucleotide sequence of the iap gene, responsible for alkaline phosphatase isoenzyme conversion in Escherichia coli, and identification of the gene product. *Journal of Bacteriology*. https://doi.org/10.1128/jb.169.12.5429-5433.1987

Isono, Kyo-ichi, Fujimura, Y., Shinga, J., Yamaki, M., O-Wang, J., Takihara, Y., Murahashi, Y., Takada, Y., Mizutani-Koseki, Y., & Koseki, H. (2005). Mammalian Polyhomeotic Homologues Phc2 and Phc1 Act in Synergy To Mediate Polycomb Repression of Hox Genes. *Molecular and Cellular Biology*. https://doi.org/10.1128/mcb.25.15.6694-6706.2005

Isono, Kyoichi, Endo, T. A., Ku, M., Yamada, D., Suzuki, R., Sharif, J., Ishikura, T., Toyoda,

T., Bernstein, B. E., & Koseki, H. (2013). SAM domain polymerization links subnuclear clustering of PRC1 to gene silencing. *Developmental Cell*. https://doi.org/10.1016/j.devcel.2013.08.016

Italiano, A., Soria, J. C., Toulmonde, M., Michot, J. M., Lucchesi, C., Varga, A., Coindre, J. M., Blakemore, S. J., Clawson, A., Suttle, B., McDonald, A. A., Woodruff, M., Ribich, S., Hedrick, E., Keilhack, H., Thomson, B., Owa, T., Copeland, R. A., Ho, P. T. C., & Ribrag, V. (2018). Tazemetostat, an EZH2 inhibitor, in relapsed or refractory B-cell non-Hodgkin lymphoma and advanced solid tumours: a first-in-human, open-label, phase 1 study. *The Lancet Oncology*. https://doi.org/10.1016/S1470-2045(18)30145-1

Izutsu, K., Ando, K., Nishikori, M., Shibayama, H., Teshima, T., Kuroda, J., Kato, K., Imaizumi, Y., Nosaka, K., Sakai, R., Hojo, S., Nakanishi, T., & Rai, S. (2021). Phase II study of tazemetostat for relapsed or refractory B-cell non-Hodgkin lymphoma with EZH2 mutation in Japan. *Cancer Science*. https://doi.org/10.1111/cas.15040

Jackson, A. L., Burchard, J., Leake, D., Reynolds, A., Schelter, J., Guo, J., Johnson, J. M., Lim, L., Karpilow, J., Nichols, K., Marshall, W., Khvorova, A., & Linsley, P. S. (2006). Position-specific chemical modification of siRNAs reduces "off-target" transcript silencing. *RNA*. https://doi.org/10.1261/rna.30706

Jacob, J., Kelsoe, G., Rajewsky, K., & Weiss, U. (1991). Intraclonal generation of antibody mutants in germinal centres. *Nature*. https://doi.org/10.1038/354389a0

Jaffe, J. D., Wang, Y., Chan, H. M., Zhang, J., Huether, R., Kryukov, G. V., Bhang, H. E. C., Taylor, J. E., Hu, M., Englund, N. P., Yan, F., Wang, Z., Mcdonald, E. R., Wei, L., Ma, J., Easton, J., Yu, Z., Debeaumount, R., Gibaja, V., … Stegmeier, F. (2013). Global chromatin profiling reveals NSD2 mutations in pediatric acute lymphoblastic leukemia. In *Nature Genetics*. https://doi.org/10.1038/ng.2777

Jain, S. U., Do, T. J., Lund, P. J., Rashoff, A. Q., Diehl, K. L., Cieslik, M., Bajic, A., Juretic, N., Deshmukh, S., Venneti, S., Muir, T. W., Garcia, B. A., Jabado, N., & Lewis, P. W. (2019). PFA ependymoma-associated protein EZHIP inhibits PRC2 activity through a H3 K27M-like mechanism. *Nature Communications*. https://doi.org/10.1038/s41467-019-09981-6

Jani, K. S., Jain, S. U., Ge, E. J., Diehl, K. L., Lundgren, S. M., Müller, M. M., Lewis, P. W., & Muir, T. W. (2019). Histone H3 tail binds a unique sensing pocket in EZH2 to activate the PRC2 methyltransferase. *Proceedings of the National Academy of Sciences of the United States of America*. https://doi.org/10.1073/pnas.1819029116

Jenuwein, T., & Allis, C. D. (2001). Translating the histone code. In *Science*. https://doi.org/10.1126/science.1063127

Jiang, Y., Ortega-Molina, A., Geng, H., Ying, H. Y., Hatzi, K., Parsa, S., McNally, D., Wang, L., Doane, A. S., Agirre, X., Teater, M., Meydan, C., Li, Z., Poloway, D., Wang, S., Ennishi, D., Scott, D. W., Stengel, K. R., Kranz, J. E., … Melnick, A. M. (2017). CREBBP inactivation promotes the development of HDAC3-dependent lymphomas. *Cancer Discovery*. https://doi.org/10.1158/2159-8290.CD-16-0975

Jinek, M., Chylinski, K., Fonfara, I., Hauer, M., Doudna, J. A., & Charpentier, E. (2012). A programmable dual-RNA-guided DNA endonuclease in adaptive bacterial immunity. *Science*. https://doi.org/10.1126/science.1225829

Jones, S., Van Heyningen, P., Berman, H. M., & Thornton, J. M. (1999). Protein-DNA interactions: A structural analysis. *Journal of Molecular Biology*. https://doi.org/10.1006/jmbi.1999.2659

Kalb, R., Latwiel, S., Baymaz, H. I., Jansen, P. W. T. C., Müller, C. W., Vermeulen, M., & Müller, J. (2014). Histone H2A monoubiquitination promotes histone H3 methylation in Polycomb repression. *Nature Structural and Molecular Biology*. https://doi.org/10.1038/nsmb.2833

Kamijo, T., Zindy, F., Roussel, M. F., Quelle, D. E., Downing, J. R., Ashmun, R. A., Grosveld, G., & Sherr, C. J. (1997). Tumor suppression at the mouse INK4a locus mediated by the alternative reading frame product p19(ARF). *Cell*. https://doi.org/10.1016/S0092-8674(00)80452-3

Kannt, A., & Đikić, I. (2021). Expanding the arsenal of E3 ubiquitin ligases for proximity-induced protein degradation. In *Cell Chemical Biology*. https://doi.org/10.1016/j.chembiol.2021.04.007

Kasinath, V., Beck, C., Sauer, P., Poepsel, S., Kosmatka, J., Faini, M., Toso, D., Aebersold, R., & Nogales, E. (2020). *JARID2 and AEBP2 regulate PRC2 activity in the presence of H2A ubiquitination or other histone modifications*. 1–20. https://doi.org/10.1101/2020.04.20.049213

Kasinath, V., Beck, C., Sauer, P., Poepsel, S., Kosmatka, J., Faini, M., Toso, D., Aebersold, R., & Nogales, E. (2021). JARID2 and AEBP2 regulate PRC2 in the presence of H2AK119ub1 and other histone modifications. *Science*. https://doi.org/10.1126/science.abc3393

Kasinath, V., Faini, M., Poepsel, S., Reif, D., Feng, X. A., Stjepanovic, G., Aebersold, R., & Nogales, E. (2018). Structures of human PRC2 with its cofactors AEBP2 and JARID2. *Science*. https://doi.org/10.1126/science.aar5700

Katoh, K., & Standley, D. M. (2013). MAFFT multiple sequence alignment software version 7: Improvements in performance and usability. *Molecular Biology and Evolution*. https://doi.org/10.1093/molbev/mst010

Kaustov, L., Ouyang, H., Amaya, M., Lemak, A., Nady, N., Duan, S., Wasney, G. A., Li, Z., Vedadi, M., Schapira, M., Min, J., & Arrowsmith, C. H. (2011). Recognition and specificity determinants of the human Cbx chromodomains. *Journal of Biological Chemistry*. https://doi.org/10.1074/jbc.M110.191411

Keats, J. J., Maxwell, C. A., Taylor, B. J., Hendzel, M. J., Chesi, M., Bergsagel, P. L., Larratt, L. M., Mant, M. J., Reiman, T., Belch, A. R., & Pilarski, L. M. (2005). Overexpression of transcripts originating from the MMSET locus characterizes all t(4;14)(p16;q32)-positive multiple myeloma patients. *Blood*. https://doi.org/10.1182/blood-2004-09-3704

Kempf, J. M., Weser, S., Bartoschek, M. D., Metzeler, K. H., Vick, B., Herold, T., Völse, K., Mattes, R., Scholz, M., Wange, L. E., Festini, M., Ugur, E., Roas, M., Weigert, O., Bultmann, S., Leonhardt, H., Schotta, G., Hiddemann, W., Jeremias, I., & Spiekermann, K. (2021). Loss-of-function mutations in the histone methyltransferase EZH2 promote chemotherapy resistance in AML. *Scientific Reports*. https://doi.org/10.1038/s41598-021-84708-6

Kennison, J. A., & Tamkun, J. W. (1988). Dosage-dependent modifiers of Polycomb and Antennapedia mutations in Drosophila. *Proceedings of the National Academy of Sciences of the United States of America*. https://doi.org/10.1073/pnas.85.21.8136

Kieffer-Kwon, K. R., Nimura, K., Rao, S. S. P., Xu, J., Jung, S., Pekowska, A., Dose, M., Stevens, E., Mathe, E., Dong, P., Huang, S. C., Ricci, M. A., Baranello, L., Zheng, Y., Ardori, F. T., Resch, W., Stavreva, D., Nelson, S., McAndrew, M., … Casellas, R. (2017). Myc Regulates Chromatin Decompaction and Nuclear Architecture during B Cell Activation. *Molecular Cell*. https://doi.org/10.1016/j.molcel.2017.07.013

Kim, H., Ekram, M. B., Bakshi, A., & Kim, J. (2015). AEBP2 as a transcriptional activator and its role in cell migration. *Genomics*. https://doi.org/10.1016/j.ygeno.2014.11.007

Kim, H., Kang, K., Ekram, M. B., Roh, T. Y., & Kim, J. (2011). Aebp2 as an epigenetic regulator for neural crest cells. *PLoS ONE*. https://doi.org/10.1371/journal.pone.0025174

Kim, H., Kang, K., & Kim, J. (2009). AEBP2 as a potential targeting protein for Polycomb

Repression Complex PRC2. *Nucleic Acids Research*. https://doi.org/10.1093/nar/gkp149
Kim, T., Chen, J., Sadoshima, J., & Lee, Y. (2004). Jumonji Represses Atrial Natriuretic Factor Gene Expression by Inhibiting Transcriptional Activities of Cardiac Transcription Factors. *Molecular and Cellular Biology*. https://doi.org/10.1128/mcb.24.23.10151-10160.2004
Kim, W., Bird, G. H., Neff, T., Guo, G., Kerenyi, M. A., Walensky, L. D., & Orkin, S. H. (2013). Targeted disruption of the EZH2-EED complex inhibits EZH2-dependent cancer. *Nature Chemical Biology*. https://doi.org/10.1038/nchembio.1331
Kimura, H. (2013). Histone modifications for human epigenome analysis. In *Journal of Human Genetics*. https://doi.org/10.1038/jhg.2013.66
Kirschbaum, M., Frankel, P., Popplewell, L., Zain, J., Delioukina, M., Pullarkat, V., Matsuoka, D., Pulone, B., Rotter, A. J., Espinoza-Delgado, I., Nademanee, A., Forman, S. J., Gandara, D., & Newman, E. (2011). Phase II study of vorinostat for treatment of relapsed or refractory indolent non-hodgkin's lymphoma and mantle cell lymphoma. *Journal of Clinical Oncology*. https://doi.org/10.1200/JCO.2010.32.1398
Klapper, W., Hoster, E., Determann, O., Oschlies, I., van der Laak, J., Berger, F., Bernd, H. W., Cabeçadas, J., Campo, E., Cogliatti, S., Leo Hansmann, M., Kluin, P. M., Kodet, R., Krivolapov, Y. A., Loddenkemper, C., Stein, H., Möller, P., Barth, T. E. F., Müller-Hermelink, K., … Dreyling, M. (2009). Ki-67 as a prognostic marker in mantle cell lymphoma-consensus guidelines of the pathology panel of the European MCL network. *Journal of Hematopathology*, *2*(2), 103–111. https://doi.org/10.1007/s12308-009-0036-x
Klein, B. J., Krajewski, K., Restrepo, S., Lewis, P. W., Strahl, B. D., & Kutateladze, T. G. (2018). Recognition of cancer mutations in histone H3K36 by epigenetic writers and readers. In *Epigenetics*. https://doi.org/10.1080/15592294.2018.1503491
Klymenko, T., & Jürg, M. (2004). The histone methyltransferases Trithorax and Ash1 prevent transcriptional silencing by Polycomb group proteins. *EMBO Reports*. https://doi.org/10.1038/sj.embor.7400111
Knutson, S. K., Kawano, S., Minoshima, Y., Warholic, N. M., Huang, K. C., Xiao, Y., Kadowaki, T., Uesugi, M., Kuznetsov, G., Kumar, N., Wigle, T. J., Klaus, C. R., Allain, C. J., Raimondi, A., Waters, N. J., Smith, J. J., Porter-Scott, M., Chesworth, R., Moyer, M. P., … Keilhack, H. (2014). Selective inhibition of EZH2 by EPZ-6438 leads to potent antitumor activity in EZH2-mutant non-Hodgkin lymphoma. *Molecular Cancer Therapeutics*. https://doi.org/10.1158/1535-7163.MCT-13-0773
Knutson, S. K., Wigle, T. J., Warholic, N. M., Sneeringer, C. J., Allain, C. J., Klaus, C. R., Sacks, J. D., Raimondi, A., Majer, C. R., Song, J., Scott, M. P., Jin, L., Smith, J. J., Olhava, E. J., Chesworth, R., Moyer, M. P., Richon, V. M., Copeland, R. A., Keilhack, H., … Kuntz, K. W. (2012). A selective inhibitor of EZH2 blocks H3K27 methylation and kills mutant lymphoma cells. *Nature Chemical Biology*. https://doi.org/10.1038/nchembio.1084
Kohli, R. M., & Zhang, Y. (2013). TET enzymes, TDG and the dynamics of DNA demethylation. In *Nature*. https://doi.org/10.1038/nature12750
Kooistra, S. M., & Helin, K. (2012a). Molecular mechanisms and potential functions of histone demethylases. *Nature Reviews Molecular Cell Biology*. https://doi.org/10.1038/nrm3327
Kooistra, S. M., & Helin, K. (2012b). Post-translational modifications: Molecular mechanisms and potential functions of histone demethylases. In *Nature Reviews Molecular Cell Biology*. https://doi.org/10.1038/nrm3327
Kouzarides, T. (2007). Chromatin Modifications and Their Function. In *Cell*. https://doi.org/10.1016/j.cell.2007.02.005
Krivtsov, A. V., & Armstrong, S. A. (2007). MLL translocations, histone modifications and

leukaemia stem-cell development. In *Nature Reviews Cancer*. https://doi.org/10.1038/nrc2253

Krivtsov, A. V., Evans, K., Gadrey, J. Y., Eschle, B. K., Hatton, C., Uckelmann, H. J., Ross, K. N., Perner, F., Olsen, S. N., Pritchard, T., McDermott, L., Jones, C. D., Jing, D., Braytee, A., Chacon, D., Earley, E., McKeever, B. M., Claremon, D., Gifford, A. J., … Armstrong, S. A. (2019). A Menin-MLL Inhibitor Induces Specific Chromatin Changes and Eradicates Disease in Models of MLL-Rearranged Leukemia. *Cancer Cell*. https://doi.org/10.1016/j.ccell.2019.11.001

Krivtsov, A. V., Feng, Z., Lemieux, M. E., Faber, J., Vempati, S., Sinha, A. U., Xia, X., Jesneck, J., Bracken, A. P., Silverman, L. B., Kutok, J. L., Kung, A. L., & Armstrong, S. A. (2008). H3K79 Methylation Profiles Define Murine and Human MLL-AF4 Leukemias. *Cancer Cell*. https://doi.org/10.1016/j.ccr.2008.10.001

Krysiak, K., Gomez, F., White, B. S., Matlock, M., Miller, C. A., Trani, L., Fronick, C. C., Fulton, R. S., Kreisel, F., Cashen, A. F., Carson, K. R., Berrien-Elliott, M. M., Bartlett, N. L., Griffith, M., Griffith, O. L., & Fehniger, T. A. (2017). Recurrent somatic mutations affecting B-cell receptor signaling pathway genes in follicular lymphoma. *Blood*. https://doi.org/10.1182/blood-2016-07-729954

Küppers, R., & Dalla-Favera, R. (2001). Mechanisms of chromosomal translocations in B cell lymphomas. In *Oncogene*. https://doi.org/10.1038/sj.onc.1204640

Kwok, H. S., Freedy, A. M., Siegenfeld, A. P., Morriss, J. W., Waterbury, A. L., Kissler, S. M., & Liau, B. (2022). Drug addiction mutations unveil a methylation ceiling in EZH2-mutant lymphoma. *BioRxiv*, 2022.04.04.486977. http://biorxiv.org/content/early/2022/04/05/2022.04.04.486977.abstract

Lachner, M., O'Carroll, D., Rea, S., Mechtler, K., & Jenuwein, T. (2001). Methylation of histone H3 lysine 9 creates a binding site for HP1 proteins. *Nature*. https://doi.org/10.1038/35065132

Langmead, B., & Salzberg, S. L. (2012). Fast gapped-read alignment with Bowtie 2. *Nature Methods*. https://doi.org/10.1038/nmeth.1923

Laugesen, A., & Helin, K. (2014). Chromatin repressive complexes in stem cells, development, and cancer. In *Cell Stem Cell*. https://doi.org/10.1016/j.stem.2014.05.006

Laugesen, A., Højfeldt, J. W., & Helin, K. (2019). Molecular Mechanisms Directing PRC2 Recruitment and H3K27 Methylation. In *Molecular Cell*. https://doi.org/10.1016/j.molcel.2019.03.011

Lavarone, E., Barbieri, C. M., & Pasini, D. (2019). Dissecting the role of H3K27 acetylation and methylation in PRC2 mediated control of cellular identity. *Nature Communications*. https://doi.org/10.1038/s41467-019-09624-w

Le Dily, F. L., Baù, D., Pohl, A., Vicent, G. P., Serra, F., Soronellas, D., Castellano, G., Wright, R. H. G., Ballare, C., Filion, G., Marti-Renom, M. A., & Beato, M. (2014). Distinct structural transitions of chromatin topological domains correlate with coordinated hormone-induced gene regulation. *Genes and Development*. https://doi.org/10.1101/gad.241422.114

Lee, C. H., Holder, M., Grau, D., Saldaña-Meyer, R., Yu, J. R., Ganai, R. A., Zhang, J., Wang, M., LeRoy, G., Dobenecker, M. W., Reinberg, D., & Armache, K. J. (2018). Distinct Stimulatory Mechanisms Regulate the Catalytic Activity of Polycomb Repressive Complex 2. *Molecular Cell*, *70*(3), 435-448.e5. https://doi.org/10.1016/j.molcel.2018.03.019

Lee, C. H., Yu, J. R., Kumar, S., Jin, Y., LeRoy, G., Bhanu, N., Kaneko, S., Garcia, B. A., Hamilton, A. D., & Reinberg, D. (2018). Allosteric Activation Dictates PRC2 Activity Independent of Its Recruitment to Chromatin. *Molecular Cell*. https://doi.org/10.1016/j.molcel.2018.03.020

Lee, C. K., Shibata, Y., Rao, B., Strahl, B. D., & Lieb, J. D. (2004). Evidence for nucleosome depletion at active regulatory regions genome-wide. *Nature Genetics*. https://doi.org/10.1038/ng1400

Lee, T. I., & Young, R. A. (2013). Transcriptional regulation and its misregulation in disease. In *Cell*. https://doi.org/10.1016/j.cell.2013.02.014

Lee, W., Teckie, S., Wiesner, T., Ran, L., Prieto Granada, C. N., Lin, M., Zhu, S., Cao, Z., Liang, Y., Sboner, A., Tap, W. D., Fletcher, J. A., Huberman, K. H., Qin, L. X., Viale, A., Singer, S., Zheng, D., Berger, M. F., Chen, Y., … Chi, P. (2014). PRC2 is recurrently inactivated through EED or SUZ12 loss in malignant peripheral nerve sheath tumors. *Nature Genetics*. https://doi.org/10.1038/ng.3095

Legesse-Miller, A., Raitman, I., Haley, E. M., Liao, A., Sun, L. L., Wang, D. J., Krishnan, N., Lemons, J. M. S., Suh, E. J., Johnson, E. L., Lund, B. A., & Coller, H. A. (2012). Quiescent fibroblasts are protected from proteasome inhibition-mediated toxicity. *Molecular Biology of the Cell*. https://doi.org/10.1091/mbc.E12-03-0192

Lemonnier, F., Couronné, L., Parrens, M., Jaïs, J. P., Travert, M., Lamant, L., Tournillac, O., Rousset, T., Fabiani, B., Cairns, R. A., Mak, T., Bastard, C., Bernard, O. A., De Leval, L., & Gaulard, P. (2012). Recurrent TET2 mutations in peripheral T-cell lymphomas correlate with TFH-like features and adverse clinical parameters. *Blood*. https://doi.org/10.1182/blood-2012-02-408542

Lemonnier, F., Dupuis, J., Sujobert, P., Tournillhac, O., Cheminant, M., Sarkozy, C., Pelletier, L., Marçais, A., Robe, C., Fataccioli, V., Haioun, C., Hermine, O., Gaulard, P., & Delarue, R. (2018). Treatment with 5-azacytidine induces a sustained response in patients with angioimmunoblastic T-cell lymphoma. In *Blood*. https://doi.org/10.1182/blood-2018-04-840538

Levine, S. S., Weiss, A., Erdjument-Bromage, H., Shao, Z., Tempst, P., & Kingston, R. E. (2002). The Core of the Polycomb Repressive Complex Is Compositionally and Functionally Conserved in Flies and Humans. *Molecular and Cellular Biology*. https://doi.org/10.1128/mcb.22.17.6070-6078.2002

Lewis, E. B. (1978). A gene complex controlling segmentation in Drosophila. In *Nature*. https://doi.org/10.1038/276565a0

Li, E., & Zhang, Y. (2014). DNA methylation in mammals. *Cold Spring Harbor Perspectives in Biology*. https://doi.org/10.1101/cshperspect.a019133

Li, Haojie, Liefke, R., Jiang, J., Kurland, J. V., Tian, W., Deng, P., Zhang, W., He, Q., Patel, D. J., Bulyk, M. L., Shi, Y., & Wang, Z. (2017). Polycomb-like proteins link the PRC2 complex to CpG islands. *Nature*. https://doi.org/10.1038/nature23881

Li, Hongxiu, Kaminski, M. S., Li, Y., Yildiz, M., Ouillette, P., Jones, S., Fox, H., Jacobi, K., Saiya-Cork, K., Bixby, D., Lebovic, D., Roulston, D., Shedden, K., Sabel, M., Marentette, L., Cimmino, V., Chang, A. E., & Malek, S. N. (2014). Mutations in linker histone genes HIST1H1 B, C, D, and E; OCT2 (POU2F2); IRF8; and ARID1A underlying the pathogenesis of follicular lymphoma. *Blood*. https://doi.org/10.1182/blood-2013-05-500264

Liao, Y., Smyth, G. K., & Shi, W. (2014). FeatureCounts: An efficient general purpose program for assigning sequence reads to genomic features. *Bioinformatics*. https://doi.org/10.1093/bioinformatics/btt656

Liefke, R., Karwacki-Neisius, V., & Shi, Y. (2016). EPOP Interacts with Elongin BC and USP7 to Modulate the Chromatin Landscape. *Molecular Cell*. https://doi.org/10.1016/j.molcel.2016.10.019

Liu, X., Zhang, J., Liu, L., Jiang, Y., Ji, J., Yan, R., Zhu, Z., & Yu, Y. (2018). Protein arginine methyltransferase 5-mediated epigenetic silencing of IRX1 contributes to tumorigenicity and metastasis of gastric cancer. *Biochimica et Biophysica Acta -*

Molecular Basis of Disease. https://doi.org/10.1016/j.bbadis.2018.05.015
Liu, Y., Easton, J., Shao, Y., Maciaszek, J., Wang, Z., Wilkinson, M. R., McCastlain, K., Edmonson, M., Pounds, S. B., Shi, L., Zhou, X., Ma, X., Sioson, E., Li, Y., Rusch, M., Gupta, P., Pei, D., Cheng, C., Smith, M. A., … Mullighan, C. G. (2017). The genomic landscape of pediatric and young adult T-lineage acute lymphoblastic leukemia. *Nature Genetics*. https://doi.org/10.1038/ng.3909
Liu, Z., Hu, X., Wang, Q., Wu, X., Zhang, Q., Wei, W., Su, X., He, H., Zhou, S., Hu, R., Ye, T., Zhu, Y., Wang, N., & Yu, L. (2021). Design and Synthesis of EZH2-Based PROTACs to Degrade the PRC2 Complex for Targeting the Noncatalytic Activity of EZH2. *Journal of Medicinal Chemistry*. https://doi.org/10.1021/acs.jmedchem.0c02234
Loh, M. L., Ma, X., Rusch, M., Wu, G., Harvey, R. C., Wheeler, D. A., Hampton, O. A., Carroll, W. L., Chen, I.-M., Gerhard, D. S., Gastier-Foster, J. M., Relling, M. V., Smith, M. A., Devidas, M., Auvil, J. M. G., Downing, J. R., Willman, C. L., Mullighan, C. G., & Hunger, S. P. (2013). Comparison Of Mutational Profiles Of Diagnosis and Relapsed Pediatric B-Acute Lymphoblastic Leukemia: A Report From The COG ALL Target Project. *Blood*.
Love, M. I., Huber, W., & Anders, S. (2014). Moderated estimation of fold change and dispersion for RNA-seq data with DESeq2. *Genome Biology*. https://doi.org/10.1186/s13059-014-0550-8
Lu, C., Jain, S. U., Hoelper, D., Bechet, D., Molden, R. C., Ran, L., Murphy, D., Venneti, S., Hameed, M., Pawel, B. R., Wunder, J. S., Dickson, B. C., Lundgren, S. M., Jani, K. S., De Jay, N., Papillon-Cavanagh, S., Andrulis, I. L., Sawyer, S. L., Grynspan, D., … Lewis, P. W. (2016). Cancer: Histone H3K36 mutations promote sarcomagenesis through altered histone methylation landscape. *Science*. https://doi.org/10.1126/science.aac7272
Lucas Farnung, Moritz Ochmann, Gaurika Garg, Seychelle M.Vos, P., & Cramer. (2022). Article Structure of a backtracked hexasomal intermediate of nucleosome transcription. *Molecular Cell*, *82*(17), 3126–3134.
Luger, K., Mäder, A. W., Richmond, R. K., Sargent, D. F., & Richmond, T. J. (1997). Crystal structure of the nucleosome core particle at 2.8 Å resolution. *Nature*. https://doi.org/10.1038/38444
Lunning, M. A., & Green, M. R. (2015). Mutation of chromatin modifiers; an emerging hallmark of germinal center B-cell lymphomas. In *Blood Cancer Journal*. https://doi.org/10.1038/bcj.2015.89
Madeira, F., Park, Y. M., Lee, J., Buso, N., Gur, T., Madhusoodanan, N., Basutkar, P., Tivey, A. R. N., Potter, S. C., Finn, R. D., & Lopez, R. (2019). The EMBL-EBI search and sequence analysis tools APIs in 2019. *Nucleic Acids Research*. https://doi.org/10.1093/nar/gkz268
Maës, J., Maleszewska, M., Guillemin, C., Pflumio, F., Six, E., André-Schmutz, I., Cavazzana-Calvo, M., Charron, D., Franeastel, C., & Goodhardt, M. (2008). Lymphoid-affiliated genes are associated with active histone modifications in human hematopoietic stem cells. *Blood*. https://doi.org/10.1182/blood-2008-02-140806
Marcovitz, A., & Levy, Y. (2011). Frustration in protein-DNA binding influences conformational switching and target search kinetics. *Proceedings of the National Academy of Sciences of the United States of America*. https://doi.org/10.1073/pnas.1109594108
Margueron, R., Justin, N., Ohno, K., Sharpe, M. L., Son, J., Drury, W. J., Voigt, P., Martin, S. R., Taylor, W. R., De Marco, V., Pirrotta, V., Reinberg, D., & Gamblin, S. J. (2009). Role of the polycomb protein EED in the propagation of repressive histone marks. *Nature*. https://doi.org/10.1038/nature08398

Margueron, R., Li, G., Sarma, K., Blais, A., Zavadil, J., Woodcock, C. L., Dynlacht, B. D., & Reinberg, D. (2008). Ezh1 and Ezh2 Maintain Repressive Chromatin through Different Mechanisms. *Molecular Cell*. https://doi.org/10.1016/j.molcel.2008.11.004

Marjon, K., Cameron, M. J., Quang, P., Clasquin, M. F., Mandley, E., Kunii, K., McVay, M., Choe, S., Kernytsky, A., Gross, S., Konteatis, Z., Murtie, J., Blake, M. L., Travins, J., Dorsch, M., Biller, S. A., & Marks, K. M. (2016). MTAP Deletions in Cancer Create Vulnerability to Targeting of the MAT2A/PRMT5/RIOK1 Axis. *Cell Reports*. https://doi.org/10.1016/j.celrep.2016.03.043

McCabe, M. T., Graves, A. P., Ganji, G., Diaz, E., Halsey, W. S., Jiang, Y., Smitheman, K. N., Ott, H. M., Pappalardi, M. B., Allen, K. E., Chen, S. B., Pietra, A. Della, Dul, E., Hughes, A. M., Gilbert, S. A., Thrall, S. H., Tummino, P. J., Kruger, R. G., Brandt, M., … Creasy, C. L. (2012). Mutation of A677 in histone methyltransferase EZH2 in human B-cell lymphoma promotes hypertrimethylation of histone H3 on lysine 27 (H3K27). *Proceedings of the National Academy of Sciences of the United States of America*. https://doi.org/10.1073/pnas.1116418109

McCabe, M. T., Ott, H. M., Ganji, G., Korenchuk, S., Thompson, C., Van Aller, G. S., Liu, Y., Pietra, A. Della, LaFrance, L. V., Mellinger, M., Duquenne, C., Tian, X., Kruger, R. G., McHugh, C. F., Miller, W. H., Dhanak, D., Verma, S. K., Tummino, P. J., Creasy, C. L., … Diaz, E. (2012). EZH2 inhibition as a therapeutic strategy for lymphoma with EZH2-activating mutations. In *Nature*. https://doi.org/10.1038/nature11606

Mcheyzer-Williams, L. J., Milpied, P. J., Okitsu, S. L., & Mcheyzer-Williams, M. G. (2015). Class-switched memory B cells remodel BCRs within secondary germinal centers. *Nature Immunology*. https://doi.org/10.1038/ni.3095

Meyer, S. N., Scuoppo, C., Vlasevska, S., Bal, E., Holmes, A. B., Holloman, M., Garcia-Ibanez, L., Nataraj, S., Duval, R., Vantrimpont, T., Basso, K., Brooks, N., Dalla-Favera, R., & Pasqualucci, L. (2019). Unique and Shared Epigenetic Programs of the CREBBP and EP300 Acetyltransferases in Germinal Center B Cells Reveal Targetable Dependencies in Lymphoma. *Immunity*. https://doi.org/10.1016/j.immuni.2019.08.006

Meyers, R. M., Bryan, J. G., McFarland, J. M., Weir, B. A., Sizemore, A. E., Xu, H., Dharia, N. V., Montgomery, P. G., Cowley, G. S., Pantel, S., Goodale, A., Lee, Y., Ali, L. D., Jiang, G., Lubonja, R., Harrington, W. F., Strickland, M., Wu, T., Hawes, D. C., … Tsherniak, A. (2017). Computational correction of copy number effect improves specificity of CRISPR-Cas9 essentiality screens in cancer cells. *Nature Genetics*. https://doi.org/10.1038/ng.3984

Milne, T. A., Martin, M. E., Brock, H. W., Slany, R. K., & Hess, J. L. (2005). Leukemogenic MLL fusion proteins bind across a broad region of the Hox a9 locus, promoting transcription and multiple histone modifications. *Cancer Research*. https://doi.org/10.1158/0008-5472.CAN-05-1041

Min, J., Zhang, Y., & Xu, R. M. (2003). Structural basis for specific binding of polycomb chromodomain to histone H3 methylated at Lys 27. *Genes and Development*. https://doi.org/10.1101/gad.269603

Mlynarczyk, C., Fontán, L., & Melnick, A. (2019). Germinal center-derived lymphomas: The darkest side of humoral immunity. In *Immunological Reviews*. https://doi.org/10.1111/imr.12755

Mohammad, F., Weissmann, S., Leblanc, B., Pandey, D. P., Højfeldt, J. W., Comet, I., Zheng, C., Johansen, J. V., Rapin, N., Porse, B. T., Tvardovskiy, A., Jensen, O. N., Olaciregui, N. G., Lavarino, C., Suñol, M., De Torres, C., Mora, J., Carcaboso, A. M., & Helin, K. (2017). EZH2 is a potential therapeutic target for H3K27M-mutant pediatric gliomas. *Nature Medicine*. https://doi.org/10.1038/nm.4293

Mohan, M., Lin, C., Guest, E., & Shilatifard, A. (2010). Licensed to elongate: A molecular

mechanism for MLL-based leukaemogenesis. In *Nature Reviews Cancer*. https://doi.org/10.1038/nrc2915

Moll, P., Ante, M., Seitz, A., & Reda, T. (2014). QuantSeq 3′ mRNA sequencing for RNA quantification. *Nature Methods*. https://doi.org/10.1038/nmeth.f.376

Morey, L., & Helin, K. (2010). Polycomb group protein-mediated repression of transcription. In *Trends in Biochemical Sciences*. https://doi.org/10.1016/j.tibs.2010.02.009

Morin, R. D., Johnson, N. A., Severson, T. M., Mungall, A. J., An, J., Goya, R., Paul, J. E., Boyle, M., Woolcock, B. W., Kuchenbauer, F., Yap, D., Humphries, R. K., Griffith, O. L., Shah, S., Zhu, H., Kimbara, M., Shashkin, P., Charlot, J. F., Tcherpakov, M., … Marra, M. A. (2010). Somatic mutations altering EZH2 (Tyr641) in follicular and diffuse large B-cell lymphomas of germinal-center origin. *Nature Genetics*. https://doi.org/10.1038/ng.518

Morin, R. D., Mendez-Lago, M., Mungall, A. J., Goya, R., Mungall, K. L., Corbett, R. D., Johnson, N. A., Severson, T. M., Chiu, R., Field, M., Jackman, S., Krzywinski, M., Scott, D. W., Trinh, D. L., Tamura-Wells, J., Li, S., Firme, M. R., Rogic, S., Griffith, M., … Marra, M. A. (2011). Frequent mutation of histone-modifying genes in non-Hodgkin lymphoma. *Nature*. https://doi.org/10.1038/nature10351

Moris, N., Pina, C., & Arias, A. M. (2016). Transition states and cell fate decisions in epigenetic landscapes. In *Nature Reviews Genetics*. https://doi.org/10.1038/nrg.2016.98

Morishima, S., Ishitsuka, K., Izutsu, K., Kusumoto, S., Makiyama, J., Utsunomiya, A., Nosaka, K., Ishida, T., Imaizumi, Y., Yamauchi, N., Araki, K., Adachi, N., Yamashita, T., Atsumi, R., Tsukasaki, K., & Tobinai, K. (2019). First-in-Human Study of the EZH1/2 Dual Inhibitor Valemetostat in Relapsed or Refractory Non-Hodgkin Lymphoma (NHL) - Updated Results Focusing on Adult T-Cell Leukemia-Lymphoma (ATL). *Blood*. https://doi.org/10.1182/blood-2019-125507

Morschhauser, F., Tilly, H., Chaidos, A., McKay, P., Phillips, T., Assouline, S., Batlevi, C. L., Campbell, P., Ribrag, V., Damaj, G. L., Dickinson, M., Jurczak, W., Kazmierczak, M., Opat, S., Radford, J., Schmitt, A., Yang, J., Whalen, J., Agarwal, S., … Salles, G. (2020). Tazemetostat for patients with relapsed or refractory follicular lymphoma: an open-label, single-arm, multicentre, phase 2 trial. *The Lancet Oncology*. https://doi.org/10.1016/S1470-2045(20)30441-1

Müller, J., Hart, C. M., Francis, N. J., Vargas, M. L., Sengupta, A., Wild, B., Miller, E. L., O'Connor, M. B., Kingston, R. E., & Simon, J. A. (2002). Histone Methyltransferase Activity of a Drosophila Polycomb Group Repressor Complex decisions are made by transiently acting transcription. *Cell*.

Mullighan, C. G., Zhang, J., Kasper, L. H., Lerach, S., Payne-Turner, D., Phillips, L. A., Heatley, S. L., Holmfeldt, L., Collins-Underwood, J. R., Ma, J., Buetow, K. H., Pui, C. H., Baker, S. D., Brindle, P. K., & Downing, J. R. (2011). CREBBP mutations in relapsed acute lymphoblastic leukaemia. *Nature*. https://doi.org/10.1038/nature09727

Munakata, W., Shirasugi, Y., Tobinai, K., Onizuka, M., Makita, S., Suzuki, R., Maruyama, D., Kawai, H., Izutsu, K., Nakanishi, T., Shiba, S., Hojo, S., & Ando, K. (2021). Phase 1 study of tazemetostat in Japanese patients with relapsed or refractory B-cell lymphoma. *Cancer Science*. https://doi.org/10.1111/cas.14822

Musselman, C. A., Lalonde, M. E., Côté, J., & Kutateladze, T. G. (2012). Perceiving the epigenetic landscape through histone readers. In *Nature Structural and Molecular Biology*. https://doi.org/10.1038/nsmb.2436

Muto, T., Sashida, G., Oshima, M., Wendt, G. R., Mochizuki-Kashio, M., Sanada, M., Miyagi, S., Saraya, A., Nakaseko, C., Yokote, K., Shimoda, K., Koseki, H., Suzuki, Y., Sugano, S., Ogawa, S., & Iwama, A. (2013). Concurrent Loss Of Ezh2 and Tet2 Cooperates In The Pathogenesis Of Myelodysplastic Disorders,. *Blood*.

https://doi.org/10.1182/blood.v122.21.480.480
Nabet, B., Roberts, J. M., Buckley, D. L., Paulk, J., Dastjerdi, S., Yang, A., Leggett, A. L., Erb, M. A., Lawlor, M. A., Souza, A., Scott, T. G., Vittori, S., Perry, J. A., Qi, J., Winter, G. E., Wong, K. K., Gray, N. S., & Bradner, J. E. (2018). The dTAG system for immediate and target-specific protein degradation. *Nature Chemical Biology*. https://doi.org/10.1038/s41589-018-0021-8
Nekrasov, M., Klymenko, T., Fraterman, S., Papp, B., Oktaba, K., Köcher, T., Cohen, A., Stunnenberg, H. G., Wilm, M., & Müller, J. (2007). Pcl-PRC2 is needed to generate high levels of H3-K27 trimethylation at Polycomb target genes. *EMBO Journal*. https://doi.org/10.1038/sj.emboj.7601837
Nerlov, C., Querfurth, E., Kulessa, H., & Graf, T. (2000). GATA-1 interacts with the myeloid PU.1 transcription factor and represses PU.1-dependent transcription. *Blood*. https://doi.org/10.1182/blood.v95.8.2543
Neumann, M., Vosberg, S., Schlee, C., Heesch, S., Schwartz, S., Gökbuget, N., Hoelzer, D., Graf, A., Krebs, S., Bartram, I., Blum, H., Brüggemann, M., Hecht, J., Bohlander, S. K., Greif, P. A., & Baldus, C. D. (2015). Mutational spectrum of adult T-ALL. *Oncotarget*. https://doi.org/10.18632/oncotarget.2218
Nikoloski, G., Langemeijer, S. M. C., Kuiper, R. P., Knops, R., Massop, M., Tönnissen, E. R. L. T. M., Van Der Heijden, A., Scheele, T. N., Vandenberghe, P., De Witte, T., Van Der Reijden, B. A., & Jansen, J. H. (2010). Somatic mutations of the histone methyltransferase gene EZH2 in myelodysplastic syndromes. *Nature Genetics*. https://doi.org/10.1038/ng.620
Nishiyama, A., Mulholland, C. B., Bultmann, S., Kori, S., Endo, A., Saeki, Y., Qin, W., Trummer, C., Chiba, Y., Yokoyama, H., Kumamoto, S., Kawakami, T., Hojo, H., Nagae, G., Aburatani, H., Tanaka, K., Arita, K., Leonhardt, H., & Nakanishi, M. (2020). Two distinct modes of DNMT1 recruitment ensure stable maintenance DNA methylation. *Nature Communications*. https://doi.org/10.1038/s41467-020-15006-4
Nora, E. P., Lajoie, B. R., Schulz, E. G., Giorgetti, L., Okamoto, I., Servant, N., Piolot, T., Van Berkum, N. L., Meisig, J., Sedat, J., Gribnau, J., Barillot, E., Blüthgen, N., Dekker, J., & Heard, E. (2012). Spatial partitioning of the regulatory landscape of the X-inactivation centre. *Nature*. https://doi.org/10.1038/nature11049
Nowosad, C. R., Spillane, K. M., & Tolar, P. (2016). Germinal center B cells recognize antigen through a specialized immune synapse architecture. *Nature Immunology*. https://doi.org/10.1038/ni.3458
Ntziachristos, P., Tsirigos, A., Vlierberghe, P. Van, Nedjic, J., Trimarchi, T., Flaherty, M. S., Ferres-Marco, D., Da Ros, V., Tang, Z., Siegle, J., Asp, P., Hadler, M., Rigo, I., De Keersmaecker, K., Patel, J., Huynh, T., Utro, F., Poglio, S., Samon, J. B., … Aifantis, I. (2012). Genetic inactivation of the polycomb repressive complex 2 in T cell acute lymphoblastic leukemia. *Nature Medicine*. https://doi.org/10.1038/nm.2651
Nutt, S. L., Hodgkin, P. D., Tarlinton, D. M., & Corcoran, L. M. (2015). The generation of antibody-secreting plasma cells. *Nature Reviews Immunology*. https://doi.org/10.1038/nri3795
O'Riordan, M., & Grosschedl, R. (1999). Coordinate regulation of B cell differentiation by the transcription factors EBF and E2A. *Immunity*. https://doi.org/10.1016/S1074-7613(00)80078-3
Okosun, J., Bödör, C., Wang, J., Araf, S., Yang, C. Y., Pan, C., Boller, S., Cittaro, D., Bozek, M., Iqbal, S., Matthews, J., Wrench, D., Marzec, J., Tawana, K., Popov, N., O'riain, C., O'shea, D., Carlotti, E., Davies, A., … Fitzgibbon, J. (2014). Integrated genomic analysis identifies recurrent mutations and evolution patterns driving the initiation and progression of follicular lymphoma. *Nature Genetics*. https://doi.org/10.1038/ng.2856

Olins, A. L., & Olins, D. E. (1974). Spheroid chromatin units (v bodies). *Science*. https://doi.org/10.1126/science.183.4122.330

Olivieri, M., Cho, T., Álvarez-Quilón, A., Li, K., Schellenberg, M. J., Zimmermann, M., Hustedt, N., Rossi, S. E., Adam, S., Melo, H., Heijink, A. M., Sastre-Moreno, G., Moatti, N., Szilard, R. K., McEwan, A., Ling, A. K., Serrano-Benitez, A., Ubhi, T., Feng, S., … Durocher, D. (2020). A Genetic Map of the Response to DNA Damage in Human Cells. *Cell*. https://doi.org/10.1016/j.cell.2020.05.040

Oliviero, G., Brien, G. L., Waston, A., Streubel, G., Jerman, E., Andrews, D., Doyle, B., Munawar, N., Wynne, K., Crean, J., Bracken, A. P., & Cagney, G. (2016). Dynamic protein interactions of the polycomb repressive complex 2 during differentiation of pluripotent cells. *Molecular and Cellular Proteomics*. https://doi.org/10.1074/mcp.M116.062240

Oricchio, E., Katanayeva, N., Donaldson, M. C., Sungalee, S., Joyce, P. P., Béguelin, W., Battistello, E., Sanghvi, V. R., Jiang, M., Jiang, Y., Teater, M., Parmigiani, A., Budanov, A. V., Chan, F. C., Shah, S. P., Kridel, R., Melnick, A. M., Ciriello, G., & Wendel, H. G. (2017). Genetic and epigenetic inactivation of SESTRIN1 controls mTORC1 and response to EZH2 inhibition in follicular lymphoma. *Science Translational Medicine*. https://doi.org/10.1126/scitranslmed.aak9969

Orkin, S. H., & Zon, L. I. (2008). Hematopoiesis: An Evolving Paradigm for Stem Cell Biology. In *Cell*. https://doi.org/10.1016/j.cell.2008.01.025

Orlando, D. A., Chen, M. W., Brown, V. E., Solanki, S., Choi, Y. J., Olson, E. R., Fritz, C. C., Bradner, J. E., & Guenther, M. G. (2014). Quantitative ChIP-Seq normalization reveals global modulation of the epigenome. *Cell Reports*. https://doi.org/10.1016/j.celrep.2014.10.018

Ortega-Molina, A., Boss, I. W., Canela, A., Pan, H., Jiang, Y., Zhao, C., Jiang, M., Hu, D., Agirre, X., Niesvizky, I., Lee, J. E., Chen, H. T., Ennishi, D., Scott, D. W., Mottok, A., Hother, C., Liu, S., Cao, X. J., Tam, W., … Wendel, H. G. (2015). The histone lysine methyltransferase KMT2D sustains a gene expression program that represses B cell lymphoma development. *Nature Medicine*. https://doi.org/10.1038/nm.3943

Pajtler, K. W., Wen, J., Sill, M., Lin, T., Orisme, W., Tang, B., Hübner, J. M., Ramaswamy, V., Jia, S., Dalton, J. D., Haupfear, K., Rogers, H. A., Punchihewa, C., Lee, R., Easton, J., Wu, G., Ritzmann, T. A., Chapman, R., Chavez, L., … Ellison, D. W. (2018). Molecular heterogeneity and CXorf67 alterations in posterior fossa group A (PFA) ependymomas. *Acta Neuropathologica*. https://doi.org/10.1007/s00401-018-1877-0

Pal, S., Vishwanath, S. N., Erdjument-Bromage, H., Tempst, P., & Sif, S. (2004). Human SWI/SNF-Associated PRMT5 Methylates Histone H3 Arginine 8 and Negatively Regulates Expression of ST7 and NM23 Tumor Suppressor Genes . *Molecular and Cellular Biology*. https://doi.org/10.1128/mcb.24.21.9630-9645.2004

Pasini, D., Bracken, A. P., Hansen, J. B., Capillo, M., & Helin, K. (2007). The Polycomb Group Protein Suz12 Is Required for Embryonic Stem Cell Differentiation. *Molecular and Cellular Biology*. https://doi.org/10.1128/mcb.01432-06

Pasqualucci, L., Dominguez-Sola, D., Chiarenza, A., Fabbri, G., Grunn, A., Trifonov, V., Kasper, L. H., Lerach, S., Tang, H., Ma, J., Rossi, D., Chadburn, A., Murty, V. V., Mullighan, C. G., Gaidano, G., Rabadan, R., Brindle, P. K., & Dalla-Favera, R. (2011). Inactivating mutations of acetyltransferase genes in B-cell lymphoma. *Nature*. https://doi.org/10.1038/nature09730

Pasqualucci, L., Khiabanian, H., Fangazio, M., Vasishtha, M., Messina, M., Holmes, A. B., Ouillette, P., Trifonov, V., Rossi, D., Tabbò, F., Ponzoni, M., Chadburn, A., Murty, V. V., Bhagat, G., Gaidano, G., Inghirami, G., Malek, S. N., Rabadan, R., & Dalla-Favera, R. (2014). Genetics of Follicular Lymphoma Transformation. *Cell Reports*.

https://doi.org/10.1016/j.celrep.2013.12.027
Pasqualucci, L., Migliazza, A., Basso, K., Houldsworth, J., Chaganti, R. S. K., & Dalla-Favera, R. (2003). Mutations of the BCL6 proto-oncogene disrupt its negative autoregulation in diffuse large B-cell lymphoma. *Blood*. https://doi.org/10.1182/blood-2002-11-3387
Pasqualucci, L., Trifonov, V., Fabbri, G., Ma, J., Rossi, D., Chiarenza, A., Wells, V. A., Grunn, A., Messina, M., Elliot, O., Chan, J., Bhagat, G., Chadburn, A., Gaidano, G., Mullighan, C. G., Rabadan, R., & Dalla-Favera, R. (2011). Analysis of the coding genome of diffuse large B-cell lymphoma. *Nature Genetics*. https://doi.org/10.1038/ng.892
Perino, M., Van Mierlo, G., Karemaker, I. D., Van Genesen, S., Vermeulen, M., Marks, H., Van Heeringen, S. J., & Veenstra, G. J. C. (2018). MTF2 recruits Polycomb Repressive Complex 2 by helical-shape-selective DNA binding. *Nature Genetics*. https://doi.org/10.1038/s41588-018-0134-8
Persky, D. O., Li, H., Rimsza, L. M., Barr, P. M., Popplewell, L. L., Bane, C. L., Von Gehr, A., LeBlanc, M., Fisher, R. I., Smith, S. M., & Friedberg, J. W. (2018). A phase I/II trial of vorinostat (SAHA) in combination with rituximab-CHOP in patients with newly diagnosed advanced stage diffuse large B-cell lymphoma (DLBCL): SWOG S0806. *American Journal of Hematology*. https://doi.org/10.1002/ajh.25010
Pertea, M., Kim, D., Pertea, G. M., Leek, J. T., & Salzberg, S. L. (2016). Transcript-level expression analysis of RNA-seq experiments with HISAT, StringTie and Ballgown. *Nature Protocols*. https://doi.org/10.1038/nprot.2016.095
Piunti, A., & Shilatifard, A. (2016). Epigenetic balance of gene expression by polycomb and compass families. In *Science*. https://doi.org/10.1126/science.aad9780
Piunti, A., & Shilatifard, A. (2021). The roles of Polycomb repressive complexes in mammalian development and cancer. In *Nature Reviews Molecular Cell Biology*. https://doi.org/10.1038/s41580-021-00341-1
Piunti, A., Smith, E. R., Morgan, M. A. J., Ugarenko, M., Khaltyan, N., Helmin, K. A., Ryan, C. A., Murray, D. C., Rickels, R. A., Yilmaz, B. D., Rendleman, E. J., Savas, J. N., Singer, B. D., Bulun, S. E., & Shilatifard, A. (2019). Catacomb: An endogenous inducible gene that antagonizes H3K27 methylation activity of Polycomb repressive complex 2 via an H3K27M-like mechanism. *Science Advances*. https://doi.org/10.1126/sciadv.aax2887
Poepsel, S., Kasinath, V., & Nogales, E. (2018). Cryo-EM structures of PRC2 simultaneously engaged with two functionally distinct nucleosomes. *Nature Structural and Molecular Biology*. https://doi.org/10.1038/s41594-018-0023-y
Potjewyd, F., Turner, A. M. W., Beri, J., Rectenwald, J. M., Norris-Drouin, J. L., Cholensky, S. H., Margolis, D. M., Pearce, K. H., Herring, L. E., & James, L. I. (2020). Degradation of Polycomb Repressive Complex 2 with an EED-Targeted Bivalent Chemical Degrader. *Cell Chemical Biology*. https://doi.org/10.1016/j.chembiol.2019.11.006
Poulard, C., Corbo, L., & Le Romancer, M. (2016). Protein arginine methylation/demethylation and cancer. In *Oncotarget*. https://doi.org/10.18632/oncotarget.11376
Prof Yuqin Song, M., Prof Yanyan Liu, M., Prof Zhi-Ming Li, M., Prof Lanfang Li, M., Prof Hang Su, M., Zhengming Jin, B., Xuelan Zuo, M., Jianyuan Wu, P., Prof Hui Zhou, M., Prof Kunyan Li, M., Prof Chuan He, M., Prof Jianfeng Zhou, M., Junyuan Qi, M., Prof Siguo Hao, M., Prof Zhen Cai, M., Yijing Li, M., Weiwei Wang, M., Xiaojing Zhang, M., Jianjun Zou, M., … van der Laak, J. (2022). SHR2554, an EZH2 inhibitor, in relapsed or refractory mature lymphoid neoplasms: a first-in-human, dose-escalation, dose-expansion, and clinical expansion phase 1 trial. *The Lancet Haematology*, *9*(7),

E493-503. https://doi.org/https://doi.org/10.1016/S2352-3026(22)00134-X
Qi, W., Chan, H. M., Teng, L., Li, L., Chuai, S., Zhang, R., Zeng, J., Li, M., Fan, H., Lin, Y., Gu, J., Ardayfio, O., Zhang, J. H., Yan, X., Fang, J., Mi, Y., Zhang, M., Zhou, T., Feng, G., … Li, E. (2012). Selective inhibition of Ezh2 by a small molecule inhibitor blocks tumor cells proliferation. *Proceedings of the National Academy of Sciences of the United States of America*. https://doi.org/10.1073/pnas.1210371110
Qi, W., Zhao, K., Gu, J., Huang, Y., Wang, Y., Zhang, H., Zhang, M., Zhang, J., Yu, Z., Li, L., Teng, L., Chuai, S., Zhang, C., Zhao, M., Chan, H., Chen, Z., Fang, D., Fei, Q., Feng, L., … Li, E. (2017). An allosteric PRC2 inhibitor targeting the H3K27me3 binding pocket of EED. *Nature Chemical Biology*, *13*(4), 381–388. https://doi.org/10.1038/nchembio.2304
Qin, W., Wolf, P., Liu, N., Link, S., Smets, M., Mastra, F. La, Forné, I., Pichler, G., Hörl, D., Fellinger, K., Spada, F., Bonapace, I. M., Imhof, A., Harz, H., & Leonhardt, H. (2015). DNA methylation requires a DNMT1 ubiquitin interacting motif (UIM) and histone ubiquitination. *Cell Research*. https://doi.org/10.1038/cr.2015.72
Raaphorst, F. M., van Kemenade, F. J., Fieret, E., Hamer, K. M., Satijn, D. P. E., Otte, A. P., & Meijer, C. J. L. M. (2000). Cutting Edge: Polycomb Gene Expression Patterns Reflect Distinct B Cell Differentiation Stages in Human Germinal Centers. *The Journal of Immunology*. https://doi.org/10.4049/jimmunol.164.1.1
Ragazzini, R., Pérez-Palacios, R., Baymaz, I. H., Diop, S., Ancelin, K., Zielinski, D., Michaud, A., Givelet, M., Borsos, M., Aflaki, S., Legoix, P., Jansen, P. W. T. C., Servant, N., Torres-Padilla, M. E., Bourc'his, D., Fouchet, P., Vermeulen, M., & Margueron, R. (2019). EZHIP constrains Polycomb Repressive Complex 2 activity in germ cells. *Nature Communications*. https://doi.org/10.1038/s41467-019-11800-x
Rajewsky, K. (1996). Clonal selection and learning in the antibody system. In *Nature*. https://doi.org/10.1038/381751a0
Ramachandran, S., Ahmad, K., & Henikoff, S. (2017). Transcription and Remodeling Produce Asymmetrically Unwrapped Nucleosomal Intermediates. *Molecular Cell*. https://doi.org/10.1016/j.molcel.2017.11.015
Ramírez, F., Dündar, F., Diehl, S., Grüning, B. A., & Manke, T. (2014). DeepTools: A flexible platform for exploring deep-sequencing data. *Nucleic Acids Research*. https://doi.org/10.1093/nar/gku365
Ramírez, F., Ryan, D. P., Grüning, B., Bhardwaj, V., Kilpert, F., Richter, A. S., Heyne, S., Dündar, F., & Manke, T. (2016). deepTools2: a next generation web server for deep-sequencing data analysis. *Nucleic Acids Research*. https://doi.org/10.1093/NAR/GKW257
Rea, S., Eisenhaber, F., O'Carroll, D., Strahl, B. D., Sun, Z. W., Schmid, M., Opravil, S., Mechtier, K., Ponting, C. P., Allis, C. D., & Jenuwein, T. (2000). Regulation of chromatin structure by site-specific histone H3 methyltransferases. *Nature*. https://doi.org/10.1038/35020506
Reddy, A., Zhang, J., Davis, N. S., Moffitt, A. B., Love, C. L., Waldrop, A., Leppa, S., Pasanen, A., Meriranta, L., Karjalainen-Lindsberg, M. L., Nørgaard, P., Pedersen, M., Gang, A. O., Høgdall, E., Heavican, T. B., Lone, W., Iqbal, J., Qin, Q., Li, G., … Dave, S. S. (2017). Genetic and Functional Drivers of Diffuse Large B Cell Lymphoma. *Cell*. https://doi.org/10.1016/j.cell.2017.09.027
Reichel, J., Chadburn, A., Rubinstein, P. G., Giulino-Roth, L., Tam, W., Liu, Y., Gaiolla, R., Eng, K., Brody, J., Inghirami, G., Carlo-Stella, C., Santoro, A., Rahal, D., Totonchy, J., Elemento, O., Cesarman, E., & Roshal, M. (2015). Flow sorting and exome sequencing reveal the oncogenome of primary Hodgkin and Reed-Sternberg cells. *Blood*. https://doi.org/10.1182/blood-2014-11-610436

Reimold, A. M., Iwakoshi, N. N., Manis, J., Vallabhajosyula, P., Szomolanyi-Tsuda, E., Gravallese, E. M., Friend, D., Grusby, M. J., Alt, F., & Glimcher, L. H. (2001). Plasma cell differentiation requires the transcription factor XBP-1. *Nature*. https://doi.org/10.1038/35085509

Ribrag, V., Michot, J.-M., Igleias, L., Tan, D., Ma, B., Duca, M., Wainberg, Z. A., Fan, Y. Y., Suenaga, N., Cheng, Y., Lai, C., & Yokota, T. (2021). Phase I/II Study of MAK683 in Patients with Advanced Malignancies, Including Diffuse Large B-Cell Lymphoma. *Blood*. https://doi.org/10.1182/blood-2021-147904

Ringrose, L., & Paro, R. (2004). Epigenetic regulation of cellular memory by the polycomb and trithorax group proteins. In *Annual Review of Genetics*. https://doi.org/10.1146/annurev.genet.38.072902.091907

Roberts, C. W. M., & Orkin, S. H. (2004). The SWI/SNF complex - Chromatin and cancer. In *Nature Reviews Cancer*. https://doi.org/10.1038/nrc1273

Roller, A., Grossmann, V., Bacher, U., Poetzinger, F., Weissmann, S., Nadarajah, N., Boeck, L., Kern, W., Haferlach, C., Schnittger, S., Haferlach, T., & Kohlmann, A. (2013). Landmark analysis of DNMT3A mutations in hematological malignancies. In *Leukemia*. https://doi.org/10.1038/leu.2013.65

Rosenberg, S. A. (1985). The low-grade non-Hodgkin's lymphomas: Challenges and opportunities. In *Journal of Clinical Oncology*.

Sahtoe, D. D., Van Dijk, W. J., Ekkebus, R., Ovaa, H., & Sixma, T. K. (2016). BAP1/ASXL1 recruitment and activation for H2A deubiquitination. *Nature Communications*. https://doi.org/10.1038/ncomms10292

Sakamoto, K. M., Kim, K. B., Kumagai, A., Mercurio, F., Crews, C. M., & Deshaies, R. J. (2001). Protacs: Chimeric molecules that target proteins to the Skp1-Cullin-F box complex for ubiquitination and degradation. *Proceedings of the National Academy of Sciences of the United States of America*. https://doi.org/10.1073/pnas.141230798

Salamero, O., Montesinos, P., Willekens, C., Pérez-Simón, J. A., Pigneux, A., Récher, C., Popat, R., Carpio, C., Molinero, C., Mascaró, C., Vila, J., Isabel Arévalo, M., Maes, T., Buesa, C., Bosch, F., & Somervaille, T. C. P. (2020). First-in-Human Phase I Study of Iadademstat (ORY-1001): A First-in-Class Lysine-Specific Histone Demethylase 1A Inhibitor, in Relapsed or Refractory Acute Myeloid Leukemia. *Journal of Clinical Oncology*. https://doi.org/10.1200/JCO.19.03250

Sanson, K. R., Hanna, R. E., Hegde, M., Donovan, K. F., Strand, C., Sullender, M. E., Vaimberg, E. W., Goodale, A., Root, D. E., Piccioni, F., & Doench, J. G. (2018). Optimized libraries for CRISPR-Cas9 genetic screens with multiple modalities. *Nature Communications*. https://doi.org/10.1038/s41467-018-07901-8

Sanulli, S., Justin, N., Teissandier, A., Ancelin, K., Portoso, M., Caron, M., Michaud, A., Lombard, B., da Rocha, S. T., Offer, J., Loew, D., Servant, N., Wassef, M., Burlina, F., Gamblin, S. J., Heard, E., & Margueron, R. (2015). Jarid2 Methylation via the PRC2 Complex Regulates H3K27me3 Deposition during Cell Differentiation. *Molecular Cell*. https://doi.org/10.1016/j.molcel.2014.12.020

Sarkozy, C., Morschhauser, F., Dubois, S., Molina, T., Michot, J. M., Cullières-Dartigues, P., Suttle, B., Karlin, L., Le Gouill, S., Picquenot, J. M., Dubois, R., Tilly, H., Herbaux, C., Jardin, F., Salles, G., & Ribrag, V. (2020). A LYSA phase Ib study of tazemetostat (EPZ-6438) plus R-CHOP in patients with newly diagnosed diffuse large B-cell lymphoma (DLBCL) with poor prognosis features. *Clinical Cancer Research*. https://doi.org/10.1158/1078-0432.CCR-19-3741

Sarma, K., Margueron, R., Ivanov, A., Pirrotta, V., & Reinberg, D. (2008). Ezh2 Requires PHF1 To Efficiently Catalyze H3 Lysine 27 Trimethylation In Vivo. *Molecular and Cellular Biology*. https://doi.org/10.1128/mcb.02017-07

Scelfo, A., Fernández-Pérez, D., Tamburri, S., Zanotti, M., Lavarone, E., Soldi, M., Bonaldi, T., Ferrari, K. J., & Pasini, D. (2019). Functional Landscape of PCGF Proteins Reveals Both RING1A/B-Dependent-and RING1A/B-Independent-Specific Activities. *Molecular Cell*. https://doi.org/10.1016/j.molcel.2019.04.002

Scheuermann, J. C., De Ayala Alonso, A. G., Oktaba, K., Ly-Hartig, N., McGinty, R. K., Fraterman, S., Wilm, M., Muir, T. W., & Müller, J. (2010). Histone H2A deubiquitinase activity of the Polycomb repressive complex PR-DUB. *Nature*. https://doi.org/10.1038/nature08966

Schmitges, F. W., Prusty, A. B., Faty, M., Stützer, A., Lingaraju, G. M., Aiwazian, J., Sack, R., Hess, D., Li, L., Zhou, S., Bunker, R. D., Wirth, U., Bouwmeester, T., Bauer, A., Ly-Hartig, N., Zhao, K., Chan, H., Gu, J., Gut, H., … Thomä, N. H. (2011). Histone Methylation by PRC2 Is Inhibited by Active Chromatin Marks. *Molecular Cell*. https://doi.org/10.1016/j.molcel.2011.03.025

Schmitz, R., Wright, G. W., Huang, D. W., Johnson, C. A., Phelan, J. D., Wang, J. Q., Roulland, S., Kasbekar, M., Young, R. M., Shaffer, A. L., Hodson, D. J., Xiao, W., Yu, X., Yang, Y., Zhao, H., Xu, W., Liu, X., Zhou, B., Du, W., … Staudt, L. M. (2018). Genetics and Pathogenesis of Diffuse Large B-Cell Lymphoma. *New England Journal of Medicine*. https://doi.org/10.1056/nejmoa1801445

Schuettengruber, B., Bourbon, H. M., Di Croce, L., & Cavalli, G. (2017). Genome Regulation by Polycomb and Trithorax: 70 Years and Counting. In *Cell*. https://doi.org/10.1016/j.cell.2017.08.002

Schwartz, Y. B., Kahn, T. G., Nix, D. A., Li, X. Y., Bourgon, R., Biggin, M., & Pirrotta, V. (2006). Genome-wide analysis of Polycomb targets in Drosophila melanogaster. *Nature Genetics*. https://doi.org/10.1038/ng1817

Sean, D., & Meltzer, P. S. (2007). GEOquery: A bridge between the Gene Expression Omnibus (GEO) and BioConductor. *Bioinformatics*. https://doi.org/10.1093/bioinformatics/btm254

Sexton, T., Yaffe, E., Kenigsberg, E., Bantignies, F., Leblanc, B., Hoichman, M., Parrinello, H., Tanay, A., & Cavalli, G. (2012). Three-dimensional folding and functional organization principles of the Drosophila genome. *Cell*. https://doi.org/10.1016/j.cell.2012.01.010

Shailesh, H., Zakaria, Z. Z., Baiocchi, R., & Sif, S. (2018). Protein arginine methyltransferase 5 (PRMT5) dysregulation in cancer. *Oncotarget*. https://doi.org/10.18632/oncotarget.26404

Shaknovich, R., Geng, H., Johnson, N. A., Tsikitas, L., Cerchietti, L., Greally, J. M., Gascoyne, R. D., Elemento, O., & Melnick, A. (2010). DNA methylation signatures define molecular subtypes of diffuse large B-cell lymphoma. *Blood*. https://doi.org/10.1182/blood-2010-05-285320

Shalem, O., Sanjana, N. E., Hartenian, E., Shi, X., Scott, D. A., Mikkelsen, T. S., Heckl, D., Ebert, B. L., Root, D. E., Doench, J. G., & Zhang, F. (2014). Genome-scale CRISPR-Cas9 knockout screening in human cells. *Science*. https://doi.org/10.1126/science.1247005

Shen, Y., Yue, F., Mc Cleary, D. F., Ye, Z., Edsall, L., Kuan, S., Wagner, U., Dixon, J., Lee, L., Ren, B., & Lobanenkov, V. V. (2012). A map of the cis-regulatory sequences in the mouse genome. *Nature*. https://doi.org/10.1038/nature11243

Shi, J., Wang, E., Milazzo, J. P., Wang, Z., Kinney, J. B., & Vakoc, C. R. (2015). Discovery of cancer drug targets by CRISPR-Cas9 screening of protein domains. *Nature Biotechnology*. https://doi.org/10.1038/nbt.3235

Shi, Y., Lan, F., Matson, C., Mulligan, P., Whetstine, J. R., Cole, P. A., Casero, R. A., & Shi, Y. (2004). Histone demethylation mediated by the nuclear amine oxidase homolog

LSD1. *Cell*. https://doi.org/10.1016/j.cell.2004.12.012
Shirendeb, U., Hishikawa, Y., Moriyama, S., Win, N., Thu, M. M. M., Mar, K. S., Khatanbaatar, G., Masuzaki, H., & Koji, T. (2009). Human papillomavirus infection and its possible correlation with p63 expression in cervical cancer in Japan, Mongolia, and Myanmar. *Acta Histochemica et Cytochemica*. https://doi.org/10.1267/ahc.09030
Shlush, L. I., Zandi, S., Mitchell, A., Chen, W. C., Brandwein, J. M., Gupta, V., Kennedy, J. A., Schimmer, A. D., Schuh, A. C., Yee, K. W., McLeod, J. L., Doedens, M., Medeiros, J. J. F., Marke, R., Kim, H. J., Lee, K., McPherson, J. D., Hudson, T. J., Brown, A. M. K., … Dick, J. E. (2014). Identification of pre-leukaemic haematopoietic stem cells in acute leukaemia. *Nature*. https://doi.org/10.1038/nature13038
Sigvardsson, M., Clark, D. R., Fitzsimmons, D., Doyle, M., Åkerblad, P., Breslin, T., Bilke, S., Li, R., Yeamans, C., Zhang, G., & Hagman, J. (2002). Early B-Cell Factor, E2A, and Pax-5 Cooperate To Activate the Early B Cell-Specific mb-1 Promoter . *Molecular and Cellular Biology*. https://doi.org/10.1128/mcb.22.24.8539-8551.2002
Simon, C., Chagraoui, J., Krosl, J., Gendron, P., Wilhelm, B., Lemieux, S., Boucher, G., Chagnon, P., Drouin, S., Lambert, R., Rondeau, C., Bilodeau, A., Lavallée, S., Sauvageau, M., Hébert, J., & Sauvageau, G. (2012). A key role for EZH2 and associated genes in mouse and human adult T-cell acute leukemia. *Genes and Development*. https://doi.org/10.1101/gad.186411.111
Siu, L. L., Rasco, D. W., Vinay, S. P., Romano, P. M., Menis, J., Opdam, F. L., Heinhuis, K. M., Egger, J. L., Gorman, S. A., Parasrampuria, R., Wang, K., Kremer, B. E., & Gounder, M. M. (2019). METEOR-1: A phase I study of GSK3326595, a first-in-class protein arginine methyltransferase 5 (PRMT5) inhibitor, in advanced solid tumours. *Annals of Oncology*. https://doi.org/10.1093/annonc/mdz244
Smith, C. R., Aranda, R., Bobinski, T. P., Briere, D. M., Burns, A. C., Christensen, J. G., Clarine, J., Engstrom, L. D., Gunn, R. J., Ivetac, A., Jean-Baptiste, R., Ketcham, J. M., Kobayashi, M., Kuehler, J., Kulyk, S., Lawson, J. D., Moya, K., Olson, P., Rahbaek, L., … Marx, M. A. (2022). Fragment-Based Discovery of MRTX1719, a Synthetic Lethal Inhibitor of the PRMT5•MTA Complex for the Treatment of MTAP-Deleted Cancers. *Journal of Medicinal Chemistry*. https://doi.org/10.1021/acs.jmedchem.1c01900
Smith, Z. D., & Meissner, A. (2013). DNA methylation: Roles in mammalian development. In *Nature Reviews Genetics*. https://doi.org/10.1038/nrg3354
Smits, A. H., Jansen, P. W. T. C., Poser, I., Hyman, A. A., & Vermeulen, M. (2013). Stoichiometry of chromatin-associated protein complexes revealed by label-free quantitative mass spectrometry-based proteomics. *Nucleic Acids Research*. https://doi.org/10.1093/nar/gks941
Sneeringer, C. J., Scott, M. P., Kuntz, K. W., Knutson, S. K., Pollock, R. M., Richon, V. M., & Copeland, R. A. (2010). Coordinated activities of wild-type plus mutant EZH2 drive tumor-associated hypertrimethylation of lysine 27 on histone H3 (H3K27) in human B-cell lymphomas. *Proceedings of the National Academy of Sciences of the United States of America*. https://doi.org/10.1073/pnas.1012525107
Snyder, L. B., Flanagan, J. J., Qian, Y., Gough, S. M., Andreoli, M., Bookbinder, M., Cadelina, G., Bradley, J., Rousseau, E., Chandler, J., Willard, R., Pizzano, J., Crews, C. M., Crew, A. P., Houston, J., Moore, M. D., Peck, R., & Taylor, I. (2021). Abstract 44: The discovery of ARV-471, an orally bioavailable estrogen receptor degrading PROTAC for the treatment of patients with breast cancer. *Cancer Research*. https://doi.org/10.1158/1538-7445.am2021-44
Souroullas, G. P., Jeck, W. R., Parker, J. S., Simon, J. M., Liu, J. Y., Paulk, J., Xiong, J., Clark, K. S., Fedoriw, Y., Qi, J., Burd, C. E., Bradner, J. E., & Sharpless, N. E. (2016). An oncogenic Ezh2 mutation induces tumors through global redistribution of histone 3

lysine 27 trimethylation. *Nature Medicine*. https://doi.org/10.1038/nm.4092
Stawiski, E. W., Gregoret, L. M., & Mandel-Gutfreund, Y. (2003). Annotating nucleic acid-binding function based on protein structure. *Journal of Molecular Biology*. https://doi.org/10.1016/S0022-2836(03)00031-7
Steffen, P. A., & Ringrose, L. (2014). What are memories made of? How polycomb and trithorax proteins mediate epigenetic memory. In *Nature Reviews Molecular Cell Biology*. https://doi.org/10.1038/nrm3789
Steger, D. J., Lefterova, M. I., Ying, L., Stonestrom, A. J., Schupp, M., Zhuo, D., Vakoc, A. L., Kim, J.-E., Chen, J., Lazar, M. A., Blobel, G. A., & Vakoc, C. R. (2008). DOT1L/KMT4 Recruitment and H3K79 Methylation Are Ubiquitously Coupled with Gene Transcription in Mammalian Cells. *Molecular and Cellular Biology*. https://doi.org/10.1128/mcb.02076-07
Stein, E. M., Garcia-Manero, G., Rizzieri, D. A., Tibes, R., Berdeja, J. G., Savona, M. R., Jongen-Lavrenic, M., Altman, J. K., Thomson, B., Blakemore, S. J., Daigle, S. R., Waters, N. J., Suttle, A. B., Clawson, A., Pollock, R., Krivtsov, A., Armstrong, S. A., DiMartino, J., Hedrick, E., … Tallman, M. S. (2018). The DOT1L inhibitor pinometostat reduces H3K79 methylation and has modest clinical activity in adult acute leukemia. *Blood*. https://doi.org/10.1182/blood-2017-12-818948
Stopa, N., Krebs, J. E., & Shechter, D. (2015). The PRMT5 arginine methyltransferase: Many roles in development, cancer and beyond. In *Cellular and Molecular Life Sciences*. https://doi.org/10.1007/s00018-015-1847-9
Straus, D. J., Hamlin, P. A., Matasar, M. J., Lia Palomba, M., Drullinsky, P. R., Zelenetz, A. D., Gerecitano, J. F., Noy, A., Hamilton, A. M., Elstrom, R., Wegner, B., Wortman, K., & Cella, D. (2015). Phase I/II trial of vorinostat with rituximab, cyclophosphamide, etoposide and prednisone as palliative treatment for elderly patients with relapsed or refractory diffuse large B-cell lymphoma not eligible for autologous stem cell transplantation. *British Journal of Haematology*. https://doi.org/10.1111/bjh.13195
Strecker, J., Jones, S., Koopal, B., Schmid-Burgk, J., Zetsche, B., Gao, L., Makarova, K. S., Koonin, E. V., & Zhang, F. (2019). Engineering of CRISPR-Cas12b for human genome editing. *Nature Communications*. https://doi.org/10.1038/s41467-018-08224-4
Streubel, G., Watson, A., Jammula, S. G., Scelfo, A., Fitzpatrick, D. J., Oliviero, G., McCole, R., Conway, E., Glancy, E., Negri, G. L., Dillon, E., Wynne, K., Pasini, D., Krogan, N. J., Bracken, A. P., & Cagney, G. (2018). The H3K36me2 Methyltransferase Nsd1 Demarcates PRC2-Mediated H3K27me2 and H3K27me3 Domains in Embryonic Stem Cells. *Molecular Cell*. https://doi.org/10.1016/j.molcel.2018.02.027
Struhl, G., & Akam, M. (1985). Altered distributions of Ultrabithorax transcripts in extra sex combs mutant embryos of Drosophila. *The EMBO Journal*. https://doi.org/10.1002/j.1460-2075.1985.tb04075.x
Su, I. H., Basavaraj, A., Krutchinsky, A. N., Hobert, O., Ullrich, A., Chait, B. T., & Tarakhovsky, A. (2003). Ezh2 controls B cell development through histone H3 methylation and Igh rearrangement. *Nature Immunology*. https://doi.org/10.1038/ni876
Sugishita, H., Kondo, T., Ito, S., Nakayama, M., Yakushiji-Kaminatsui, N., Kawakami, E., Koseki, Y., Ohinata, Y., Sharif, J., Harachi, M., Blackledge, N. P., Klose, R. J., & Koseki, H. (2021). Variant PCGF1-PRC1 links PRC2 recruitment with differentiation-associated transcriptional inactivation at target genes. *Nature Communications*. https://doi.org/10.1038/s41467-021-24894-z
Sun, A., Li, F., Liu, Z., Jiang, Y., Zhang, J., Wu, J., & Shi, Y. (2018). Structural and biochemical insights into human zinc finger protein AEBP2 reveals interactions with RBBP4. In *Protein and Cell*. https://doi.org/10.1007/s13238-017-0483-6
Szilágyi, A., & Skolnick, J. (2006). Efficient Prediction of Nucleic Acid Binding Function

from Low-resolution Protein Structures. *Journal of Molecular Biology*. https://doi.org/10.1016/j.jmb.2006.02.053

Taberlay, P. C., Achinger-Kawecka, J., Lun, A. T. L., Buske, F. A., Sabir, K., Gould, C. M., Zotenko, E., Bert, S. A., Giles, K. A., Bauer, D. C., Smyth, G. K., Stirzaker, C., O'Donoghue, S. I., & Clark, S. J. (2016). Three-dimensional disorganization of the cancer genome occurs coincident with long-range genetic and epigenetic alterations. *Genome Research*. https://doi.org/10.1101/gr.201517.115

Taherbhoy, A. M., Huang, O. W., & Cochran, A. G. (2015). BMI1-RING1B is an autoinhibited RING E3 ubiquitin ligase. *Nature Communications*. https://doi.org/10.1038/ncomms8621

Tamburri, S., Lavarone, E., Fernández-Pérez, D., Conway, E., Zanotti, M., Manganaro, D., & Pasini, D. (2020). Histone H2AK119 Mono-Ubiquitination Is Essential for Polycomb-Mediated Transcriptional Repression. *Molecular Cell*. https://doi.org/10.1016/j.molcel.2019.11.021

Tan, J., Yang, X., Zhuang, L., Jiang, X., Chen, W., Puay, L. L., Karuturi, R. K. M., Tan, P. B. O., Liu, E. T., & Yu, Q. (2007). Pharmacologic disruption of polycomb-repressive complex 2-mediated gene repression selectively induces apoptosis in cancer cells. *Genes and Development*. https://doi.org/10.1101/gad.1524107

Tanay, A., O'Donnell, A. H., Damelin, M., & Bestor, T. H. (2007). Hyperconserved CpG domains underlie Polycomb-binding sites. *Proceedings of the National Academy of Sciences of the United States of America*. https://doi.org/10.1073/pnas.0609746104

Tatton-Brown, K., Murray, A., Hanks, S., Douglas, J., Armstrong, R., Banka, S., Bird, L. M., Clericuzio, C. L., Cormier-Daire, V., Cushing, T., Flinter, F., Jacquemont, M. L., Joss, S., Kinning, E., Lynch, S. A., Magee, A., Mcconnell, V., Medeira, A., Ozono, K., … Rahman, N. (2013). Weaver syndrome and EZH2 mutations: Clarifying the clinical phenotype. *American Journal of Medical Genetics, Part A*. https://doi.org/10.1002/ajmg.a.36229

Terns, M. P., & Terns, R. M. (2011). CRISPR-based adaptive immune systems. In *Current Opinion in Microbiology*. https://doi.org/10.1016/j.mib.2011.03.005

The Uniprot Consortium, . (2019). UniProt: a worldwide hub of protein knowledge The UniProt Consortium. *Nucleic Acids Research*.

Tolhuis, B., Muijrers, I., De Wit, E., Teunissen, H., Talhout, W., Van Steensel, B., & Van Lohuizen, M. (2006). Genome-wide profiling of PRC1 and PRC2 Polycomb chromatin binding in Drosophila melanogaster. *Nature Genetics*. https://doi.org/10.1038/ng1792

Tsai, S. Q., Zheng, Z., Nguyen, N. T., Liebers, M., Topkar, V. V., Thapar, V., Wyvekens, N., Khayter, C., Iafrate, A. J., Le, L. P., Aryee, M. J., & Joung, J. K. (2015). GUIDE-seq enables genome-wide profiling of off-target cleavage by CRISPR-Cas nucleases. *Nature Biotechnology*. https://doi.org/10.1038/nbt.3117

Tsujimoto, Y., Cossman, J., Jaffe, E., & Croce, C. M. (1985). Involvement of the bcl-2 gene in human follicular lymphoma. *Science*. https://doi.org/10.1126/science.3874430

Tulstrup, M., Soerensen, M., Hansen, J. W., Gillberg, L., Needhamsen, M., Kaastrup, K., Helin, K., Christensen, K., Weischenfeldt, J., & Grønbæk, K. (2021). TET2 mutations are associated with hypermethylation at key regulatory enhancers in normal and malignant hematopoiesis. *Nature Communications*. https://doi.org/10.1038/s41467-021-26093-2

Van Der Meulen, J., Sanghvi, V., Mavrakis, K., Durinck, K., Fang, F., Matthijssens, F., Rondou, P., Rosen, M., Pieters, T., Vandenberghe, P., Delabesse, E., Lammens, T., De Moerloose, B., Menten, B., Van Roy, N., Verhasselt, B., Poppe, B., Benoit, Y., Taghon, T., … Van Vlierberghe, P. (2015). The H3K27me3 demethylase UTX is a gender-specific tumor suppressor in T-cell acute lymphoblastic leukemia. *Blood*.

https://doi.org/10.1182/blood-2014-05-577270
Van Der Meulen, J., Speleman, F., & Van Vlierberghe, P. (2014). The H3K27me3 demethylase UTX in normal development and disease. In *Epigenetics*. https://doi.org/10.4161/epi.28298
van Galen, J. C., Dukers, D. F., Giroth, C., Sewalt, R. G. A. B., Otte, A. P., Meijer, C. J. L. M., & Raaphorst, F. M. (2004). Distinct expression patterns of polycomb oncoproteins and their binding partners during the germinal center reaction. *European Journal of Immunology*. https://doi.org/10.1002/eji.200424985
Van Haaften, G., Dalgliesh, G. L., Davies, H., Chen, L., Bignell, G., Greenman, C., Edkins, S., Hardy, C., O'Meara, S., Teague, J., Butler, A., Hinton, J., Latimer, C., Andrews, J., Barthorpe, S., Beare, D., Buck, G., Campbell, P. J., Cole, J., … Futreal, P. A. (2009). Somatic mutations of the histone H3K27 demethylase gene UTX in human cancer. *Nature Genetics*. https://doi.org/10.1038/ng.349
Van Kemenade, F. J., Raaphorst, F. M., Blokzijl, T., Fieret, E., Hamer, K. M., Satijn, D. P. E., Otte, A. P., & Meijer, C. J. L. M. (2001). Coexpression of BMI-1 and EZH2 polycomb-group proteins is associated with cycling cells and degree of malignancy in B-cell non-Hodgkin lymphoma. *Blood*. https://doi.org/10.1182/blood.V97.12.3896
Vastenhouw, N. L., & Schier, A. F. (2012). Bivalent histone modifications in early embryogenesis. In *Current Opinion in Cell Biology*. https://doi.org/10.1016/j.ceb.2012.03.009
Velichutina, I., Shaknovich, R., Geng, H., Johnson, N. A., Gascoyne, R. D., Melnick, A. M., & Elemento, O. (2010). EZH2-mediated epigenetic silencing in germinal center B cells contributes to proliferation and lymphomagenesis. *Blood*. https://doi.org/10.1182/blood-2010-04-280149
Verma, S. K., Tian, X., Lafrance, L. V., Duquenne, C., Suarez, D. P., Newlander, K. A., Romeril, S. P., Burgess, J. L., Grant, S. W., Brackley, J. A., Graves, A. P., Scherzer, D. A., Shu, A., Thompson, C., Ott, H. M., Van Aller, G. S., MacHutta, C. A., Diaz, E., Jiang, Y., … Miller, W. H. (2012). Identification of potent, selective, cell-Active inhibitors of the histone lysine methyltransferase EZH2. *ACS Medicinal Chemistry Letters*. https://doi.org/10.1021/ml3003346
Victora, G. D., & Nussenzweig, M. C. (2012). Germinal centers. In *Annual Review of Immunology*. https://doi.org/10.1146/annurev-immunol-020711-075032
Victora, G. D., Schwickert, T. A., Fooksman, D. R., Kamphorst, A. O., Meyer-Hermann, M., Dustin, M. L., & Nussenzweig, M. C. (2010). Germinal center dynamics revealed by multiphoton microscopy with a photoactivatable fluorescent reporter. *Cell*. https://doi.org/10.1016/j.cell.2010.10.032
Waddington, C. H. (1942). Canalization of development and the inheritance of acquired characters. *Nature*. https://doi.org/10.1038/150563a0
Wang, C. Y., Colognori, D., Sunwoo, H., Wang, D., & Lee, J. T. (2019). PRC1 collaborates with SMCHD1 to fold the X-chromosome and spread Xist RNA between chromosome compartments. *Nature Communications*. https://doi.org/10.1038/s41467-019-10755-3
Wang, H., Wang, L., Erdjument-Bromage, H., Vidal, M., Tempst, P., Jones, R. S., & Zhang, Y. (2004). Role of histone H2A ubiquitination in Polycomb silencing. *Nature*. https://doi.org/10.1038/nature02985
Wang, J. H., Nichogiannopoulou, A., Wu, L., Sun, L., Sharpe, A. H., Bigby, M., & Georgopoulos, K. (1996). Selective defects in the development of the fetal and adult lymphoid system in mice with an Ikaros null mutation. *Immunity*. https://doi.org/10.1016/S1074-7613(00)80269-1
Wang, P., Wang, Z., & Liu, J. (2020). Role of HDACs in normal and malignant hematopoiesis. In *Molecular Cancer*. https://doi.org/10.1186/s12943-019-1127-7

Wang, Xing, Wang, D., Ding, N., Mi, L., Yu, H., Wu, M., Feng, F., Hu, L., Zhang, Y., Zhong, C., Ye, Y., Li, J., Fang, W., Shi, Y., Deng, L., Ying, Z., Song, Y., & Zhu, J. (2021). The synergistic anti-tumor activity of ezh2 inhibitor shr2554 and hdac inhibitor chidamide through orc1 reduction of dna replication process in diffuse large b cell lymphoma. *Cancers*. https://doi.org/10.3390/cancers13174249

Wang, Xueyin, Paucek, R. D., Gooding, A. R., Brown, Z. Z., Ge, E. J., Muir, T. W., & Cech, T. R. (2017). Molecular analysis of PRC2 recruitment to DNA in chromatin and its inhibition by RNA. *Nature Structural and Molecular Biology*. https://doi.org/10.1038/nsmb.3487

Wassef, M., Luscan, A., Aflaki, S., Zielinski, D., Jansen, P. W. T. C., Baymaz, H. I., Battistella, A., Kersouani, C., Servant, N., Wallace, M. R., Romero, P., Kosmider, O., Just, P. A., Hivelin, M., Jacques, S., Vincent-Salomon, A., Vermeulen, M., Vidaud, M., Pasmant, E., & Margueron, R. (2019). EZH1/2 function mostly within canonical PRC2 and exhibit proliferation-dependent redundancy that shapes mutational signatures in cancer. *Proceedings of the National Academy of Sciences of the United States of America*. https://doi.org/10.1073/pnas.1814634116

Waterhouse, A. M., Procter, J. B., Martin, D. M. A., Clamp, M., & Barton, G. J. (2009). Jalview Version 2-A multiple sequence alignment editor and analysis workbench. *Bioinformatics*. https://doi.org/10.1093/bioinformatics/btp033

Watts, J. M., Bradley, T. J., Thomassen, A., Brunner, A. M., Minden, M. D., Papadantonakis, N., Abedin, S., Baines, A. J., Barbash, O., Gorman, S., Kremer, B. E., & Borthakur, G. M. (2019). A Phase I/II Study to Investigate the Safety and Clinical Activity of the Protein Arginine Methyltransferase 5 Inhibitor GSK3326595 in Subjects with Myelodysplastic Syndrome and Acute Myeloid Leukemia. *Blood*. https://doi.org/10.1182/blood-2019-130337

Weishaupt, H., Sigvardsson, M., & Attema, J. L. (2010). Epigenetic chromatin states uniquely define the developmental plasticity of murine hematopoietic stem cells. *Blood*. https://doi.org/10.1182/blood-2009-07-235176

Wiedenheft, B., Sternberg, S. H., & Doudna, J. A. (2012). RNA-guided genetic silencing systems in bacteria and archaea. In *Nature*. https://doi.org/10.1038/nature10886

Willcockson, M. A., Healton, S. E., Weiss, C. N., Bartholdy, B. A., Botbol, Y., Mishra, L. N., Sidhwani, D. S., Wilson, T. J., Pinto, H. B., Maron, M. I., Skalina, K. A., Toro, L. N., Zhao, J., Lee, C. H., Hou, H., Yusufova, N., Meydan, C., Osunsade, A., David, Y., … Skoultchi, A. I. (2021). H1 histones control the epigenetic landscape by local chromatin compaction. *Nature*. https://doi.org/10.1038/s41586-020-3032-z

Woodley, C. M., Romer, A. S., Wang, J., Guarnaccia, A. D., Elion, D. L., Maxwell, J. N., Guerrazzi, K., McCann, T. S., Popay, T. M., Matlock, B. K., Flaherty, D. K., Lorey, S. L., Liu, Q., Tansey, W. P., & Weissmiller, A. M. (2021). Multiple interactions of the oncoprotein transcription factor MYC with the SWI/SNF chromatin remodeler. *Oncogene*. https://doi.org/10.1038/s41388-021-01804-7

Woyach, J. A., Furman, R. R., Liu, T.-M., Ozer, H. G., Zapatka, M., Ruppert, A. S., Xue, L., Li, D. H.-H., Steggerda, S. M., Versele, M., Dave, S. S., Zhang, J., Yilmaz, A. S., Jaglowski, S. M., Blum, K. A., Lozanski, A., Lozanski, G., James, D. F., Barrientos, J. C., … Byrd, J. C. (2014). Resistance Mechanisms for the Bruton's Tyrosine Kinase Inhibitor Ibrutinib. *New England Journal of Medicine*. https://doi.org/10.1056/nejmoa1400029

Wright, G. W., Huang, D. W., Phelan, J. D., Coulibaly, Z. A., Roulland, S., Young, R. M., Wang, J. Q., Schmitz, R., Morin, R. D., Tang, J., Jiang, A., Bagaev, A., Plotnikova, O., Kotlov, N., Johnson, C. A., Wilson, W. H., Scott, D. W., & Staudt, L. M. (2020). A Probabilistic Classification Tool for Genetic Subtypes of Diffuse Large B Cell

Lymphoma with Therapeutic Implications. *Cancer Cell*. https://doi.org/10.1016/j.ccell.2020.03.015

Xie, X. P., Laks, D. R., Sun, D., Ganbold, M., Wang, Z., Pedraza, A. M., Bale, T., Tabar, V., Brennan, C., Zhou, X., & Parada, L. F. (2022). Quiescent human glioblastoma cancer stem cells drive tumor initiation, expansion, and recurrence following chemotherapy. *Developmental Cell*. https://doi.org/10.1016/j.devcel.2021.12.007

Xu, A. Q., Barbosa, R. R., & Calado, D. P. (2020). Genetic timestamping of plasma cells in vivo reveals tissue-specific homeostatic population turnover. *ELife*. https://doi.org/10.7554/eLife.59850

Xu, Y., Yue, L., Wang, Y., Xing, J., Chen, Z., Shi, Z., Liu, R., Liu, Y. C., Luo, X., Jiang, H., Chen, K., Luo, C., & Zheng, M. (2016). Discovery of Novel Inhibitors Targeting the Menin-Mixed Lineage Leukemia Interface Using Pharmacophore- and Docking-Based Virtual Screening. *Journal of Chemical Information and Modeling*. https://doi.org/10.1021/acs.jcim.6b00185

Yamane, K., Toumazou, C., Tsukada, Y. ichi, Erdjument-Bromage, H., Tempst, P., Wong, J., & Zhang, Y. (2006). JHDM2A, a JmjC-Containing H3K9 Demethylase, Facilitates Transcription Activation by Androgen Receptor. *Cell*. https://doi.org/10.1016/j.cell.2006.03.027

Yang, Liubin, Rau, R., & Goodell, M. A. (2015). DNMT3A in haematological malignancies. *Nature Reviews Cancer*. https://doi.org/10.1038/nrc3895

Yang, Liubin, Rodriguez, B., Mayle, A., Park, H. J., Lin, X., Luo, M., Jeong, M., Curry, C. V., Kim, S. B., Ruau, D., Zhang, X., Zhou, T., Zhou, M., Rebel, V. I., Challen, G. A., Göttgens, B., Lee, J. S., Rau, R., Li, W., & Goodell, M. A. (2016). Erratum: DNMT3A Loss Drives Enhancer Hypomethylation in FLT3-ITD-Associated Leukemias (Cancer Cell (2016) 29(6) (922–934) (S1535610816302082) (10.1016/j.ccell.2016.05.003)). In *Cancer Cell*. https://doi.org/10.1016/j.ccell.2016.07.015

Yang, Lu, Chan, A. K. N., Miyashita, K., Delaney, C. D., Wang, X., Li, H., Pokharel, S. P., Li, S., Li, M., Xu, X., Lu, W., Liu, Q., Mattson, N., Chen, K. Y., Wang, J., Yuan, Y. C., Horne, D., Rosen, S. T., Soto-Feliciano, Y., … Chen, C. W. (2021). High-resolution characterization of gene function using single-cell CRISPR tiling screen. *Nature Communications*. https://doi.org/10.1038/s41467-021-24324-0

Yang, W., Soares, J., Greninger, P., Edelman, E. J., Lightfoot, H., Forbes, S., Bindal, N., Beare, D., Smith, J. A., Thompson, I. R., Ramaswamy, S., Futreal, P. A., Haber, D. A., Stratton, M. R., Benes, C., McDermott, U., & Garnett, M. J. (2013). Genomics of Drug Sensitivity in Cancer (GDSC): A resource for therapeutic biomarker discovery in cancer cells. *Nucleic Acids Research*. https://doi.org/10.1093/nar/gks1111

Yang, X. J., & Seto, E. (2007). HATs and HDACs: From structure, function and regulation to novel strategies for therapy and prevention. In *Oncogene*. https://doi.org/10.1038/sj.onc.1210599

Yao, G. (2014). Modelling mammalian cellular quiescence. In *Interface Focus*. https://doi.org/10.1098/rsfs.2013.0074

Yap, D. B., Chu, J., Berg, T., Schapira, M., Cheng, S. W. G., Moradian, A., Morin, R. D., Mungall, A. J., Meissner, B., Boyle, M., Marquez, V. E., Marra, M. A., Gascoyne, R. D., Humphries, R. K., Arrowsmith, C. H., Morin, G. B., & Aparicio, S. A. J. R. (2011). Somatic mutations at EZH2 Y641 act dominantly through a mechanism of selectively altered PRC2 catalytic activity, to increase H3K27 trimethylation. *Blood*. https://doi.org/10.1182/blood-2010-11-321208

Yelagandula, R., Stecher, K., Novatchkova, M., Michetti, L., Michlits, G., Wang, J., Hofbauer, P., Pribitzer, C., Vainorius, G., Isbel, L., Mendjan, S., Schübeler, D., Elling, U., Brennecke, J., & Bell, O. (2021). ZFP462 targets heterochromatin to transposon-

derived enhancers restricting transcription factor binding and expression of lineage-specifying genes. *BioRxiv*.
Yokoyama, A., Somervaille, T. C. P., Smith, K. S., Rozenblatt-Rosen, O., Meyerson, M., & Cleary, M. L. (2005). The menin tumor suppressor protein is an essential oncogenic cofactor for MLL-associated leukemogenesis. *Cell*. https://doi.org/10.1016/j.cell.2005.09.025
Youmans, D. T., Gooding, A. R., Dowell, R. D., & Cech, T. R. (2021). Competition between PRC2.1 and 2.2 subcomplexes regulates PRC2 chromatin occupancy in human stem cells. *Molecular Cell*. https://doi.org/10.1016/j.molcel.2020.11.044
Youmans, D. T., Schmidt, J. C., & Cech, T. R. (2018). Live-cell imaging reveals the dynamics of PRC2 and recruitment to chromatin by SUZ12-associated subunits. *Genes and Development*. https://doi.org/10.1101/gad.311936.118
Yu, J. R., Lee, C. H., Oksuz, O., Stafford, J. M., & Reinberg, D. (2019). PRC2 is high maintenance. In *Genes and Development*. https://doi.org/10.1101/gad.325050.119
Yuan, W., Xu, M., Huang, C., Liu, N., Chen, S., & Zhu, B. (2011). H3K36 methylation antagonizes PRC2-mediated H3K27 methylation. *Journal of Biological Chemistry*. https://doi.org/10.1074/jbc.M110.194027
Yunis, J. J., Frizzera, G., Oken, M. M., McKenna, J., Theologides, A., & Arnesen, M. (1987). Multiple Recurrent Genomic Defects in Follicular Lymphoma. *New England Journal of Medicine*. https://doi.org/10.1056/nejm198701083160204
Yusufova, N., Kloetgen, A., Teater, M., Osunsade, A., Camarillo, J. M., Chin, C. R., Doane, A. S., Venters, B. J., Portillo-Ledesma, S., Conway, J., Phillip, J. M., Elemento, O., Scott, D. W., Béguelin, W., Licht, J. D., Kelleher, N. L., Staudt, L. M., Skoultchi, A. I., Keogh, M. C., … Melnick, A. M. (2021). Histone H1 loss drives lymphoma by disrupting 3D chromatin architecture. *Nature*. https://doi.org/10.1038/s41586-020-3017-y
Zappia, V., Della Ragione, F., Pontoni, G., Gragnaniello, V., & Cartenì-Farina, M. (1988). Human 5'-deoxy-5'-methylthioadenosine phosphorylase: kinetic studies and catalytic mechanism. In *Advances in experimental medicine and biology*. https://doi.org/10.1007/978-1-4684-5637-0_15
Zauderer, M. G., Szlosarek, P. W., Le Moulec, S., Popat, S., Taylor, P., Planchard, D., Scherpereel, A., Jahan, T. M., Koczywas, M., Forster, M., Cameron, R. B., Peikert, T., Argon, E. K., Michaud, N., Yang, J., Kansra, V., & Fennell, D. A. (2020). Safety and efficacy of tazemetostat, an enhancer of zeste-homolog 2 inhibitor, in patients with relapsed or refractory malignant mesothelioma. *Journal of Clinical Oncology*. https://doi.org/10.1200/jco.2020.38.15_suppl.9058
Zhang, Jenny, Jima, D., Moffitt, A. B., Liu, Q., Czader, M., Hsi, E. D., Fedoriw, Y., Dunphy, C. H., Richards, K. L., Gill, J. I., Sun, Z., Love, C., Scotland, P., Lock, E., Levy, S., Hsu, D. S., Dunson, D., & Dave, S. S. (2014). The genomic landscape of mantle cell lymphoma is related to the epigenetically determined chromatin state of normal B cells. *Blood*. https://doi.org/10.1182/blood-2013-07-517177
Zhang, Jiyuan, Dominguez-Sola, D., Hussein, S., Lee, J. E., Holmes, A. B., Bansal, M., Vlasevska, S., Mo, T., Tang, H., Basso, K., Ge, K., Dalla-Favera, R., & Pasqualucci, L. (2015). Disruption of KMT2D perturbs germinal center B cell development and promotes lymphomagenesis. *Nature Medicine*. https://doi.org/10.1038/nm.3940
Zhang, Jiyuan, Vlasevska, S., Wells, V. A., Nataraj, S., Holmes, A. B., Duval, R., Meyer, S. N., Mo, T., Basso, K., Brindle, P. K., Hussein, S., Dalla-Favera, R., & Pasqualucci, L. (2017). The CREBBP acetyltransferase is a haploinsufficient tumor suppressor in B-cell lymphoma. *Cancer Discovery*. https://doi.org/10.1158/2159-8290.CD-16-1417
Zhang, M., Wang, Y., Jones, S., Sausen, M., McMahon, K., Sharma, R., Wang, Q., Belzberg,

A. J., Chaichana, K., Gallia, G. L., Gokaslan, Z. L., Riggins, G. J., Wolinksy, J. P., Wood, L. D., Montgomery, E. A., Hruban, R. H., Kinzler, K. W., Papadopoulos, N., Vogelstein, B., & Bettegowda, C. (2014). Somatic mutations of SUZ12 in malignant peripheral nerve sheath tumors. *Nature Genetics*. https://doi.org/10.1038/ng.3116

Zhang, P., Zhang, X., Iwama, A., Yu, C., Smith, K. A., Mueller, B. U., Narravula, S., Torbett, B. E., Orkin, S. H., & Tenen, D. G. (2000). PU.1 inhibits GATA-1 function and erythroid differentiation by blocking GATA-1 DNA binding. *Blood*. https://doi.org/10.1182/blood.v96.8.2641.h8002641_2641_2648

Zhang, Q., Agius, S. C., Flanigan, S. F., Uckelmann, M., Levina, V., Owen, B. M., & Davidovich, C. (2021). PALI1 facilitates DNA and nucleosome binding by PRC2 and triggers an allosteric activation of catalysis. *Nature Communications*. https://doi.org/10.1038/s41467-021-24866-3

Zhang, Q., McKenzie, N. J., Warneford-Thomson, R., Gail, E. H., Flanigan, S. F., Owen, B. M., Lauman, R., Levina, V., Garcia, B. A., Schittenhelm, R. B., Bonasio, R., & Davidovich, C. (2019). RNA exploits an exposed regulatory site to inhibit the enzymatic activity of PRC2. *Nature Structural and Molecular Biology*. https://doi.org/10.1038/s41594-019-0197-y

zhang, Q., wang, W., & gao, Q. (2020). β-TRCP-mediated AEBP2 ubiquitination and destruction controls cisplatin resistance in ovarian cancer. *Biochemical and Biophysical Research Communications*. https://doi.org/10.1016/j.bbrc.2019.12.050

Zhang, Yaqin, Dong, W., Zhu, J., Wang, L., Wu, X., & Shan, H. (2017). Combination of EZH2 inhibitor and BET inhibitor for treatment of diffuse intrinsic pontine glioma. *Cell and Bioscience*. https://doi.org/10.1186/s13578-017-0184-0

Zhang, Yong, Liu, T., Meyer, C. A., Eeckhoute, J., Johnson, D. S., Bernstein, B. E., Nussbaum, C., Myers, R. M., Brown, M., Li, W., & Shirley, X. S. (2008). Model-based analysis of ChIP-Seq (MACS). *Genome Biology*. https://doi.org/10.1186/gb-2008-9-9-r137

Zhang, Z., Jones, A., Sun, C. W., Li, C., Chang, C. W., Joo, H. Y., Dai, Q., Mysliwiec, M. R., Wu, L. C., Gou, Y., Yang, W., Liu, K., Pawlik, K. M., Erdjument-Bromage, H., Tempst, P., Lee, Y., Min, J., Townes, T. M., & Wang, H. (2011). PRC2 complexes with JARID2, MTF2, and esPRC2p48 in ES cells to modulate ES cell pluripotency and somatic cell reprograming. *Stem Cells*. https://doi.org/10.1002/stem.578